universität wien

DISSERTATION / DOCTORAL THESIS

Titel der Dissertation /Title of the Doctoral Thesis

„Prodrug and passive targeting strategies for anticancer therapeutics“

verfasst von / submitted by

Dipl.-Ing. Marlene Mathuber, BSc

angestrebter akademischer Grad / in partial fulfilment of the requirements for the degree of

Doktorin der Naturwissenschaften (Dr. rer. nat.)

Wien, 2021 / Vienna 2021

Studienkennzahl lt. Studienblatt / degree programme code as it appears on the student record sheet:	UA 796 605 419
Dissertationsgebiet lt. Studienblatt / field of study as it appears on the student record sheet:	Chemie
Betreut von / Supervisor:	Assoz. Prof. Mag. Dr. Christian Kowol
Betreut von / Supervisor:	o. Univ.-Prof. Dr. Dr. Bernhard Keppler

TO MY PARENTS, CLAUDIA AND JOHANN MATHUBER

ACKNOWLEDGMENTS

I would like to dedicate this part to all those who made this work possible and accompanied me on this journey. My sincerest gratitude goes to:

My supervisor **Assoc.-Prof. Dr. Christian Kowol** for the chance to work on these interesting projects, the countless hours discussing about them and for always keeping me motivated. Thank you very much for your guidance and encouragement as well as the delightful non-work related talks.

The head of the institute and supervisor **o. Univ.-Prof. Dr. Dr. Bernhard K. Keppler** for offering me the opportunity to be part of this research group and to work in such extraordinary well-equipped facilities.

Univ.-Prof. Dr. Walter Berger, Univ.-Prof. Dr. Petra Heffeter, **Michael Gutmann, Sonja Hager, Anna Lämmerer, Mery La Franca, Patrick Moser, Hemma Schüffl,** and **Petra Vician** from the Institute of Cancer Research and Comprehensive Cancer Center of the Medical University of Vienna for the countless biological experiments, interesting discussions and fruitful collaborations.

Assoc.-Prof. Dr. Éva Anna Enyedy and **Dr. Dömötör Orsolya** for the nice time in Hungary during my time abroad and contribution to this work.

Mag. Elfriede Limberger and **Mag. Veronika Knoll** for having always an open ear, the nice talks and their outstanding administrative support.

Sylwia Kur and **Sabrina Unterburg** for ordering chemicals and other administrative support. **Norbert Kandler** for the technical support and the countless hours together repairing the HPLCs.

For measuring numberless samples **Ao.-Prof. Dr. Mathea Galanski** and the **NMR team**, the whole group of the **mass center** and **Johannes Theiner** as well as the **elemental analysis team.**

My former and current lab/office colleagues: **Philipp Fronik, Sebastian Kallus, Marianne Lahnsteiner, Julia Bormio Nunes, Alexander Unterlercher** and **Martijn Dijkstra** for the pleasant working atmosphere. In particular **Esra Ahmed, Florian Bachmann, Björn Bielec** and **Anja Federa** for the funny times and wonderful talks outside the lab. **Alexander Kastner** for becoming a real friend, I am really going to miss you and “Alex und Marlene regeln Dinge”!

The whole research group including **Gui, Heiko, Lisa, Sophia, Valentin, Aleks, Daniel, Ines, Henrik, Yvonne, Tom, Max, Amitava** and all whose acquaintance I was allowed to make over the years for the nice times and great memories.

My family and friends for taking my mind off during stressful times, their precious advices and continuous support.

Birgit Ringhofer for your patience, understanding and encouragement. Thank you for staying by my side over all these years!

Last but most importantly to my parents **Claudia** and **Johann Mathuber** for their unconditional love and support from day one throughout my whole life. Thank you for always believing in me and giving me the opportunity to develop myself freely. I would not be here without you!

PUBLICATIONS AND MANUSCRIPTS

This dissertation is based on the following publications and manuscript:

Improving the Stability of EGFR Inhibitor Cobalt(III) Prodrugs

Marlene Mathuber, Hemma Schueffl, Orsolya Dömötör, Claudia Karnthaler, Éva A. Enyedy, Petra Heffeter, Bernhard K. Keppler and Christian R. Kowol

Inorganic Chemistry **2020**, 59, 23, 17794–17810

Development of a cobalt(III)-based ponatinib prodrug system

Marlene Mathuber, Michael Gutmann, Mery La Franca, Petra Vician, Anna Laemmerer, Patrick Moser, Bernhard K. Keppler, Walter Berger and Christian R. Kowol

Inorganic Chemistry Frontiers **2021**, 8, 2468–2485

Liposomal formulations of anticancer copper(II) thiosemicarbazone complexes

Marlene Mathuber, Sonja Hager, Bernhard K. Keppler, Petra Heffeter and Christian R. Kowol

Submitted to *Dalton Transactions*

ABSTRACT

Despite all scientific advances in the last few decades, cancer is still an immense burden to humanity, being the second leading cause of death globally. Although various treatment options are available, in most cases, severe adverse effects are dose-limiting factors and often rapidly developing resistances occur. One strategy to optimize the therapeutic index of compounds are prodrugs, a concept where the drug can be specifically activated at the target site. Another approach is the use of drug delivery systems (passive targeting), which exploit the enhanced permeability and retention (EPR) effect. By encapsulation of the drug into nanoparticles, the plasma half-life times and tumor accumulation can be increased.

Targeted therapy, including small molecule tyrosine kinase inhibitors (TKIs) and monoclonal antibodies, revolutionized cancer treatment over the past 20 years. Even though TKIs target oncogene-dependent cancer cells, resistances and lack of tumor specificity restrict them in their clinical use. Consequently, within this work prodrugs of TKIs were developed to overcome these limitations. Aim of the first project was to improve the stability of an epidermal growth factor receptor (EGFR) inhibitor-based cobalt(III) prodrug system, which can be activated *via* hypoxia. Modification of the ligands led to a decreased reduction potential (and therefore higher stability) of the complexes whilst retaining their anticancer activity *in vitro*. However, the resulting data also revealed that the direct attachment of the chelating ethylenediamine moiety to the quinazoline ring of the EGFR inhibitor is unfavorable. Consequently, in the second project cobalt(III) complexes of the clinically approved multi-kinase inhibitor ponatinib (containing a -CH_2- spacer unit at this crucial position) were designed and indeed distinctly lower reduction potentials and increased stabilities could be observed. Interestingly, *in vivo* studies showed that the most stable complex was less active, suggesting that too high stability can prevent sufficient activation *via* hypoxia.
The third project of this thesis focused on α-*N*-heterocyclic thiosemicarbazones (TSCs), which are currently under clinical investigation as anticancer drugs. Unfortunately, one of the most prominent representatives, Triapine, showed hardly any efficacy against solid cancer types, most likely due to a very short plasma half-life and fast metabolisation. Encapsulation into nanoparticles is therefore an interesting strategy to bypass these disadvantages. Liposomal formulations of copper(II) complexes of Triapine and another clinically investigated TSC (COTI-2) were developed and characterized. The liposomes of copper(II) Triapine showed the most encouraging results in cell culture experiments. *In vivo* a slow and continuous release of the drug could be observed in plasma, proving its stable encapsulation and promising properties as drug delivery system.

ZUSAMMENFASSUNG

Krebs ist, trotz aller wissenschaftlichen Fortschritte in den letzten Jahrzehnten, immer noch die zweithäufigste Todesursache weltweit und stellt für Erkrankte sowie Angehörige eine enorme Belastung dar. Die derzeit zur Verfügung stehenden Behandlungsmöglichkeiten werden häufig durch das Auftreten schwerwiegender Nebenwirkungen eingeschränkt oder verlieren ihre Wirkung durch sich rasch bildende Resistenzen. Eine vielversprechende Strategie zur Optimierung des therapeutischen Index einer Substanz ist der Einsatz sogenannter Prodrugs. Durch spezifische Mechanismen kann das Arzneimittel gezielt an der gewünschten Wirkungsstelle aktiviert werden, was Nebenwirkungen minimiert. Eine weitere aussichtsreiche Methode ist die Verwendung von „Drug Delivery"-Systemen (*passive targeting*), welche den EPR-Effekt (*enhanced permeability and retention*) nutzen. Hierbei werden Substanzen in Nanopartikel eingeschlossen, wodurch Plasma-Halbwertszeiten erhöht und die Tumorakkumulation deutlich verbessert werden können.

In den letzten 20 Jahren hat die Substanzklasse der gezielten Krebstherapeutika („*Targeted Therapeutics*"), bestehend aus Tyrosinkinase-Inhibitoren (TKIs) und monoklonalen Antikörpern, die Krebstherapie revolutioniert. Nichtsdestotrotz werden TKIs aufgrund mangelnder Tumorspezifität und auftretender Resistenzen oft in ihrer klinischen Verwendung eingeschränkt. Im Rahmen dieser Arbeit wurden daher Prodrugs von TKIs entwickelt, um diese Nachteile zu überwinden.

Ziel des ersten Projekts war es, die Stabilität einer Co(III)-basierten Prodrug zu verbessern, welche eine epidermale Wachstumsfaktorrezeptor (EGFR) inhibitierende Einheit besitzt und im hypoxischen Milieu des Tumors aktiviert werden kann. Die Modifikation der Liganden resultierte in einem geringeren Reduktionspotential (und damit in der gewünschten erhöhten Stabilität) der Komplexe, die ihre Antitumoraktivität *in vitro* behielten. Es stellte sich jedoch heraus, dass die direkte Bindung der chelatisierenden Ethylendiamin-Gruppe an den Chinazolinring des EGFR-Inhibitors nicht von Vorteil ist. Infolgedessen wurden im zweiten Projekt Co(III)-Komplexe des klinisch zugelassenen Multikinase-Inhibitors Ponatinib, welches an ebenjener Stelle einen -CH_2-Spacer in seiner molekularen Struktur trägt, synthetisiert. Tatsächlich konnten deutlich niedrigere Reduktionspotentiale und erhöhte Stabilitäten erzielt werden. Interessanterweise zeigte sich in *In-vivo*-Studien, dass der stabilste Komplex eine geringere Wirkung aufwies. Dies deutet darauf hin, dass eine ausreichende hypoxische Aktivierung wohl durch eine zu hohe Stabilität des Komplexes verhindert wird.

Das dritte Projekt dieser Arbeit befasste sich mit α-*N*-heterocyclischen Thiosemicarbazonen (TSCs), welche derzeit als potentielle Krebstherapeutika klinisch untersucht werden. Leider weist Triapin, einer der prominentesten Vertreter, kaum Wirksamkeit gegen solide Tumore auf, was höchstwahrscheinlich auf zu kurze Plasma-Halbwertszeiten und rasche Metabolisierung

zurückzuführen ist. Der Einschluss dieser Substanz(en) in Nanopartikel stellt eine interessante Strategie zur Umgehung dieser Nachteile dar. Daher wurden liposomale Formulierungen der Cu(II)-Komplexen von Triapin und COTI-2, einem weiterem klinisch untersuchten TSC, synthetisiert und charakterisiert. Die Liposomen von Cu(II)-Triapin zeigten die vielversprechendsten Ergebnisse in Zellkulturexperimenten. Anschließend konnte *in vivo* eine langsame und kontinuierliche Freisetzung des Wirkstoffs in das Plasma beobachtet werden, was auf einen stabilen Einschluss und somit auf eine vielversprechende Anwendung als „Drug Delivery"-System schließen lässt.

TABLE OF CONTENT

1 INTRODUCTION

1.1 Cancer and the human mankind

Despite remarkable progresses in scientific and medical terms, cancer is still one of the leading causes of death worldwide (right after cardiovascular diseases). Expressed in figures almost 10 million people have died in 2020 as a consequences of a cancer, on a global scale almost 1 in 6 deaths is a result of this illness, and 19.3 million new cases were recorded. The most common cancer types (in terms of cases) from last year for both sexes are: Breast (2.26 million), lung (2.21 million), colon and rectum (1.93 million), prostate (1.41 million), skin (non-melanoma) (1.20 million) and stomach (1.09 million) with lung cancer showing the highest mortality (Figure 1).[1-2]

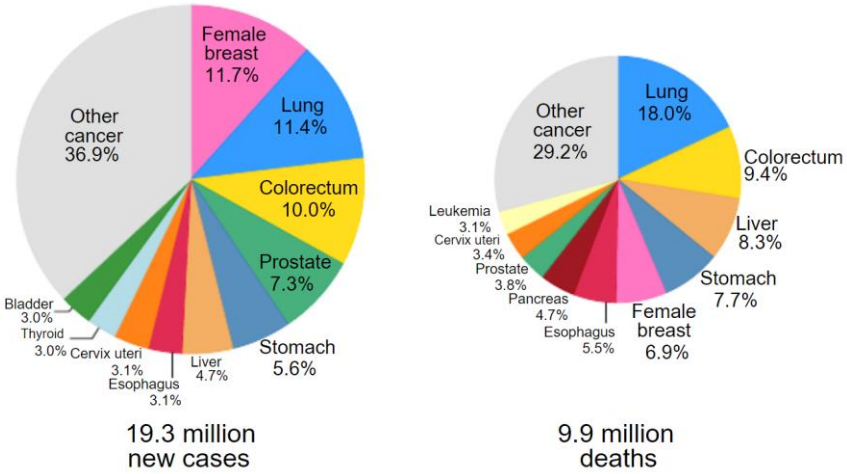

Figure 1: Incidences and mortalities for the most common cancer types in both sexes from 2020. Non-melanoma skin cancers are assigned to the other cancer category. Figure from reference [2].

This trend will continue in the future, as prognosis models suggest a surge of cancer incidences by ~14% and cancer deaths by ~16% between 2009 and 2030 for example in Austria.[3] There are a variety of reasons associated with this phenomenon including the steady growth of the population, increasing life expectancy as well as social and economic developments (e.g. tobacco/alcohol consume, diet or living conditions).[1] Consequently, cancer will still represent a major challenge for future generations and strategies are urgently in demand to at least stabilize cancer incidences worldwide. Besides screening, early detection and raised awareness campaigns, the development of improved anticancer therapeutics is of uttermost importance to achieve higher survival and cure rates. Cancer as collective term was excellently described by R.W. Ruddon “as an abnormal growth of cells caused by multiple changes in gene expression leading to dysregulated balance of cell proliferation and cell death and ultimately evolving into a population of cells that can invade tissues and metastasize to distant sites, causing significant morbidity and, if untreated, death of the host”.[4]

Notably, any part of the human body can be affected by cancer, resulting in more than 200 different types and variations. A general distinction of the most common forms can be made between carcinomas (solid tumors deriving from epithelial cells), sarcomas (cancers deriving from cartilage, soft tissues or bones), leukemia (blood malignancies deriving from bone marrow) and lymphoma (blood malignancies deriving from lymphocytes).[5] As cancers originate from a person's healthy cells it can be defined as deeply personal diseases, for which no universal treatments exist.

1.2 Forms of cancer treatment

For the treatment of cancer several options and combination possibilities are available today depending on the type of cancer and its development stage.[6] One of the oldest oncological disciplines is surgery, which has been in use for more than thousand years and improved tremendously with time. Nevertheless, surgery is most of the times restricted to primary tumors and due to its interfering nature not available for all organs. Hence, this approach is often combined with other treatments such as radiotherapy and/or chemotherapy.[7] In radiotherapy, another physical method, ionizing radiation (generated from outer or inner sources) is used to specifically destroy cancer cells by e.g. damaging their DNA. Radiotherapy is mostly applied as neoadjuvant (shrinking the tumor before main treatment) or adjuvant (preventing relapse after the main treatment) therapy.[8] Chemotherapy is still one of the most widely used therapy options worldwide, especially in combination with the above mentioned treatment forms. In general, a classic chemotherapeutic agent interrupts mechanisms responsible for cell division (mainly by targeting the DNA and associated processes), resulting in the forced apoptosis of cancer cells.[9] Theoretically, selectivity should be achieved as malignant cells show a higher turnover than healthy cells. Unfortunately, severe adverse events almost always occur during the treatment with such cytostatic drugs, starting from gastrointestinal problems or hair loss to life-threatening issues like anemia or cardiac vascular events. This results from a lack of distinction as also fast replicating normal cells (e.g. hair, bone marrows or blood) are affected by these drugs.[10] Conventional chemotherapeutics can be classified into several subgroups, which differ in their mode of action: DNA alkylating agents such as nitrogen mustards and nitrosoureas (e.g. cyclophosphamide and carmustine), antimetabolites (e.g. fluorouracil, gemcitabine, capecitabine), antimitotic agents such as topoisomerase inhibitors (e.g. topotecan, irinotecan) and platinum complexes (cisplatin, oxaliplatin, carboplatin).[11] As classic chemotherapeutics suffer from these strong side effects, novel approaches were sought after, with the aim to specifically target cancer cells while sparing the healthy cells. An intensively explored and well-known example in modern cancer medicine is immunotherapy, which was recently awarded with a Nobel Prize in 2018. As malignant cells develop from the body's own cells, the immune system is not able to recognize and destroy them.

Overexpression of certain inhibitory receptors or production of immunosuppressive mediators allows malignant cells to evade and protect themselves from immune response. Cancer immunotherapy enables the detection of these "evasion" mechanisms, supporting the immune system to identify and target abnormal cells.[12] Another alternative to classic treatments, is hormonal therapy. However, this option is only available for certain cancers types (e.g. breast, prostate or female reproductive organs), which are induced by dysfunctional steroid hormones. By inhibiting the production and/or effect of the respective hormones in the body, the growth of tumors can be reduced or stopped.[13] One major treatment option, which revolutionized cancer treatment in the last two decades, is targeted therapy. As its name suggests, in this therapy, antineoplastic agents (small molecule or monoclonal antibody tyrosine kinase inhibitors [TKIs]) specifically act on oncogenic targets and pathways crucial for carcinogenesis. In this way a distinction between normal and malignant cells can be achieved, resulting in decreased systemic toxicities.[14] Foundation for the targeted therapy approach was the steadily growing understanding of the signaling pathways involved in the development of cancer. These underlying mechanisms responsible for the complex biology of cancers can be described by the so-called hallmarks of cancer. Such hallmarks targeted by targeted therapeutics are for example activation of invasion and metastasis, sustainment of proliferative signaling or inducement of angiogenesis (Figure 2).[15]

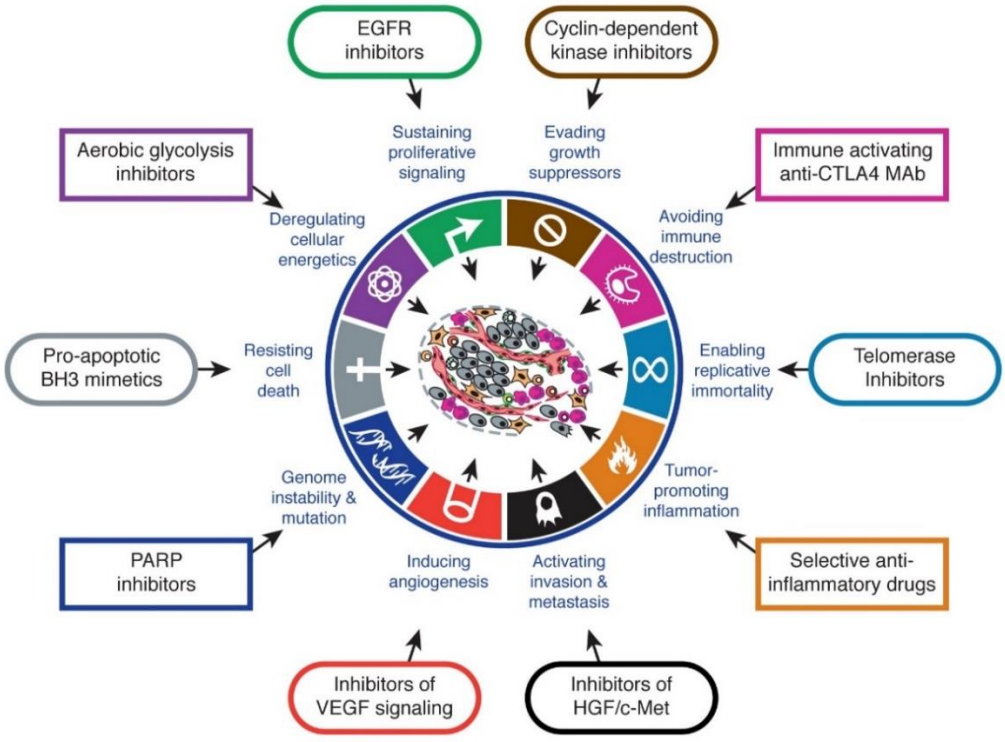

Figure 2: The hallmarks of cancer and selected examples of therapeutics targeting them. Figure from reference [15]. EGFR: epidermal growth factor receptor; CTLA4: cytotoxic T-lymphocyte-associated protein 4; mAb: monoclonal antibody; HGF: hepatocyte growth factor; c-Met: proto-oncogene receptor tyrosine kinase; VEGF: vascular endothelial growth factor; PARP: poly adenosine diphosphate ribose polymerase; BH3: apoptosis regulator Bcl-2 homology domain 3.

2 CLASSES OF ANTICANCER THERAPEUTICS WORKED WITHIN THIS THESIS

Within this thesis I have worked with two of the above mentioned anticancer compound classes: 1) the development of prodrug systems for tyrosine kinase inhibitors and 2) passive drug targeting strategies for α-*N*-heterocyclic thiosemicarbazones chemotherapeutics. Therefore, in the next chapters I will introduce these two compound classes in more detail.

2.1 Targeted Therapy - Tyrosine Kinases

Tyrosine kinases (TKs) are a subclass of protein kinases and catalyze the transfer of γ-phosphate groups from adenosine triphosphate (ATP) to tyrosine residues on protein substrates.[16] Thus, they play a crucial role in cell-regulating signaling processes including proliferation, cell-cycle control, differentiation, metabolism, survival and apoptosis.[17] Roughly 518 kinases can be found in the human genome of which 90 encode for TKs. These TKs are grouped into 58 receptor tyrosine kinases (RTKs) and 32 intracellular, non-receptor tyrosine kinases (NRTKs).[18] In general, the molecular architecture of RTKs consists of an extracellular ligand-binding domain, a cytoplasmic region containing the protein TK (plus extra regulatory domains) and a connecting single transmembrane helix.[19] The binding of receptor-specific ligands (e.g. growth/differentiation factors or hormones) to the extracellular region of the RTK leads to an intermolecular dimerization and/or oligomerization of the tyrosine kinase domain (TKD). These conformational alterations start the autophosphorylation cascade of the TKD's tyrosine residues, activating the intracellular kinase moiety thereby. Subsequently, various downstream-signaling processes are initiated, which then propagate critical cellular signaling pathways (Figure 3).[19-20]

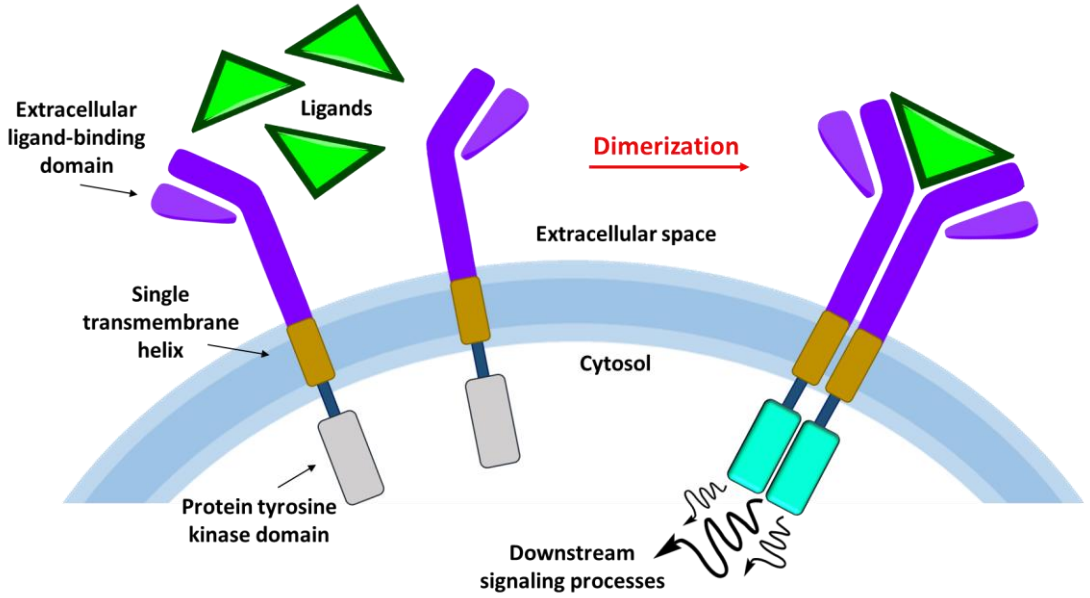

Figure 3: General ligand-mediated activation mechanism of tyrosine kinase receptors. After binding of the growth factor ligand, the connection between two monomeric receptors is stabilized resulting in the formation of a dimer. Subsequently the (*via* autophosphorylation) activated intracellular kinase induces several downstream signaling processes. Figure adapted from reference [21].

Deregulation of these signaling processes has been associated with the development of various diseases, most prominently cancer.[20] Malignant transformations can arise from abnormal activity of RTKs, which can be caused by (roughly divided) four principal mechanisms: gain-of-function mutations, genomic amplification, chromosomal translocation, and/or autocrine activation.[17, 20] Since more than 70% of known oncogenes and proto-oncogenes involve TKs,[22] inhibition of those is a promising and versatile approach in cancer therapy.[23]

2.1.1 Tyrosine Kinase Inhibitors

Tyrosine kinase inhibitors (TKIs), consisting of small molecules and monoclonal antibodies, belong to the group of targeted therapeutics and represent one of the most prominent compound classes in modern cancer therapy. The fundamental research of TKIs started over 70 years ago with the discovery of protein kinase activity, followed by the identification of the epidermal growth factor receptor (EGFR) as first RTK. [17, 24] Understanding the role of TK signaling cascades in carcinogenesis initiated the studies of TKIs in the late 1980s. This research resulted in the clinical approval of the small molecule TKI imatinib (BCR-ABL inhibitor) by the U.S. Food and Drug Administration (FDA) in 2001 and marked the breakthrough of targeted cancer therapy.[21] Small molecule TKIs target the ATP-binding site of TKs in multiple ways (e.g. by reversible/irreversible binding), leading to the inactivation of the respective domain and subsequently inhibition of cellular processes.[25-27]

More than 60 small molecule TKIs have been clinically approved by the FDA after imatinib revolutionizing cancer therapy ever after (Table 1).[28] However, (severe) adverse effects and rapidly emerging resistances limit their clinical use.[29] Therefore, strategies to overcome these disadvantages are of great interest.

Table 1: List of all FDA- approved small molecule TKIs as of March 2021.[28] (for multi-kinase inhibitors only their main therapeutic targets are provided). All compounds are applied orally.

Drug	Approved	Primary targets	Main therapeutic indications
Abemaciclib	2017	CDK4/6	Combination therapy/monotherapy for breast cancer
Acalabrutinib	2017	BTK	Mantle cell lymphomas, CLL
Afatinib	2013	ErbB1/2/4	NSCLC
Alectinib	2015	ALK, RET	ALS-positive NSCLC
Avapritinib	2020	PDGFRα	GIST with *PDGFRα* exon 18 mutations
Axitinib	2012	VEGFR1/2/3	RCG
Binimetinib	2018	MEK1/2	Combination therapy with encorafenib for $BRAF^{V600E/K}$ melanomas
Bosutinib	2012	BCR-Abl	CML
Brigatinib	2017	ALK, RET	ALK-positive NSCLC
Cabozantinib	2012	RET, VEGFR2	Medullary thyroid cancers, RCC, HCC
Capmatinib	2020	c-MET	NSCLC with *MET* exon 14 skipping mutations
Ceritinib	2014	ALK	ALK-positive NSCLC resistant to crizotinib
Cobimetinib	2015	MEK1/2	$BRAF^{V600E/K}$ melanomas in combination with vemurafenib
Crizotinib	2011	ALK, ROS1	ALK or ROS1-postive NSCLC
Dabrafenib	2013	B-Raf	$BRAF^{V600E/K}$ melanomas, $BRAF^{V600E}$ NSCLC, $BRAF^{V600E}$, anaplastic thyroid cancers
Dacomitinib	2018	EGFR	*EGFFR*-mutant NSCLC
Dasatinib	2006	BCR-Abl	CML
Encorafenib	2018	B-Raf	Combination therapy with binimetinib for melanomas $BRAF^{V600E/K}$
Entrectinib	2019	TRKA/B/C, ROS1	Solid tumors with NTRK fusion proteins, ROS1-positive NSCLC
Erdafitinib	2019	FGFR1/2/3/4	Urothelial bladder cancers
Erlotinib	2004	EGFR	NSCLC, pancreatic cancers
Everolimus	2009	FKBP12/mTOR	HER2-negative breast cancers, pancreatic neuroendocrine tumors, etc.
Fedratinib	2019	JAK2	Myelofibrosis
Fostamatinib	2018	Syk	Chronic immune thrombocytopenia
Gefitinib	2003	EGFR	NSCLC
Gilteritinib	2018	Flt3	AML
Ibrutinib	2013	BTK	CLL, mantle cell lymphomas, marginal zone lymphomas, graft vs. host disease
Imatinib	2001	BCR-Abl	Ph^+ CML or ALL, aggressive systemic mastocytosis, etc.
Lapatinib	2007	EGFR, ErbB2/HER2	HER2-positive breast cancer

Larotrectinib	2018	TRKA/B/C	Solid tumors with NTRK fusion proteins
Lenvatinib	2015	VEGFR, RET	Differentiated thyroid cancers
Lorlatinib	2018	ALK	ALK-positive NSCLC
Midostaurin	2017	Flt3	AML, mastocytosis, mast cell leukemia
Neratinib	2017	ErbB2/HER2	HER2-positive breast cancers
Nilotinib	2007	BCR-Abl	Ph^+ CML
Nintedanib	2014	FGFR1/2/3/4	Idiopathic pulmonary fibrosis
Osimertinib	2015	EGFR, T790M	NSCLC
Palbociclib	2015	CDK4/6	Estrogen receptor- and HER2- positive breast cancers
Pazopanib	2009	VEGFR1/2/3	RCC, soft tissue sarcomas
Pemigatinib	2020	FGFR2	Advanced cholangiocarcinoma with a FGFR2 fusion or rearrangement
Pexidartinib	2019	CSF1R	Tenosynovial giant cell tumors
Ponatinib	2012	BCR-Abl	Ph^+ CML or ALL
Pralsetinib	2020	RET	RET-fusion (i) NSCLC, (ii) medullary thyroid cancer, (iii) thyroid cancer
Regorafenib	2012	VEGFR1/2/3	Colorectal cancers
Ribociclib	2017	CDK4/6	Combination therapy with an aromatase inhibitor for breast cancers
Ripretinib	2020	Kit, PDGFRα	Fourth-line treatment for GIST
Ruxolitinib	2011	JAK1/2/3, Tyk	Myelofibrosis, polycythemia vera
Selpercatinib	2020	RET	RET fusion NSCLC and thyroid cancers, RET mutant medullary thyroid cancers
Selumetinib	2020	MEK1/2	Neurofibromatosis type I
Sorafenib	2005	VEGFR1/2/3	HCC, RCC, thyroid cancer (differentiated)
Sunitinib	2006	VEGFR2	GIST, pancreatic neuroendocrine tumors, RCC
Trametinib	2013	MEK1/2	*BRAF*$^{V600E/K}$ melanomas, *BRAF*^{V600E} NSCLC
Tucatinib	2020	ErbB2/HER2	Combination second-line treatment for HER2-positive breast cancers
Vandetanib	2011	VEGFR2	Medullary thyroid cancers
Vemurafenib	2011	B-Raf	*BRAF*$^{V600E/K}$ melanomas
Zanubrutinib	2019	BTK	Mantle cell lymphomas

ALK, anaplastic lymphoma kinase; ALL, acute lymphoblastic leukemias; AML, acute myelogenous leukemias; BCR-ABL, fusion gene of the Philadelphia chromosome; BTK, Bruton's tyrosine kinase; CLL, chronic lymphocytic leukemias; CML, chronic myelogenous leukemias; c-Met, MET proto-oncogene receptor tyrosine kinase; EGFR, epidermal growth factor receptor; ErbB2/HER2, human epidermal growth factor receptor-2; FGFR, fibroblast growth factor receptor; GIST, gastrointestinal stromal tumors; HCC, hepatocellular carcinomas; JAK, Janus kinase; KIT, proto-oncogene receptor tyrosine kinase or mast/stem cell growth factor receptor; mTOR, mechanistic target of rapamycin; MEK1/2, Mitogen-activated protein kinase; PDGFR, platelet-derived growth factor receptor; NSCLC, non-small-cell lung carcinoma; Ph+, Philadelphia chromosome positive; Raf, Raf proto-oncogene serine/threonine kinase; RCC, renal cell carcinomas; Ret, RET proto-oncogene receptor tyrosine kinase; ROS1, ROS proto-oncogene 1 receptor tyrosine kinase; TRK, tropomyosin receptor kinase; VEGFR, vascular endothelial growth factor.

The smaller but yet important compound class of TKIs consists of monoclonal antibodies (mAbs), which inhibit ligand-receptor interactions extracellularly and can even support the immune response against cancerous cells (in the case of trastuzumab or pertuzumab).[30]

Several TK targeting mABs have been clinically approved since 1998, with trastuzumab (targeting HER) being the first one, including panitumumab (targeting EGFR; approval in 2006), ramucirumab (targeting VEGFR2; approval in 2015), pertuzumab (targeting HER2; approval in 2015), necitumumab (targeting EGFR; approval in 2015) and burosumab (targeting FGF23; approval in 2018).[31] One of the most prominent example is cetuximab, a chimeric mABS approved in 2004 for treatment of advanced colorectal cancer and late-stage head and neck cancer, which selectively binds and blocks the EGFR.[32]

First group of anticancer therapeutics worked within this thesis

2.1.1.1 EGFR-inhibitors

The epidermal growth factor receptor (EGFR) belongs to the group of RTKs and is part of the ErbB family, therefore also referred to as HER1 and ErbB1.[33] Different signaling pathways (such as the RAS-RAF-MEK-ERK MAPK or the PI3K-AKT-mTOR) induce downstream signaling processes, which lead to a cellular response and finally regulate e.g. the epithelial tissue development and homeostasis.[34] In healthy tissue, EGFRs are expressed in a range from 40,000–100,000 receptors in a single cell. However, this number is drastically increased (up to 2×10^6 EGFR molecules per cell) in various solid tumors e.g. non-small-cell lung carcinoma (NSCLC), breast, ovarian or renal cancer.[35] These deviations origin from gene amplification, protein overexpression, diverse mutations and/or in-frame deletions.[36] Since the EGFR is such a crucial key mediator in cell signaling, overexpression can lead to promotion of tumorigenesis.[36] Inhibition of the EGFR by targeted therapeutics is therefore a promising approach to more selectively treat tumor cells and spare healthy cells.[27] To this day, three generations of EGFR-targeting small molecule TKIs and three mABs (cetuximab, panitumumab and necitumumab) were clinically approved by the FDA.[28, 37] Gefitinib was the first small molecule TKI approved by the FDA for NSCLC in 2003, closely followed by erlotinib one year later in 2004 (Figure 4).[28] Their mode of action is based on a high affinity towards the active site of mutated kinases and both of them bind in a reversible fashion to the EGFR ATP binding pocket.[38] Deviations such as the exon 19 deletion or the L858R point mutation are one of the most common EGFR activating mutations and respond well to the treatment with gefitinib (response rate of 70%).[39] Studies showed that erlotinib is more effective than gefitinib, however suffers from more adverse effects at the same time.[40] Unfortunately, resistance development against the first-generation EGFR inhibitors unavoidably occurred after roughly one year of treatment mainly caused by the exon 20 point mutation T790M. Studies revealed that this mutation leads to a preference of ATP (in more than 60% of patients) to the receptor kinase exceeding the potency of the first-generation of TKIs.[41]

Therefore, a second-generation of EGFR inhibitors was developed to bind irreversibly to the ATP binding pocket overcoming the T790M mediated resistance thereby.[42] Two representatives of this second-generation, afatinib[43] and dacomitinib[44], got FDA approval as a first line therapeutic for EGFR-mutant NSCLC in 2013 and 2018 (Figure 4). Both drugs contain an electrophilic acrylamide moiety in their molecular structure, which can bind covalently to a conserved cysteine (at the active site of EGFR) *via* a Michael addition.[42, 45] Preclinical studies of afatinib and dacomitinib suggested indeed a high efficacy against T790M mutated EGFR, however they were characterized by an unbearable low maximum tolerated dose (MTD) and dose-limiting toxicities.[38] These issues origin from lack of differentiation between the mutant T790M and wild-type EGFR (or other members of the ErbB family), which limits their clinical application.[46] Consequently, a new generation of irreversible EGFR inhibitors was developed with the aim to specifically target the T790M (and other) mutations.[47] Looking at the chemical structure of osimertinib, the change from the previously established 4-anilinoquinazoline ring system to an *N*-(3-(pyrimidin-2-ylamino)phenyl) acrylamide core is evident (Figure 4).[48] Osimertinib was approved by the FDA in 2015 for patients with metastatic EGFR T790M mutation-positive NSCLC, who suffer from progression after EGFR TKI treatment.[49] In 2018 Osimertinib also got approval as first-line therapy for EGFR-mutated advanced NSCLC and in 2020 for the adjuvant treatment of patients with early-stage EGFR-mutated NSCLC.[50-52] In general, this TKI is usually well tolerated, however during the treatment eventually other resistance mechanisms emerge, resulting from a C797S point mutation or upregulation of various other kinase pathways.[53]

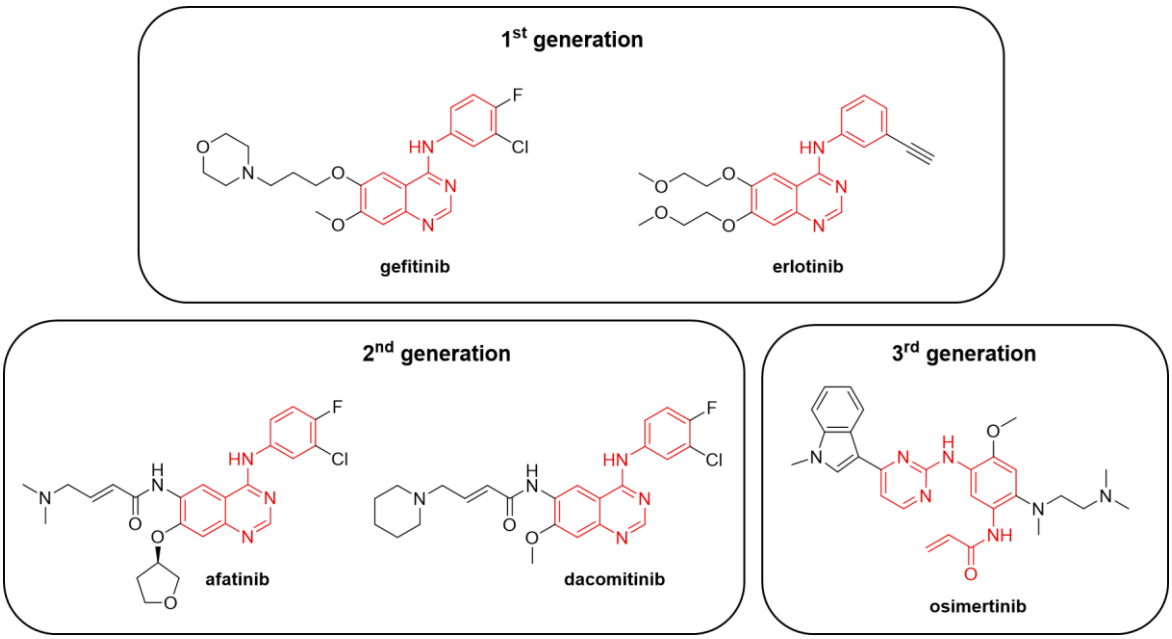

Figure 4: Clinically approved first-, second-, and third-generation of EGFR inhibitors. The core structures (4-anilinoquinazoline and *N*-(3-(pyrimidin-2-ylamino)phenyl)acrylamide for the third generation) are highlighted in red.

Despite their specific targeted approach (especially in comparison to conventional chemotherapy), severe skin- or gastrointestinal-related side effects are the still one of the main issues during the treatment with EGFR-targeting TKIs.[54] Notably, the patients who suffer from the worst adverse reaction show the best therapy response when treated with first generation EGFR-TKIs, revealing a correlation between the intensity of side effects and therapeutic potential.[55-56]

Taken together, despite their remarkable success as targeted therapeutics (especially against NSCLC), EGFR TKIs are strongly limited by acquisition of resistance mechanisms and severe adverse reactions. Even the development of new, improved generations of TKIs could not turn this disease into a chronic one, achieve long-term cure or strongly reduce side effects. Therefore, strategies to optimize the therapeutic potential of small molecule EGFR inhibitors are urgently needed.

2.1.1.2 FGFR inhibitors

The fibroblast growth factor receptor (FGFR) family consists of five transmembrane RTKs (FGFR1–5), and takes a crucial part in cell-regulating processes such as proliferation, differentiation or survival. Furthermore, they are associated with the regulation of e.g. embryonic development, tissue homeostasis and wound repair.[57] Notably, FGFR5 misses a tyrosine kinase domain and acts therefore only as a co-receptor for FGFR1.[58] Similar to other RTKs, a cascade of downstream-signaling pathways (e.g. RAS-RAF-MEK-ERK MAPK, PI3K/Akt and PLCγ) is initiated by the binding of fibroblast growth factors (FGFs) to the FGFR (followed by receptor dimerization and induced intracellular autophosphorylation).[59] Deregulation of these processes (origin from mutations and gene amplification/fusions) can result in oncogenesis and tumor progression as well as in a variety of other diseases.[60] Consequently, blocking the FGF/FGFR signaling axis by e.g. small molecule TKIs is a promising approach to target various tumor types. To this date, the FDA approved several drugs inhibiting the FGFR family including nintendanib (2014), erdaftinib (2019) and pemigatinib (2020), in addition, several others are currently investigated in clinical trials.[61]

2.1.1.3 ABL inhibitors

The Abelson (ABL) family (consisting of ABL1 and ABL2) belongs to the group of non-receptor tyrosine kinases and is encoded by the mammalian ABL genes. These kinases take part in a wide range of cellular processes including but not only cell proliferation, differentiation, survival, migration, death, DNA-damage responses and regulate a variety of other biological functions.[62] Notably, ABL1 was determined as oncogene in the development of leukemia (originated from Abelson murine leukemia virus or chromosome translocations) more than three decades ago.[63] CML (chronic myelogenous leukemia), which is diagnosed in roughly 15–20% of new leukemia cases, is caused by a deregulation of BCR-ABL1. BCR-ABL1 is encoded by the fusion gene resulting

from the t(9;22)(q34;q11) chromosomal translocation, commonly referred to as Philadelphia (Ph) chromosome.[64] The discovery of BCR-ABL1 being the driver for initiation and maintenance of CML was a "dream come true" for anticancer precision medicine and started the era of targeted therapeutics. Imatinib was the first TKI ever to get approval by the FDA in 2001, marking a milestone in cancer therapy. This drug showed promising results against CML, however occurring resistances caused by point mutations (e.g. T315I) and adverse effects entailed a second- (dasatinib, nilotinib, and bosutinib) and third-generation (ponatinib) of BCR-ABL1 inhibitors.[65-66]

2.1.1.4 Multi-kinase inhibitor Ponatinib

Cancer is an extremely complex disease and in most solid tumors, a range of various signaling pathways can be overexpressed at the same time leading to tumor progression. Therefore, it makes sense to inhibit more than one target by simultaneous administration of several "mono-targeted" TKIs. Although theoretically a promising approach, clinical studies revealed that such combinations of TKIs suffer from accumulated toxicities, frequently resulting in dose reduction for the drugs or treatment discontinuation. Furthermore, combination therapies often prove to be ineffective as the concentration of the drugs is too low (after dose reduction) to achieve any significant anticancer activity. A preferred strategy is therefore to use a single TKI, which is able to target multiple kinases at the same time (so-called multi-kinase inhibitors).[67]

One of the most prominent representatives of a multi-kinase inhibitor is ponatinib, which inhibits ABL, FGFR, platelet-derived growth factor receptor (PDGFR), vascular endothelial growth factor receptor (VEGFR) and others kinases.[68-69] Ponatinib was granted FDA approval in 2012 as second line treatment for resistant or imatinib intolerant Philadelphia chromosome-positive (Ph+) CML and acute lymphoblastic leukemia (Ph+ ALL), specifically in cases of a BCR-ABL T315I mutation.[70-71] Remarkably, only ponatinib and no other BCR-ABL1-targeting TKI (e.g. imatinib, dasatinib or nilotinib) can inhibit the T315I mutation.[72] This inhibition potential very likely results from the unique acetylene linker of ponatinib, which gives its molecular structure a certain rigidity favorable for these interactions. Crystal structures confirmed this binding mode of ponatinib with BCR-ABL1 (Figure 5)[73]: The imidazo[1,2-*b*]pyridazine core blocks the adenine pocket, the methylphenyl unit binds a hydrophobic pocket (behind the gatekeeper residue) and the trifluoromethylphenyl group fits into a pocket induced by the DFG-out (Asp-Phe-Gly = "DFG" motif). Lastly, the piperazine group is necessary for the aqueous solubility of this highly lipophilic molecule.[71]

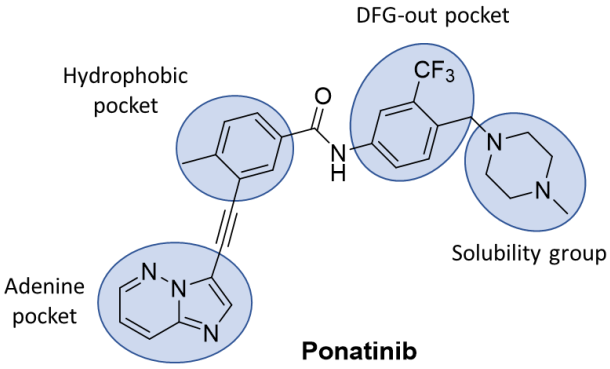

Figure 5: Chemical structure of the clinically approved ponatinib (Iclusig®) and its schematic binding mode with BCR-ABL (adapted from references[71, 73]).

Ponatinib is currently investigated in several preclinical and clinical studies on other cancers,[74] of particular interest is thereby the targeting of FGFR.[75-76]

Unfortunately, severe adverse reactions, most of them cardio-related, could be frequently observed during the treatment with ponatinib.[77] The occurrence of life-threatening arterial thrombotic events in a clinical phase III study finally led to dose-limitations and extra precautionary measures during therapy.[78-80] Thus, approaches to overcome these drawbacks and still utilize the potential of ponatinib are of high interest.

Second group of anticancer therapeutics worked within this thesis

2.2 α-*N*-Heterocyclic thiosemicarbazones and their metal complexes

α-*N*-heterocyclic thiosemicarbazones (TSCs) and their metal complexes (e.g. Cu, Fe, Zn, Ga) present a compound class with very promising anticancer (as well as antibacterial, antiviral and antifungal) properties.[81] The proposed biological mode of action of TSCs is the inhibition of ribonucleotide reductase (RR). In general, the RR converts ribonucleotides to 2'-deoxyribonucleotides, which are vital for the synthesis and repair of DNA. RRs can be roughly divided into three classes (I, II and III), which all use different metals as cofactors, whereby only class Ia is expressed in mammalians. Two dimeric subunits R1 and R2 form the tetrameric enzyme Ia RR and catalyze jointly the reduction steps. The α_2 dimer (protein R1), includes the substrate (ribonucleotide) binding site, and is activated by the electron of a tyrosyl radical, which is transferred to this moiety over a distance of around 35 Å. The smaller β_2 dimer (protein R2) consists of a diiron center and polypeptide chains, here the tyrosyl radicals are generated. After the transport of the radical to the R1 subunit, a thiyl radical is formed at the cysteine residue Cys439 (state 1; Figure 6).[82]

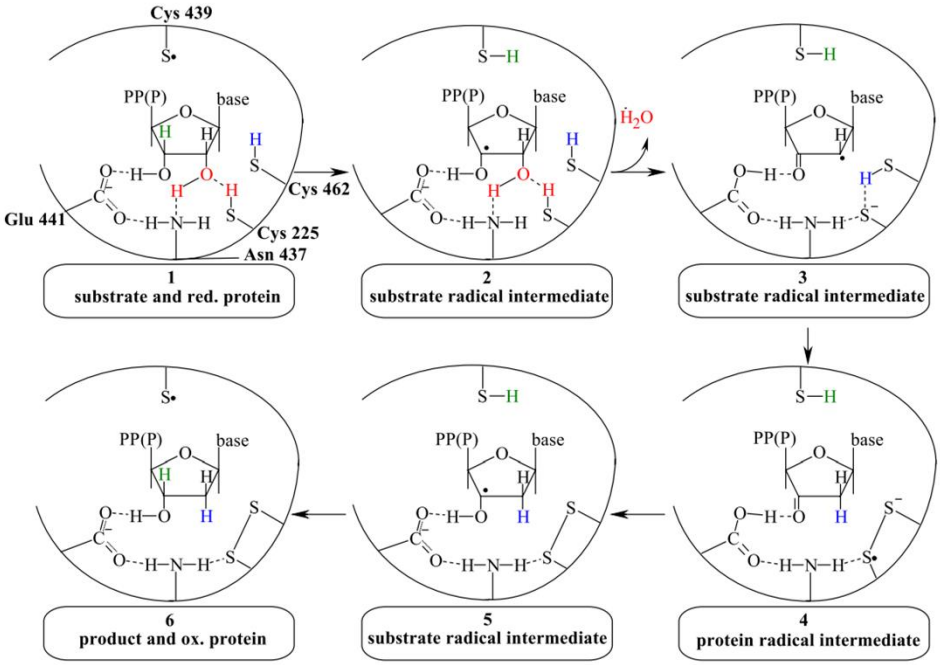

Figure 6: Proposed mechanism for the reduction of ribonucleotides by RR. Figure from reference [82]:

The proposed mechanism continuous with the abstraction of the 3'-hydrogen atom of the ribose by the thiyl radical and formation of the substrate radical intermediate (state 2). Protonation of 2'-OH and subsequent elimination of water leads to the 2'-ketyl radical (state 3). In the next step, a hydrogen atom is transferred to the 2'-position, generating a disulfide anion radical intermediate (state 4), which is then transported back to ribose, restoring the substrate radical intermediate (state 5). Finally, the hydrogen atom from the Cys439, which initiated the cycle, is moved to the substrate re-generating the thiyl radical (state 6). The radical is transferred back to the R2 subunit where it forms again the tyrosyl radical. Then the reduction of the disulfide bond (by thioredoxin or glutaredoxin and the NADPH binding flavoprotein thioredoxin reductase) completes the turnover.[82] The thiyl radical would very likely disturb the reduction of the disulfide bond, which is the reason for the interim transfer of the radical to the R2 subunit.

Among the compound class of TSCs, 3-aminopyridine-2-carboxaldehyde thiosemicarbazone, (Triapine, Figure 7) is by far the best-studied representative being evaluated in more than 30 clinical phase I and II trials.[83] Several possible modes of action have been suggested for Triapine, with the iron cofactor of the R2 subunit being most likely its target. Although, the exact mechanism is yet to be elucidated, the work of Aye *et al* proposes the formation of an iron complex by the reaction of the tridentate NNS donor atoms with the labile intracellular iron (Figure 7).[84]

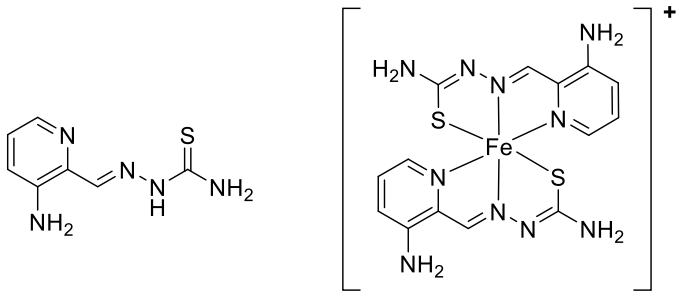

Figure 7: Triapine (left) and its iron(III) complex (right).

Notably, Triapine showed encouraging results against hematological cancers such as advanced leukemia,[85] but was hardly effective against solid tumor types (e.g. renal cell carcinoma or NSCLC) and at best only achieved stabilization of tumor size.[86-87] Thus, further clinical trials focused on combinational therapies and a phase III study with cisplatin and radiation is currently executed.[88-89] Recent studies from our group suggested that the rapid metabolism/excretion and poor tumor accumulation of Triapine are likely reasons for its insufficient activity against solid tumor types.[90-92] Furthermore the occurrence of methemoglobinemia, a condition where methemoglobin (metHB) blood levels are increased, could be frequently noticed during clinical trials.[93] The formation of iron(III) Triapine complexes in the blood stream and their subsequently redox reaction with oxyhemoglobin (HBO_2) explains this phenomena.[94] Consequently, new strategies for enhanced plasma half-life time and tumor specificity/accumulation are of high interest.

In the last decade, new generations of TSCs were developed with the aim to further improve the anticancer activity of this compound class. Well studied examples are di-2-pyridylketone 4,4-dimethyl3-thiosemicarbazone (Dp44mT) and its successor di-2-pyridylketone 4-cyclohexyl-4-methyl-3-thiosemicarbazone (DpC), both possessing terminally disubstituted NH_2 groups (Figure 8). Notably, these TSCs are characterized by extraordinarily increased *in vitro* anticancer activity (~500-fold) in comparison to Triapine. This significant differences can probably be attributed to the intracellular formation of very stable copper complexes of the terminally disubstituted TSCs.[95] DpC was studied in a clinical phase I trial in 2016.[96]

Another promising next-generation TSC is represented by 4-(pyridine-2-yl)-N-([(8E)-5,6,7,8-tetrahydroquinolin-8-ylidene]amino)piperazine-1-carbothioamide (COTI-2), which deviates a bit more from the classical TSC structure (Figure 8). *In vitro* experiments showed also a cytotoxicity in the nanomolar range and encouraging results could be achieved *in vivo*.[97] Hence, this TSC was recently investigated in a phase Ib/IIa clinical trial against gynecologic malignancies.[98] Studies

demonstrated that COTI-2 affects the tumor suppressor functionality by restoring mutated p53, revealing a new mode of action for this compound class.[99-100]

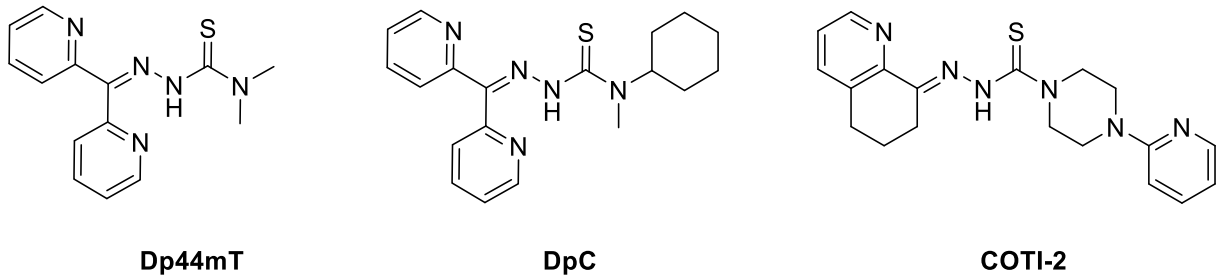

Dp44mT **DpC** **COTI-2**

Figure 8: Chemical structures of the next generation TSCs Dp44mT, DpC and COTI-2.

3 APPROACHES TO REDUCE THE ADVERSE EFFECTS OF ANTICANCER THERAPEUTICS

The scientific efforts in the last decades led to the further optimization of already established anticancer therapeutics and discovery of novel, promising strategies (e.g. targeted therapy). Nevertheless, the occurrence of treatment-induced side effects still remains one the main issues of modern anticancer therapy. Adverse events (caused by small-molecule drugs) can be divided in so-called on-target and off-target effects. In general, on-target effects are the consequence of target inhibition in the healthy tissue, thus can be described as loss of selectivity. Whereas off-target effects occur rather unrelated and are induced by activity modulation of proteins that can be (but does not have to be) biologically linked to the target protein.[101] To reduce adverse reactions, the enhancement of the tumor selectivity and/or increase of the tumor accumulation of the respective drug are promising strategies. Consequently, two major concepts, namely the prodrug and drug targeting approach, have been vastly explored and applied to the compound class of small molecule therapeutics. Both approaches will be briefly discussed and addressed in more detail in the later chapters.

Prodrugs are defined as inactivated, non-toxic compounds, which release the active drug after specific activation at the tumor site.[102] Regarding the drug targeting approach a distinction is made between the passive- (or tumor) targeting and the active- (or ligand based) targeting approach. In the passive-targeting approach, the drug is encapsulated into nanoparticles, which specifically accumulate in the tumor. The active-targeting approach utilizes ligands, which are attached to the anticancer therapeutic and can interact with (overexpressed) receptors on cancer cells leading to an increased uptake.[103-104] Some drugs even combine both passive- and active targeting approaches at the same time (e.g. surface-modified polymeric nanoparticles).[105]

The joint strategy of all three approaches is the release of the active drug, in whichever way, inside the tumor tissue, sparring the healthy cells thereby. When administered to the patient, prodrugs are distributed throughout the whole body comparable to conventional therapeutics (Figure 9A/B). However, the active compound is released by tumor-specific triggers, hence mainly affects cancer tissue. The drug distribution properties of the targeting approach distinctly differs: In both cases (active and passive targeting strategy) the drug carrier is accumulated at the tumor site (where it releases the drug) and not equally distributed throughout the body (Figure 9C).

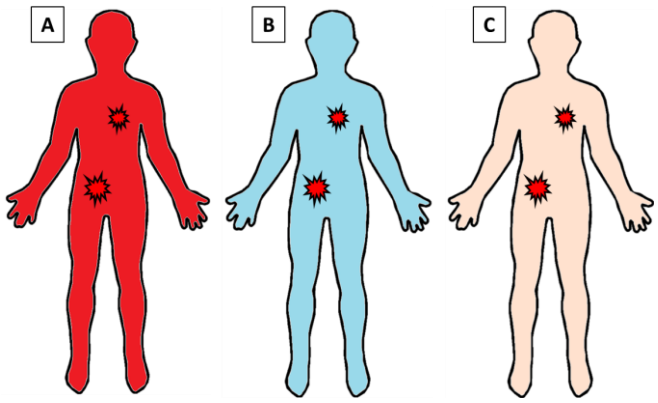

Figure 9: Schematic illustration of (A) conventional chemotherapy, (B) the prodrug and (C) the drug-targeting approach; the tumors are represented by the red irregular shapes. Chemotherapeutics distribute in the whole body effecting not only cancer cells but also rapidly, dividing healthy cells (symbolized in red = active). Prodrugs likewise circulate in the whole body but are non-toxic until they release their active moiety after a tumor-specific trigger event (symbolized in blue = inactive and red = active). In the case of the drug-targeting approaches, the carrier is accumulated at the tumor site and subsequently releases the drug in an unspecific (passive) or specific (active) way (symbolized in beige = not accumulated and red = active).

3.1 Prodrugs

As mentioned briefly before, prodrugs are inactivated parent compounds, which only release their cytotoxic moiety after a tumor-specific trigger event, sparring healthy cells thereby. In general, the molecular structure of prodrugs usually consists of a trigger unit, the bioactive drug itself and in most cases some kind of linker to connect them. To successfully develop a prodrug, the molecular structure of the chosen compound needs to A) allow reversible, chemical modifications without losing its anticancer properties and B) possess this modified part in the right position to ensure triggered tumor selectivity. The activation mechanisms are versatile and depend on the microenvironment of the tumor. Well-known examples include the overexpression of certain enzymes, hypoxic milieu, decreased pH levels and oxidative or reductive conditions.[102] Regardless of the activation trigger, to achieve selectivity in the tumor tissue, several crucial characteristics need to be fulfilled. First and foremost the prodrug must exhibit a high stability in healthy tissue while being labile and thus activatable at the target site.

Secondly, the solubility and bioavailability of the prodrug must be given under the required circumstances. Furthermore, it must be taken into consideration that the pharmacokinetics, which describe the administration, distribution, metabolization and excretion (ADME) of the respective compound are altered after chemical derivatization compared to the parent drug. The most prominent and in this thesis used prodrug approaches will be discussed in following chapters.

3.1.1 Release mechanism of prodrugs

3.1.1.1 pH-sensitive prodrugs

Notably, the extracellular pH value of cancer cells is distinctly lower compared to healthy cells (usually 0.5–1.0 units), as a high rate of glycolysis is maintained even under hypoxia. Consequently, the lack of oxygen leads to an excess of lactic and carbonic acid, which in turn results in the drop of the extracellular pH value. This difference between healthy and cancer cells represents therefore an interesting approach for the development of prodrugs.[106] To achieve selective activation the prodrug needs to be stable at physiological conditions (blood or extracellular space) and release its bioactive moiety only after hydrolysis in an acidic environment. Functional groups sensitive to pH value used for this strategy include imines, actetals/ketals, hydrazones and carboxylic hydrazones (Figure 10A).[102, 106] One of the most successful representatives of this approach is aldoxorubicin, an albumin-binding prodrug of doxorubicin bearing an acid-cleavable moiety [(6-maleimidocaproyl) hydrazone], which is currently investigated in several clinical phase II and III trials (Figure 10B).[107]

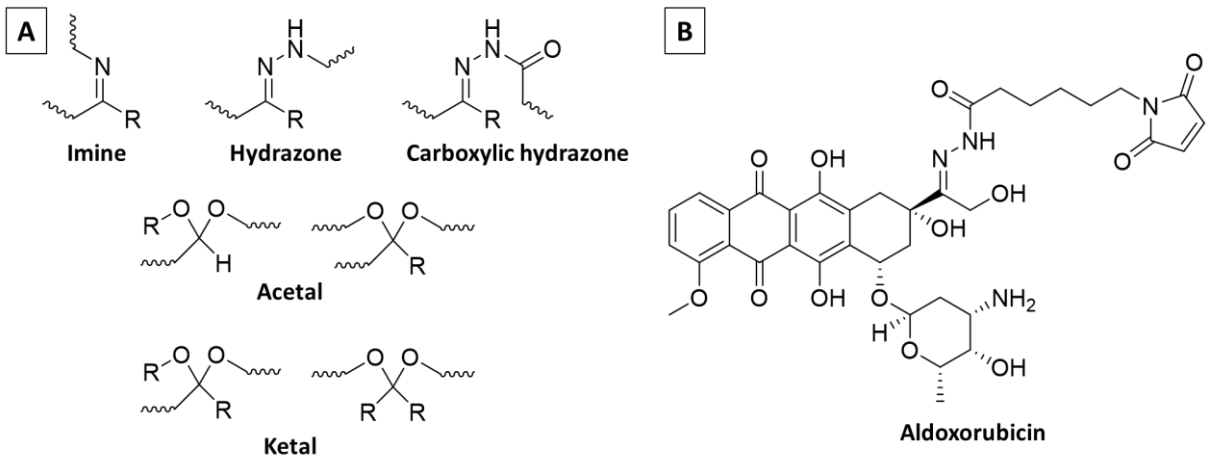

Figure 10: (A) pH-sensitive linkers regularly used in prodrugs. (B) Aldoxorubicin as representative of acid-cleavable prodrugs in clinical trials.

3.1.1.2 Enzymatic-sensitive prodrugs

Another property, which can be exploited for the prodrug approach, is the upregulation of specific enzyme in cancer cells.[106] A well-studied and one of the most frequently used examples of such enzymes is Cathepsin B, an intracellular cysteine protease highly overexpressed in tumors. As for the mode of action of enzymatic-sensitive prodrugs, these overexpressed enzymes specifically cleave selected peptide linkers, resulting in the release of the bioactive unity.[108] Therefore, the choice of the cleavable linkers is crucial to achieve a specific activation. Studies of cathepsin B-sensitive prodrugs of doxorubicin showed the high efficacy of dipeptide motives such as Phenylalanine-Lysine (Phe-Lys) and Valine-Citrulline (Val-Cit). Furthermore, a self-immolative spacer such as p-aminobenzycarbonyl (PABC) was integrated in the prodrug structure to control the steric interactions.[109] One of the most successful representative is the antibody-drug conjugate (ADC) brentuximab vedotin (for Hodgkin's lymphoma and anaplastic large cell lymphoma), which is composed of the mAb brentuximab (carrier unit), Val-Cit (cathepsin B-cleavable moiety), PABC (self-immolative linker) and monomethyl-auristatin E (MMAE; antimitotic drug) (Figure 11).[108]

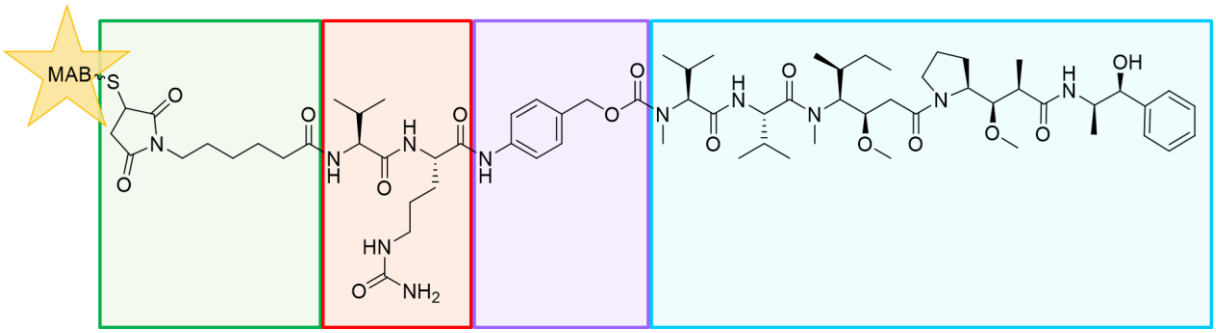

Figure 11: Chemical structure of brentuximab vedotin. Monoclonal antibody brentuximab (star); maleimide unit as attachment group (green); cathepsin B-cleavable Val-Cit peptide linker (red); self-immolative PABC spacer (purple); cytotoxic agent MMAE (blue).

3.1.1.3 Hypoxia-sensitive prodrugs

Another intensively explored characteristic of cancer utilized for the prodrug approach is the hypoxic environment of tumors. In general, hypoxia describes a lack of oxygen in the body and is caused in solid tumors by their fast and uncontrolled growth. The defective vasculature of tumors is characterized by its disorganized blood vessel networks and leakages, which prevents an even distribution of oxygen. At the same time, the rapid proliferation of tumor cells as well as infiltration of healthy tissue demands a high but not sustainable oxygen supply. Both features lead to an imbalance between oxygen delivery and consumption, resulting in hypoxic tissue. Hypoxia is related to an upregulation of the hypoxia-inducible transcription factor (HIF) and takes therefore a crucial part in cancer progression and metastasis. Furthermore, it is associated with the occurrence of resistances to conventional therapies, leading to a poor prognosis. As hypoxic

regions (to varying degrees) can be found in 50–60% of solid tumors, this characteristic is a promising target for cancer therapy.[110-111]

Various different hypoxia activated prodrugs (HAPs) have been developed over the past last decades.[112] The general idea behind this approach is to develop a prodrug that exhibits high stability under normoxic conditions and only releases its active moiety in a hypoxic environment. Thus, an enhanced selectivity between the healthy and tumor cells can be achieved, resulting in less adverse effects. As for the proposed mode of action, in the first step the HAP is reduced by enzymes (one-electron oxidoreductases) turning into an oxygen-sensitive radical intermediate. This radical is instantly re-oxidized by molecular oxygen in healthy tissue (normoxia) generating again the parental prodrug. Due to the insufficient oxygen supply in the hypoxic regions of the tumor, an irreversible reduction takes place and the bioactive unit is released from the prodrug (Figure 12).[112]

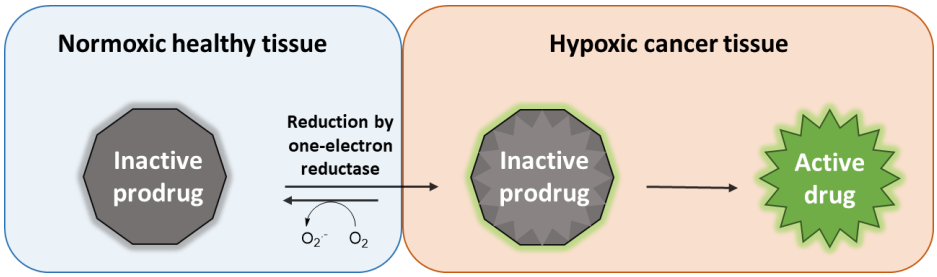

Figure 12: Proposed mechanism for HAPs. In the presence of molecular oxygen (healthy tissue) the prodrug stays in its inactive form, as a re-oxidation step takes immediately place after the initial one-electron bio-reduction. However, under hypoxic conditions (cancer tissue) the lability of the formed radical leads to a consecutive reaction (e.g. reduction, dissociation or fragmentation of the prodrug), resulting in the release of the bioactive species.

Well-known one-electron oxidoreductases, which are overexpressed in solid tumor cells and able to reduce HAPs, include NADH-cytochrome b_5 reductases, nitric oxide synthases, and NADPH-cytochrome P450 reductase. In addition, two-electron oxidoreductases can be involved in the activation of HAPs, in this case the activation mechanism is changed as no radical is formed. Overexpression of these enzymes can lead to off-target effects, but at the same time offer another target for HAPs.[113]

The four big compound classes, which are known for their suitable redox properties and possible application as HAPs consist of quinones, N-oxides, nitroaromatics and transition metal complexes (Figure 13).[112] Quinones are well suited for this approach, as they can be reduced to hydroquinones forming a stable, fully aromatic ring system thereby. Mitomycin C, a DNA crosslinking anticancer antibiotic, was discovered more than six decades ago and is considered one of the first bioreductive prodrugs.[112] Derived from this drug, several compounds have been synthesized with apaziquone

being studied in clinical phase III.[114] Another compound class, which can be selectively reduced in the hypoxic tumor environment, are N-oxides. Depending on the molecular structure of the N-oxides, different enzymes are involved in the reduction process. In the case of aromatic systems, one-electron reduction cause the formation of labile radicals.[112] A well-studied example of such a prodrug is tirapazamine, which was clinically investigated in several phase III trials.[115] Regarding aliphatic N-oxides such as banoxantrone, reduction by two-electron oxidoreductases forms the corresponding active tertiary amines.[116] The third group of triggers reducible under biological conditions are nitroaromatics such as nitrobenzyls or nitroimidazoles. Their activation mechanism is again based on an enzyme controlled reduction process, generating a nitro radical anion thereby. Under normoxic conditions this radical intermediate is re-oxidized to the parental compound, whereas the lack of oxygen results in the decomposition of the prodrug and release of the bioactive moiety. Two of the most prominent representatives are evofosfamid (TH-302) and tarloxotinib (TH-4000), which both use nitroimidazoles as trigger unit. The most advanced in terms of clinical investigations (several phase III trials) is evofosfamid, the prodrug of an ifosfamide derivative. Tarloxotinib is one of the few TK-inhibiting (EGFR) HAPs and was investigated in several clinical phase II trials.[112]

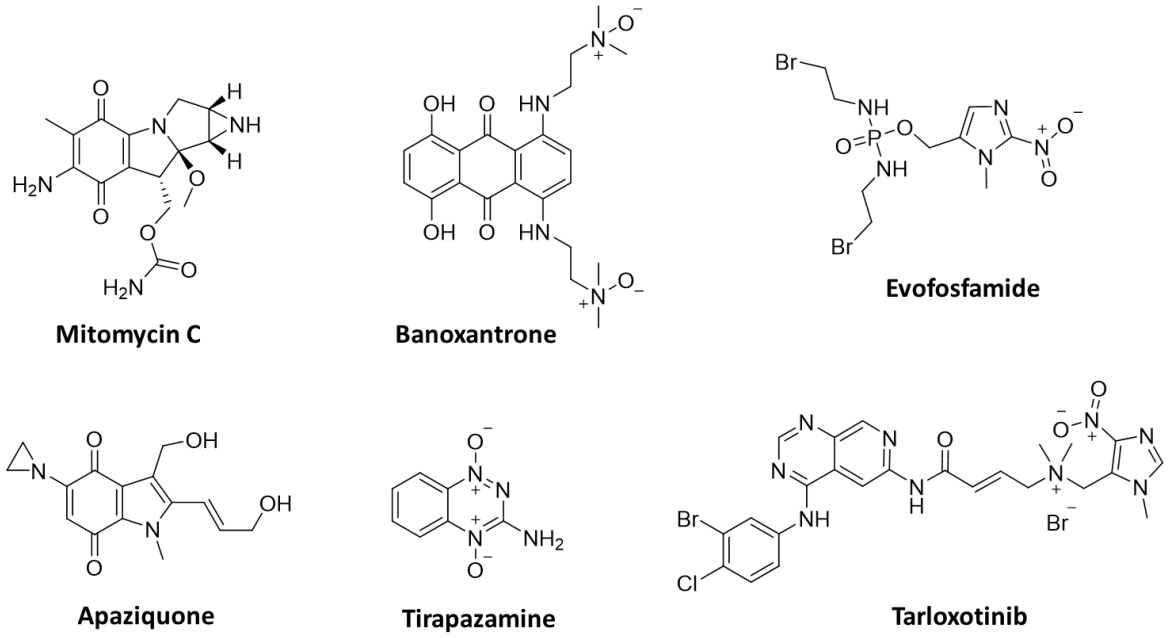

Figure 13: Representatives of different compound classes of HAPs, which have been or are currently clinically investigated as HAPs. The approved bioreductive drug mitomycin c once initiated the development of quinone based HAPs.

The fourth compound class suitable for this approach is transition metal complexes (e.g. cobalt or copper). In general, these metals are characterized by two main oxidation states, which exhibit different stabilities, and their well adjustable redox properties. Under normoxia the complex with

the higher oxidation state is stable and therefore inactivated. Whereas under hypoxia, the complex is reduced to the labile lower oxidation state, resulting in release of the (bioactive) ligands.[112, 117] The most prominent element for metal complex-based HAPs is cobalt, with a well-studied coordination chemistry. The redox potential of cobalt(III)/(II) complexes can be fine-tuned by appropriate ligand selection to lie within the redox range of cells.[118] Notably, the octahedral cobalt(III) complexes show high stabilities due to kinetic inertness, whereas the cobalt(II) state is characterized by kinetic lability (leading to a several magnitudes higher ligand exchange rate).[119] This outstanding difference can be exploited for the hypoxic environment of a tumor in form of a HAP as described above. Regarding the choice of ligands, Ware *et al* revealed that bidentate chelating ligands ensure sufficient stability under normoxia unlike the previously used monodentate aziridine ligands.[120] For this prodrug strategy, a well-balanced equilibrium between the two oxidation states needs to be attained: The cobalt(III) complex must be stable enough in healthy tissue to reduce adverse effects. At the same time dissociation of the reduced cobalt(II) complex should only take place in a hypoxic environment at the target site. Comparable to pure organic hypoxia-activatable drugs (see above) it is frequently suggest that in healthy tissues the cobalt(III) species is instantly restored by oxygen after reduction, inhibiting the release of the bioactive ligand thereby.[121-122] However, pulse radiolysis measurements contradicted this theory, as the re-oxidation rates were too slow under normoxic conditions. Instead a competition between the cobalt(III) complexes and molecular oxygen for one-electron reductants is proposed.[123] Even though the exact mode of action is yet to be elucidated, several promising cobalt(III) complexes have been synthesized over the last years using various anticancer drugs as ligands such as alkylating agents (e.g. nitrogen mustards), matrix metalloproteinase (MMP) inhibitors (e.g. marimastat) or TKIs (e.g. EGFR inhibitor) (Figure 14).[124-125]

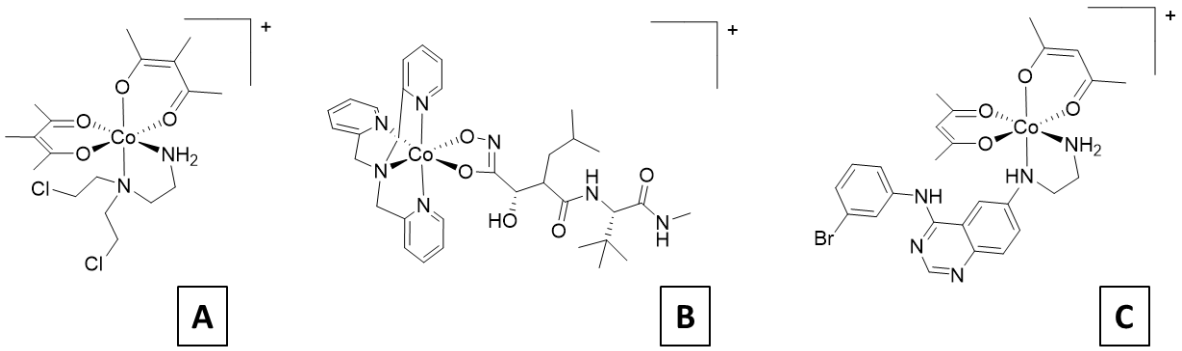

Figure 14: Representatives of cobalt(III) based HAPs using different anticancer agents such as (A) nitrogen mustards[120], (B) marimastat[126] or (C) an EGFR inhibitor[127].

Notably, most of the hypoxia-activatable prodrugs use chemotherapeutics and especially DNA alkylating agents as active moiety. Unfortunately, despite promising results in various clinical phase

I and II studies (e.g. for evofosfamide or tirapazamine), the respective phase III could not be successfully completed for any HAP until now.[128] Interestingly, only in the past few years, this approach has been applied also to the large class of small molecule TKIs.[129-132]

3.2 Drug delivery systems in anticancer therapy

Another promising strategy to reduce adverse effects by enhancing the tumor selectivity of anticancer therapeutics is the use of so-called drug or targeted delivery systems.[103-104] In general, drug delivery systems can be divided into passive- and active targeting approaches, which utilizes different delivery strategies, targets and activation mechanisms (Figure 15).[133] Both approaches will be discussed in detail in the following chapters.

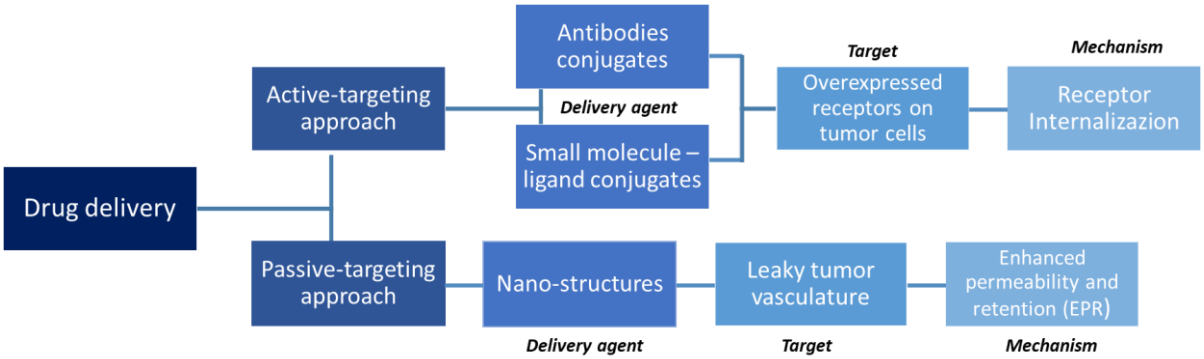

Figure 15: Active- and passive targeting strategies in drug delivery. Figure adapted from reference [133].

3.2.1 Passive targeting approach – EPR effect

The enhanced permeability and retention (EPR) effect is the basis for passive targeting strategies and was discovered first by Maeda and Matsumura more than four decades ago.[134-135] This pathological condition is caused by the fast and uncontrolled growth (angiogenesis) of tumors, which entails the formation of abnormal (in terms of size and form) and leaky blood vessels. As a result, the endothelial cells are not properly arranged and large gaps (in the range of 200–2000 nm) between them can be found. Macromolecules (e.g. nanoparticles, proteins or polymers) can diffuse into the tumor tissue through these openings and accumulate there (= enhanced permeability effect). On the contrary, the healthy tissue is not exposed to macromolecules as it is delimited by its intact endothelial cells (Figure 16).[136-137] The other aspect is the defective lymphatic drainage system of the tumor, which ensures a sufficient accumulation of the respective macromolecule at the target site (retention effect) (Figure 16).[138] Both features combined result in the EPR effect, which is already successfully utilized in clinics (e.g. liposomal doxorubicin, see

below).[139] However, it should be mentioned that factors such as hypoxia, inhomogeneities in the tumor tissue or the cancer type itself could reduce or even prevent the impact of the EPR effect.[140]

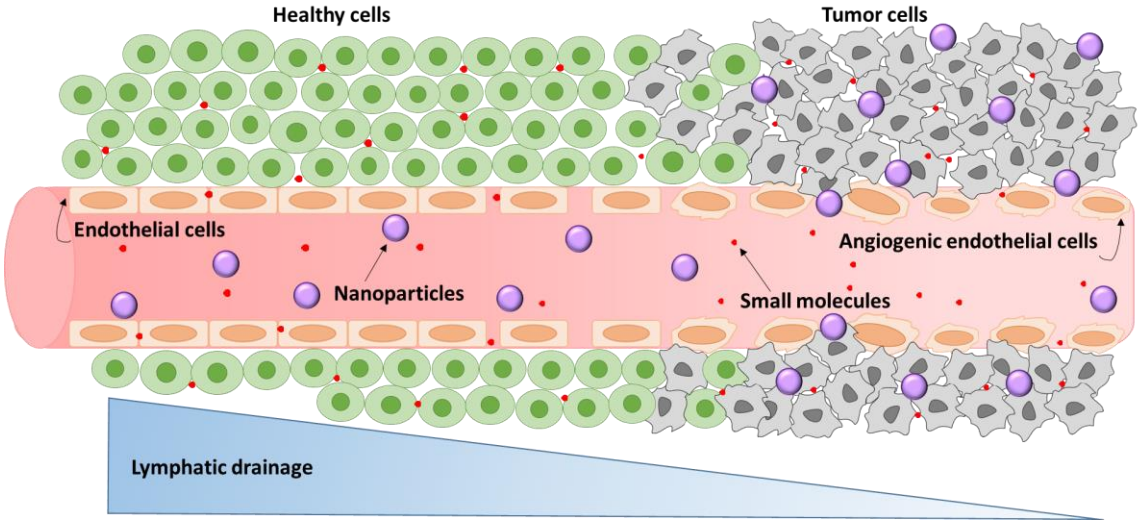

Figure 16: Schematic illustration of the enhanced permeability and retention (EPR) effect. In healthy tissue, small molecules (here illustrated as red dots) can easily cross the endothelial cells unlike e.g. nanoparticles (here illustrated as purple circles), which are hindered by their size. However, in cancerous tissue, the misshaped angiogenic endothelial cells enable an entering of macromolecules. In this manner, an accumulation of the encapsulated drug at the target site can be achieved. Furthermore, the lymphatic drainage of tumors does not function properly leading to aggravated removal of the drug carrier. Figure adapted from reference [141].

3.2.1.1 Nanoparticulate formulations for passive drug targeting

The history of nanoparticles in medicine goes back more than 50 years, when Bangham *et al* discovered and reported the properties of swollen phospholipids.[142] Formulations used for anticancer drug delivery include lipid- (e.g. liposomes) or polymer- (e.g. micelles) based nanocarriers, drug conjugates (e.g. antibody or protein) and various inorganic nanoparticles (e.g. generated from gold, silica or hafnium oxide) (Figure 17).[143]

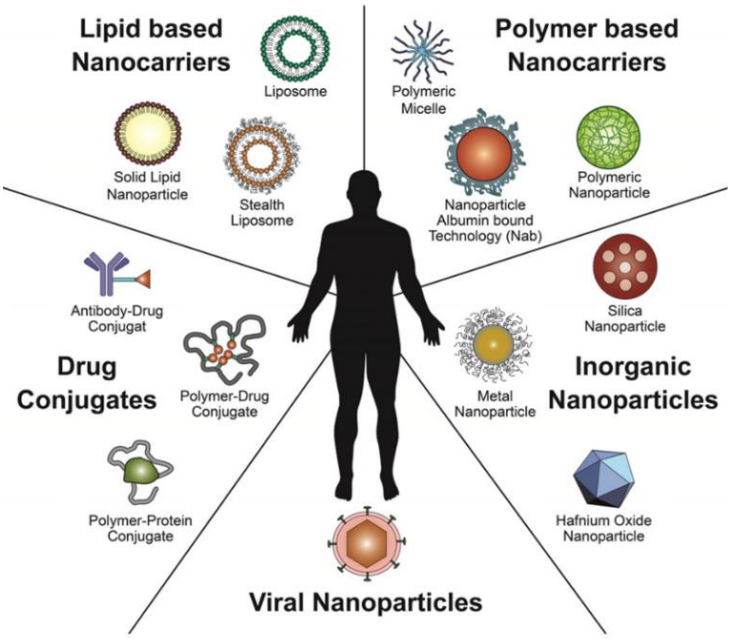

Figure 17: Schematic overview of various types of nanoparticulate formulations used in cancer therapy. From reference [143].

To be suitable for the drug delivery approach these formulations must fulfill a number of requirements such as a high encapsulation efficiency (EE), a slow and continuous release of the drug, low toxicities as well as an enhanced accumulation in cancerous tissue.[104] Furthermore, the drug loaded carrier system must show a long-term circulation and a high level of stability in the blood stream. After accumulation at the target site, a certain period of time or specific trigger events should lead to the controlled release of the drug. Derived from these requirements, the main properties of nanoparticulate formulations are their size and size distribution, zeta potential (surface charge), as well as drug loading and drug release behavior.

The **size of nanoparticles** in context of drug targeting is determined between 1–1000 nm. However, depending on the class of drug carriers a much narrower size range can be specified: For example the size of gold particles is around ~13–60 nm, of polymer based nanocarriers between ~50–500 and of liposomes ~80–200.[144-145] Notably, studies showed that a size below 400 nm of the drug carrier is favorable for an efficient transport as well as an increased accumulation at the target site.[146] To examine the size of nanoparticles dynamic light scattering is used, a method, which exploits the Brownian movement of suspended particles (in general, smaller particles tend to move faster in comparison to larger particles). This technique uses monochromatic laser light to irradiate the sample and detects the resulting scattered light, which is then analyzed for its intensity. A dependency of the scattering intensity from fluctuation of the nanoparticles exists, which in turn reveals the rate of diffusion and thereby size.[147]

Another characteristic, which can be acquired *via* this method, is the so-called **polydispersity index (PDI)**. The PDI is an important parameter in the preparation of nanoparticles as it describes their size distribution and therefore quality of the formulation. As a general rule, a PDI below 0.15 displays a narrow size-distributions, suggesting a monodisperse behavior.[147] Another important characteristic is the electrostatic surface potential, which is referred to as **zeta potential**. The zeta potential arises from dissociation/ionization of the used particle material and the adsorption of ions on the particle surface.[148] Studies showed that a slightly negative or neutral charge allows nanoparticles to evade interactions with plasma proteins and reduces the adsorption by them (opsonization). This in turn leads to an increased long-term circulation in the body.[149] Since a direct measurement of the zeta potential is not possible, an electric field is applied to the nanoparticulate formulation and the resulting electrophoretic mobility is determined. Subsequently, the acquired data is mathematically processed by the Henry's equation to calculate the zeta potential.[150]
To describe the drug loading capacity the **encapsulation efficiency (EE)** is given. This parameter indicates the percentage of the compound, which could be successfully encapsulated into the respective nanoformulation.

The final (and perhaps most important) property of nanoparticles is their **drug release** behavior. On the one hand, the drug must be stably enclosed inside the nanoparticulate formulation, as a fast release counteracts the targeting effect. On the other hand, a controlled release of the compound is necessary to achieve a constant drug concentration at the desired target site. In general, the drug can be released in various manners e.g. by diffusion through the nanoparticles matrix, and/or degradation and/or erosion of the nanoparticle itself.[151] To evaluate the release profile a range of techniques is available (e.g. size exclusion chromatography, flow cytometry or fluorescence assays[152]), depending on the nature of the encapsulated drug and nanoparticles. One of the easiest to apply and frequently used methods is the so-called dialysis bag diffusion method.[153] In this technique, a certain volume of the sample is filled into a dialysis bag, which is then transferred into an acceptor liquid. Over time the drug is released from the nanoparticulate formulation, diffuses through the dialysis membrane and accumulates in the outer compartment until the concentration equilibrium is established. To determine the drug release, samples from the acceptor liquid are taken and analyzed for their concentration. Of course, this method is only suitable for encapsulated drugs, which possess a certain solubility in the used aqueous solution.

3.2.1.2 Liposomal Formulations

One of the most prominent and extensively investigated representatives of nanoparticles in medicine are liposomes.

Due to their size and chemical nature, they can be used as nanocarriers for various drugs and accumulate at the target site by utilizing the EPR effect. These spherical vesicles consist of a lipid bilayer, which encloses an aqueous core and is composed of natural and/or artificial phospholipids (e.g. phosphatidylglycerol, phosphatidylethanolamine or phosphatidylcholine).[154] Although these lipid bilayers are easily formed by self-assembly of phospholipids in aqueous solutions, studies showed a fast release of the encapsulated drugs. It turned out that those liposomes solely prepared from unsaturated phospholipid molecules suffered from leakiness in their layers. To solve this problem and improve the stability of the encapsulated drugs, cholesterol was included in the synthesis to ensure a tight packing of the lipids.[155] The synthesis of the first drug-loaded liposomes was already accomplished in the 1970s.[156] However, these liposomal formulations were easily detected and attacked by macrophages or the serum complement system. Furthermore, due to their lipophilic nature, they reacted with lipoproteins leading to instability and fast drug release.[157] One of the most successful strategies to overcome these drawbacks is the modification of the liposomal surface. By these alterations, the interaction and consequently binding to plasma proteins can be hindered and the circulation time thereby significantly increased. The most prominent surfactant for this is polyethylene glycol (PEG). In general, liposomal formulation prepared by this method are referred to as so-called “PEG-ylated” or “stealth” liposomes.[158-159] Other approaches to modify the liposomal surface (to accumulate at the desired target site) include the use of targeting ligands such as peptides or monoclonal antibodies.[160]

As for the preparation of liposomal formulations, several techniques are available, depending on their application and the chemical properties of the encapsulated drug. The first and still one of the most frequently used approaches is the thin lipid method, which was reported in 1965 by Bangham *et al*.[142] In this technique, the liposomal building blocks are dissolved in an organic solvent, which is subsequently evaporated leaving the eponymous thin lipid film. The following step includes the rehydration of the thin lipid film by an aqueous solution of choice to form the liposomes. Next, the liposomes are reduced and unified in their size, which can be carried out by different methods (e.g. sonication with an ultrasonic bath/probe tip sonicator or extrusion through polycarbonate filter).[161] The thin lipid film hydration method is particularly suitable for the loading of lipophilic drugs, which can be easily added at the beginning of the synthesis.[162] However, applying this approach to less lipophilic drugs resulted in a low encapsulation efficacy as the substances shows more affinity to the aqueous phase and stays dissolved in this medium. One very

successful method to overcome these drawbacks is the so-called remote loading approach in which hydrophilic or amphipathic compounds are encapsulated into preformed liposomes *via* a pH gradient.[163] In this technique, the pH gradient between the internal and the external media of the liposomal formulation "pumps" the drug inside the liposomes (Figure 18). The internal solution usually consists of salts of weak bases (e.g. ammonium) or weak acids (e.g. acetates) and is formed by rehydration of the thin lipid film.[164] By exchanging the external solution (e.g. to PBS) the difference in the proton concentration gradient is created. Due to this, the uncharged drug is forced inside the liposomes, where its protonation takes place. The loaded compound needs to feature particular characteristics to be suitable for this method: Being soluble in the external aqueous media (to at least a certain extent), exhibiting a logD in the range of –2.5 to 2 at pH 7 and a pKa ≤ 11. Furthermore, depending on the compounds pKa and the pH of the external medium, the change between its charged to uncharged form must be enabled.[163-164]

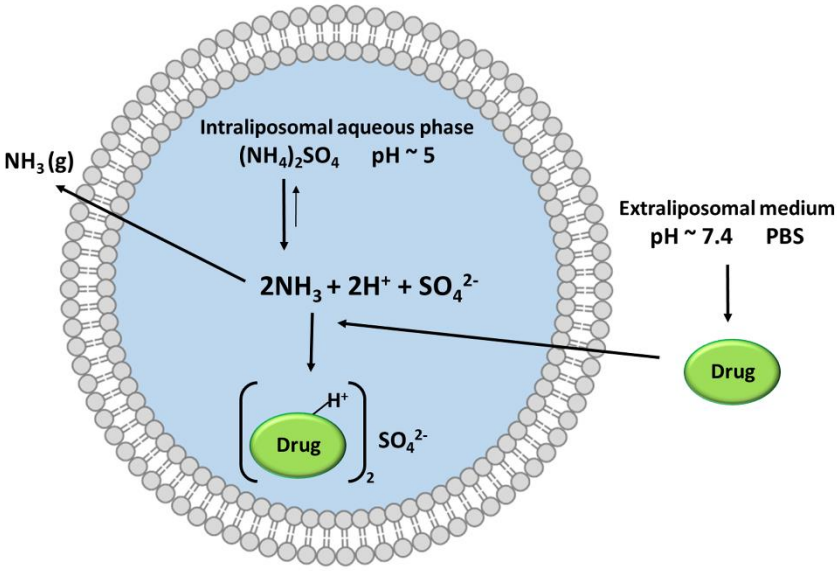

Figure 18: Schematic illustration of the remote loading approach of a weak amphipathic base *via* an ammonium sulfate gradient. Adapted from reference [163].

3.2.1.3 Nanoformulations as anticancer therapeutics in the clinic

The success story of liposomal anticancer formulations started in 1995, when Doxil®, which is a PEGylated liposomal doxorubicin, got approval by the FDA for treatment of Kaposi's sarcoma induced by HIV.[165] Doxil® marked a milestone in the (passive) drug targeting approach and is still one of its most prominent and lucrative representatives.[166] After these first promising results, a range of other liposomal formulations was developed and clinically approved. Only one year later, in 1996, DaunoXome® (liposomal Daunorubicin) was approved for the therapy of various leukemia and Kaposi's sarcoma.[143] Another liposomal formulation (loaded into non-PEGylated liposomes) of doxorubicin resulted in Myocet®, which got approval in Canada and Europe twenty years ago to

treat ovarian and breast cancers.[167] Notably, the encapsulation of doxorubicin into liposomes drastically enhanced its therapeutic potential as the plasma half-life time was increased from 0.2 h (free doxorubicin) to 2.5 h (Myocet®) or even 55 h (Doxil®).[168] Another advantageous aspect of both liposomal formulations was the reduction of dose-limiting side effects such as cardiotoxicities.[169] Lipodex® was the third liposomal formulation of doxorubicin, which got clinical approval in 2013 and demonstrated even higher circulation half-life (65 h) due to use of other liposomal building blocks.[143] Furthermore, liposomal formulations for instance of vincristine (Marqibo®) or mifarmutide (Mepact®) have been approved for the therapy of various cancers.[170] All the above described (and some more) clinically approved liposomal formulations, their trade name, approval year as well as therapeutic indications can be found in Table 2.

Table 2: A selection of FDA- approved nanoformulations.[143, 170] Only their main therapeutic indications are provided.

Drug	Trade name	Approved	Type of formulation	Main therapeutic indications
Doxorubicin	Doxil®	1995	PEGylated liposomes	Kaposi's sarcoma, ovarian cancer, multiple myeloma
Doxorubicin	Myocet®	2000	Non-PEGylated liposomes	Ovarian and breast cancer
Doxorubicin	Lipodox®	2013	PEGylated liposomes	Ovarian cancer, multiple myeloma
Daunorubicin	DaunoXome®	1996	Non-PEGylated liposomes	Various leukemias
Vincristine sulfate	Marqibo®	2012	Non-PEGylated liposomes	Leukemia, melanoma, lymphoma
Mifarmutide	Mepact®	2009	Non-PEGylated liposomes	Osteosarcoma
Irinotecan	ONIVYDE®	2015	Non-PEGylated liposomes	Metastatic pancreatic cancer

Furthermore, liposomal formulations of other anticancer drugs are currently investigated in several clinical trials: Liposomal cisplatin in form of Lipoplatin (phase III) and SPI-77 (phase II) (both PEGylated liposomes) or liposomal paclitaxel in form of EndoTAG-I (phase II) and LEP-ETU (phase II) (both non-PEGylated liposomes).[143, 171-172] Also novel (e.g. thermosensitive) liposomal formulations of doxorubicin are developed (Thermodox in a phase III and MM-302 in a phase II/III trials, both PEGylated liposomes).[170] The other important group of nanoformulations, which can be used as drug-carrier in anticancer therapy, consists of polymeric nanoparticles. Although, possessing encouraging properties such as prolonged half-life time and controlled release behavior, no representative of this compound class has gotten approval so far.[173] However, many polymeric nanoparticles are currently investigated in various clinical phase III trials e.g. Opaxio and NK105 (both paclitaxel loaded polymeric nanoparticle formulations) or NC-6004 (nanoparticle formulations of cisplatin).[174] All above described (and some more) clinically investigated liposomal

formulations or polymeric nanoparticles, their trade name, clinical phase as well as therapeutic targets can be found in Table 3.

Table 3: A selection of currently clinical investigated nanoformulations.[143, 170] Only their main therapeutic indications are provided.

Drug	Trade name	Clinical phase	Type of formulation	Main therapeutic indications
Cisplatin	Lipoplatin	Phase III	PEGylated liposomes	Non-small cell lung cancer
Cisplatin	SPI-77	Phase II	PEGylated liposomes	Ovarian cancer
Doxorubicin	Thermodox	Phase III	PEGylated liposomes	Breast cancer
Doxorubicin	MM-302	Phase II/III	PEGylated liposomes	Breast cancer
Paclitaxel	EndoTAG-I	Phase II	Non-PEGylated liposomes	Breast and pancreatic cancer
Paclitaxel	LEP-ETU	Phase II	Non-PEGylated liposomes	Ovarian and breast cancer
Paclitaxel	Opaxio	Phase III	Polymeric nanoparticles	Lung and ovarian cancer
Paclitaxel	NK105	Phase III	Polymeric nanoparticles	Breast cancer
Doxorubicin	Transdrug BA-003	Phase III	Polymeric nanoparticles	Hepatocellular carcinoma
Docetaxel	BIND-014	Phase II	Polymeric nanoparticles	Various cancers
Cisplatin	NC-6004	Phase II	Polymeric nanoparticles	Pancreatic cancer

3.2.2 Active Targeting

While the passive targeting approach utilizes the EPR effect, active targeting drugs interact with their target (e.g. overexpressed receptors in cancer cells) *via* various ligands. Tumors often exhibit a dysregulated expression of various receptors, which distinguishes them from healthy cells. Selected ligands, which are attached to the actual drug actively target and bind to these overexpressed receptors. By this enhanced affinity to the cancer cells, an increased uptake (mainly *via* endocytosis) and thereby accumulation of the drug in the tumor tissue can be achieved. Ligands used for this kind of approach include peptides, vitamins, lipids, sugars, or aptamers.[175] Despite promising results in several preclinical and clinical trials, to this date no active tumor-targeting drug is clinically approved by the FDA or any other drug regulatory authority.[176] Poor tumor penetration, inhomogeneities in the tumor tissue, toxicities or endosomal escape are still the main issues of this compound class.[177] Some drugs even combine the active- and passive-targeting approach, resulting in a strong synergism from the EPR effect and selective cell-uptake. Prominent representatives of this mixed compound class are antibody-drug conjugates (ADC) and NPs with a ligand-modified surface (e.g. polymer-caged nanobins).[178]

4 RESEARCH OBJECTIVES

Within this thesis, different strategies are applied to two anticancer compound classes (TKIs and TSCs) in order to overcome their respective drawbacks. Although small molecule TKIs marked a milestone in targeted cancer therapy two decades ago, severe treatment-related toxicities frequently lead to dose-reductions or therapy discontinuation. Moreover, the occurrence of rapidly developing resistances limits their application potential and period. Combination therapy of two TKIs can indeed result in strong synergistic effects as a range of signaling pathways is targeted at the same time, bypassing resistance mechanisms in this way. Unfortunately, the combined adverse effects of both drugs are frequently severe during this kind of treatment. Therefore, approaches to reduce the side effects of TKIs are urgently required to further improve the potential of this compound class.

The first part of this work deals with the development of prodrug systems of TKIs with the aim to enhance their tumor selectivity whilst retaining their potent anticancer properties. In a previous work, we established the first hypoxia-activatable cobalt(III) prodrug (**Co-EGFR**) bearing a novel EGFR-inhibiting ligand (KP2187).[127] Although promising results were obtained in initial *in vivo* experiments, the stability of the complex towards reduction in serum/tissue showed potential for improvement. Consequently, the first objective of this thesis was the enhancement of the stability of **Co-EGFR** by decreasing its reduction potential. To this end, the EGFR inhibiting moiety and/or ancillary ligands were methylated, a strategy proposed by Denny *et al* for other types of cobalt(III) prodrugs (Figure 19).[120]

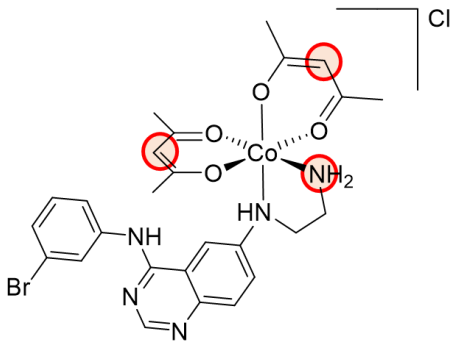

Figure 19: The previously synthesized cobalt(III) complex **Co-EGFR** bearing the EGFR-inhibiting moiety (KP2187).[127] Highlighted in red are the positions methylated with the aim to lower its cobalt redox potential and increase the complex stability.

The resulting, novel derivatives were characterized by various methods (NMR, mass spectrometry and elemental analysis) and their redox potential was investigated by cyclic voltammetry. Furthermore, the stability of the complexes was examined in the presence of naturally occurring

reducing agents and in fetal calf serum. Subsequently, their anticancer activity was evaluated under normoxic/hypoxic conditions *in vitro* and correlated with the previously obtained physico-chemical data.

One likely explanation for the high reduction potential of **Co-EGFR** (and thereof low stability in vivo), is the direct attachment of the metal-chelating moiety to the aromatic ring system (Figure 19). In general, aromatic ring systems withdraw the electron density from adjacent groups, in this case the metal center, leading to increased reduction potentials. Thus, in the second project the already established cobalt(III) prodrug approach was implemented to the clinically approved mulitkinase-inhibitor ponatinib. Ponatinib is an ideal candidate for this kind of strategy as the piperazine group mostly acts as a solubilizing unit, and thus can be substituted with an ethylendiamine bridge. More importantly, there is a $–CH_2$ spacer unit between the piperazine moiety and the aromatic ring system, which should result in higher electron density at the cobalt and therefore lower reduction potentials (in comparison to KP2187). Thus, a novel ligand based on ponatinib was developed with a metal-chelating ethylendiamine moiety in place of the original piperazine group (Figure 20).

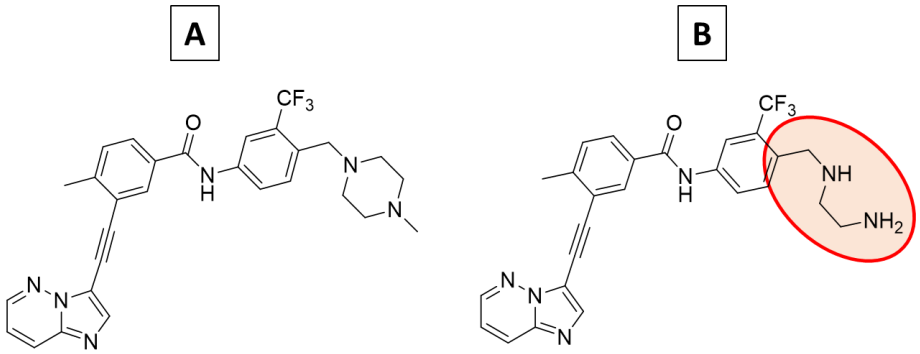

Figure 20: Molecular structure of (A) the clinically approved multi-kinase inhibitor ponatinib and (B) the novel ponatinib-based ligand. Highlighted in red is the moiety relevant for metal coordination and its connection to the aromatic ring system.

At first, molecular docking studies showed if the novel ligand displays a similar binding behavior as ponatinib and if the two cobalt(III) complexes are indeed too bulky to fit into the respective binding pockets (to act as prodrugs). Afterwards synthesis and complete characterization of two of the proposed compounds with different auxiliary ligands (acetylacetone or methylacetylacetone) was performed. The impact of the $–CH_2$ group was investigated by cyclic voltammetry and the stability of the novel complexes was studied under physiological and biological relevant conditions. Biological investigations such as *in vitro* tests in various cancer cell lines under normoxic/hypoxic conditions revealed the differences of the release of the ligand from the cobalt(III) complex and its

antineoplastic properties. *In vivo* tests were performed to correlate the reduction potential of the complexes with their tolerability and anticancer activity.

The second part of this work deals with the compound class of TSCs, which exhibit strong anticancer properties and are currently examined in various clinical trials. However, one of its most prominent drug candidates, Triapine, is widely not effective against solid tumors most likely due to its short plasma half-life time and poor tumor accumulation. A promising approach to overcome these drawbacks and increase the tumor targeting properties of TSCs is their encapsulation into nanoparticles (such as liposomes) exploiting the EPR effect thereby. We successfully demonstrated this strategy in a previous work, however, for Triapine no stable encapsulation could be reached.[179] Therefore, we decided to encapsulate its copper(II) complex as it behaves as prodrug, releasing Triapine after reduction.[95, 180] This strategy was also tested for the promising third generation TSC COTI-2, and its copper(II) complex (Figure 21).

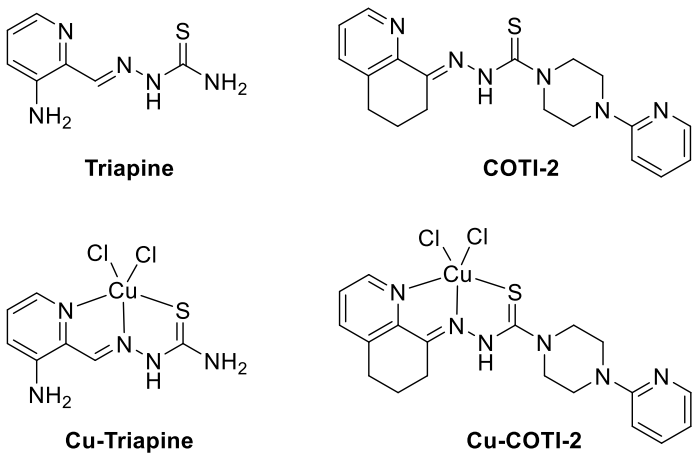

Figure 21: The clinically investigated TSCs Triapine and COTI-2 as well as their copper(II) complexes.

First of all a series of different encapsulation methods and conditions was investigated to find the optimal synthetic strategies for the two different drugs. After encapsulation, the physico-chemical properties (e.g. particle size, surface charge, size distribution, encapsulation efficiency) and drug release kinetics of the synthesized liposomal formulation were examined. The liposomes were evaluated and compared with the free ligands/complexes regarding their anticancer properties *in vitro*. Subsequently, the most promising liposomal formulations was tested for their release properties and anticancer activity *in vivo*. Furthermore, the extent of methemoglobin formation, a frequently observed side effect during the administration of Triapine, was analyzed.

5 ABBREVIATIONS

ABL	Abelson kinase
ADC	antibody-drug conjugates
ALL	acute lymphoblastic leukemia
ATP	adenosine triphosphate
CML	chronic myeloid leukemia
DNA	deoxyribonucleic acid
DLS	dynamic light scattering
EGFR	epidermal growth factor receptor
EPR	enhanced permeability and retention
FDA	U.S. Food and Drug Administration
FGFR	fibroblast growth factor receptor
HbO_2	oxyhemoglobin
HER	human epidermal growth factor receptor
HSA	human serum albumin
MAb	monoclonal antibody
metHb	methemoglobin
NMR	nuclear magnetic resonance
NSCLC	non-small-cell lung cancer
NRTK	non-receptor tyrosine kinases
PDI	polydispersity index
PDGFR	platelet-derived growth factor receptor
PEG	polyethylene glycol
RR	ribonucleotide reductase
RTK	receptor tyrosine kinase
TK	tyrosine kinase
TKI	tyrosine kinase inhibitors
VEGFR	vascular endothelial growth factor receptor
WHO	World Health Organization

6 REFERENCES

1. WHO. https://www.who.int/news-room/fact-sheets/detail/cancer (17.06.2021).
2. Sung, H.; Ferlay, J.; Siegel, R. L.; Laversanne, M.; Soerjomataram, I.; Jemal, A.; Bray, F., Global cancer statistics 2020: GLOBOCAN estimates of incidence and mortality worldwide for 36 cancers in 185 countries. *CA: A Cancer Journal for Clinicians* **2021,** *71* (3), 209-249.
3. Klotz, J.; Hackl, M.; Schwab, M.; Hanika, A.; Haluza, D., Combining population projections with quasi-likelihood models: A new way to predict cancer incidence and cancer mortality in Austria up to 2030. *Demographic Research* **2019,** *40*, 503-532.
4. Ruddon, R. W., *Cancer Biology*. Oxford University Press: 2007.
5. Pardee, A. B.; Stein, G. S., *The biology and treatment of cancer: Understanding cancer*. John Wiley & Sons: 2011.
6. National Cancer Institute. https://www.cancer.gov/about-cancer/treatment/types (17.06.2021).
7. Wyld, L.; Audisio, R. A.; Poston, G. J., The evolution of cancer surgery and future perspectives. *Nature Reviews Clinical Oncology* **2015,** *12* (2), 115-124.
8. Chen, H. H.; Kuo, M. T., Improving radiotherapy in cancer treatment: Promises and challenges. *Oncotarget* **2017,** *8* (37), 62742.
9. Fernando, J.; Jones, R., The principles of cancer treatment by chemotherapy. *Surgery (Oxford)* **2015,** *33* (3), 131-135.
10. Knowles, M.; Selby, P., *Introduction to the cellular and molecular biology of cancer*. Oxford university press: 2005.
11. Falzone, L.; Salomone, S.; Libra, M., Evolution of cancer pharmacological treatments at the turn of the third millennium. *Frontiers in Pharmacology* **2018,** *9*, 1300.
12. Waldman, A. D.; Fritz, J. M.; Lenardo, M. J., A guide to cancer immunotherapy: from T cell basic science to clinical practice. *Nature Reviews Immunology* **2020,** *20* (11), 651-668.
13. Abraham, J.; Staffurth, J., Hormonal therapy for cancer. *Medicine* **2016,** *44* (1), 30-33.
14. Baudino, T., Targeted cancer therapy: the next generation of cancer treatment. *Current Drug Discovery Technologies* **2015,** *12* (1), 3-20.
15. Hanahan, D.; Weinberg, R. A., Hallmarks of cancer: the next generation. *Cell* **2011,** *144* (5), 646-674.
16. Hubbard, S. R.; Till, J. H., Protein tyrosine kinase structure and function. *Annual Review of Biochemistry* **2000,** *69* (1), 373-398.
17. Paul, M. K.; Mukhopadhyay, A. K., Tyrosine kinase–role and significance in cancer. *International Journal of Medical Sciences* **2004,** *1* (2), 101.
18. Manning, G.; Plowman, G. D.; Hunter, T.; Sudarsanam, S., Evolution of protein kinase signaling from yeast to man. *Trends in Biochemical Sciences* **2002,** *27* (10), 514-520.
19. Lemmon, M. A.; Schlessinger, J., Cell signaling by receptor tyrosine kinases. *Cell* **2010,** *141* (7), 1117-1134.
20. Du, Z.; Lovly, C. M., Mechanisms of receptor tyrosine kinase activation in cancer. *Molecular Cancer* **2018,** *17* (1), 1-13.
21. Pottier, C.; Fresnais, M.; Gilon, M.; Jérusalem, G.; Longuespée, R.; Sounni, N. E., Tyrosine kinase inhibitors in cancer: breakthrough and challenges of targeted therapy. *Cancers* **2020,** *12* (3), 731.
22. Pelengaris, S.; Khan, M., *The molecular biology of cancer: A bridge from bench to bedside*. John Wiley & Sons: 2013.
23. Gschwind, A.; Fischer, O. M.; Ullrich, A., The discovery of receptor tyrosine kinases: targets for cancer therapy. *Nature Reviews Cancer* **2004,** *4* (5), 361-370.
24. Cohen, P., The origins of protein phosphorylation. *Nature Cell Biology* **2002,** *4* (5), E127-E130.
25. Wu, P.; Nielsen, T. E.; Clausen, M. H., FDA-approved small-molecule kinase inhibitors. *Trends in Pharmacological Sciences* **2015,** *36* (7), 422-439.
26. Lamba, V.; Ghosh, I., New directions in targeting protein kinases: focusing upon true allosteric and bivalent inhibitors. *Current Pharmaceutical Design* **2012,** *18* (20), 2936-2945.
27. Zhong, L.; Li, Y.; Xiong, L.; Wang, W.; Wu, M.; Yuan, T.; Yang, W.; Tian, C.; Miao, Z.; Wang, T., Small molecules in targeted cancer therapy: advances, challenges, and future perspectives. *Signal Transduction and Targeted Therapy* **2021,** *6* (1), 1-48.
28. Roskoski, R., Properties of FDA-approved small molecule protein kinase inhibitors: a 2021 update. *Pharmacological Research* **2021**, 105463.
29. Cohen, P.; Cross, D.; Jänne, P. A., Kinase drug discovery 20 years after imatinib: progress and future directions. *Nature Reviews Drug Discovery* **2021**, 1-19.

30. Fauvel, B.; Yasri, A., Antibodies directed against receptor tyrosine kinases: Current and future strategies to fight cancer. *MAbs* **2014,** *6* (4), 838-851.
31. Lu, R.-M.; Hwang, Y.-C.; Liu, I.-J.; Lee, C.-C.; Tsai, H.-Z.; Li, H.-J.; Wu, H.-C., Development of therapeutic antibodies for the treatment of diseases. *Journal of Biomedical Science* **2020,** *27* (1), 1-30.
32. Yazdi, M. H.; Faramarzi, M. A.; Nikfar, S.; Abdollahi, M., A comprehensive review of clinical trials on EGFR inhibitors such as cetuximab and panitumumab as monotherapy and in combination for treatment of metastatic colorectal cancer. *Avicenna Journal of Medical Biotechnology* **2015,** *7* (4), 134.
33. Chen, J.; Zeng, F.; Forrester, S. J.; Eguchi, S.; Zhang, M.-Z.; Harris, R. C., Expression and function of the epidermal growth factor receptor in physiology and disease. *Physiological Reviews* **2016,** *96* (3), 1025-1069.
34. Wee, P.; Wang, Z., Epidermal growth factor receptor cell proliferation signaling pathways. *Cancers* **2017,** *9* (5), 52.
35. Herbst, R. S., Review of epidermal growth factor receptor biology. *International Journal of Radiation Oncology* Biology* Physics* **2004,** *59* (2), S21-S26.
36. Roskoski Jr, R., The ErbB/HER family of protein-tyrosine kinases and cancer. *Pharmacological Research* **2014,** *79*, 34-74.
37. Cai, W.-Q.; Zeng, L.-S.; Wang, L.-F.; Wang, Y.-Y.; Cheng, J.-T.; Zhang, Y.; Han, Z.-W.; Zhou, Y.; Huang, S.-L.; Wang, X.-W., The latest battles between EGFR monoclonal antibodies and resistant tumor cells. *Frontiers in Oncology* **2020,** *10*, 1249.
38. Ayati, A.; Moghimi, S.; Salarinejad, S.; Safavi, M.; Pouramiri, B.; Foroumadi, A., A review on progression of epidermal growth factor receptor (EGFR) inhibitors as an efficient approach in cancer targeted therapy. *Bioorganic Chemistry* **2020,** *99*, 103811.
39. Lynch, T. J.; Bell, D. W.; Sordella, R.; Gurubhagavatula, S.; Okimoto, R. A.; Brannigan, B. W.; Harris, P. L.; Haserlat, S. M.; Supko, J. G.; Haluska, F. G., Activating mutations in the epidermal growth factor receptor underlying responsiveness of non–small-cell lung cancer to gefitinib. *New England Journal of Medicine* **2004,** *350* (21), 2129-2139.
40. Yang, Z.; Hackshaw, A.; Feng, Q.; Fu, X.; Zhang, Y.; Mao, C.; Tang, J., Comparison of gefitinib, erlotinib and afatinib in non-small cell lung cancer: A meta-analysis. *International Journal of Cancer* **2017,** *140* (12), 2805-2819.
41. Pao, W.; Miller, V. A.; Politi, K. A.; Riely, G. J.; Somwar, R.; Zakowski, M. F.; Kris, M. G.; Varmus, H., Acquired resistance of lung adenocarcinomas to gefitinib or erlotinib is associated with a second mutation in the EGFR kinase domain. *PLOS Medicine* **2005,** *2* (3), e73.
42. Xu, J.; Wang, J.; Zhang, S., Mechanisms of resistance to irreversible epidermal growth factor receptor tyrosine kinase inhibitors and therapeutic strategies in non-small cell lung cancer. *Oncotarget* **2017,** *8* (52), 90557.
43. Helena, A. Y.; Pao, W., Targeted therapies: Afatinib—new therapy option for EGFR-mutant lung cancer. *Nature Reviews Clinical Oncology* **2013,** *10* (10), 551.
44. Gonzales, A. J.; Hook, K. E.; Althaus, I. W.; Ellis, P. A.; Trachet, E.; Delaney, A. M.; Harvey, P. J.; Ellis, T. A.; Amato, D. M.; Nelson, J. M., Antitumor activity and pharmacokinetic properties of PF-00299804, a second-generation irreversible pan-erbB receptor tyrosine kinase inhibitor. *Molecular Cancer Therapeutics* **2008,** *7* (7), 1880-1889.
45. Solca, F.; Dahl, G.; Zoephel, A.; Bader, G.; Sanderson, M.; Klein, C.; Kraemer, O.; Himmelsbach, F.; Haaksma, E.; Adolf, G. R., Target binding properties and cellular activity of afatinib (BIBW 2992), an irreversible ErbB family blocker. *Journal of Pharmacology and Experimental Therapeutics* **2012,** *343* (2), 342-350.
46. Camidge, D. R.; Pao, W.; Sequist, L. V., Acquired resistance to TKIs in solid tumours: learning from lung cancer. *Nature Reviews Clinical Oncology* **2014,** *11* (8), 473.
47. Steuer, C. E.; Khuri, F. R.; Ramalingam, S. S., The next generation of epidermal growth factor receptor tyrosine kinase inhibitors in the treatment of lung cancer. *Cancer* **2015,** *121* (8), E1-E6.
48. Cross, D. A.; Ashton, S. E.; Ghiorghiu, S.; Eberlein, C.; Nebhan, C. A.; Spitzler, P. J.; Orme, J. P.; Finlay, M. R. V.; Ward, R. A.; Mellor, M. J., AZD9291, an irreversible EGFR TKI, overcomes T790M-mediated resistance to EGFR inhibitors in lung cancer. *Cancer discovery* **2014,** *4* (9), 1046-1061.
49. Greig, S. L., Osimertinib: first global approval. *Drugs* **2016,** *76* (2), 263-273.
50. Lamb, Y. N.; Scott, L. J., Osimertinib: a review in T790M-positive advanced non-small cell lung cancer. *Targeted Oncology* **2017,** *12* (4), 555-562.
51. Soria, J.-C.; Ohe, Y.; Vansteenkiste, J.; Reungwetwattana, T.; Chewaskulyong, B.; Lee, K. H.; Dechaphunkul, A.; Imamura, F.; Nogami, N.; Kurata, T., Osimertinib in untreated EGFR-mutated advanced non–small-cell lung cancer. *New England Journal of Medicine* **2018,** *378* (2), 113-125.

52. Drugs. https://www.drugs.com/newdrugs/tagrisso-approved-us-adjuvant-patients-early-stage-egfr-mutated-non-small-cell-lung-cancer-5411.html (17.06.2021).
53. Lazzari, C.; Gregorc, V.; Karachaliou, N.; Rosell, R.; Santarpia, M., Mechanisms of resistance to osimertinib. *Journal of Thoracic Disease* **2020,** *12* (5), 2851.
54. Aw, D. C. W.; Tan, E. H.; Chin, T. M.; Lim, H. L.; Lee, H. Y.; Soo, R. A., Management of epidermal growth factor receptor tyrosine kinase inhibitor-related cutaneous and gastrointestinal toxicities. *Asia-Pacific Journal of Clinical Oncology* **2018,** *14* (1), 23-31.
55. Kiyohara, Y.; Yamazaki, N.; Kishi, A., Erlotinib-related skin toxicities: treatment strategies in patients with metastatic non-small cell lung cancer. *Journal of the American Academy of Dermatology* **2013,** *69* (3), 463-472.
56. Kudo, K.; Hotta, K.; Bessho, A.; Nogami, N.; Kozuki, T.; Kuyama, S.; Inoue, K.; Harita, S.; Okada, T.; Genba, K., Development of skin rash within the 1st week is a potential surrogate marker of therapeutic effect in afatinib monotherapy in patients with EGFR-mt non-small-cell lung cancer (NSCLC): Okayama Lung Cancer Study Group Experience. American Society of Clinical Oncology: 2015.
57. Turner, N.; Grose, R., Fibroblast growth factor signalling: from development to cancer. *Nature Reviews Cancer* **2010,** *10* (2), 116-129.
58. Regeenes, R.; Silva, P. N.; Chang, H. H.; Arany, E. J.; Shukalyuk, A. I.; Audet, J.; Kilkenny, D. M.; Rocheleau, J. V., Fibroblast growth factor receptor 5 (FGFR5) is a co-receptor for FGFR1 that is up-regulated in beta-cells by cytokine-induced inflammation. *Journal of Biological Chemistry* **2018,** *293* (44), 17218-17228.
59. Ornitz, D. M.; Itoh, N., The fibroblast growth factor signaling pathway. *Wiley Interdisciplinary Reviews: Developmental Biology* **2015,** *4* (3), 215-266.
60. Babina, I. S.; Turner, N. C., Advances and challenges in targeting FGFR signalling in cancer. *Nature Reviews Cancer* **2017,** *17* (5), 318.
61. Yue, S.; Li, Y.; Chen, X.; Wang, J.; Li, M.; Chen, Y.; Wu, D., FGFR-TKI resistance in cancer: current status and perspectives. *Journal of Hematology & Oncology* **2021,** *14* (1), 1-14.
62. Wang, J. Y., The capable ABL: what is its biological function? *Molecular and Cellular Biology* **2014,** *34* (7), 1188-1197.
63. Greuber, E. K.; Smith-Pearson, P.; Wang, J.; Pendergast, A. M., Role of ABL family kinases in cancer: from leukaemia to solid tumours. *Nature Reviews Cancer* **2013,** *13* (8), 559-571.
64. Soverini, S.; Mancini, M.; Bavaro, L.; Cavo, M.; Martinelli, G., Chronic myeloid leukemia: the paradigm of targeting oncogenic tyrosine kinase signaling and counteracting resistance for successful cancer therapy. *Molecular Cancer* **2018,** *17* (1), 1-15.
65. Jabbour, E.; Kantarjian, H.; Cortes, J., Use of second-and third-generation tyrosine kinase inhibitors in the treatment of chronic myeloid leukemia: an evolving treatment paradigm. *Clinical Lymphoma Myeloma and Leukemia* **2015,** *15* (6), 323-334.
66. Braun, T. P.; Eide, C. A.; Druker, B. J., Response and resistance to BCR-ABL1-targeted therapies. *Cancer Cell* **2020,** *37* (4), 530-542.
67. Broekman, F.; Giovannetti, E.; Peters, G. J., Tyrosine kinase inhibitors: Multi-targeted or single-targeted? *World Journal of Clinical Oncology* **2011,** *2* (2), 80.
68. Tan, F. H.; Putoczki, T. L.; Stylli, S. S.; Luwor, R. B., Ponatinib: a novel multi-tyrosine kinase inhibitor against human malignancies. *OncoTargets and Therapy* **2019,** *12*, 635.
69. Huang, W.-S.; Metcalf, C. A.; Sundaramoorthi, R.; Wang, Y.; Zou, D.; Thomas, R. M.; Zhu, X.; Cai, L.; Wen, D.; Liu, S., Discovery of 3-[2-(imidazo [1, 2-b] pyridazin-3-yl) ethynyl]-4-methyl-N-{4-[(4-methylpiperazin-1-yl) methyl]-3-(trifluoromethyl) phenyl} benzamide (AP24534), a potent, orally active pan-inhibitor of breakpoint cluster region-abelson (BCR-ABL) kinase including the T315I gatekeeper mutant. *Journal of Medicinal Chemistry* **2010,** *53* (12), 4701-4719.
70. Hoy, S. M., Ponatinib: a review of its use in adults with chronic myeloid leukaemia or Philadelphia chromosome-positive acute lymphoblastic leukaemia. *Drugs* **2014,** *74* (7), 793-806.
71. O'Hare, T.; Shakespeare, W. C.; Zhu, X.; Eide, C. A.; Rivera, V. M.; Wang, F.; Adrian, L. T.; Zhou, T.; Huang, W.-S.; Xu, Q., AP24534, a pan-BCR-ABL inhibitor for chronic myeloid leukemia, potently inhibits the T315I mutant and overcomes mutation-based resistance. *Cancer Cell* **2009,** *16* (5), 401-412.
72. Soverini, S.; Colarossi, S.; Gnani, A.; Rosti, G.; Castagnetti, F.; Poerio, A.; Iacobucci, I.; Amabile, M.; Abruzzese, E.; Orlandi, E., Contribution of ABL kinase domain mutations to imatinib resistance in different subsets of Philadelphia-positive patients: by the GIMEMA Working Party on Chronic Myeloid Leukemia. *Clinical Cancer Research* **2006,** *12* (24), 7374-7379.
73. Zhou, T.; Commodore, L.; Huang, W. S.; Wang, Y.; Thomas, M.; Keats, J.; Xu, Q.; Rivera, V. M.; Shakespeare, W. C.; Clackson, T., Structural mechanism of the pan-BCR-ABL inhibitor ponatinib (AP24534): lessons for overcoming kinase inhibitor resistance. *Chemical Biology & Dug Design* **2011,** *77* (1), 1-11.

74. Musumeci, F.; Greco, C.; Grossi, G.; Molinari, A.; Schenone, S., Recent studies on ponatinib in cancers other than chronic myeloid leukemia. *Cancers* **2018,** *10* (11), 430.
75. Roskoski Jr, R., The role of fibroblast growth factor receptor (FGFR) protein-tyrosine kinase inhibitors in the treatment of cancers including those of the urinary bladder. *Pharmacological Research* **2020,** *151*, 104567.
76. Ren, M.; Qin, H.; Ren, R.; Cowell, J. K., Ponatinib suppresses the development of myeloid and lymphoid malignancies associated with FGFR1 abnormalities. *Leukemia* **2013,** *27* (1), 32-40.
77. Chan, O.; Talati, C.; Isenalumhe, L.; Shams, S.; Nodzon, L.; Fradley, M.; Sweet, K.; Pinilla-Ibarz, J., Side-effects profile and outcomes of ponatinib in the treatment of chronic myeloid leukemia. *Blood Advances* **2020,** *4* (3), 530-538.
78. Lipton, J. H.; Chuah, C.; Guerci-Bresler, A.; Rosti, G.; Simpson, D.; Assouline, S.; Etienne, G.; Nicolini, F. E.; le Coutre, P.; Clark, R. E., Ponatinib versus imatinib for newly diagnosed chronic myeloid leukaemia: an international, randomised, open-label, phase 3 trial. *The Lancet Oncology* **2016,** *17* (5), 612-621.
79. Dorer, D. J.; Knickerbocker, R. K.; Baccarani, M.; Cortes, J. E.; Hochhaus, A.; Talpaz, M.; Haluska, F. G., Impact of dose intensity of ponatinib on selected adverse events: multivariate analyses from a pooled population of clinical trial patients. *Leukemia Research* **2016,** *48*, 84-91.
80. Gainor, J. F.; Chabner, B. A., Ponatinib: accelerated disapproval. *Oncologist* **2015,** *20* (8), 847.
81. Heffeter, P.; Pape, V. F.; Enyedy, É. A.; Keppler, B. K.; Szakacs, G.; Kowol, C. R., Anticancer thiosemicarbazones: chemical properties, interaction with iron metabolism, and resistance development. *Antioxidants & Redox Signaling* **2019,** *30* (8), 1062-1082.
82. Kolberg, M.; Strand, K. R.; Graff, P.; Andersson, K. K., Structure, function, and mechanism of ribonucleotide reductases. *Biochimica et Biophysica Acta (BBA)-Proteins and Proteomics* **2004,** *1699* (1-2), 1-34.
83. Miah, A.; Harrington, K.; Nutting, C., Triapine in clinical practice. *The European Journal of Clinical & Medical Oncology* **2010,** *2* (1), 1.
84. Aye, Y.; Long, M. J.; Stubbe, J., Mechanistic studies of semicarbazone triapine targeting human ribonucleotide reductase in vitro and in mammalian cells: tyrosyl radical quenching not involving reactive oxygen species. *Journal of Biological Chemistry* **2012,** *287* (42), 35768-35778.
85. Karp, J. E.; Giles, F. J.; Gojo, I.; Morris, L.; Greer, J.; Johnson, B.; Thein, M.; Sznol, M.; Low, J., A Phase I study of the novel ribonucleotide reductase inhibitor 3-aminopyridine-2-carboxaldehyde thiosemicarbazone (3-AP, Triapine®) in combination with the nucleoside analog fludarabine for patients with refractory acute leukemias and aggressive myeloproliferative disorders. *Leukemia Research* **2008,** *32* (1), 71-77.
86. Knox, J. J.; Hotte, S. J.; Kollmannsberger, C.; Winquist, E.; Fisher, B.; Eisenhauer, E. A., Phase II study of Triapine® in patients with metastatic renal cell carcinoma: a trial of the National Cancer Institute of Canada Clinical Trials Group (NCIC IND. 161). *Investigational New Drugs* **2007,** *25* (5), 471-477.
87. Ma, B.; Goh, B. C.; Tan, E. H.; Lam, K. C.; Soo, R.; Leong, S. S.; Wang, L. Z.; Mo, F.; Chan, A. T.; Zee, B., A multicenter phase II trial of 3-aminopyridine-2-carboxaldehyde thiosemicarbazone (3-AP, Triapine®) and gemcitabine in advanced non-small-cell lung cancer with pharmacokinetic evaluation using peripheral blood mononuclear cells. *Investigational New Drugs* **2008,** *26* (2), 169-173.
88. Kunos, C. A.; Ivy, S. P., Triapine radiochemotherapy in advanced stage cervical cancer. *Frontiers in Oncology* **2018,** *8*, 149.
89. Ratner, E. S.; Zhu, Y.-L.; Penketh, P. G.; Berenblum, J.; Whicker, M. E.; Huang, P. H.; Lee, Y.; Ishiguro, K.; Zhu, R.; Sartorelli, A. C., Triapine potentiates platinum-based combination therapy by disruption of homologous recombination repair. *British Journal of Cancer* **2016,** *114* (7), 777-786.
90. Pelivan, K.; Miklos, W.; van Schoonhoven, S.; Koellensperger, G.; Gille, L.; Berger, W.; Heffeter, P.; Kowol, C. R.; Keppler, B. K., Differences in protein binding and excretion of Triapine and its Fe (III) complex. *Journal of Inorganic Biochemistry* **2016,** *160*, 61-69.
91. Miklos, W.; Pelivan, K.; Kowol, C.; Pirker, C.; Dornetshuber-Fleiss, R.; Spitzwieser, M.; Englinger, B.; van Schoonhoven, S.; Cichna-Markl, M.; Koellensperger, G., Triapine-mediated ABCB1 induction via PKC induces widespread therapy unresponsiveness but is not underlying acquired triapine resistance. *Cancer Letters* **2015,** *361* (1), 112-120.
92. Pelivan, K.; Frensemeier, L.; Karst, U.; Koellensperger, G.; Bielec, B.; Hager, S.; Heffeter, P.; Keppler, B. K.; Kowol, C. R., Understanding the metabolism of the anticancer drug triapine: electrochemical oxidation, microsomal incubation and in vivo analysis using LC-HRMS. *Analyst* **2017,** *142* (17), 3165-3176.
93. Quach, P.; Gutierrez, E.; Basha, M. T.; Kalinowski, D. S.; Sharpe, P. C.; Lovejoy, D. B.; Bernhardt, P. V.; Jansson, P. J.; Richardson, D. R., Methemoglobin formation by triapine, di-2-pyridylketone-4, 4-dimethyl-3-thiosemicarbazone (Dp44mT), and other anticancer thiosemicarbazones: identification of novel

thiosemicarbazones and therapeutics that prevent this effect. *Molecular Pharmacology* **2012,** *82* (1), 105-114.
94. Basha, M. T.; Bordini, J.; Richardson, D. R.; Martinez, M.; Bernhardt, P. V., Kinetico-mechanistic studies on methemoglobin generation by biologically active thiosemicarbazone iron (III) complexes. *Journal of Inorganic Biochemistry* **2016,** *162*, 326-333.
95. Hager, S.; Pape, V. F.; Pósa, V.; Montsch, B.; Uhlik, L.; Szakács, G.; Tóth, S.; Jabronka, N.; Keppler, B. K.; Kowol, C. R., High Copper Complex Stability and Slow Reduction Kinetics as Key Parameters for Improved Activity, Paraptosis Induction, and Impact on Drug-Resistant Cells of Anticancer Thiosemicarbazones. *Antioxidants & Redox Signaling* **2020,** *33* (6), 395-414.
96. Guo, Z.-L.; Richardson, D. R.; Kalinowski, D. S.; Kovacevic, Z.; Tan-Un, K. C.; Chan, G. C.-F., The novel thiosemicarbazone, di-2-pyridylketone 4-cyclohexyl-4-methyl-3-thiosemicarbazone (DpC), inhibits neuroblastoma growth in vitro and in vivo via multiple mechanisms. *Journal of Hematology & Oncology* **2016,** *9* (1), 1-16.
97. Salim, K. Y.; Vareki, S. M.; Danter, W. R.; Koropatnick, J., Abstract A25: COTI-2, a novel small molecule that is effective against multiple human cancer cell lines in vitro and in vivo. AACR: 2017.
98. Salim, K. Y.; Maleki Vareki, S.; Danter, W. R.; Koropatnick, J., COTI-2, a new anticancer drug currently under clinical investigation, targets mutant p53 and negatively modulates the PI3K/AKT/mTOR pathway. *European Journal of Cancer* **2016,** *69*, S19.
99. Salim, K. Y.; Vareki, S. M.; Danter, W. R.; Koropatnick, J., COTI-2, a novel small molecule that is active against multiple human cancer cell lines in vitro and in vivo. *Oncotarget* **2016,** *7* (27), 41363.
100. Lindemann, A.; Patel, A. A.; Silver, N. L.; Tang, L.; Liu, Z.; Wang, L.; Tanaka, N.; Rao, X.; Takahashi, H.; Maduka, N. K., COTI-2, a novel thiosemicarbazone derivative, exhibits antitumor activity in HNSCC through p53-dependent and-independent mechanisms. *Clinical Cancer Research* **2019,** *25* (18), 5650-5662.
101. Rudmann, D. G., On-target and off-target-based toxicologic effects. *Toxicologic Pathology* **2013,** *41* (2), 310-314.
102. Kratz, F.; Müller, I. A.; Ryppa, C.; Warnecke, A., Prodrug strategies in anticancer chemotherapy. *ChemMedChem* **2008,** *3* (1), 20-53.
103. Rosenblum, D.; Joshi, N.; Tao, W.; Karp, J. M.; Peer, D., Progress and challenges towards targeted delivery of cancer therapeutics. *Nature Communications* **2018,** *9* (1), 1-12.
104. Kratz, F.; Senter, P.; Steinhagen, H., *Drug Delivery in Oncology: From Basic Research to Cancer Therapy*. John Wiley & Sons: 2013.
105. Ahmed, A.; Sarwar, S.; Hu, Y.; Munir, M. U.; Nisar, M. F.; Ikram, F.; Asif, A.; Rahman, S. U.; Chaudhry, A. A.; Rehman, I. U., Surface-modified polymeric nanoparticles for drug delivery to cancer cells. *Expert Opinion on Drug Delivery* **2021,** *18* (1), 1-24.
106. Zhang, X.; Li, X.; You, Q.; Zhang, X., Prodrug strategy for cancer cell-specific targeting: A recent overview. *European Journal of Medicinal Chemistry* **2017,** *139*, 542-563.
107. Cranmer, L. D., Spotlight on aldoxorubicin (INNO-206) and its potential in the treatment of soft tissue sarcomas: Evidence to date. *OncoTargets and Therapy* **2019,** *12*, 2047.
108. Katz, J.; Janik, J. E.; Younes, A., Brentuximab vedotin (SGN-35). *Clinical Cancer Research* **2011,** *17* (20), 6428-6436.
109. Dubowchik, G. M.; Firestone, R. A.; Padilla, L.; Willner, D.; Hofstead, S. J.; Mosure, K.; Knipe, J. O.; Lasch, S. J.; Trail, P. A., Cathepsin B-labile dipeptide linkers for lysosomal release of doxorubicin from internalizing immunoconjugates: model studies of enzymatic drug release and antigen-specific in vitro anticancer activity. *Bioconjugate Chemistry* **2002,** *13* (4), 855-869.
110. Rankin, E. B.; Giaccia, A. J., Hypoxic control of metastasis. *Science* **2016,** *352* (6282), 175-180.
111. Vaupel, P.; Mayer, A., Hypoxia in cancer: significance and impact on clinical outcome. *Cancer and Metastasis Reviews* **2007,** *26* (2), 225-239.
112. Sharma, A.; Arambula, J. F.; Koo, S.; Kumar, R.; Singh, H.; Sessler, J. L.; Kim, J. S., Hypoxia-targeted drug delivery. *Chemical Society Reviews* **2019,** *48* (3), 771-813.
113. Wilson, W. R.; Hay, M. P., Targeting hypoxia in cancer therapy. *Nature Reviews Cancer* **2011,** *11* (6), 393-410.
114. Phillips, R. M.; Hendriks, H. R.; Sweeney, J. B.; Reddy, G.; Peters, G. J., Efficacy, pharmacokinetic and pharmacodynamic evaluation of apaziquone in the treatment of non-muscle invasive bladder cancer. *Expert Opinion on Drug Metabolism & Toxicology* **2017,** *13* (7), 783-791.
115. Marcu, L.; Olver, I., Tirapazamine: from bench to clinical trials. *Current Clinical Pharmacology* **2006,** *1* (1), 71-79.
116. Patterson, L.; McKeown, S., AQ4N: a new approach to hypoxia-activated cancer chemotherapy. *British Journal of Cancer* **2000,** *83* (12), 1589-1593.

117. Jungwirth, U.; Kowol, C. R.; Keppler, B. K.; Hartinger, C. G.; Berger, W.; Heffeter, P., Anticancer activity of metal complexes: involvement of redox processes. *Antioxidants & Redox Signaling* **2011,** *15* (4), 1085-1127.
118. Comba, P.; Sickmüller, A. F., Modeling of the redox properties of (hexaamine) cobalt (III/II) couples. *Inorganic Chemistry* **1997,** *36* (20), 4500-4507.
119. Bernhardt, P. V.; Jones, L. A.; Sharpe, P. C., Structural and electron self-exchange rate variations in isomeric (Hexaamine) cobalt (III/II) complexes. *Inorganic Chemistry* **1997,** *36* (11), 2420-2425.
120. Ware, D. C.; Palmer, B. D.; Wilson, W. R.; Denny, W. A., Hypoxia-selective antitumor agents. 7. Metal complexes of aliphatic mustards as a new class of hypoxia-selective cytotoxins. Synthesis and evaluation of cobalt (III) complexes of bidentate mustards. *Journal of Medicinal Chemistry* **1993,** *36* (13), 1839-1846.
121. Graf, N.; Lippard, S. J., Redox activation of metal-based prodrugs as a strategy for drug delivery. *Advanced Drug Delivery Reviews* **2012,** *64* (11), 993-1004.
122. Heffern, M. C.; Yamamoto, N.; Holbrook, R. J.; Eckermann, A. L.; Meade, T. J., Cobalt derivatives as promising therapeutic agents. *Current Opinion in Chemical Biology* **2013,** *17* (2), 189-196.
123. Anderson, R.; Denny, W.; Ware, D.; Wilson, W., Pulse radiolysis studies on the hypoxia-selective toxicity of a colbalt-mustard complex. *British Journal of Cancer* **1996,** *27*, S48.
124. Renfrew, A. K.; O'Neill, E. S.; Hambley, T. W.; New, E. J., Harnessing the properties of cobalt coordination complexes for biological application. *Coordination Chemistry Reviews* **2018,** *375*, 221-233.
125. Munteanu, C. R.; Suntharalingam, K., Advances in cobalt complexes as anticancer agents. *Dalton Transactions* **2015,** *44* (31), 13796-13808.
126. Failes, T. W.; Cullinane, C.; Diakos, C. I.; Yamamoto, N.; Lyons, J. G.; Hambley, T. W., Studies of a cobalt (III) complex of the MMP inhibitor marimastat: a potential hypoxia-activated prodrug. *Chemistry — A European Journal* **2007,** *13* (10), 2974-2982.
127. Karnthaler-Benbakka, C.; Groza, D.; Kryeziu, K.; Pichler, V.; Roller, A.; Berger, W.; Heffeter, P.; Kowol, C. R., Tumor-Targeting of EGFR Inhibitors by Hypoxia-Mediated Activation. *Angewandte Chemie International Edition* **2014,** *53* (47), 12930-12935.
128. Spiegelberg, L.; Houben, R.; Niemans, R.; de Ruysscher, D.; Yaromina, A.; Theys, J.; Guise, C. P.; Smaill, J. B.; Patterson, A. V.; Lambin, P., Hypoxia-activated prodrugs and (lack of) clinical progress: The need for hypoxia-based biomarker patient selection in phase III clinical trials. *Clinical and Translational Radiation Oncology* **2019,** *15*, 62-69.
129. Karnthaler-Benbakka, C.; Koblmüller, B.; Mathuber, M.; Holste, K.; Berger, W.; Heffeter, P.; Kowol, C. R.; Keppler, B. K., Synthesis, Characterization and in vitro Studies of a Cathepsin B-Cleavable Prodrug of the VEGFR Inhibitor Sunitinib. *Chemistry & Biodiversity* **2019,** *16* (1), e1800520.
130. Karnthaler-Benbakka, C.; Groza, D.; Koblmüller, B.; Terenzi, A.; Holste, K.; Haider, M.; Baier, D.; Berger, W.; Heffeter, P.; Kowol, C. R., Targeting a targeted drug: an approach toward hypoxia-activatable tyrosine kinase inhibitor prodrugs. *ChemMedChem* **2016,** *11* (21), 2410.
131. Bielec, B.; Schueffl, H.; Terenzi, A.; Berger, W.; Heffeter, P.; Keppler, B. K.; Kowol, C. R., Development and biological investigations of hypoxia-sensitive prodrugs of the tyrosine kinase inhibitor crizotinib. *Bioorganic Chemistry* **2020,** *99*, 103778.
132. Huang, Q.; Zhou, C.; Chen, X.; Dong, B.; Chen, S.; Zhang, N.; Liu, Y.; Li, A.; Yao, M.; Miao, J., Prodrug AST-003 improves the therapeutic index of the multi-targeted tyrosine kinase inhibitor sunitinib. *PLOS One* **2015,** *10* (10), e0141395.
133. Kue, C. S.; Kamkaew, A.; Burgess, K.; Kiew, L. V.; Chung, L. Y.; Lee, H. B., Small molecules for active targeting in cancer. *Medicinal Research Reviews* **2016,** *36* (3), 494-575.
134. Maeda, H.; Matsumura, Y., Tumoritropic and lymphotropic principles of macromolecular drugs. *Critical Reviews in Therapeutic Drug Carrier Systems* **1989,** *6* (3), 193-210.
135. Matsumura, Y.; Maeda, H., A new concept for macromolecular therapeutics in cancer chemotherapy: mechanism of tumoritropic accumulation of proteins and the antitumor agent smancs. *Cancer Research* **1986,** *46* (12 Part 1), 6387-6392.
136. Fang, J.; Nakamura, H.; Maeda, H., The EPR effect: unique features of tumor blood vessels for drug delivery, factors involved, and limitations and augmentation of the effect. *Advanced Drug Delivery Reviews* **2011,** *63* (3), 136-151.
137. Hobbs, S. K.; Monsky, W. L.; Yuan, F.; Roberts, W. G.; Griffith, L.; Torchilin, V. P.; Jain, R. K., Regulation of transport pathways in tumor vessels: role of tumor type and microenvironment. *Proceedings of the National Academy of Sciences* **1998,** *95* (8), 4607-4612.
138. Konno, T.; Maeda, H.; Iwai, K.; Maki, S.; Tashiro, S.; Uchida, M.; Miyauchi, Y., Selective targeting of anti-cancer drug and simultaneous image enhancement in solid tumors by arterially administered lipid contrast medium. *Cancer* **1984,** *54* (11), 2367-2374.

139. Maeda, H., The 35th Anniversary of the Discovery of EPR Effect: A New Wave of Nanomedicines for Tumor-Targeted Drug Delivery—Personal Remarks and Future Prospects. *Journal of Personalized Medicine* **2021,** *11* (3), 229.
140. Bjornmalm, M.; Thurecht, K. J.; Michael, M.; Scott, A. M.; Caruso, F., Bridging bio–nano science and cancer nanomedicine. *ACS Nano* **2017,** *11* (10), 9594-9613.
141. Grumezescu, A. M., *Multifunctional systems for combined delivery, biosensing and diagnostics*. William Andrew: 2017.
142. Bangham, A.; Standish, M. M.; Watkins, J. C., Diffusion of univalent ions across the lamellae of swollen phospholipids. *Journal of Molecular Biology* **1965,** *13* (1), 238-IN27.
143. Wicki, A.; Witzigmann, D.; Balasubramanian, V.; Huwyler, J., Nanomedicine in cancer therapy: challenges, opportunities, and clinical applications. *Journal of Controlled Release* **2015,** *200*, 138-157.
144. Duncan, R.; Gaspar, R., Nanomedicine (s) under the microscope. *Molecular Pharmaceutics* **2011,** *8* (6), 2101-2141.
145. Gaumet, M.; Vargas, A.; Gurny, R.; Delie, F., Nanoparticles for drug delivery: the need for precision in reporting particle size parameters. *European Journal of Pharmaceutics and Biopharmaceutics* **2008,** *69* (1), 1-9.
146. Alexis, F.; Pridgen, E.; Molnar, L. K.; Farokhzad, O. C., Factors affecting the clearance and biodistribution of polymeric nanoparticles. *Molecular pharmaceutics* **2008,** *5* (4), 505-515.
147. Müller, R. H.; Schuhmann, R., *Teilchengrössenmessung in der Laborpraxis: kurzes Lehrbuch mit Einführung in die Theorie: Photonenkorrelationsspektroskopie (PCS)-Laserdiffraktometrie (LD)-Coulter-Meßprinzip (CM) und Meßbeispielen aus dem Schwerpunktbereich der Koaleszenzuntersuchungen, Stuttgart:*. Wiss. Verlag-Ges.: 1996.
148. Hunter, R. J., *Zeta potential in colloid science: principles and applications*. Academic Press: 2013; Vol. 2.
149. Owens III, D. E.; Peppas, N. A., Opsonization, biodistribution, and pharmacokinetics of polymeric nanoparticles. *International Journal of Pharmaceutics* **2006,** *307* (1), 93-102.
150. Bhattacharjee, S., DLS and zeta potential–what they are and what they are not? *Journal of Controlled Release* **2016,** *235*, 337-351.
151. Singh, R.; Lillard Jr, J. W., Nanoparticle-based targeted drug delivery. *Experimental and Molecular Pathology* **2009,** *86* (3), 215-223.
152. Bouchaala, R.; Richert, L.; Anton, N.; Vandamme, T. F.; Djabi, S.; Mély, Y.; Klymchenko, A. S., Quantifying Release from Lipid Nanocarriers by Fluorescence Correlation Spectroscopy. *ACS Omega* **2018,** *3* (10), 14333-14340.
153. Benita, S., *Microencapsulation: methods and industrial applications*. CRC Press: 2005.
154. Pattni, B. S.; Chupin, V. V.; Torchilin, V. P., New developments in liposomal drug delivery. *Chemical Reviews* **2015,** *115* (19), 10938-10966.
155. Briuglia, M.-L.; Rotella, C.; McFarlane, A.; Lamprou, D. A., Influence of cholesterol on liposome stability and on in vitro drug release. *Drug Delivery and Translational Research* **2015,** *5* (3), 231-242.
156. Gregoriadis, G., Drug entrapment in liposomes. *FEBS Letters* **1973,** *36* (3), 292-296.
157. Immordino, M. L.; Dosio, F.; Cattel, L., Stealth liposomes: review of the basic science, rationale, and clinical applications, existing and potential. *International Journal of Nanomedicine* **2006,** *1* (3), 297.
158. Yan, X.; Scherphof, G. L.; Kamps, J. A., Liposome opsonization. *Journal of Liposome Research* **2005,** *15* (1-2), 109-139.
159. Xu, X.; Ho, W.; Zhang, X.; Bertrand, N.; Farokhzad, O., Cancer nanomedicine: from targeted delivery to combination therapy. *Trends in Molecular Medicine* **2015,** *21* (4), 223-232.
160. Sapra, P.; Allen, T., Ligand-targeted liposomal anticancer drugs. *Progress in Lipid Research* **2003,** *42* (5), 439-462.
161. Akbarzadeh, A.; Rezaei-Sadabady, R.; Davaran, S.; Joo, S. W.; Zarghami, N.; Hanifehpour, Y.; Samiei, M.; Kouhi, M.; Nejati-Koshki, K., Liposome: classification, preparation, and applications. *Nanoscale Research Letters* **2013,** *8* (1), 1-9.
162. Sharma, A.; Sharma, U. S., Liposomes in drug delivery: progress and limitations. *International Journal of Pharmaceutics* **1997,** *154* (2), 123-140.
163. Zucker, D.; Marcus, D.; Barenholz, Y.; Goldblum, A., Liposome drugs' loading efficiency: a working model based on loading conditions and drug's physicochemical properties. *Journal of Controlled Release* **2009,** *139* (1), 73-80.
164. Clerc, S.; Barenholz, Y., Loading of amphipathic weak acids into liposomes in response to transmembrane calcium acetate gradients. *Biochimica et Biophysica Acta (BBA)-Biomembranes* **1995,** *1240* (2), 257-265.

165. Barenholz, Y. C., Doxil®—the first FDA-approved nano-drug: lessons learned. *Journal of Controlled Release* **2012,** *160* (2), 117-134.
166. Grand View Research. https://www.grandviewresearch.com/industry-analysis/liposomal-doxorubicin-market (17.06.2021).
167. Batist, G.; Barton, J.; Chaikin, P.; Swenson, C.; Welles, L., Myocet (liposome-encapsulated doxorubicin citrate): a new approach in breast cancer therapy. *Expert Opinion on Pharmacotherapy* **2002,** *3* (12), 1739-1751.
168. Chang, H.-I.; Yeh, M.-K., Clinical development of liposome-based drugs: formulation, characterization, and therapeutic efficacy. *International Journal of Nanomedicine* **2012,** *7*, 49.
169. Ansari, L.; Shiehzadeh, F.; Taherzadeh, Z.; Nikoofal-Sahlabadi, S.; Momtazi-Borojeni, A.; Sahebkar, A.; Eslami, S., The most prevalent side effects of pegylated liposomal doxorubicin monotherapy in women with metastatic breast cancer: a systematic review of clinical trials. *Cancer Gene Therapy* **2017,** *24* (5), 189-193.
170. Anselmo, A. C.; Mitragotri, S., Nanoparticles in the clinic: An update. *Bioengineering & Translational Medicine* **2019,** *4* (3), e10143.
171. Seetharamu, N.; Kim, E.; Hochster, H.; Martin, F.; Muggia, F., Phase II study of liposomal cisplatin (SPI-77) in platinum-sensitive recurrences of ovarian cancer. *Anticancer Research* **2010,** *30* (2), 541-545.
172. Slingerland, M.; Guchelaar, H.-J.; Rosing, H.; Scheulen, M. E.; van Warmerdam, L. J.; Beijnen, J. H.; Gelderblom, H., Bioequivalence of Liposome-Entrapped Paclitaxel Easy-To-Use (LEP-ETU) formulation and paclitaxel in polyethoxylated castor oil: a randomized, two-period crossover study in patients with advanced cancer. *Clinical Therapeutics* **2013,** *35* (12), 1946-1954.
173. Pérez-Herrero, E.; Fernández-Medarde, A., Advanced targeted therapies in cancer: Drug nanocarriers, the future of chemotherapy. *European Journal of Pharmaceutics and Biopharmaceutics* **2015,** *93*, 52-79.
174. Vale, N., *Biomedical Chemistry: Current Trends and Developments*. Walter de Gruyter GmbH & Co KG: 2015.
175. Yoo, J.; Park, C.; Yi, G.; Lee, D.; Koo, H., Active targeting strategies using biological ligands for nanoparticle drug delivery systems. *Cancers* **2019,** *11* (5), 640.
176. Yan, W.; Leung, S. S.; To, K. K., Updates on the use of liposomes for active tumor targeting in cancer therapy. *Nanomedicine* **2020,** *15* (3), 303-318.
177. Dawidczyk, C. M.; Kim, C.; Park, J. H.; Russell, L. M.; Lee, K. H.; Pomper, M. G.; Searson, P. C., State-of-the-art in design rules for drug delivery platforms: lessons learned from FDA-approved nanomedicines. *Journal of Controlled Release* **2014,** *187*, 133-144.
178. Lee, J. H.; Nan, A., Combination drug delivery approaches in metastatic breast cancer. *Journal of Drug Delivery* **2012,** *2012*.
179. Fischer, B.; Kryeziu, K.; Kallus, S.; Heffeter, P.; Berger, W.; Kowol, C. R.; Keppler, B. K., Nanoformulations of anticancer thiosemicarbazones to reduce methemoglobin formation and improve anticancer activity. *RSC Advances* **2016,** *6* (61), 55848-55859.
180. Popović-Bijelić, A.; Kowol, C. R.; Lind, M. E.; Luo, J.; Himo, F.; Enyedy, É. A.; Arion, V. B.; Gräslund, A., Ribonucleotide reductase inhibition by metal complexes of Triapine (3-aminopyridine-2-carboxaldehyde thiosemicarbazone): a combined experimental and theoretical study. *Journal of Inorganic Biochemistry* **2011,** *105* (11), 1422-1431.

7 PUBLICATION AND MANUSCRIPT

7.1 Improving the Stability of EGFR Inhibitor Cobalt(III) Prodrugs

Marlene Mathuber[a], Hemma Schueffl[b], Orsolya Dömötör[c,d], Claudia Karnthaler[a], Éva A. Enyedy[c,d], Petra Heffeter[b,e], Bernhard K. Keppler[a,e] and Christian R. Kowol[a,e,*]

Inorganic Chemistry, published on November 21st, 2020

[a] Institute of Inorganic Chemistry, Faculty of Chemistry, University of Vienna, Waehringer Straße 42, 1090 Vienna, Austria

[b] Institute of Cancer Research and Comprehensive Cancer Center, Medical University of Vienna, Borschkegasse 8A, 1090 Vienna, Austria

[c] Department of Inorganic and Analytical Chemistry, University of Szeged, Dóm tér 7, H-6720 Szeged, Hungary

[d] MTA-SZTE Lendület Functional Metal Complexes Research Group, University of Szeged, Dóm tér 7, H-6720 Szeged, Hungary

[e] Research Cluster ''Translational Cancer Therapy Research'', University of Vienna and Medical University of Vienna, 1090 Vienna, Austria

* Corresponding author. E-mail address: christian.kowol@univie.ac.at

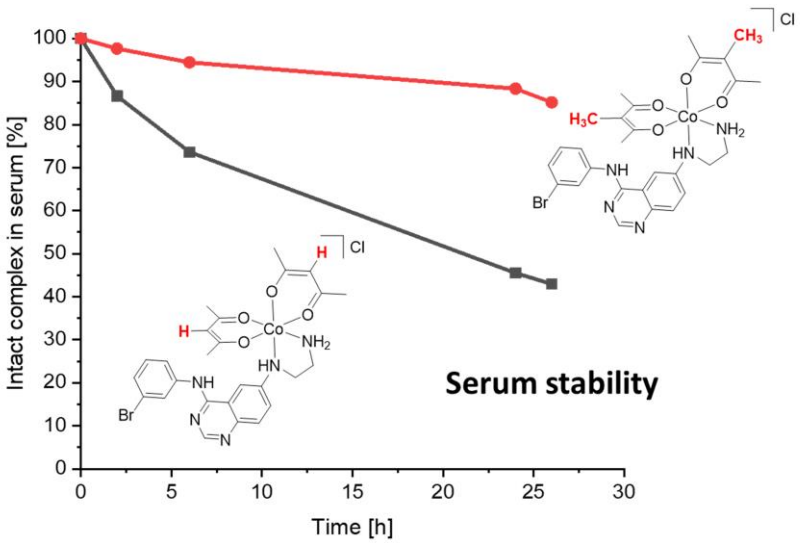

As the first author, I (re)synthesized and characterized all compounds, determined their fluorescence properties, investigated their reduction potential, evaluated their stability under biological relevant conditions and wrote the majority of the manuscript.

Inorganic Chemistry

pubs.acs.org/IC Article

Improving the Stability of EGFR Inhibitor Cobalt(III) Prodrugs

Marlene Mathuber, Hemma Schueffl, Orsolya Dömötör, Claudia Karnthaler, Éva A. Enyedy, Petra Heffeter, Bernhard K. Keppler, and Christian R. Kowol*

Cite This: *Inorg. Chem.* 2020, 59, 17794–17810

Read Online

ACCESS | Metrics & More | Article Recommendations | Supporting Information

ABSTRACT: Although tyrosine kinase inhibitors (TKIs) have revolutionized cancer therapy in the past two decades, severe drawbacks such as strong adverse effects and drug resistance limit their clinical application. Prodrugs represent a valuable approach to overcoming these disadvantages by administration of an inactive drug with tumor-specific activation. We have recently shown that hypoxic prodrug activation is a promising strategy for a cobalt(III) complex bearing a TKI of the epidermal growth factor receptor (EGFR). The aim of this study was the optimization of the physicochemical properties and enhancement of the stability of this compound class. Therefore, we synthesized a series of novel derivatives to investigate the influence of the electron-donating properties of methyl substituents at the metal-chelating moiety of the EGFR inhibitor and/or the ancillary acetylacetonate (acac) ligand. To understand the effect of the different methylations on the redox properties, the newly synthesized complexes were analyzed by cyclic voltammetry and their behavior was studied in the presence of natural low-molecular weight reducing agents. Furthermore, it was proven that reduction to cobalt(II) resulted in a lower stability of the complexes and subsequent release of the coordinated TKI ligand. Moreover, the stability of the cobalt(III) prodrugs was investigated in blood serum as well as in cell culture by diverse cell and molecular biological methods. These analyses revealed that the complexes bearing the methylated acac ligand are characterized by distinctly enhanced stability. Finally, the cytotoxic activity of all new compounds was tested in cell culture under normoxic and various hypoxic conditions, and their prodrug nature could be correlated convincingly with the stability data. In summary, the performed chemical modifications resulted in new cobalt(III) prodrugs with strongly improved stabilities together with retained hypoxia-activatable properties.

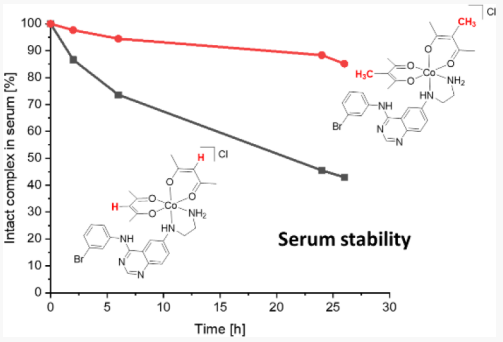

INTRODUCTION

The epidermal growth factor receptor (EGFR) belongs to the family of receptor tyrosine kinases, a group of proteins that are responsible for numerous signal transduction processes in the human body (e.g., cell growth, differentiation, and metabolism).[1] Hence, an overexpression of the EGFR can be observed in various types of solid tumors, including those of lung, head and neck, ovary, breast, and colon.[2,3] Especially in non-small-cell lung cancer (NSCLC), which is still one of the leading causes of cancer-related deaths worldwide, the EGFR is overexpressed in at least 50% of the patients.[4] Moreover, "activating mutations" of the EGFR protein have been observed in ≤20% of the patients, which results in a permanent activation of this signaling pathway.[5] As such, cancer cells are highly dependent on the respective growth signals and the development of EGFR inhibitors as targeted therapeutics has been of great interest over the past two decades. As a result of this intensive research, several small-molecule or antibody inhibitors targeting the EGFR have been clinically developed mainly for NSCLC treatment.[6] The mode of action of low-molecular weight EGFR tyrosine kinase inhibitors (TKIs) is the (ir)reversible binding into the ATP-binding pocket, which hampers the activation of the downstream signaling [e.g., phosphorylation of extracellular signal-regulated kinases (ERKs)].[7] The clinically approved EGFR TKIs comprise gefitinib (Iressa, 2003), erlotinib (Tarceva, 2004), afatinib (Gilotrif, 2013), and osimertinib (Tagrisso, 2017), which are all used for the treatment of NSCLC.[6] In addition, erlotinib (in combination with gemcitabine) is approved for advanced and metastatic pancreatic cancer.[8]

Unfortunately, besides the rapid development of drug resistance, EGFR- targeting TKIs in clinical application found their limitations in insufficient tumor accumulation and induction of side effects such as severe papulopustular skin rashes, gastrointestinal-related adverse events, or fatigue.[9] It is noteworthy that the intensity of these observed "on-target" adverse effects directly correlates with therapy response.[10,11] Thus, patients suffering from the most severe side effects (and consequently most likely to have to discontinue therapy) are the

Received: October 16, 2020
Published: November 21, 2020

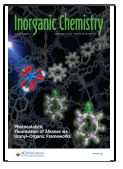

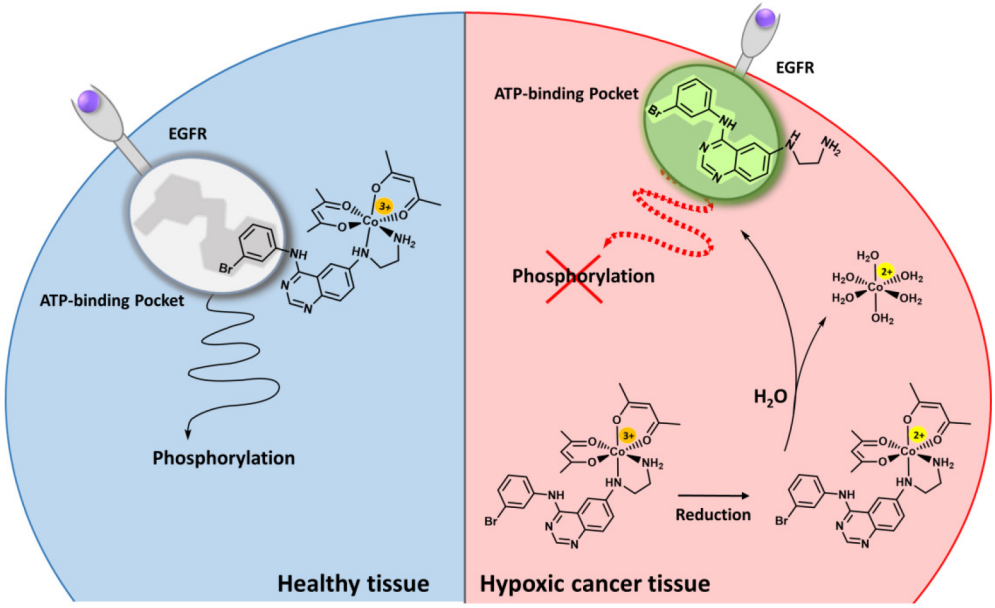

Figure 1. Proposed mechanism of the hypoxia-activated cobalt(III) prodrug system. In healthy tissue (left), the cobalt(III) complex is too bulky to fit into the ATP-binding pocket of the EGFR and is therefore biologically inactive. In the hypoxic environment of the tumor (right) an irreversible reduction takes place. This results in the release of the TKI ligand with formation of cobalt(II) species {$[Co(H_2O)_6]^{2+}$ and mixed acac/H_2O complexes} and subsequent inhibition of EGFR-downstream signaling.

Scheme 1. Chemical Structures of EGFR Inhibitor Ligands L and MeL as well as Cobalt(III) Complexes $Co(acac)_2L^+$, $Co(Meacac)_2L^+$, $Co(acac)_2MeL^+$, and $Co(Meacac)_2MeL^+$

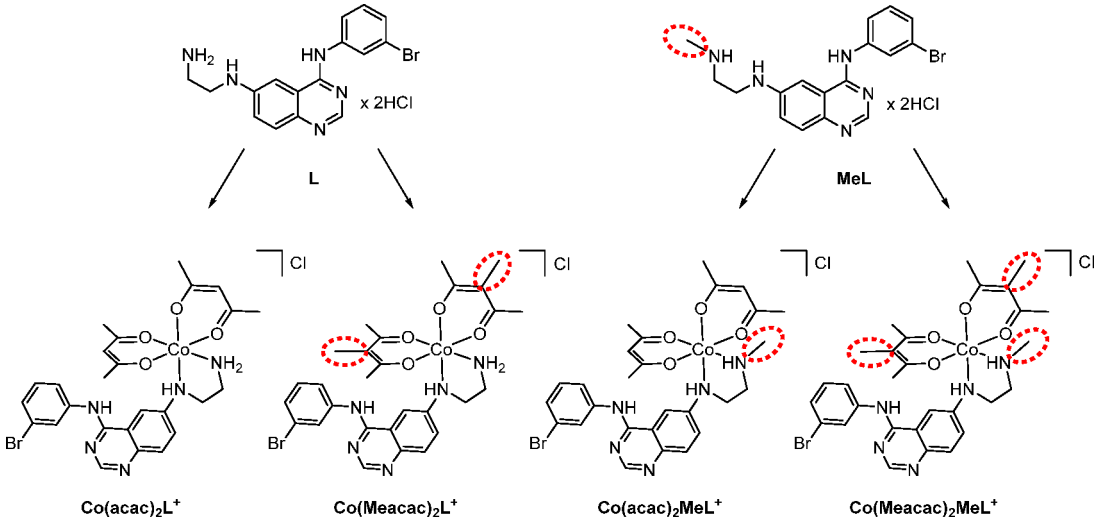

ones who would benefit most from EGFR inhibitor treatment.[10] Because adverse effects usually arise from a lack of tumor specificity, the use of prodrug systems is a promising approach to overcoming these drawbacks. Anticancer prodrugs are defined as inactivated (nontoxic) derivatives of drugs, which ideally release their active moiety at the desired site of action (e.g., tumors) by specific activation.[12] Cancer tissue distinguishes itself from the healthy surroundings in different ways.[13] One well-researched example is the occurrence of hypoxic areas in solid tumors caused by insufficient blood supply based on their uncontrolled and fast growth.[14,15] To exploit these tumor characteristics, several substance classes of hypoxia-activated prodrugs such as nitroaromatics, quinones, transition metal complexes [especially cobalt(III) systems], and aromatic *N*-oxides have been developed. Some of these compounds [e.g., tirapazamine, TH-302 (evofosfamide), and apaziquone] have already been investigated even in clinical phase III studies; however, no representative has reached clinical approval so far.[16] Notably, for the large class of existing TKIs, only a few attempts have been made to convert them into prodrugs that can be activated under hypoxic conditions.[17−20]

With regard to metal-based drugs, cobalt complexes can be used as attractive prodrug systems due to their adjustable redox potential and well-established coordination chemistry.[21−23] Most important for this prodrug system is the kinetic inertness of octahedral cobalt(III) complexes, whereas (after a one-electron reduction) the cobalt(II) state is labile with fast ligand exchange processes.[21,24] Applying this mechanism to the hypoxic environment of a tumor, the inactive prodrug will undergo an irreversible reduction in the hypoxic tissue with

https://dx.doi.org/10.1021/acs.inorgchem.0c03083
Inorg. Chem. 2020, 59, 17794−17810

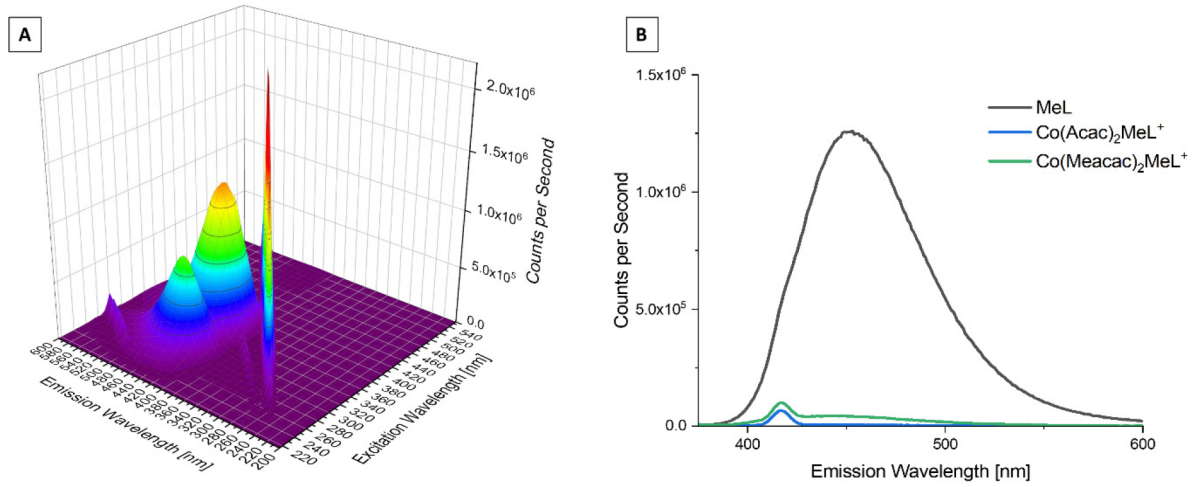

Figure 2. (A) 3D full excitation−emission landscape of **MeL** (Rayleigh scattering of first and second order appears as diagonal ridges). (B) Fluorescence emission spectra at a λ_{ex} of 365 nm of **MeL**, **Co(acac)$_2$MeL$^+$**, and **Co(Meacac)$_2$MeL$^+$** (the peaks at 420 nm are caused by Raman scattering[28]). All measurements were performed in PBS at pH 7.40 (30 μM ligand, 30 μM complex, and 25.0 °C).

subsequent ligand release. In contrast, in healthy tissues the complex is stable, preventing the ligand from exerting its biological activity. It is noteworthy that Ware et al. already showed that in the case of monodentate aziridine ligands, the cobalt(II) complexes do not have sufficient stability under normoxic conditions. Consequently, bidentate chelating ligands are preferred for the design of novel prodrug complexes.[21] We have recently successfully developed the first cobalt(III)-based prodrug [**Co(acac)$_2$L$^+$**] for a new EGFR inhibitor (denoted as **L**)[17] (Figure 1). Notably, the potential of this new compound class could be observed in several cancer cell models *in vitro* and demonstrated encouraging results *in vivo* using xenograft tumor models in mice. However, subsequent investigations showed only moderate stability of the complex toward reduction in blood serum. Consequently, the aim of this study was to further improve this substance class by decreasing the cobalt redox potential leading to higher stability. Therefore, we synthesized several novel derivatives, evaluated their properties (electrochemical potential, interaction with natural reducing agents, and serum stability), and correlated them with their cytotoxic activity against cancer cell lines.

RESULTS AND DISCUSSION

Synthesis and Characterization. To design an EGFR inhibitor that can coordinate to cobalt(III), we used in our previous study the typical quinazoline ring of most approved EGFR inhibitors but modified the 6 position by introducing an ethylenediamine ("en") type metal-binding moiety [**L** (Scheme 1)].[17] Reaction with Na[Co(acac)$_2$(NO$_2$)$_2$] (acac = acetylacetonate) yielded the cobalt(III) EGFR inhibitor ternary complex **Co(acac)$_2$L$^+$**. To develop derivatives with lower redox potentials and consequently higher expected (blood plasma) stabilities, we followed two strategies: (1) introduction of an electron-donating methyl group at the "en" moiety (**MeL**) and/or (2) using methylacetylacetone (Meacac) instead of acac as the ancillary ligand.

MeL was synthesized using *N*-(3-bromophenyl)quinazoline-4,6-diamine, *N*-Boc-(methylamino)-acetaldehyde, and sodium cyanoborohydride. After deprotection with HCl, **MeL** could be obtained in ∼80% yield as a dihydrochloride salt. The cobalt(III) complexes were synthesized by reaction of Na[Co(acac)$_2$(NO$_2$)$_2$] or Na[Co(Meacac)$_2$(NO$_2$)$_2$] with **L** or **MeL** in a water/methanol mixture in the presence of activated charcoal following a procedure described by Denny et al.[21] (Scheme 1). Finally, addition of brine to the reaction mixture resulted in the precipitation of the complex as a chloride salt. Afterward, the crude product was purified by reversed-phase high-performance liquid chromatography (HPLC) (without addition of acids to the eluent to avoid a counter ion exchange). The novel compounds were characterized by mass spectrometry, ^{1}H and ^{13}C one- and two-dimensional nuclear magnetic resonance (NMR) spectroscopy, and elemental analysis.

Of note are especially the NMR spectra of the cobalt(III) complexes. In the case of **Co(acac)$_2$L$^+$**[17] and **Co(Meacac)$_2$L$^+$**, two independent signal sets can be observed, belonging to two pairs of diastereomers (Figure S1 and ref 17). The two stereogenic centers originate from the propeller chirality of the complex itself and the anilinic NH group. In the case of methylated ligand **MeL**, an additional stereocenter is formed,[25,26] resulting in four sets of signals for complexes **Co(acac)$_2$MeL$^+$** and **Co(Meacac)$_2$MeL$^+$** (Figures S2 and S3). The presence of these isomers can be easily seen in the ^{1}H NMR spectra, where depending on the complex, two or four separated singlets of the NH group appear (Figure S4). However, especially in the aromatic area and within the "en" bridge the protons tend to overlap. Therefore, an exact assignment of all NMR signals could not be achieved (see Experimental Section). Isolation of pure diastereomers by reversed-phase HPLC was not possible, because the product peaks could not be separated (also a change in the gradient or solvent and the addition of formic acid did not result in sufficient separation).

Fluorescence Properties. In our previous work,[17] we showed that EGFR inhibitor ligand **L** possesses distinct fluorescence properties with an emission maximum at 455 nm upon irradiation at 370 nm. This fluorescence is completely quenched by coordination to the cobalt(III) ion [**Co(acac)$_2$L$^+$**]. Therefore, we also examined the fluorescence of **MeL** and the novel complexes in phosphate-buffered saline (PBS) at pH 7.40. The three-dimensional (3D) spectrum of **MeL** (Figure 2A) is similar in intensity and maxima (λ_{em} = 455 nm, and λ_{ex} = 365 nm) compared to **L**. In agreement to our previous data, the fluorescence of all cobalt(III) complexes is negligible, most probably due to the metal center, resulting in extremely fast intersystem crossing rates in the excited state[27] [Figure 2B for

https://dx.doi.org/10.1021/acs.inorgchem.0c03083
Inorg. Chem. 2020, 59, 17794−17810

$Co(acac)_2MeL^+$ and $Co(Meacac)_2MeL^+$]. Therefore, we could exploit the fluorescence properties for stability studies of the complexes.

Lipophilicity. The first physicochemical property we investigated was the lipophilicity of the complexes, because it is a critical parameter for passing biological membranes. Distribution coefficients ($D_{7.4}$) presented in Table 1 were determined by the traditional shake-flask method in an *n*-octanol/buffered aqueous solution at physiological pH. All compounds containing an EGFR inhibitor ligand (**L** or **MeL**) show highly lipophilic character, despite the positive charge of the complexes. As expected, the methylated compounds are more lipophilic than $Co(acac)_2L^+$ (Table 1). However, all complexes still show good water solubility. The active EGFR inhibitor ligand **L** itself proved to be highly lipophilic ($logD_{7.40}$ = 1.86).[29] Therefore, the lipophilic character of the complexes is mainly based on the coordinating EGFR inhibitor ligand and just slightly modulated by the attachment of the cobalt-(methyl)acetylacetonato fragment [the simple model complex $Co(acac)_2en^+$ is very hydrophilic with a log $D_{7.40}$ value of −1.86]. The highly lipophilic character of the complexes apparently contradicts the relatively good water solubility (0.5−1.0 mM in water or PBS). Variation of the composition of the aqueous phase in the case of $Co(acac)_2L^+$ revealed a strong dependence of the distribution coefficient on the ion content of the aqueous solution (see footnote of Table 1). This phenomenon refers to ion pair formation taking place between the single positively charged complex and anions like Cl^- and $H_2PO_4^-$ present in the buffer system. Distribution coefficients determined in 20 mM phosphate and 0.1 M KCl probably represent best the lipophilicity of the complexes under physiological conditions.

These results are in line with HPLC measurements, where the retention time of the complexes increases with the number of methyl substituents resulting in the following order: $Co(acac)_2L^+$ < $Co(acac)_2MeL^+$ < $Co(Meacac)_2L^+$ < $Co(Meacac)_2MeL^+$.

Cyclic Voltammetry. As the reduction process is crucial for the activation of cobalt(III)-based prodrug systems, the redox properties of the complexes were investigated to elucidate the effects of ligand methylation at different positions. Cyclic voltammetry measurements were performed in aqueous solution at pH 7.40 (10 mM phosphate buffer with 0.1 M KCl). The voltammograms at a scan speed of 30 mV/s showed a single irreversible cathodic peak in the range of 4−120 mV versus the normal hydrogen electrode (NHE), which can be assigned to the reduction of cobalt(III) to cobalt(II) (Figure 3).

Table 1. Distribution Coefficients ($D_{7.40}$) of the Complexes at pH 7.40 [T = 25.0 °C, and I = 0.1 M (KCl)]

complex	log $D_{7.40}$
$Co(acac)_2L^+$[a]	1.59 ± 0.06
$Co(Meacac)_2L^+$	2.24 ± 0.04
$Co(acac)_2MeL^+$	2.05 ± 0.17
$Co(Meacac)_2MeL^+$	>2.7
$Co(acac)_2en^+$	−1.86 ± 0.05
L	1.86 ± 0.03[29]

[a]Distribution coefficients measured under different conditions: log D = −0.55 ± 0.01 (water, pH ~6.5), −0.09 ± 0.03 [20 mM phosphate buffer (pH 7.40)], and 2.22 ± 0.03 [20 mM phosphate buffer and 0.58 M KCl (pH 7.40)].

Also, at a much higher scan speed of 1000 mV/s, the redox processes were still completely irreversible (Figure S5).

Compared to reference compound $Co(acac)_2L^+$ with a cathodic peak at 62 mV versus NHE, the methylation of the acac ligand $Co(Meacac)_2L^+$ resulted in the desired lower cathodic peak potential at 4 mV versus NHE. This trend is also in agreement with literature data of cobalt(III) prodrug systems containing nitrogen mustard ligands.[21] In contrast to the expectations, methylation of the "en" moiety of the EGFR inhibitor ligand $Co(Meacac)_2MeL^+$ did not further decrease the reduction potential but resulted in a slightly higher cathodic potential (17 mV vs NHE). Analogously, $Co(acac)_2MeL^+$ also showed an increased potential (120 mV vs NHE) compared to that of $Co(acac)_2L^+$ (62 mV vs NHE).

Notably, the reduction potential of reference compound $Co(acac)_2en^+$ was distinctly lower with a value of −141 mV versus NHE even compared to the most promising representative of the EGFR inhibitor-containing complexes, $Co(Meacac)_2L^+$, at 4 mV versus NHE. To verify that the adjacent aromatic moiety of the quinazoline is responsible for this shift and that methylation of the "en" moiety indeed increases the redox potential, additional model complexes were synthesized (Figure 4): (1) $Co(acac)_2PhEn^+$ to determine the influence of the phenyl moiety and (2) $Co(Meacac)_2en^+$, $Co(acac)_2MeEn^+$, and $Co(Meacac)_2MeEn^+$ to confirm the shifts of the cathodic peak potential as a result of the different methylations (MeEn = *N*-methylethylenediamine; PhEn = *N*-phenylethylenediamine). The synthesis of the complexes followed a similar procedure as described above, and the only difference was the use of ammonium hexafluorophosphate for precipitation of the complexes (see details in the Experimental Section).

Indeed, cyclic voltammetric measurements performed for $Co(acac)_2PhEn^+$ showed a strong shift of the cathodic peak potential to 49 mV in comparison to that of $Co(acac)_2en^+$ at −141 mV (Figure 4). This can be explained by the electron-withdrawing effect of the phenyl ring, which distinctly increases the redox potential of the cobalt center. With regard to the methylations at the "en" versus the acac moiety, the model complexes confirmed (even more pronounced) the tendencies observed for the EGFR inhibitor-containing complexes [except $Co(acac)_2MeEn^+$ with a slightly lower E_c value]. The introduction of the methylated acac moiety led to a significantly

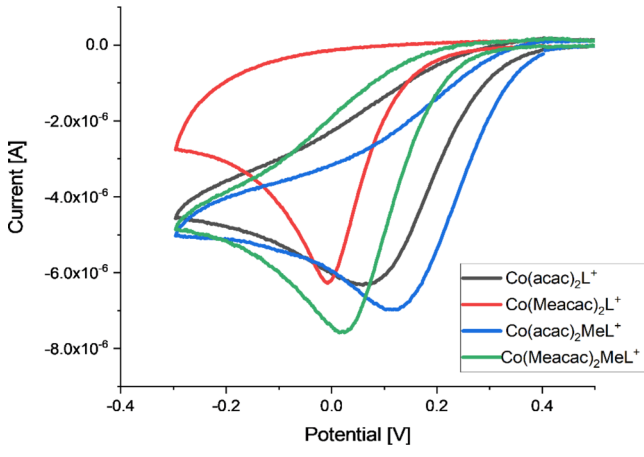

Figure 3. Cyclic voltammograms of $Co(acac)_2L^+$, $Co(Meacac)_2L^+$, $Co(acac)_2MeL^+$, and $Co(Meacac)_2MeL^+$ in 10 mM phosphate buffer (pH 7.40) (1.5 mM complex, I = 0.10 M KCl, scan rate of 30 mV/s, 25.0 °C). Potentials are referenced to the NHE.

https://dx.doi.org/10.1021/acs.inorgchem.0c03083
Inorg. Chem. 2020, 59, 17794−17810

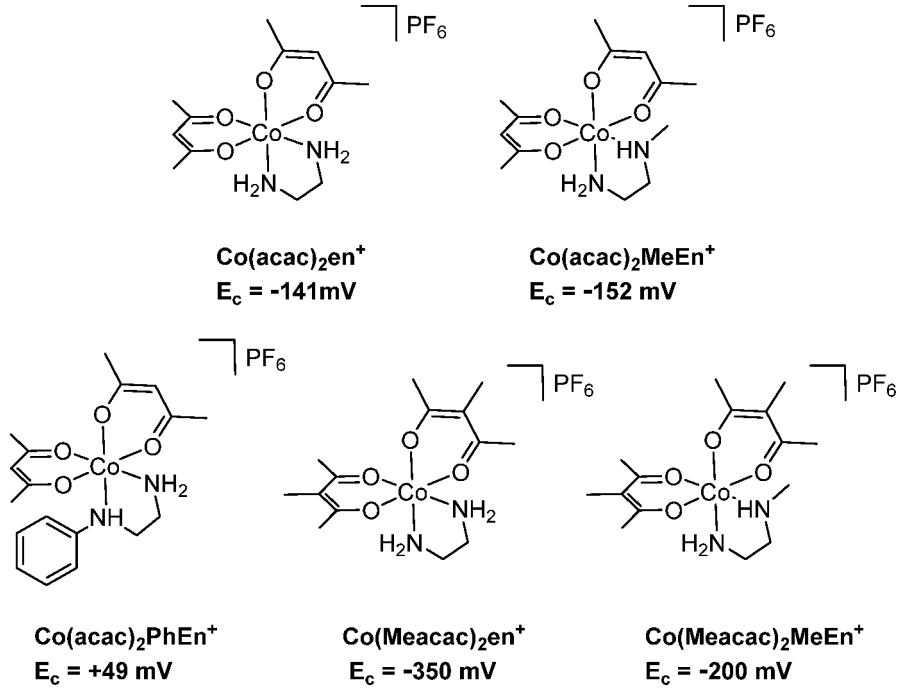

Figure 4. Cobalt(III) model complexes synthesized to investigate the effect of the methyl and phenyl substitution at the "en" and/or acac moiety. E_c is the cathodic peak potential vs NHE of the cobalt complexes measured at a scan rate of 30 mV/s in 10 mM phosphate buffer (pH 7.4).

Table 2. Proton Dissociation Constants (K_a) of Hacac as well as Fully Protonated MeEn and PhEn Together with the Overall Stability Constants (β) for the Binary and Ternary Cobalt(II) Complexes Determined by pH-Potentiometric Measurements[a]

	acac (A)		MeEn (B)	PhEn (B)
pK_{a1}	8.80 ± 0.01[b]	pK_{a1}	7.04 ± 0.02	1.85 ± 0.01[c]
pK_{a2}	–	pK_{a2}	9.98 ± 0.01	9.34 ± 0.01[c]
		Log β Values of the Binary Complexes[c]		
$[Co(II)L]^+$	5.05 ± 0.02[b]	$[Co(II)L]^{2+}$	5.26 ± 0.01	3.63 ± 0.05
$[Co(II)L_2]^0$	8.66 ± 0.05[b]	$[Co(II)L_2]^{2+}$	9.15 ± 0.02	6.75 ± 0.09
$[Co(II)L_3]^-$	–	$[Co(II)L_3]^{2+}$	12.94 ± 0.04	–
		Log β Values of the Ternary Complexes		
		$[Co(II)AB]^+$	9.82 ± 0.05	8.03 ± 0.15
		$[Co(II)A_2B]^0$	12.73 ± 0.09	12.08 ± 0.09
		$[Co(II)AB_2]^+$	13.20 ± 0.12	11.29 ± 0.13

[a]In ternary (mixed-ligand) complexes, "A" denotes acac and "B" denotes MeEn or PhEn [25.0 °C; I = 0.1 M (KCl)]. [b]Reported data for the cobalt(II) acac system: pK_{a1} = 8.83, log β[CoL] = 5.10, and log β[CoL_2] = 9.08 (25 °C; I = 0.1 M $NaClO_4$).[40] [c]pK_a values of 1.76 ± 0.03 and 9.42 ± 0.03, and 1.73 ± 0.03 and 9.37 ± 0.03, determined by ultraviolet−visible and spectrofluorometric titrations, respectively.

decreased reduction potential, whereas the methylation of the "en" ligand showed the opposite effect. Therefore, in the case of **Co(Meacac)$_2$MeEn$^+$**, the influence of the methylated acac moiety is widely annihilated by the methylation of "en".

Notably, all reduction processes were completely irreversible independent of the scan speed (30−1000 mV/s). In the literature, the proposed mechanism for cobalt(III) prodrugs usually comprises that in healthy tissues, which are provided with a sufficient supply of oxygen, and after the reduction to cobalt(II), an immediate re-oxidation step occurs, regenerating the inert cobalt(III) complex.[23,30] However, at the same time for most of the cobalt(III) complexes in the literature, the redox process in an aqueous solution is completely irreversible.[31−34] This is in line with pulse radiolysis studies also revealing that the re-oxidation rates under normoxic conditions are too slow.[35] Instead, competition between oxygen and the cobalt(III) complexes for one-electron reductants was suggested. Interestingly, despite this irreversibility, e.g., cobalt(III) nitrogen mustard complexes showed promising hypoxia selective anticancer activity.[32] In particular, Ware et al. tried to optimize the electrochemical properties of cobalt(III) prodrug systems, resulting in (partially) reversible complexes with highly hypoxia selective activity against cancer cells.[36] Unfortunately, their lead compound did not show significant activity in a mouse model. However, as our compound class, which displays irreversible electrochemical properties, also possesses hypoxia-dependent anticancer activity in a mouse model,[17] this indicates that the irreversibility of the reduction process does not interfere with the in vivo effectiveness. Therefore, it is currently unknown how the exact mechanism of the hypoxic selectivity of cobalt(III) complexes works and which electrochemical properties are ideal.

Aqueous Solution Stability of the Formed Cobalt(II) Complexes. After reductive activation of the cobalt(III) prodrugs, it is essential to investigate whether the formed cobalt(II) complexes indeed can release the coordinated targeting ligand. For this reason, we selected two ternary

https://dx.doi.org/10.1021/acs.inorgchem.0c03083
Inorg. Chem. 2020, 59, 17794−17810

systems as models to study the potential liberation of the (N,N) ligand from the mixed-ligand cobalt complex upon reduction. Thus, the aqueous stability of several cobalt(II) complexes was investigated under strictly anaerobic conditions. Due to the limited water solubility of cobalt(II) chloride complexes with **L**, model ligands with better solubility, namely, MeEn and PhEn, were used. First, deprotonation processes of the acetylacetone (Hacac) and the fully protonated MeEn and PhEn ligands were followed at pH 2.0−11.5 (Table 2). The calculated pK_a for Hacac of 8.80 is in good agreement with literature data (pK_a = 8.82) reported at I = 0.1 M $NaClO_4$.[37] The two pK_a values of MeEn [pK_{a1} = 7.04 ($MeNH_2^+$); pK_{a2} = 9.98 (NH_3^+)] correspond well to the deprotonation constants of the fully protonated form of "en",[38,39] but the pK_{a1} dramatically differs from that of $PhEnH_2^{2+}$ (pK_{a1} = 1.85; pK_{a2} = 9.34). The latter model ligand is quite comparable to EGFR inhibitor **L** (pK_{a1} < 1.0; pK_{a2} = 9.21) investigated in our previous work.[29]

Following the determination of the stability constants for the binary complexes (Table 2), overall stability constants for the mixed-ligand complexes formed in the cobalt(II)−acac−MeEn and cobalt(II)−acac−PhEn ternary systems were calculated on the basis of pH-potentiometric titrations. Three types of complexes were formed, $[CoAB]^+$, $[CoA_2B]$, and $[CoAB_2]^+$, where "A" denotes acac and "B" refers to MeEn or PhEn. Concentration distribution curves in Figure 5 were computed using the stability constants of the 1:2:1 cobalt(II)−acac−PhEn composition that corresponds to the reduced form of **Co(II)(acac)$_2$L^0**. On the basis of these data, negligible amounts (<1%) of PhEn are coordinated to cobalt(II) at pH 7.4. For the 1:2:1 cobalt(II)−acac−MeEn system, ∼11% are still coordinated to cobalt(II) at pH 7.4 (Figure S6). However, it has to be mentioned that these calculations were performed for 1 mM cobalt(II) (where the titrations were performed), and the amount of the intact ternary complex further decreases with lower concentrations [e.g., in the latter system at pH 7.4 and 0.1 mM cobalt(II), the coordinated MeEn fraction is only ∼2%].

As a conclusion, these measurements strongly support the assumption that after reduction of the cobalt(III) complexes, the respective EGFR-targeting ligand completely dissociates, which enables subsequent inhibition of the EGFR-downstream signaling.

Interaction with Natural Low-Molecular Weight Reducing Agents. Next, we investigated if common biologically relevant low-molecular weight reducing agents can reduce **Co(acac)$_2$L$^+$** or **Co(Meacac)$_2$L$^+$**. Glutathione (GSH) and reduced nicotinamide adenine dinucleotide (phosphate) (NADH/NADPH) are responsible for the redox equilibrium in the cytosol, while ascorbic acid (AA) is found in both extra- and intracellular space. Among them, NADH is the strongest reducing agent (formal potential at pH 7.0 of −0.32 V for NAD^+/NADH[41]), followed by GSH (−0.24 V for GSSG/GSH at pH 7.0[41]). For AA, usually 0.06 V for dehydro-L-ascorbate/AA at pH 7.0 is reported.[42] However, recent literature also suggests even higher values in the range of 0.35−0.50 V.[43,44] GSH is produced in cells at concentrations (1−10 mM) at least one order of magnitude higher than those of NADH (30−100 μM).[45,46]

The interaction of AA, GSH, and NADH at pH 7.40 (phosphate buffer) was investigated exemplarily for **Co(acac)$_2$L$^+$** and **Co(Meacac)$_2$L$^+$**. The reaction was followed by ultraviolet−visible (UV−vis) and fluorometric detection at 25 °C with a 10-fold excess of reducing agent. Spectrofluorometry was proven to be an effective technique for monitoring this redox reaction, because the free EGFR inhibitor ligand **L** is highly fluorescent, while its cobalt(III) complex has negligible emission (*vide supra*).[17] Accordingly, an increase in the emission intensity is expected upon reduction and concomitant release of the free ligand. Figure 6 indicates practically no reduction process of **Co(Meacac)$_2$L$^+$** in the presence of 10 equiv of GSH, and no significant amount of free **L** appeared in samples even after 24 h. The same tendency was observed by UV−vis detection (data not shown). For **Co(acac)$_2$L$^+$**, again no liberation of the active ligand could be detected within 24 h. AA and NADH were also not able to reduce the two complexes even after 24 h. These data show that the complexes are highly stable in aqueous solution and biologically relevant low-molecular weight non-enzymatic reducing agents are not responsible for the reduction of the cobalt(III) complexes. For other hypoxia-activatable drugs like tirapazamine and its second-generation analogue SN30000, P450 oxidoreductases (POR) have been proposed as proteins responsible for reduction.[47] However, Ware and co-workers[36] and Wilson and co-workers[48] showed for different types of cobalt(III) complexes that the cytotoxicity did not change in cells overexpressing POR

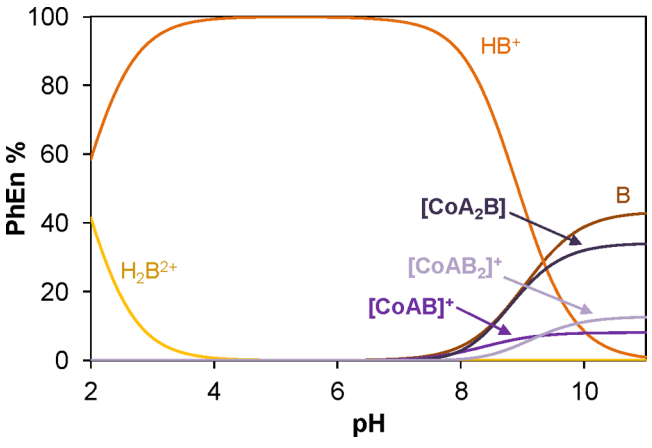

Figure 5. Concentration distribution diagram for the 1:2:1 cobalt(II)−acac−PhEn system. A = acac; B = PhEn [1 mM cobalt(II); I = 0.10 M (KCl); 25.0 °C].

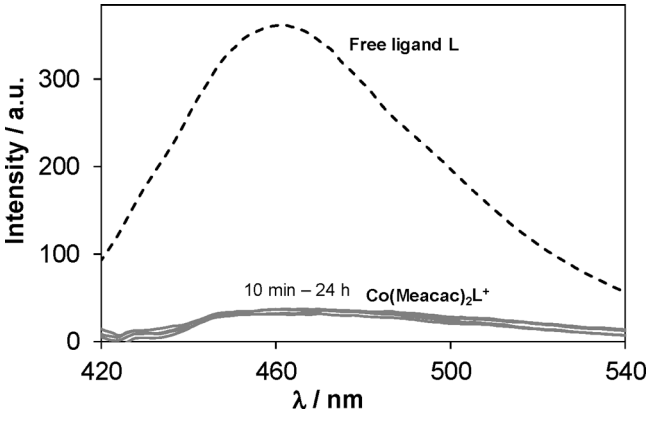

Figure 6. Fluorescence emission spectra of **Co(Meacac)$_2$L$^+$** in the presence of 10 equiv of GSH followed for 24 h. The dashed spectrum corresponds to the emission spectrum of free EGFR inhibitor **L** [$c_{complex}$ = 15 μM; $c_{free\ ligand}$ = 15 μM; λ_{EX} = 350 nm; pH 7.40 (10 mM phosphate buffer and 0.1 M KCl); 25.0 °C].

https://dx.doi.org/10.1021/acs.inorgchem.0c03083
Inorg. Chem. 2020, 59, 17794−17810

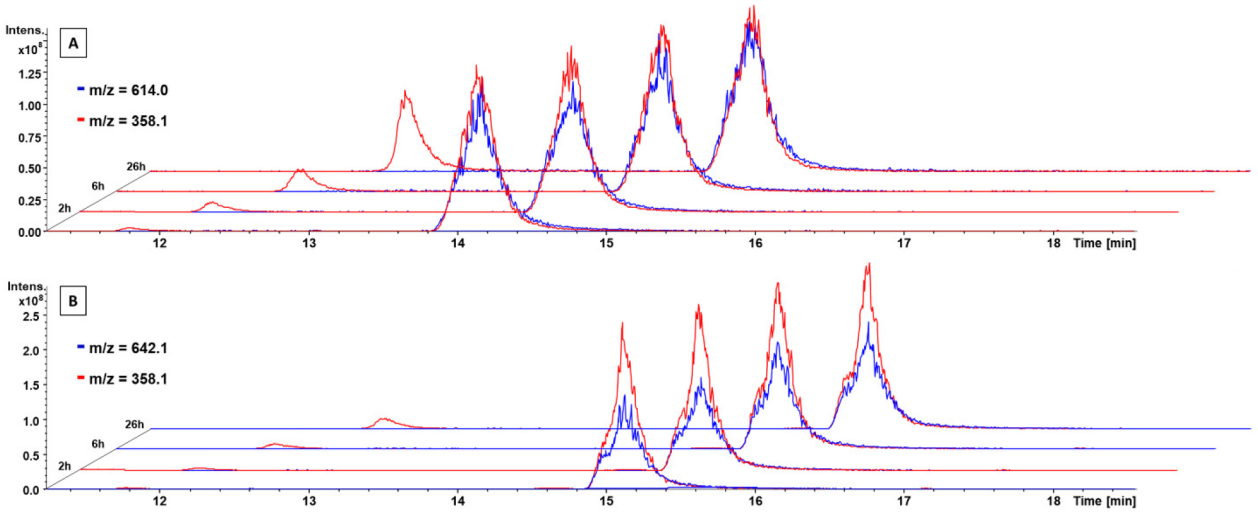

Figure 7. Time-dependent stability of (A) $\mathbf{Co(acac)_2L^+}$ and (B) $\mathbf{Co(Meacac)_2L^+}$ incubated in FCS at 37 °C (pH 7.4, 150 mM phosphate buffer) and analyzed by HPLC–mass spectrometry (depicted are the extracted ion mass chromatograms). Due to the different ionization properties, the intensities of the free ligand (m/z 358.1) and cobalt(III) complexes (m/z 614.0 or 642.1) cannot be directly compared.

compared to the parental cell line. Therefore, the actual reducing molecules or reductase(s) are still unknown.

Serum Stability. The data presented in the previous sections indicate that even in the presence of low-molecular weight reducing agents the cobalt(III) complexes are completely stable. Therefore, we wanted to investigate if this is still true in a more elaborate biological environment like blood serum. To this end, the four EGFR inhibitor complexes were dissolved in 50 mM phosphate puffer and mixed in a 1:10 ratio with fetal calf serum (FCS; buffered with 150 mM phosphate buffer to keep a stable pH of 7.4) to a final concentration of 50 μM. The samples were incubated at 37 °C and after 0, 2, 6, 24, and 26 h extracted with acetonitrile and measured by HPLC-MS. The extracted ion mass chromatogram of $\mathbf{Co(acac)_2L^+}$ clearly showed the time-dependent release of the free EGFR inhibitor (Figure 7A; red peak at 11.8 min, m/z 358.1). The intact complex could be observed at 14.2 min (blue peak, m/z 614.0). The red signal at the same retention time (Figure 7A; 14.2 min, m/z 358.1) is a mass spectrometry artifact and belongs to the free ligand generated during ionization of the complex. In contrast, the mass spectra of $\mathbf{Co(Meacac)_2L^+}$ incubated in serum revealed much smaller amounts of the released ligand (Figure 7B).

The same trend was observed for $\mathbf{Co(acac)_2MeL^+}$ and $\mathbf{Co(Meacac)_2MeL^+}$ (Figure S7). Therefore, in this experiment, a distinct increase in the stability in the presence of the Meacac ligand could be observed in both complexes with ~85% intact compound after serum incubation for 26 h at 37 °C. The stability of these complexes was much higher than that of $\mathbf{Co(acac)_2L^+}$ and $\mathbf{Co(acac)_2MeL^+}$, having only 43% and 50% intact compound after 26 h, respectively (Figure 8). In general, these results are in accordance with the cyclic voltammetry measurements, where $\mathbf{Co(Meacac)_2L^+}$ and $\mathbf{Co(Meacac)_2MeL^+}$ showed the lowest redox potential of the four complexes. Together, this indicates a strong influence of the methylation of acac for the stability of cobalt(III) prodrugs; however, no beneficial effect was seen in the case of methylation of the "en" moiety.

Biological Investigations. *Evaluation of the Complex Stability in the Presence of Cells under Normoxic Conditions.* As a next step, we addressed the question of whether the new derivatives are also more stable than $\mathbf{Co(acac)_2L^+}$ in the

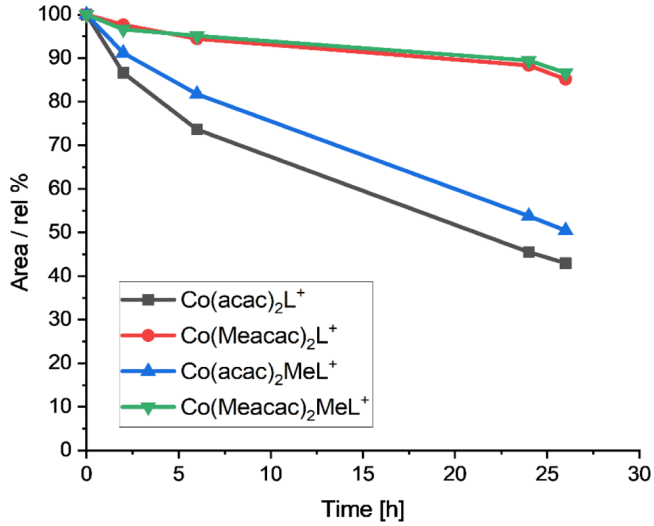

Figure 8. Stability measurements of $\mathbf{Co(acac)_2L^+}$, $\mathbf{Co(Meacac)_2L^+}$, $\mathbf{Co(acac)_2MeL^+}$, and $\mathbf{Co(Meacac)_2MeL^+}$ incubated in FCS at 37 °C (pH 7.4, 150 mM phosphate buffer) and analyzed by mass spectrometry over a period of 26 h. The y-axis shows the relative ratio of the integrated peak areas of the intact complex over time (in percent) compared to the area at the starting point (0 h).

presence of cells under normoxic cell culture conditions (medium containing 10% serum at 37 °C, 21% O_2, and 5% CO_2). Therefore, the stability of the cobalt(III) complexes was monitored indirectly by microscopy as well as flow cytometry in A431 cells by exploiting the fluorescence of released ligands **L** and **MeL**. As shown in Figure 9, the stability of the compounds bearing a Meacac ligand was distinctly increased compared to those of the acac derivatives. Consequently, while in case of the acac drugs most of the ligand was already released after 24 h (clearly visible by the blue fluorescence of the cells), the micrographs of the Meacac compounds remained widely unchanged.

This also could be confirmed by subsequently performed flow cytometry investigations (Figure 10). In detail, the evaluation of the fluorescence intensities showed that the cobalt complexation led to a 1.9–2.6-fold reduced mean fluorescence and a 4–90-

https://dx.doi.org/10.1021/acs.inorgchem.0c03083
Inorg. Chem. 2020, 59, 17794–17810

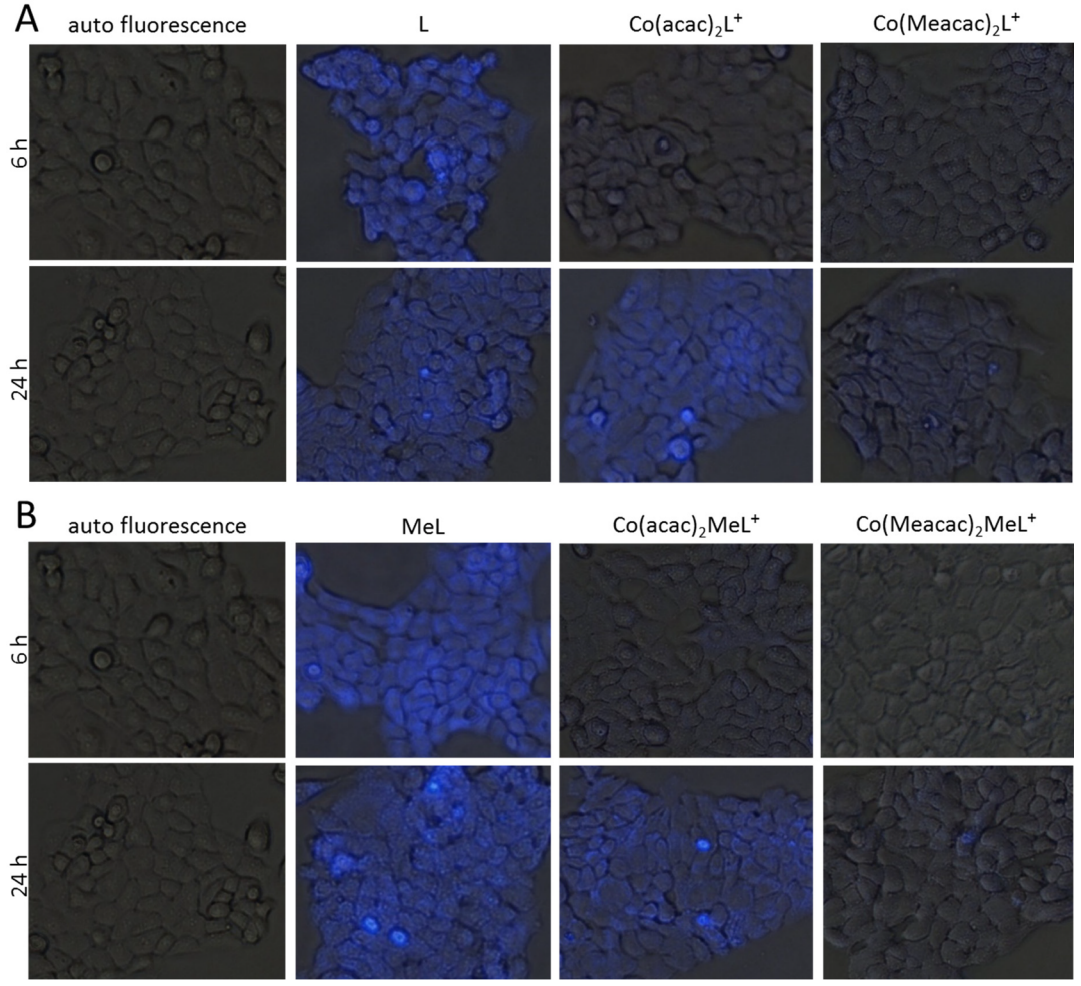

Figure 9. Fluorescence microscopic measurements indicating the release of the ligand from the different cobalt(III) complexes. Release of (A) **L** and (B) **MeL** from the different cobalt(III) complexes under normoxic cell culture conditions (37 °C, 21% O_2, and 5% CO_2) using UV fluorescence microscopy. A431 cells were incubated with 10 μM drugs for 6 or 24 h. Images are overlays of representative fluorescence and differential interference contrast microscopies (10× objective) of the different treatments processed by ImageJ software.

fold reduced number of ligand-positive cells at the 6 h time point. This is in good agreement with the already published data on **Co(acac)$_2$L$^+$**.[17] However, after incubation for 24 h 100% of cells treated with the two acac complexes became ligand-positive, resulting in a mean fluorescence similar to that of the samples treated with the free ligand. In contrast, in the samples of the Meacac-containing group, the mean fluorescence was much less affected, as the percentage of ligand-positive cells increased only from 2.2% to 18.4% and from 1% to 7.5%, in the cases of **Co(Meacac)$_2$L$^+$** and **Co(Meacac)$_2$MeL$^+$**, respectively. This indicates that in contrast to the acac-auxiliary ligand, the cobalt(III) complexes bearing a Meacac moiety are highly stable under normoxic cell culture conditions for more than 1 day.

To evaluate if cobalt complexation also prevents EGFR inhibition under normoxic conditions, Western blot analyses of the EGFR phosphorylation at position Y1068 (activating phosphorylation) as well as the activation of the EGFR downstream protein ERK 1/2 were performed. To ensure an EGFR-dependent signaling, A431 cells were serum-starved for 24 h, incubated with the indicated cobalt(III) drugs at three different concentrations for 2 h, and stimulated by EGF for 10 min prior to protein isolation (Figure 11). In agreement with our stability data, the Meacac ligand set efficiently prevented the release of both **L** and **MeL**, indicated by the distinctly weakened EGFR-inhibitory potential of **Co(Meacac)$_2$L$^+$** and **Co(Meacac)$_2$MeL$^+$** in comparison to **Co(acac)$_2$L$^+$** and **Co(acac)$_2$MeL$^+$**. The potent EGFR inhibition by free **MeL** and **L** under these conditions is shown in Figure S8 and ref 17, respectively.

Hypoxia-Dependent Cytotoxicity of the Cobalt Complexes. Finally, we wanted to evaluate whether the Meacac coordination sphere also affects the hypoxic activation of the complexes. To characterize the activity of the free EGFR inhibitor ligands, prior to the assessment of their anticancer activity in cell culture, the EGFR-inhibitory potential was investigated in a cell-free kinase inhibition assays in the presence of a 10-fold excess of ATP. The results showed that the methylation at the terminal amino group slightly reduced the EGFR inhibition potential from an IC_{50} value of 0.29 nM for **L** to a value of 0.41 nM for **MeL** (Figure S9).

Subsequently, MTT-based cytotoxicity assays of the complexes in comparison to the respective metal-free ligands were performed under different O_2 levels (21%, 5%, 1%, or 0.1%) (Table 3 and Figure 12). As expected, the two EGFR inhibitor ligands **L** and **MeL** did not show distinct differences in their anticancer activity in normoxic versus the different hypoxic conditions. However, **MeL** was approximately twice as effective as **L**. This is interesting, as the kinase assay mentioned above did

https://dx.doi.org/10.1021/acs.inorgchem.0c03083
Inorg. Chem. 2020, 59, 17794−17810

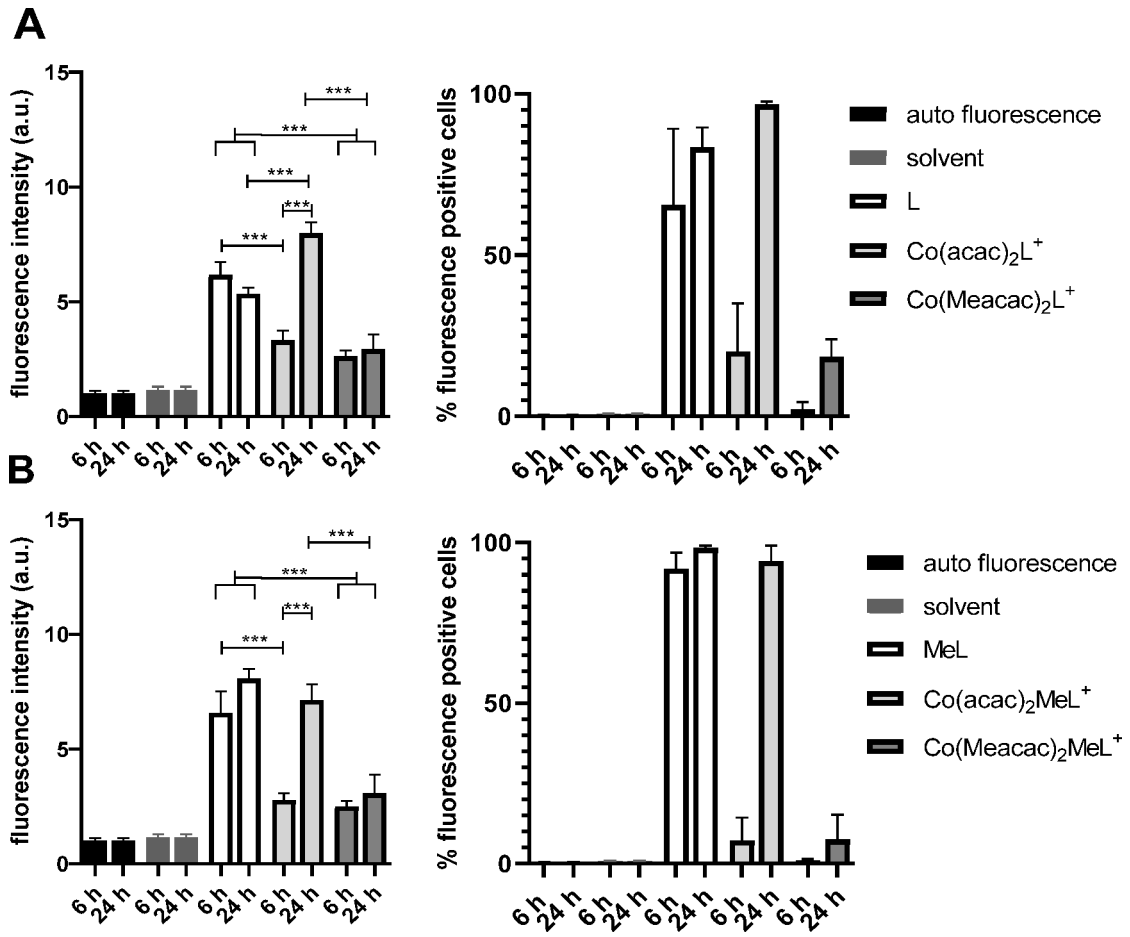

Figure 10. Release of (A) **L** or (B) **MeL** from the indicated cobalt(III) complexes under normoxic cell culture conditions (37 °C, 21% O_2, and 5% CO_2) by flow cytometry. A431 cells were incubated with 10 μM drugs for 6 or 24 h, and the fold change in fluorescence intensity (left, after normalization with fluorescence intensity of the cells) and the percent of fluorescence-positive cells (right) were evaluated using Diva Software and GraphPad Prism. Statistical significance was calculated via two-way analysis of variance with a multiple-comparison test and Bonferroni correction with $p < 0.001$ (***).

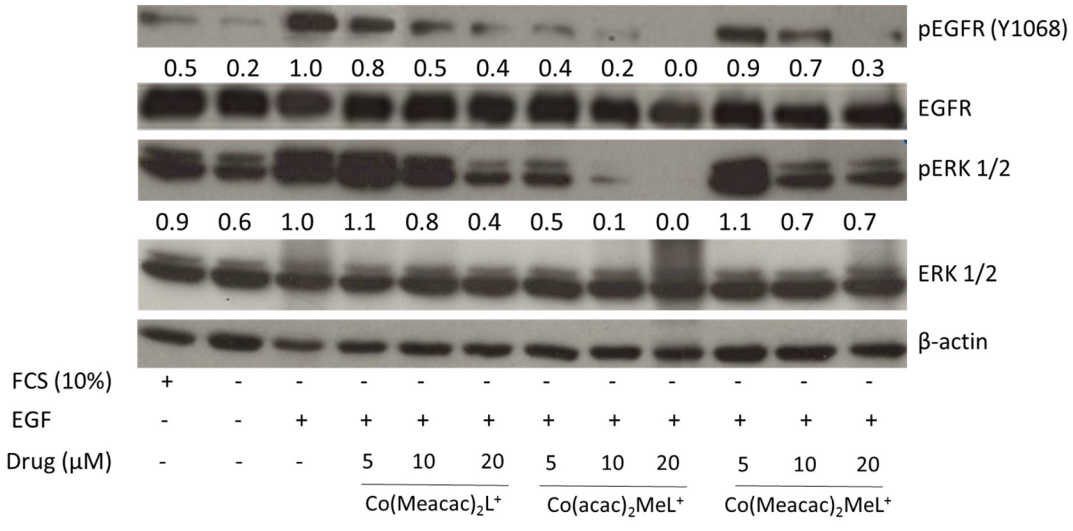

Figure 11. Impact of new cobalt(III) complexes on the EGFR signaling cascade (pEGFR, pERK 1/2) under normoxic conditions. A431 cells were grown in medium with or without FCS and treated with the indicated drug for 2 h. After EGFR stimulation with 50 ng/mL EGF for 10 min, cells were harvested, lysated, and further analyzed by Western blotting. The ratios of pEGFR or pERK 1/2 levels of the treated samples (after normalization to the loading control β-actin) to the levels of the control (−FCS and +EGF) are given below the respective bands.

https://dx.doi.org/10.1021/acs.inorgchem.0c03083
Inorg. Chem. 2020, 59, 17794−17810

Table 3. IC_{50} Values of L and MeL in Comparison to the Respective Cobalt(III) Prodrugs against A431 Cancer Cells after Treatment for 72 h under Different O_2 Levels (21% to 0.1%)[a]

	IC_{50} (μM ± SD)			
drug	normoxia	hypoxia with 5% O_2	hypoxia with 1% O_2	hypoxia with 0.1% O_2
L	12.0 ± 1.3	12.8 ± 0.9	12.7 ± 2.0	13.7 ± 2.9
MeL	6.9 ± 1.8	8.7 ± 1.2	5.5 ± 0.4	5.4 ± 0.8
$Co(acac)_2L^+$	22.9 ± 5.7[b]	18.7 ± 4.0[b]	13.4 ± 0.3	7.2 ± 1.4
$Co(Meacac)_2L^+$	51.9 ± 9.4[c,e]	45.5 ± 2.7[c]	25.3 ± 3.9	23.5 ± 5.1
$Co(acac)_2MeL^+$	15.1 ± 1.6	13.5 ± 3.2	12.5 ± 3.1	11.9 ± 3.5
$Co(Meacac)_2MeL^+$	58.6 ± 4.4[c,e]	55.2 ± 1.4[c]	32.0 ± 2.9[d]	19.9 ± 1.0
erlotinib	13.3 ± 4.7	nd	14.4 ± 4.0	nd

[a]Values are given as means ± SD of at least three independent experiments performed in triplicate. Statistical significance, between the drugs under normoxic and different hypoxic conditions, was calculated via one-way analysis of variance with a multiple-comparison test and Bonferroni correction. [b]$p < 0.01$ compared to hypoxia with 0.1% O_2. [c]$p < 0.001$ compared to hypoxia with 1% and 0.1% O_2. [d]$p < 0.05$ compared to hypoxia with 0.1% O_2. [e]$p < 0.001$ compared to the corresponding ligand and $Co(acac)_2X^+$ derivative under normoxia.

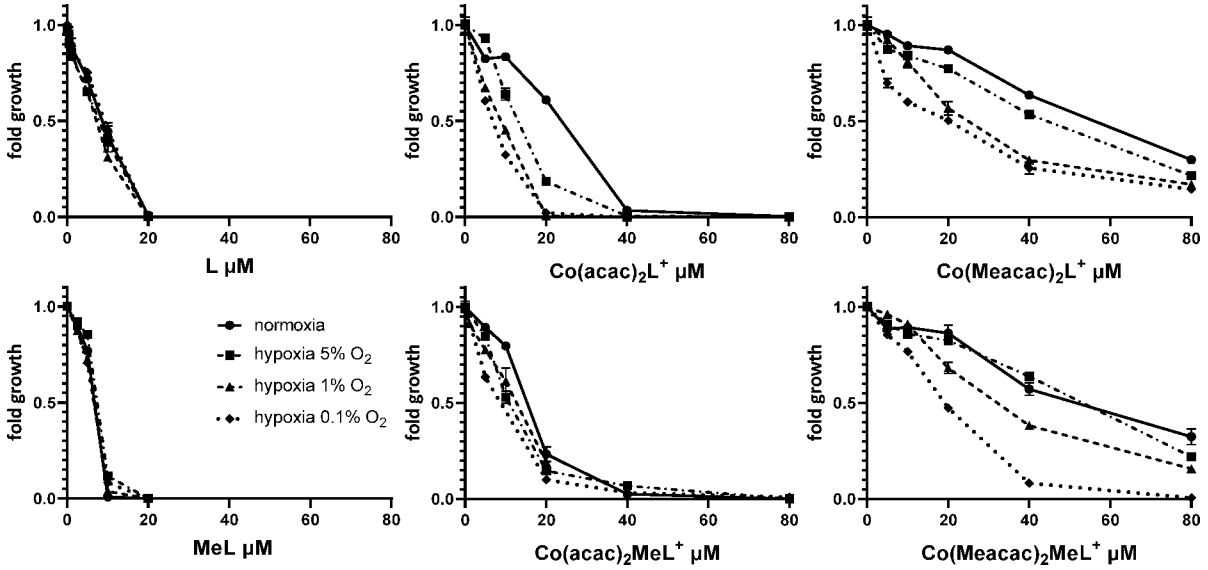

Figure 12. Cytotoxic activity of the indicated compounds against A431 cancer cells. The incubation time of the compounds on the cells was 72 h under normoxic and three different hypoxic conditions (5%, 1%, or 0.1% O_2). Values are given as means ± the standard deviation of one representative experiment performed in triplicate.

not show a higher EGFR inhibitor potency for this new inhibitor, probably indicating a shift in the target kinase spectrum.

In good agreement with our previous study,[17] the formerly investigated **$Co(acac)_2L^+$** exhibited an ~2-fold weaker anticancer activity under normoxia (Table 3) than under reduced oxygen conditions (≤1%). Also in the case of **$Co(acac)_2MeL^+$**, the cobalt complex was ~2-fold less active than the respective free ligand. However, under hypoxic conditions, **$Co(acac)_2MeL^+$** did not show full **MeL** activity even under the lowest oxygen levels of 0.1%. In contrast, the two Meacac-containing cobalt(III) complexes both showed IC_{50} values of >50 μM under normoxic conditions and also weak hypoxia with 5% O_2 did not enhance the activity to a relevant extent. However, the reduction of oxygen levels to 1% significantly ($p < 0.001$) increased the cytotoxic activity of the two prodrugs, resulting in IC_{50} values of ~25 and ~32 μM for **$Co(Meacac)_2L^+$** and **$Co(Meacac)_2MeL^+$**, respectively. In the case of **$Co(Meacac)_2L^+$**, a further decrease in the O_2 levels from 1% to 0.1% generated similar results. In contrast, for **$Co(Meacac)_2MeL^+$**, the presence of 0.1% O_2 induced an additional significant ($p < 0.05$) improvement in drug efficacy (IC_{50} value of ~20 μM) compared to that for 1% O_2 hypoxia, resulting in a 2.9-fold increase in cytotoxicity compared to that under normoxic conditions.

It is well-known that cobalt(II) ions have some biological effects like an upregulation of the expression of the hypoxia inducible factor (HIF).[49] Furthermore, a possible effect could also arise from iron(III) binding of released Meacac.[50] However, we already investigated in our previous work[17] $CoCl_2$ as well as the complexes $[Co(II)(acac)_2en]$ and $[Co(III)(acac)_2en]PF_6$ with a simple ethylenediamine ligand without an EGFR-binding moiety. No significant cytotoxic activity could be observed against A431 cells under both normoxia and hypoxia. Therefore, we can widely exclude a contribution of Co(II) ions or released acac (and subsequent iron chelation) on the anticancer activity of EGFR inhibitor-bearing cobalt(III) prodrugs.

CONCLUSIONS

Despite the revolutionizing effect they have had on cancer therapy, TKIs are limited in their clinical application due to severe side effects and rapid development of drug resistance. Hence, the design of tumor-specifically activated prodrugs is an important strategy for reducing these adverse effects. We

https://dx.doi.org/10.1021/acs.inorgchem.0c03083
Inorg. Chem. 2020, 59, 17794−17810

recently established a hypoxia-activatable cobalt(III) prodrug bearing an EGFR inhibitor ligand [**Co(acac)$_2$L$^+$**], which showed promising results *in vitro* as well as *in vivo*.[17] The aim of this study was to further improve the stability of this type of prodrug by introducing electron-donating methyl groups to lower the reduction potential. Methylation was performed at the chelating moiety of the EGFR inhibitor and/or the acac ancillary ligand. Interestingly, methylation of the EGFR inhibitor ligand [**Co(acac)$_2$MeL$^+$**] alone did not result in the expected lower cobalt(III) reduction potential. However, this aim was reached using Meacac as the ancillary ligand, and complexes **Co(Meacac)$_2$L$^+$** and **Co(Meacac)$_2$MeL$^+$** showed highly increased stability in blood plasma. This stability trend could also be confirmed in cell culture using fluorescence microscopy and flow cytometry, exploiting the quenched fluorescence of the EGFR inhibitor ligand when coordinated to cobalt(III). Evaluation of the cytotoxic activity of all compounds under normoxia versus hypoxia revealed that the complexes with distinctly higher stability still possess promising hypoxia-activatable properties. However, the IC_{50} values at 0.1% O_2 after 72 h were significantly higher compared to those of the free EGFR inhibitor ligands. More in-depth studies are now needed to evaluate the underlying reasons for this effect. Finally, a balance between sufficient stability of the complex and tumor-specific release of the EGFR inhibitor ligand is needed. However, only evaluation in future *in vivo* experiments will reveal whether **Co(Meacac)$_2$MeL$^+$** is a promising candidate with both high stability and activity.

EXPERIMENTAL SECTION

Materials and Methods. All solvents and reagents were obtained from commercial suppliers. They were, unless stated otherwise, used without further purification. Anhydrous MeOH and tetrahydrofuran over molecular sieves were bought from Fisher Chemicals. The precursors Na[Co(acac)$_2$(NO$_2$)$_2$] and Na[Co(Meacac)$_2$(NO$_2$)$_2$] were obtained following the protocol of Denny et al.[21] **Co(acac)$_2$en$^+$**, **Co(acac)$_2$L$^+$**, and **L** were synthesized according to our previous publication.[17]

For all HPLC measurements, Milli-Q water (18.2 MΩ cm, Merck Milli-Q Advantage, Merck, Darmstadt, Germany) was used. Preparative RP-HPLC was performed on an Agilent 1200 Series system controlled by Chemstation software. As the stationary phase, either a XBridge BEH C18 OBD Prep Column (130 Å, 5 μm, 19 mm × 250 mm) or an Atlantis T3 OBD Prep Column (100 Å, 10 μm, 19 mm × 250 mm), each from Waters Corp., was used. The general procedure included a flow rate of 17.06 mL/min, an injection volume of ≤10 mL, and a column temperature of 25 °C. Milli-Q water and acetonitrile (ACN) without addition of acids were used as eluents unless stated otherwise. Stability and kinetic experiments were analyzed on an Agilent 1260 Infinity system using a Waters Atlantis T3 column (150 mm × 4.6 mm) coupled to a Bruker amaZon SL ESI mass spectrometer. If not stated otherwise, water (containing 0.1% formic acid) and ACN (containing 0.1% formic acid) were used as eluents with a gradient of 1% to 99% ACN within 29 min. Elemental analyses were performed by the Microanalytical Laboratory of the University of Vienna on a Perkin Elmer 2400 CHN Elemental Analyzer. Electrospray ionization (ESI) mass spectra were recorded on a Bruker amaZon SL ion trap mass spectrometer in positive and/or negative mode by direct infusion. High-resolution mass spectra were recorded on a Bruker maXis UHR ESI time-of-flight mass spectrometer. Expected and experimental isotope distributions were compared. ^{1}H and ^{13}C NMR one- and two-dimensional spectra were recorded in DMSO-d_6 with a Bruker FT-NMR AV NEO 500 MHz spectrometer at 500.10 (^{1}H) and 125.75 (^{13}C) MHz at 298 K or a Bruker FT-NMR AVIII 600 MHz spectrometer at 600.25 MHz (^{1}H) and 150.93 MHz (^{13}C). Chemical shifts (parts per million) were referenced internally to the solvent residual peaks. For the description of the spin multiplicities the following abbreviations were used: s, singlet; d, doublet; t, triplet; q, quartet; m, multiplet. For the NMR description of the synthesized compounds, the following abbreviations were used: acac, acetylacetone; Meacac, methylacetylacetone; en, ethylenediamine; MeEn, *N*-methylethylenediamine; phEn, *N*-phenylethylenediamine; ph, phenyl; quin, quinazoline.

Synthesis. *tert-Butyl [2-({4-[(3-Bromophenyl)amino]quinazolin-6-yl}amino)ethyl](methyl)carbamate.* *N*-(3-Bromophenyl)-quinazoline-4,6-diamine (1.5 g, 4.81 mmol) was dissolved in absolute MeOH (47 mL) under an argon atmosphere. Freshly distilled acetic acid (276 μL, 4.81 mmol) and molecular sieves (823 mg, 3−4 Å, dried overnight at 150 °C) were added. *N*-Boc-(methylamino)-acetaldehyde (1 g, 5.77 mmol) was dissolved in absolute MeOH (5 mL), and the mixture was added dropwise to the yellow reaction solution. After the mixture had been stirred for 1 h, sodium cyanoborohydride (363 mg, 5.77 equiv) was added in small portions and the reaction mixture was allowed to stir overnight under an argon atmosphere. The next day the solvent was removed, and the yellow residue was extracted in 600 mL of EtOAc and washed with 400 mL of 1 M HCl, saturated $NaHCO_3$, and brine. The organic phase was separated, dried over Na_2SO_4, and concentrated *in vacuo*. The crude product was purified via flash chromatography (15:1 dichloromethane/MeOH). Yield: 1.48 g (65%). ^{1}H NMR (500.1 MHz, DMSO-d_6): δ 1.19 (s, 6H), 1.39 (s, 3H), 1.41 (s, 3H), 2.77−2.93 (m, 2H), 3.42−3.50 (m, 2H), 6.31 (d, J = 8.0 Hz, 1H), 7.91−7.31 (m, 3H), 7.35 (t, 1H), 7.56 (d, J = 2.0 Hz, 1H), 7.91 (d, J = 2.0 Hz, 1H), 8.17 (s, 1H), 8.39 (s, 1H), 9.34 (d, J = 6.0 Hz, 1H).

*N^4-(3-Bromophenyl)-N^6-[2-(methylamino)ethyl]quinazoline-4,6-diamine Dihydrochloride (**MeL**).* To a solution of *tert*-butyl [2-({4-[(3-bromophenyl)amino]quinazolin-6-yl}amino)ethyl](methyl)-carbamate (1.48 g, 3.12 mmol) in EtOH (30 mL) was added concentrated HCl (1.25 mL, 40.0 mmol), and the reaction mixture was refluxed for 3 h. The solution was cooled to room temperature and stored overnight at 4 °C. The yellow precipitate was filtered off, washed with EtOH, and dried *in vacuo*. Yield: 1.11 g (80%). ^{1}H NMR (600.25 MHz, DMSO-d_6): δ 2.61 (t, 3H, H23), 3.15 (m, 2H, H21), 3.67 (m, 2H, H20), 7.19 (s, 1H, H18), 7.45 (t, 3H, H16), 7.48−7.54 (m, 2H, H2, H15), 7.77 (d, 1H, J = 2.0 Hz, H3), 7.88 (d, 1H, J = 2.0 Hz, H11), 8.00 (s, 1H, H6), 8.13 (s, 1H, H13), 8.78 (s, 1H, H8), 9.09 (s, 2H, H22), 11.50 (s, 1H, H17). ^{13}C NMR (150.93 MHz, DMSO-d_6): δ 32.45 (C23), 38.93 (C21), 46.20 (C20), 98.57 (C6), 115.42 (C5), 120.73 (C3), 121.00 (C14), 123.71 (C11), 126.53 (C2), 127.23 (C13), 128.72 (C15), 130.41 (C16), 130.88 (C4), 138.67 (C12), 146.30 (C8), 148.57 (C1), 158.23 (C10). MS: calcd for $[C_{17}H_{18}BrN_5]^+$, 372.08; found, 372.08. Anal. Calcd for $C_{17}H_{18}BrN_5 \cdot 2HCl$ (M_r = 445.18 g/mol): C, 45.86; H, 4.53; N, 15.73. Found: C, 45.75; H, 4.22; N, 15.47.

*Bis(3-methyl-2,4-pentanedionato) N^6-(2-Aminoethyl)-N^4-(3-bromophenyl)quinazoline-4,6-diamine Cobalt(III) Chloride [**Co(Meacac)$_2$L$^+$**].* Na[Co(Meacac)$_2$(NO$_2$)$_2$] (84.4 mg, 0.22 mmol) was dissolved in H_2O (1.6 mL) and MeOH (4.5 mL). **L** (100 mg, 0.23 mmol) was dissolved in H_2O (1 mL), neutralized with NaOH (1.65 mL, 0.28 M in MeOH), and subsequently added to the cobalt precursor solution together with activated charcoal (64 mg). The resulting mixture was stirred for 1 h at room temperature, filtered through Celite, and washed with small amounts of a MeOH/H_2O mixture (1:1). Brine

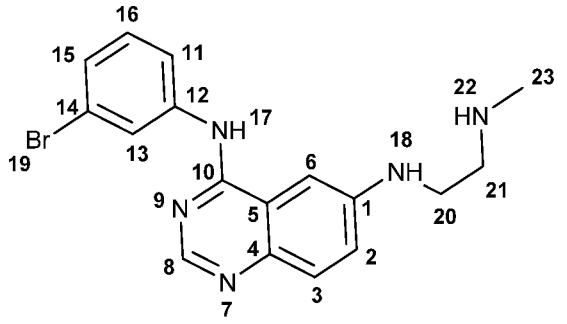

MeL

https://dx.doi.org/10.1021/acs.inorgchem.0c03083
Inorg. Chem. 2020, 59, 17794−17810

(30 mL) was added to the filtrate, and the resulting solution was left at 4 °C overnight. The formed green precipitate was filtered off the next day. The crude product (250 mg of a dark green solid) was purified by RP-HPLC (Xbridge, H_2O/MeOH, isocratic 57:43, without formic acid or TFA to avoid counter ion exchange). Yield: 67 mg (44%). The ratio of the two isomers was 1:0.36.

Shifts of the main isomer. ^{1}H NMR (500.1 MHz, DMSO-d_6): δ 1.00 (s, 3H, CH_3, Meacac), 1.65 (s, 3H, CH_3, Meacac), 1.88 (s, 3H, CH_3, Meacac), 2.05−2.06 (m, 6H, CH_3, Meacac), 2.35 (s, 3H, CH_3, Meacac), 2.67−2.97 (m, 3H, CH_2, en), 3.60−3.69 (m, 1H, CH_2, en), 5.28−5.37 [m, 1H, CH, NH_2(en)], 5.73−5.80 [m, 1H, CH, NH_2(en)], 7.36−7.43 (m, 2H, ph), 7.52 (dd, 1H, J = 9 Hz, J = 2 Hz, quin), 7.67 (d, 1H, J = 9 Hz, quin), 7.82−7.89 (m, 1H, ph), 7.93 [d, 1H, NH(en)], 8.10 (s, 1H, ph), 8.14−8.17 (m, 1H, quin), 8.65−8.70 (m, 1H, quin), 10.12 (s, 1H, NH). ^{13}C NMR (125.75 MHz, DMSO-d_6): δ 13.8 (CH_3, Meacac), 14.9 (CH_3, Meacac), 26.1 (2C, CH_3, Meacac), 26.5 (2C, CH_3, Meacac), 41.8 (CH_2, en), 50.9 (CH_2, en), 98.3 (C_q, Meacac), 100.5 (C_q, Meacac), 113.4 (CH, quin)*, 121.2 (C_q, ph), 121.3 (CH, ph), 124.7 (CH, ph), 126.5 (2C, CH, quin + ph), 130.0 (CH, quin)*, 130.6 (CH, ph), 140.6 (C_q, ph), 142.8 (Cq, quin), 153.7 (CH, quin)*, 157.0 (C_q, quin), 186.2 (C_q, acac), 186.9 (C_q, acac), 187.3 (C_q, acac), 187.9 (C_q, acac).

Shifts of the minor isomer. ^{1}H NMR (500.1 MHz, DMSO-d_6): δ 1.77 (s, 3H, CH_3, Meacac), 1.78 (s, 3H, CH_3, Meacac), 1.99 (s, 3H, CH_3, Meacac), 2.05−2.06 (m, 3H, CH_3, Meacac), 2.20 (s, 3H, CH_3, Meacac), 2.34 (s, 3H, CH_3, Meacac), 2.67−2.97 (m, 3H, en), 3.72−3.80 (m, 1H, en), 5.28−5.37 [m, 1H, NH_2(en)], 5.73−5.80 [m, 1H, NH_2(en)], 7.18 (dd, 1H, J = 9 Hz, J = 2 Hz, quin), 7.36−7.43 (m, 2H, ph), 7.46 [m, 1H, NH(en)], 7.71 (d, 1H, J = 9 Hz, quin), 7.82−7.89 (m, 1H, ph), 8.14−8.17 (m, 1H, ph), 8.65−8.70 (m, 2H, quin), 10.25 (s, 1H, NH). ^{13}C NMR (125.75 MHz, DMSO-d_6): δ 14.7 (CH_3, Meacac), 14.9 (CH_3, Meacac)*, 25.9 (CH_3, Meacac), 26.6 (CH_3, Meacac), 26.8 (CH_3, Meacac), 26.7 (CH_3, Meacac), 51.2 (CH_2, en)*, 52.2 (CH_2, en)*, 100.4 (C_q, Meacac), 100.6 (C_q, Meacac), 114 (2C, CH, quin)*, 121.3 (CH, ph)*, 124.7 (CH, ph)*, 126.5 (2C, CH, -quin + ph)*, 129.3 (CH, quin)*, 130.6 (CH, ph)*, 153.7 (CH, quin)*, 187.7 (C_q, Meacac), 188.2 (C_q, Meacac).

MS: calcd for $[C_{28}H_{34}BrCoN_5O_4]^+$, 642.11; found, 642.28. Anal. Calcd for $C_{28}H_{34}BrClCoN_5O_4{\cdot}2H_2O$ (M_r = 714.92 g/mol): C, 47.04; H, 5.36; N, 9.80. Found: C, 46.85; H, 5.09; N, 9.68. *Detected only in two-dimensional (2D) NMR.

*Bis(2,4-pentanedionato) N^4-(3-Bromophenyl)-N^6-[2-(methylamino)ethyl]quinazoline-4,6-diamine Cobalt(III) Chloride [**Co(acac)$_2$MeL**$^+$].* $Na[Co(acac)_2(NO_2)_2]$ (83.6 mg, 0.23 mmol) was dissolved in H_2O (1.6 mL) and MeOH (1.6 mL). **MeL** (105 mg, 0.24 mmol) was dissolved in H_2O (1.1 mL), neutralized with NaOH (1.9 mL, 0.25 M in MeOH), and subsequently added to the cobalt complex solution with activated charcoal (55.2 mg). The resulting mixture was stirred for 1 h at room temperature, filtered through Celite, and washed with small amounts of MeOH. Brine (6.1 mL) was added to the filtrate, and the resulting solution was extracted with dichloromethane (3 × 10 mL). The organic phase was separated, dried with Na_2SO_4, and evaporated. The crude product (115 mg of a dark green solid) was purified by RP-HPLC (H_2O/ACN, 30−42% ACN, 26 min, without formic acid or TFA to avoid counter ion exchange). Yield: 63 mg (40%). The ratio of the four isomers (A:B:C:D) was 1:0.42:0.33:0.20.

Shifts of the main isomer A. ^{1}H NMR (500.1 MHz, DMSO-d_6): δ 1.56 (s, 3H, CH_3, acac), 1.77 (d, 3H, J = 6 Hz, CH_3, MeEn), 2.01 (s, 3H, CH_3, acac), 2.02 (s, 3H, CH_3, acac), 2.30 (s, 3H, CH_3, acac), 2.58−3.04 (m, 3H, CH_2, MeEn), 3.68−3.92 (m, 1H, CH_2, MeEn), 4.79 (s, 1H, CH, acac), 5.67−5.75 (m, 1H, CH, acac), 6.74 [m, 1H, NH(en)], 7.33−7.43 (m, 2H, CH, ph), 7.46 (dd, 1H, CH, J = 8 Hz, J = 2 Hz, quin), 7.61−7.73 (m, 1H, CH, quin), 7.83−7.94 (m, 1H, CH, ph), 8.13 (t, 1H, CH, ph), 8.23−8.27 (m, 1H, CH, quin), 8.29−8.38 [m, 1H, NH(en)], 8.62−8.70 (m, 1H, CH, quin), 10.13 (s, 1H, NH). ^{13}C NMR (125.75 MHz, DMSO-d_6): δ 26.2 (CH_3, acac), 26.4 (CH_3, acac), 26.5 (CH_3, acac), 26.6 (CH_3, acac), 37.5 (CH_3, MeEn), 50.8 (CH_2, MeEn), 53.1 (CH_2, MeEn), 96.4 (CH, acac), 98.8 (CH, acac), 115.7 (C_q, quin)*, 121.6 (C_q, ph), 121.8 (CH, ph), 125.3 (CH, ph), 127.0 (CH, ph), 127.5 (CH, quin), 130.9 (CH, quin), 131.0 (CH, ph), 141.1 (C_q, ph), 142.7 (C_q, quin), 148.5 (Cq, quin)*, 157.5 (Cq, quin), 189.6 (C_q, acac), 189.7 (C_q, acac), 190.0 (C_q, acac), 190.9 (C_q, acac).

Shifts of isomer B. ^{1}H NMR (500.1 MHz, DMSO-d_6): δ 1.68 (s, 3H, CH_3, acac), 2.06 (d, 3H, J = 6 Hz, CH_3, MeEn), 2.03 (s, 3H, CH_3, acac), 2.11 (s, 3H, CH_3, acac), 2.26 (s, 3H, CH_3, acac), 2.58−3.04 (m, 3H, CH_2, MeEn), 3.68−3.92 (m, 1H, CH_2, MeEn), 5.55 (s, 1H, CH, acac), 5.67−5.75 (m, 1H, CH, acac), 6.18 [m, 1H, NH(en)], 7.29 (dd, 1H, CH, J = 8 Hz, J = 2 Hz, quin), 7.33−7.43 (m, 2H, CH, ph), 7.61−7.73 (m, 1H, CH, quin), 7.83−7.94 [m, 2H, CH, ph + NH(en)], 8.16 (m, 1H, CH, ph), 8.62−8.70 (m, 1H, CH, quin), 8.70−8.74 (m, 1H, CH, quin), 10.23 (s, 1H, NH). ^{13}C NMR (125.75 MHz, DMSO-d_6): δ 26.5 (CH_3, acac), 26.8 (CH_3, acac), 26.9 (CH_3, acac), 27.0 (CH_3, acac), 35.8 (CH_3, MeEn), 49.8 (CH_2, MeEn), 53.5 (CH_2, MeEn), 98.3 (2C, CH, acac), 115.7 (C_Q, quin)*, 116.1 (CH, quin)*, 121.6 (C_q, ph), 121.7 (CH, ph), 125.2 (CH, ph), 126.9 (CH, ph), 127.5 (CH, quin), 129.6 (CH, quin), 131.0 (CH, ph), 141.3 (C_q, ph), 142.5 (C_q, quin), 148.5 (C_q, quin)*, 157.8 (C_q, quin), 189.0 (C_q, acac), 189.7 (C_q, acac), 189.8 (C_q, acac), 190.1 (C_q, acac).

Shifts of isomer C. ^{1}H NMR (500.1 MHz, DMSO-d_6): δ 1.76 (s, 3H, CH_3, acac), 1.90 (d, 3H, J = 6 Hz, CH_3, MeEn), 1.99 (s, 3H, CH_3, acac), 2.07 (s, 3H, CH_3, acac), 2.26 (s, 3H, CH_3, acac), 2.58−3.04 (m, 3H, CH_2, MeEn), 4.16−4.27 (m, 1H, CH_2, MeEn), 5.51 (s, 1H, CH, acac), 5.67−5.75 (m, 1H, CH, acac), 6.87 [m, 1H, NH(en)], 7.25 (dd, 1H, CH, J = 8 Hz, J = 2 Hz, quin), 7.33−7.43 (m, 2H, CH, ph), 7.61−7.73 (m, 1H, CH, quin), 7.83−7.94 [m, 1H, NH(en)], 7.98 (d, 1H, J = 9.0 Hz, CH, ph), 8.16 (m, 1H, CH, ph), 8.62−8.70 (m, 1H, CH, quin), 8.98 (s, 1H, CH, quin), 10.33 (s, 1H, NH). ^{13}C NMR (125.75 MHz, DMSO-d_6): δ 26.5 (CH_3, acac)*, 26.7 (CH_3, acac)*, 27.0 (CH_3, acac)*, 27.1 (CH_3, acac)*, 36.6 (CH_3, MeEn)*, 52.9 (CH_2, MeEn)*, 51.1 (CH_2, MeEn)*, 98.1 (CH, acac), 114.4 (CH, quin)*, 115.7 (C_q, quin)*, 117.0 (CH, quin)*, 121.6 (C_q, ph)*, 122.0 (CH, ph), 125.6 (CH, ph), 127.0 (CH, ph)*, 127.5 (CH, quin), 129.6 (CH, quin), 131.0 (CH, ph), 141.3 (C_q, ph), 142.1 (C_q, quin)*, 148.5 (C_q, quin)*, 189.6 (C_q, acac), 190.1 (C_q, acac), 190.4 (C_q, acac).

Shifts of isomer D. ^{1}H NMR (500.1 MHz, DMSO-d_6): δ 1.71 (s, 3H, CH_3, acac), 1.88 (s, 3H, CH_3, acac), 2.19 (d, 3H, J = 6 Hz, CH_3, -MeEn), 2.58−3.04 (m, 3H, CH_2, MeEn), 3.68−3.92 (m, 1H, CH_2, MeEn), 4.75 (s, 1H, CH, acac), 5.67−5.75 (m, 1H, CH, acac), 6.18 [m, 1H, NH(en)], 7.33−7.43 (m, 2H, CH, ph), 7.61−7.73 (m, 1H, CH, quin), 7.83−7.94 (m, 1H, CH, ph), 8.23−8.27 (m, 1H, CH, ph), 8.29−8.38 [m, 1H, NH(en)], 8.62−8.70 (m, 1H, CH, quin), 8.70−8.74 (m, 1H, CH, quin), 10.21 (s, 1H, NH). ^{13}C NMR (125.75 MHz, DMSO-d_6): δ 26.5 (CH_3, acac)*, 26.7 (CH_3, acac)*, 35.4 (CH_3, MeEn), 53.5 (CH_2, MeEn)*, 96.5 (CH, acac)*, 98.6 (CH, acac)*, 115.7 (C_q, quin)*, 121.6 (C_q, ph)*, 122.1 (CH, ph), 125.4 (CH, ph), 127.0 (CH, ph)*, 127.5 (CH, quin), 143.4 (C_q, quin)*, 189.3 (C_q, acac)*, 189.5 (C_q, acac)*, 131.0 (CH, ph).

MS: calcd for $[C_{27}H_{32}BrCoN_5O_4]^+$, 628.10; found, 628.26. Anal. Calcd for $C_{27}H_{32}BrClCoN_5O_4{\cdot}2H_2O$ (M_r = 700.89 g/mol): C, 46.27; H, 5.18; N, 9.99. Found: C, 46.24; H, 5.05; N, 9.77. *Detected only in 2D NMR.

*Bis(3-methyl-2,4-pentanedionato) N^4-(3-Bromophenyl)-N^6-[2-(methylamino)ethyl]quinazoline-4,6-diamine Cobalt(III) Chloride [**Co(Meacac)$_2$MeL**$^+$].* $Na[Co(Meacac)_2(NO_2)_2]$ (85.6 mg, 0.21 mmol) was dissolved in H_2O (1.6 mL) and MeOH (1.2 mL). **MeL** (100 mg, 0.23 mmol) was dissolved in H_2O (1 mL), neutralized with NaOH (1.8 mL, 0.25 M in MeOH), and then added with activated charcoal (52.5 mg) to the cobalt precursor solution. The resulting mixture was stirred for 1 h at room temperature and filtered through Celite, which was washed with small amounts of MeOH. Brine (5.8 mL) was added to the filtrate, and the resulting solution was extracted with dichloromethane (3 × 10 mL). The organic phase was separated, dried with Na_2SO_4, and evaporated. The crude product (100 mg of a dark green solid) was purified by RP-HPLC (H_2O/ACN, 30−42% ACN, 26 min, without formic acid or TFA to avoid counter ion exchange). Yield: 37.6 mg (24%). The ratio of the four isomers (A:B:C:D) was 1:0.34:0.23:0.19.

Shifts of the main isomer A. ^{1}H NMR (500.1 MHz, DMSO-d_6): δ 1.00 (s, 3H, CH_3, Meacac), 1.57 (s, 3H, CH_3, Meacac), 1.67−1.72 (m, 3H, CH_3, MeEn), 1.90 (s, 3H, CH_3, Meacac), 2.08 (s, 3H, CH_3,

https://dx.doi.org/10.1021/acs.inorgchem.0c03083
Inorg. Chem. 2020, 59, 17794−17810

Meacac), 2.11 (s, 3H, CH_3, Meacac), 2.41 (s, 3H, CH_3, Meacac), 2.58−3.00 (m, 3H, CH_2, MeEn), 3.60−3.83 (m, 1H, CH_2, MeEn), 6.61−6.76 [m, 1H, NH(en)], 7.31−7.44 (m, 2H, CH, ph), 7.48 (d, 1H, CH, J = 9 Hz, -quin), 7.55−7.71 (m, 1H, CH, -quin), 7.84 (d, 1H, J = 2.0 Hz, CH, ph), 8.06−8.17 [m, 3H, CH, quin + ph + NH(en)], 8.60−8.72 (m, 1H, quin), 10.09 (s, 1H, NH). ^{13}C NMR (125.75 MHz, DMSO-d_6): δ 13.8 (CH_3, Meacac)*, 14.7 (CH_3, Meacac), 26.1 (CH_3, Meacac), 26.3 (CH_3, Meacac), 26.4 (CH_3, Meacac), 26.6 (CH_3, Meacac), 36.9 (CH_3, MeEn), 50.2 (CH_2, MeEn), 53.0 (CH_2, MeEn), 98.5 (C_q, Meacac), 101.2 (C_q, Meacac), 113.7 (CH, quin)*, 121.1 (CH, ph), 124.6 (CH, ph), 126.4 (CH, ph), 127.1 (CH, quin)*, 130.1 (CH, quin)*, 130.6 (CH, ph), 140.9 (C_q, ph), 142.5 (C_q, quin), 156.9 (C_q, quin), 187.0 (C_q, Meacac), 187.4 (C_q, Meacac), 187.5 (CC_q, Meacac), 188.2 (C_q, Meacac).

Shifts of isomer B. ^{1}H NMR (500.1 MHz, DMSO-d_6): δ 1.67−1.72 (m, 3H, CH_3, Meacac), 1.79 (s, 3H, CH_3, Meacac), 1.95 (s, 3H, CH_3, Meacac), 2.04−2.14 (m, 6H, CH_3, acac + MeEn), 2.23 (s, 3H, CH_3, Meacac), 2.33 (s, 3H, CH_3, Meacac), 2.58−3.00 (m, 3H, CH_2, MeEn), 3.60−3.83 (m, 1H, CH_2, MeEn), 5.85 [m, 1H, NH(en)], 7.13−7.23 (m, 1H, CH, quin), 7.31−7.44 (m, 2H, CH, ph), 7.55−7.71 (m, 1H, CH, -quin), 7.87−8.03 [m, 2H, CH, ph + NH(en)], 8.24 (s, 1H, CH, ph), 8.60−8.72 (m, 1H, CH, quin), 8.75 (s, 1H, CH, quin), 10.23 (s, 1H, NH). ^{13}C NMR (125.75 MHz, DMSO-d_6): δ 14.6 (CH_3, Meacac), 14.7 (CH_3, Meacac), 35.2 (CH_3, MeEn), 26.4 (CH_3, Meacac), 26.6 (CH_3, Meacac)*, 26.9 (CH_3, Meacac), 26.1 (CH_3, Meacac), 52.5 (CH_2, MeEn), 100.7 (2C, C_q, Meacac), 121.1 (CH, ph), 124.6 (CH, ph)*, 126.4 (CH, ph), 127.1 (CH, quin)*, 129.2 (CH, quin), 130.6 (CH, ph), 187.0 (C_q, Meacac), 187.3 (C_q, Meacac), 188.0 (C_q, Meacac).

Shifts of isomer C. ^{1}H NMR (500.1 MHz, DMSO-d_6): δ 1.75 (s, 3H, CH_3, Meacac), 1.77−1.83 (m, 3H, CH_3, MeEn), 1.82 (s, 3H, CH_3, Meacac), 1.97 (s, 3H, CH_3, Meacac), 2.04−2.14 (m, 3H, CH_3, Meacac), 2.19 (s, 3H, CH_3, Meacac), 2.37 (s, 3H, CH_3, Meacac), 2.58−3.00 (m, 3H, CH_2, MeEn), 3.60−3.83 (m, 1H, CH_2, MeEn), 6.61−6.76 [m, 1H, NH(en)], 7.13−7.23 (m, 1H, CH, quin), 7.31−7.44 (m, 2H, CH, ph), 7.55−7.71 (m, 1H, CH, quin), 7.87−8.03 [m, 2H, CH, ph + NH(en)], 8.19 (s, 1H, CH, ph), 8.60−8.72 (m, 1H, CH, quin), 8.90 (s, 1H, CH, -quin), 10.28 (s, 1H, NH). ^{13}C NMR (125.75 MHz, DMSO-d_6): δ 14.6 (CH_3, Meacac), 14.7 (CH_3, Meacac), 34.9 (CH_3, MeEn), 26.2 (CH_3, Meacac), 26.4 (CH_3, Meacac)*, 52.7 (CH_2, MeEn)*, 100.7 (2C, C_q, Meacac), 121.1 (CH, ph), 124.6 (CH, ph)*, 126.4 (CH, ph)*, 127.1 (CH, quin)*, 129.3 (CH, quin), 130.6 (CH, ph), 187.2 (C_q, Meacac)*, 187.5 (C, C_q, Meacac)*.

Shifts of isomer D. ^{1}H NMR (500.1 MHz, DMSO-d_6): δ 1.76 (s, 3H, CH_3, MeEn), 1.77−1.83 (m, 3H, CH_3, Meacac), 1.99 (s, 3H, CH_3, Meacac), 2.04−2.14 (m, 3H, CH_3, Meacac), 2.21−2.26 (m, 3H, CH_3, MeEn), 2.33 (s, 3H, CH_3, Meacac), 2.58−3.00 (m, 3H, CH_2, MeEn), 3.60−3.83 (m, 1H, CH_2, MeEn), 5.85 [m, 1H, NH(en)], 7.31−7.44 (m, 2H, CH, ph), 7.47 (m, 1H, CH, quin), 7.55−7.71 (m, 1H, CH, quin), 8.24 (s, 1H, CH, ph), 8.06−8.17 [m, 3H, CH, quin + ph + NH(en)], 8.60−8.72 (m, 1H, CH, quin), 10.14 (s, 1H, NH). ^{13}C NMR (125.75 MHz, DMSO-d_6): δ 14.6 (CH_3, Meacac)*, 14.8 (CH_3, Meacac)*, 36.0 (CH_3, MeEn)*, 26.4 (CH_3, Meacac)*, 121.1 (CH, ph), 124.6 (CH, ph)*, 126.4 (CH, ph)*, 127.1 (CH, quin)*, 130.1 (CH, quin)*, 130.6 (CH, ph), 186.4 (C_q, acac)*, 187.7 (C_q, Meacac)*, 188.3 (C_q, Meacac)*.

MS: calcd for $[C_{29}H_{36}BrCoN_5O_4]^+$, 656.13; found, 656.13. Anal. Calcd for $C_{29}H_{36}BrClCoN_5O_4{\cdot}2H_2O$ (M_r = 728.95 g/mol): C, 47.78; H, 5.53; N, 9.61. Found: C, 47.58; H, 5.40; N, 9.64. *Detected only in 2D NMR.

*Bis(2,4-pentanedionato) (Phenyl-1,2-ethylenediamine) Cobalt-(III) Hexafluorophosphate [**Co(acac)$_2$PhEn$^+$**].* Na[Co(acac)$_2$(NO$_2$)$_2$] (100 mg, 0.27 mmol) was dissolved in H_2O (1.5 mL) and MeOH (1 mL), and *N*-phenylethylenediamine (36.9 μL, 0.28 mmol) was added to the solution with a spatula tip of activated charcoal. The reaction mixture was stirred for 1 h at room temperature and filtered through Celite. NH_4PF_6 (152.4 mg, 0.94 mmol) was added to the filtrate, and the solution was stored at 4 °C overnight. The formed grayish violet solid was filtered off and washed with ice-cold H_2O and Et_2O. Yield: 45 mg (30%). The ratio of the two isomers was 1:0.81.

Shifts of the main isomer. ^{1}H NMR (500.1 MHz, DMSO-d_6): δ 1.69 (s, 3H, CH_3, acac), 2.00 (s, 3H, CH_3, acac), 2.10 (s, 3H, -CH_3, acac), 2.18 (s, 3H, CH_3, acac), 2.52−2.91 (m, 3H, CH_2, phEn), 3.19−3.25 (m, 1H, CH_2, phEn), 5.35 (s, 1H, NH_2), 5.56 (s, 1H, CH, acac), 5.66 (s, 1H, CH, acac), 5.88 (s, 1H, NH_2), 7.01 (d, 1H, J = 2 Hz, CH, ph), 7.15 (d, 2H, J = 3 Hz, NH), 7.19−7.35 (m, 8H, CH, ph).

Shifts of the minor isomer. ^{1}H NMR (500.1 MHz, DMSO-d_6): δ 1.70 (s, 3H, CH_3, acac), 1.95 (s, 3H, -CH_3, acac), 1.98 (s, 3H, CH_3, acac), 2.19 (s, 3H, CH_3, acac), 2.52−2.91 (m, 3H, CH_2, phEn), 3.19−3.25 (m, 1H, CH_2, phEn), 4.91 (s, 1H, CH, acac), 5.54 (s, 1H, NH_2), 5.64 (s, 1H, CH, acac), 5.64 (s, 1H, NH_2), 7.01 (d, 1H, J = 2 Hz, CH, ph), 7.19−7.35 (m, 4H, CH, ph), 7.76 (d, 2H, J = 3 Hz, NH).

MS: calcd for $[C_{18}H_{26}CoN_2O_4]^+$, 393.12; found, 393.04. Anal. Calcd for $C_{18}H_{26}CoF_6N_2O_4P{\cdot}0.5H_2O$ (M_r = 547.32 g/mol): C, 39.50; H, 4.97; N, 5.12. Found: C, 39.75; H, 4.82; N, 4.96.

*Bis(3-methyl-2,4-pentanedionato) Ethylenediamine Cobalt(III) Hexafluorophosphate [**Co(Meacac)$_2$en$^+$**].* Na[Co(Meacac)$_2$(NO$_2$)$_2$] (150 mg, 0.37 mmol) was dissolved in H_2O (2.25 mL) and MeOH (1.5 mL), and ethylenediamine (26.3 μL, 0.39 mmol) was added with a spatula tip of activated charcoal. The reaction mixture was stirred for 1.5 h at room temperature and filtered through a syringe filter. NH_4PF_6 (212 mg, 1.3 mmol) was added to the filtrate, and the solution was stored at room temperature for 2 h. Violet and orange crystals precipitated after a while. The solid was filtered off and washed with ice-cold H_2O and Et_2O. Separation of the two compounds was carried out by dissolution in MeOH. The insoluble orange crystals were filtered off, and the violet filtrate was evaporated and dried *in vacuo*. Yield: 30 mg (16%). ^{1}H NMR (500.1 MHz, DMSO-d_6): δ 1.86 (s, 6H, CH_3, Meacac), 2.13 (s, 6H, CH_3, Meacac), 2.15 (s, 6H, CH_3, Meacac), 2.34 (m, 2H, CH_2, en), 2.45 (m, 2H, CH_2, en), 4.78 (s, 2H, NH_2), 5.21 (s, 2H, NH_2). MS: calcd for $[C_{18}H_{26}CoN_2O_4]^+$, 345.12; found, 345.10. Anal. Calcd for $C_{14}H_{26}CoF_6N_2O_4P{\cdot}0.5H_2O$ (M_r = 499.27 g/mol): C, 33.68; H, 5.45; N, 5.61. Found: C, 33.85; H, 5.70; N, 5.39.

*Bis(2,4-pentanedionato) (Methyl-1,2-ethanediamine) Cobalt(III) Hexafluorophosphate [**Co(acac)$_2$MeEn$^+$**].* Na[Co(acac)$_2$(NO$_2$)$_2$] (500 mg, 1.34 mmol) was dissolved in H_2O (7.5 mL) and MeOH (5 mL), and *N*-methylethylenediamine (123 μL, 1.41 mmol) was added to the solution with a spatula tip of activated charcoal. The reaction mixture was stirred for 1.5 h at room temperature and filtered through Celite. NH_4PF_6 (763 mg, 4.68 mmol) was added to the filtrate, and the solution was stored at 4 °C for 4 days. The formed violet crystals were filtered off and washed with ice-cold H_2O and Et_2O. Yield: 252 mg (39%). ^{1}H NMR (500.1 MHz, DMSO-d_6): δ 1.67 (d, 3H, J = 9 Hz, CH_3, MeEn), 2.04 (s, 3H, CH_3, acac), 2.06 (s, 3H, CH_3, acac), 2.09 (s, 6H, CH_3, acac), 2.34−2.6 (m, 4H, CH_2, MeEn), 5.27 (m, 2H, NH_2), 5.61 (s, 1H, CH, acac), 5.63 (s, 1H, CH, acac), 6.16 (s, 1H, NH). MS: calcd for $[C_{13}H_{24}CoN_2O_4]^+$, 331.11; found, 331.10. Anal. Calcd for $C_{13}H_{24}CoF_6N_2O_4P$ (M_r = 476.24 g/mol): C, 32.79; H, 5.08; N, 5.88. Found: C, 32.57; H, 5.11; N, 5.83.

*Bis(3-methyl-2,4-pentanedionato) (Methyl-1,2-ethanediamine) Cobalt(III) Hexafluorophosphate [**Co(Meacac)$_2$MeEn$^+$**].* Na[Co(Meacac)$_2$(NO$_2$)$_2$] (100 mg, 0.25 mmol) was dissolved in H_2O (1.5 mL) and MeOH (1 mL), and *N*-methylethylenediamine (22.9 μL, 0.26 mmol) was added with a spatula tip of activated charcoal. The reaction mixture was stirred for 1.5 h at room temperature and filtered through a syringe filter. NH_4PF_6 (142 mg, 0.87 mmol) was added to the filtrate, and the solution was stored at room temperature for 2 h. The precipitated purple crystals were filtered off and washed with ice-cold H_2O and Et_2O. Yield: 20 mg (16%). The ratio of the two isomers was 1:0.30.

Shifts of the main isomer. ^{1}H NMR (500.1 MHz, DMSO-d_6): δ 1.60 (d, 3H, J = 8 Hz, CH_3, MeEn), 1.84 (s, 3H, CH_3, Meacac), 1.88 (s, 3H, CH_3, Meacac), 2.11 (s, 3H, CH_3, Meacac), 2.16 (s, 3H, CH_3, Meacac), 2.18 (s, 3H, CH_3, Meacac), 2.21 (s, 3H, CH_3, Meacac), 2.23−2.40 (m, 3H, CH_2, MeEn), 2.62 (s, 1H, CH_2, MeEn), 4.97 (s, 1H, NH_2), 5.13 (s, 1H, NH_2), 5.96 (s, 1H, NH).

Shifts of the minor isomer. ^{1}H NMR (500.1 MHz, DMSO-d_6): δ 1.86 (s, 3H, CH_3, MeEn), 1.89 (s, 3H, CH_3, Meacac), 1.95 (d, 3H, J = 11 Hz, CH_3, Meacac), 2.14 (s, 6H, CH_3, Meacac), 2.16 (s, 3H, CH_3, Meacac),

https://dx.doi.org/10.1021/acs.inorgchem.0c03083
Inorg. Chem. 2020, 59, 17794−17810

2.21 (s, 3H, CH_3, Meacac), 2.23−2.40 (m, 3H, CH_2, MeEn), 2.62 (s, 1H, CH_2, MeEn), 4.81 (s, 1H, NH), 5.35 (m, 2H, NH_2).

MS: calcd for $[C_{15}H_{28}CoN_2O_4]^+$, 359.14; found, 359.12. Anal. Calcd for $C_{15}H_{28}CoF_6N_2O_4P{\cdot}0.5H_2O$ (M_r = 522.31 g/mol): C, 35.1; H, 5.69; N, 5.46. Found: C, 35.21; H, 5.64; N, 5.16.

Kinase Screening. The EGFR (ErbB1) kinase-inhibitory potential of the novel ligand **MeL** in comparison to that of previously synthesized ligand **L** was evaluated using the Select Screen Biochemical Kinase Profiling Service at Life Technologies (ThermoFisher Scientific, Madison, WI). The test compounds were screened in a final DMSO concentration of 1% using the ZLYTE Assay in the presence of 10 μM ATP.

Fluorescence Measurements. Fluorescence measurements were performed on a Horiba FluoroMax-4 spectrofluorometer, and the data were analyzed using FluorEssence version 3.5. The tested solutions were dissolved immediately prior to analysis in PBS (10 mM, pH 7.4) with a final concentration of 3×10^{-5} M. Scans were run at room temperature with excitation and emission slit widths of 4 nm. Emission scans were run from 375 to 600 nm using an excitation wavelength of 365 nm. The 3D fluorescence spectra of **L** and **MeL** were determined at excitation wavelengths from 220 to 550 nm, and emission was recorded within the range of 200−600 nm.

Lipophilicity. Distribution coefficient ($D_{7.4}$) values of the studied cobalt(III) compounds were determined by the traditional shake-flask method in an *n*-octanol/buffered aqueous solution at pH 7.40 (PBS) and 25.0 ± 0.2 °C as described previously.[51] The complexes were dissolved in an *n*-octanol presaturated aqueous solution of the buffer at ∼100 μM. After phase separation, the UV−vis spectrum of the compound in the aqueous phase was compared to that of the original stock solution and the $D_{7.4}$ values of the compounds were calculated according to the following formula: [absorbance(original solution)/absorbance(aqueous phase after separation) − 1].

Chemicals for Analytical Measurements. All solvents were of analytical grade and used without further purification. MeEn, PhEn, acac, Meacac, KH-phthalate, $K_3[Fe(III)(CN)_6]$, KCl, NaCl, HCl, KOH, AA, GSH, and reduced NADH were products of Sigma-Aldrich. $CoCl_2{\cdot}H_2O$, NaH_2PO_4, and Na_2HPO_4 were purchased from Reanal, and the exact concentration of the $CoCl_2$ stock solution was determined by complexometry via its EDTA complex. Milli-Q water was used for sample preparation.

Cyclic Voltammetry. The compounds were dissolved in 10 mM phosphate buffer (pH 7.40), with 0.1 M KCl as the supporting electrolyte, to obtain a final concentration of 1.5 mM. Electrochemical experiments were conducted on an EG&G PARC 273A potentiostat/galvanostat with scan rates of 30 and 1000 mV/s at room temperature. Argon was bubbled through the solution before every measurement to remove oxygen. A three-electrode configuration cell was used with a glassy carbon electrode as the working electrode, which was polished before every measurement. The reference electrode was Ag/AgCl/KCl (3.5 M), and the auxiliary electrode was a platinum wire. Electrodes were conditioned regularly in 1 M H_2SO_4 for 5−10 cycles between voltage limits of −1.0 and 1.0 V at a scan rate of 100 mV/s. The system was calibrated with 1.5 mM $K_3[Fe(CN)_6]$ for every experiment. Redox potentials measured relative to the Ag/AgCl/KCl (3.5 M) reference electrode were converted for potentials against NHE by the addition of 0.205 V. Measurements were repeated at least three times, and the mean values were calculated.

Spectroscopic Studies of the Proton Dissociation and Redox Processes. Proton dissociation processes of PhEn were followed by UV−vis spectrophotometry and spectrofluorometry; samples were prepared in water containing 100 and 10 μM ligand, respectively, and 0.1 M KCl at 25 ± 0.2 °C. The proton dissociation constants and the UV−vis or fluorescence emission spectra of the individual species in the various protonation states were calculated by deconvolution of the spectra recorded in the pH range of 2.0−11.5 with PSEQUAD.[40] Reduction of the cobalt(III) compounds by AA, GSH, and NADH in aqueous solutions was followed for 24 h at 25.0 °C. All solutions were prepared under strictly oxygen-free conditions in an argon atmosphere. Batch samples contained 30 μM cobalt(III) complex and 10 equiv of AA, GSH, or NADH in PBS buffer (pH 7.40) and were used only once to record their UV−vis and fluorescence spectra. A Hewlett Packard 8452A diode array spectrophotometer was used in the interval of 200−800 nm, and a Hitachi F-4500 spectrofluorometer was applied to record the emission spectra (λ_{EX} = 290 nm and λ_{EM} = 310−450 nm in case of the titration of PhEn; λ_{EX} = 370 nm and λ_{EM} = 400−600 nm in the case of redox reactions).

pH-Potentiometric Measurements and Data Evaluation. For determination of the proton dissociation (K_a) and formation constants (β) pH-potentiometric measurements were carried out at 25 ± 0.1 °C and an ionic strength (I) of 0.10 M (KCl) to keep the activity coefficients constant. A carbonate-free KOH solution (0.10 M) was used for titrations. The exact concentrations of HCl and KOH were determined by pH-potentiometric titrations. A Metrohm-combined electrode (type 6.0234.100) connected to an Orion 710A pH-meter and a computer-controlled Methrom 665 Dosimat buret (increment, 1 μL; precision, 2 μL) were used for the pH-potentiometric measurements. The electrode system was calibrated to the pH = $-\log[H^+]$ scale by means of blank titrations (strong acid HCl vs strong base KOH), as suggested by Irving et al.[52] The determined average water ionization constant (pK_w = 13.76 ± 0.01) corresponds well to the literature data.[37] Titration points included in the calculations gave a reproducibility within 0.005 pH unit. Titrations were performed in the pH range of 2.0−11.5, and the initial volume of the samples was 10 mL. Binary systems contained 1 or 2 mM ligand, and metal:ligand ratios of 1:1, 1:2, 1:3, and 1:4 were used. In the ternary systems, the cobalt(II) concentration was 1 mM and the two types of ligands (A, acac, and B, MeEn, or PhEn) were varied as follows: 1:1:1, 1:2:1, 1:1:2, and 1:2:2 Co(II):A:B. The samples were degassed by bubbling purified argon through them for 10 min prior to the measurements, and argon was also passed over the solutions during the titrations.

The stoichiometry of the complexes and overall stability constants were established by the computer program Hyperquad2013.[53] For the general equilibrium $\beta(M_pL_qH_r)$ is defined as

$$pM + qL + rH \rightleftharpoons M_pL_qH_r \text{ as } \beta(M_pL_qH_r) = [M_pL_qH_r]/[M]^p[L]^q[H]^r \quad (1)$$

where M denotes the cobalt(II) ion and L the completely deprotonated ligand. The calculations were performed as reported in our previous work.[54]

Serum Stability Measurements. For serum stability measurements, 135 μL of FCS, buffered with 150 mM phosphate (Na_2HPO_4/NaH_2PO_4) to maintain a pH value of 7.4, was mixed with 15 μL of a 500 μM stock solution of the respective complex in 50 mM phosphate buffer to reach a final concentration of 50 μM. The samples were incubated at 37 °C. At different time points, to 20 μL of serum was added 40 μL of ACN. After being vigorously shaked for 2 min, the suspension was centrifuged at 6000 rpm for 10 min. The supernatant was taken up with a syringe and directly measured via HPLC-MS.

Biological Methods. *Chemicals for Cell Culture Tests.* All investigated drugs were dissolved in DMSO. These stock solutions (10 mM) were further diluted into culture media containing 10% FCS at the indicated concentrations. The final DMSO concentrations were always less than 1%. All other substances were purchased from Sigma-Aldrich (St. Louis, MO).

Cell Culture. Human cancer cell line A431 (epidermoid carcinoma, overexpressing EGFR/wt) was purchased from American Type Culture Collection (ATCC) (Rockville, MD). The cell line was grown, unless otherwise indicated, in humidified incubators (37 °C, 21% O_2, and 5% CO_2) in RPMI 1640 containing 10% FCS (PAA, Linz, Austria). Under hypoxic conditions, plated and treated cells were incubated in humidified incubators (ProOx model C21 system von BioSpherix) with 0.1%, 1%, or 5% CO_2 for the indicated period of time before analysis.

Cytotoxicity Assay. A431 cells were seeded (3×10^3 cells/well) in 96-well plates, and after recovery for 24 h, the dissolved drugs were added in increasing concentrations. After exposure to the drug for 72 h, the proportion of viable cells was determined by the MTT assay following the manufacturer's recommendations (EZ4U, Biomedica, Vienna, Austria). Cytotoxicity was expressed as IC_{50} values calculated from full dose−response curves using GraphPad Prism.

https://dx.doi.org/10.1021/acs.inorgchem.0c03083
Inorg. Chem. 2020, 59, 17794−17810

Western Blot Analysis. A431 cells were plated (1×10^6 cells/60 mm dish) and allowed to recover for 24 h, followed by serum starvation for 24 h (except the nonstarving control). Subsequently, the cells were treated with the drugs in different concentrations for 2 h. In the final 10 min, EGF was added with a final concentration of 50 ng/mL to stimulate EGFR. Then, cells were harvested, and proteins were isolated, resolved by sodium dodecyl sulfate−polyacrylamide gel electrophoresis, and transferred onto a polyvinylidene difluoride membrane for Western blotting as previously described.[17] The following antibodies were used: EGFR (8198), p-EGFR (Tyr1068) (3077), ERK 1/2 (9102), and p-ERK 1/2 (Thr202/Tyr204) (9101) (all monoclonal rabbit, Cell Signaling Technology, Beverly, MA) and β-actin (monoclonal mouse, Sigma). All primary antibodies were used in 1:1000 dilutions [in Tris-buffered saline containing 0.1% Triton X-100 (TBST) with 3% bovine serum albumin (BSA)]. Additionally, horseradish peroxidase-labeled anti-mouse (7076) and anti-rabbit (7074) secondary antibodies were used at working dilutions of 1:10000 (in TBST with 1% BSA).

Fluorescence Microscopy. A431 cells were seeded (5×10^5 cells/well) in six-well plates and allowed to recover overnight. Then, cells were treated with 10 μM investigated drugs (diluted with 10% FCS-containing medium) for 6 or 24 h. After incubation, the drug solutions were removed, and the cells were washed with PBS. Subsequently, microphotographs were taken using UV fluorescence microscopy (Nikon Eclipse Ti microscope with a DAPI filter and a high-pressure mercury lamp) and a 10× objective.

Flow Cytometry. For better quantification of the fluorescence intensity of released EGFR inhibitors, the previously microscoped cells were trypsinized, harvested, and centrifuged. The pellets were washed twice with PBS and further resuspended in Dulbecco's modified Eagle's medium (DMEM). Subsequently, the samples were measured on a LSR Fortessa flow cytometer (BD Biosciences, East Rutherford, NJ). The compound fluorescence was detected using 405 nm excitation and Pacific Blue (450/50 nm) band pass emission filters. Data were analyzed using the FACSDiva software and are depicted as the percent of fluorescence-positive cells and as the fluorescence intensity normalized to the autofluorescence.

■ ASSOCIATED CONTENT

Supporting Information

The Supporting Information is available free of charge at https://pubs.acs.org/doi/10.1021/acs.inorgchem.0c03083.

NMR spectroscopic data of the cobalt complexes, concentration distribution diagram for cobalt(II)-acacMeEn, extracted ion mass chromatograms of the stability of the cobalt complexes, Western blot of **MeL**, and EGFR kinase screening of **L** and **MeL** (PDF)

■ AUTHOR INFORMATION

Corresponding Author

Christian R. Kowol − *Institute of Inorganic Chemistry, Faculty of Chemistry, University of Vienna, 1090 Vienna, Austria; Research Cluster "Translational Cancer Therapy Research", University of Vienna and Medical University of Vienna, 1090 Vienna, Austria;* orcid.org/0000-0002-8311-1632; Email: christian.kowol@univie.ac.at

Authors

Marlene Mathuber − *Institute of Inorganic Chemistry, Faculty of Chemistry, University of Vienna, 1090 Vienna, Austria*

Hemma Schueffl − *Institute of Cancer Research and Comprehensive Cancer Center, Medical University of Vienna, 1090 Vienna, Austria*

Orsolya Dömötör − *Department of Inorganic and Analytical Chemistry and MTA-SZTE Lendület Functional Metal Complexes Research Group, University of Szeged, H-6720 Szeged, Hungary*

Claudia Karnthaler − *Institute of Inorganic Chemistry, Faculty of Chemistry, University of Vienna, 1090 Vienna, Austria*

Éva A. Enyedy − *Department of Inorganic and Analytical Chemistry and MTA-SZTE Lendület Functional Metal Complexes Research Group, University of Szeged, H-6720 Szeged, Hungary;* orcid.org/0000-0002-8058-8128

Petra Heffeter − *Institute of Cancer Research and Comprehensive Cancer Center, Medical University of Vienna, 1090 Vienna, Austria; Research Cluster "Translational Cancer Therapy Research", University of Vienna and Medical University of Vienna, 1090 Vienna, Austria*

Bernhard K. Keppler − *Institute of Inorganic Chemistry, Faculty of Chemistry, University of Vienna, 1090 Vienna, Austria; Research Cluster "Translational Cancer Therapy Research", University of Vienna and Medical University of Vienna, 1090 Vienna, Austria*

Complete contact information is available at: https://pubs.acs.org/10.1021/acs.inorgchem.0c03083

Notes

The authors declare no competing financial interest.

■ ACKNOWLEDGMENTS

This work was supported by the Austrian Science Fund (FWF) (Grant P28853, to C.R.K.), the National Research, Development and Innovation Office-NKFI through Projects FK124240 and PD131472, and FIKP Program TUDFO/47138-1/2019-ITM. O.D. gratefully acknowledges the financial support from a J. Bolyai Research Fellowship. The authors thank Ing. Ingo Polivka for enthusiastic synthetic help and Ms. Vivien Pósa for performing some of the solution studies.

■ REFERENCES

(1) Chen, J.; Zeng, F.; Forrester, S. J.; Eguchi, S.; Zhang, M.-Z.; Harris, R. C. Expression and function of the epidermal growth factor receptor in physiology and disease. *Physiol. Rev.* **2016**, *96* (3), 1025−1069.

(2) Hynes, N. E.; Lane, H. A. ERBB receptors and cancer: the complexity of targeted inhibitors. *Nat. Rev. Cancer* **2005**, *5* (5), 341.

(3) Sigismund, S.; Avanzato, D.; Lanzetti, L. Emerging functions of the EGFR in cancer. *Mol. Oncol.* **2018**, *12* (1), 3−20.

(4) Sharma, S. V.; Bell, D. W.; Settleman, J.; Haber, D. A. Epidermal growth factor receptor mutations in lung cancer. *Nat. Rev. Cancer* **2007**, *7* (3), 169.

(5) Gazdar, A. Activating and resistance mutations of EGFR in non-small-cell lung cancer: role in clinical response to EGFR tyrosine kinase inhibitors. *Oncogene* **2009**, *28* (1), S24−S31.

(6) Singh, M.; Jadhav, H. R. Targeting non-small cell lung cancer with small-molecule EGFR tyrosine kinase inhibitors. *Drug Discovery Today* **2018**, *23* (3), 745−753.

(7) Bhullar, K. S.; Lagarón, N. O.; McGowan, E. M.; Parmar, I.; Jha, A.; Hubbard, B. P.; Rupasinghe, H. V. Kinase-targeted cancer therapies: progress, challenges and future directions. *Mol. Cancer* **2018**, *17* (1), 48.

(8) Wang, Y.; Hu, G.-f.; Zhang, Q.-q.; Tang, N.; Guo, J.; Liu, L.-y.; Han, X.; Wang, X.; Wang, Z.-h. Efficacy and safety of gemcitabine plus erlotinib for locally advanced or metastatic pancreatic cancer: a systematic review and meta-analysis. *Drug Des., Dev. Ther.* **2016**, *10*, 1961.

(9) Aw, D. C. W.; Tan, E. H.; Chin, T. M.; Lim, H. L.; Lee, H. Y.; Soo, R. A. Management of epidermal growth factor receptor tyrosine kinase inhibitor-related cutaneous and gastrointestinal toxicities. *Asia-Pac. J. Clin. Onco.* **2018**, *14* (1), 23−31.

(10) Kiyohara, Y.; Yamazaki, N.; Kishi, A. Erlotinib-related skin toxicities: treatment strategies in patients with metastatic non-small cell lung cancer. *J. Am. Acad. Dermatol.* **2013**, *69* (3), 463−472.
(11) Kudo, K.; Hotta, K.; Bessho, A.; Nogami, N.; Kozuki, T.; Kuyama, S.; Inoue, K.; Harita, S.; Okada, T.; Genba, K.; et al. Development of skin rash within the 1st week is a potential surrogate marker of therapeutic effect in afatinib monotherapy in patients with EGFR-mt non-small-cell lung cancer (NSCLC): Okayama Lung Cancer Study Group Experience. *J. Clin. Oncol.* **2015**, *33*, e19051.
(12) Kratz, F.; Müller, I. A.; Ryppa, C.; Warnecke, A. Prodrug strategies in anticancer chemotherapy. *ChemMedChem* **2008**, *3* (1), 20−53.
(13) Fouad, Y. A.; Aanei, C. Revisiting the hallmarks of cancer. *Am. J. Cancer Res.* **2017**, *7* (5), 1016.
(14) Vaupel, P.; Mayer, A. Hypoxia in cancer: significance and impact on clinical outcome. *Cancer Metastasis Rev.* **2007**, *26* (2), 225−239.
(15) Wilson, W. R.; Hay, M. P. Targeting hypoxia in cancer therapy. *Nat. Rev. Cancer* **2011**, *11* (6), 393.
(16) Sharma, A.; Arambula, J. F.; Koo, S.; Kumar, R.; Singh, H.; Sessler, J. L.; Kim, J. S. Hypoxia-targeted drug delivery. *Chem. Soc. Rev.* **2019**, *48* (3), 771−813.
(17) Karnthaler-Benbakka, C.; Groza, D.; Kryeziu, K.; Pichler, V.; Roller, A.; Berger, W.; Heffeter, P.; Kowol, C. R. Tumor-targeting of EGFR inhibitors by hypoxia-mediated activation. *Angew. Chem., Int. Ed.* **2014**, *53* (47), 12930−12935.
(18) Karnthaler-Benbakka, C.; Groza, D.; Koblmüller, B.; Terenzi, A.; Holste, K.; Haider, M.; Baier, D.; Berger, W.; Heffeter, P.; Kowol, C. R.; Keppler, B. K. Targeting a Targeted Drug: An Approach Toward Hypoxia-Activatable Tyrosine Kinase Inhibitor Prodrugs. *ChemMedChem* **2016**, *11* (21), 2410−2421.
(19) Patterson, A. V.; Silva, S.; Guise, C.; Bull, M.; Abbattista, M.; Hsu, A.; Sun, J. D.; Hart, C. P.; Pearce, T. E.; Smaill, J. B. TH-4000, a hypoxia-activated EGFR/Her2 inhibitor to treat EGFR-TKI resistant T790M-negative NSCLC. *J. Clin. Oncol.* **2015**, *33*, e13548.
(20) Bielec, B.; Schueffl, H.; Terenzi, A.; Berger, W.; Heffeter, P.; Keppler, B. K.; Kowol, C. R. Development and biological investigations of hypoxia-sensitive prodrugs of the tyrosine kinase inhibitor crizotinib. *Bioorg. Chem.* **2020**, *99*, 103778.
(21) Ware, D. C.; Palmer, B. D.; Wilson, W. R.; Denny, W. A. Hypoxia-selective antitumor agents. 7. Metal complexes of aliphatic mustards as a new class of hypoxia-selective cytotoxins. Synthesis and evaluation of cobalt (III) complexes of bidentate mustards. *J. Med. Chem.* **1993**, *36* (13), 1839−1846.
(22) Jungwirth, U.; Kowol, C. R.; Keppler, B. K.; Hartinger, C. G.; Berger, W.; Heffeter, P. Anticancer activity of metal complexes: involvement of redox processes. *Antioxid. Redox Signaling* **2011**, *15* (4), 1085−1127.
(23) Heffern, M. C.; Yamamoto, N.; Holbrook, R. J.; Eckermann, A. L.; Meade, T. J. Cobalt derivatives as promising therapeutic agents. *Curr. Opin. Chem. Biol.* **2013**, *17* (2), 189−196.
(24) Ware, D. C.; Siim, B.; Robinson, K.; Denny, W.; Brothers, P.; Clark, G. Synthesis and characterization of aziridine complexes of cobalt (III) and chromium (III) designed as hypoxia-selective cytotoxins. X-ray crystal structure of trans-$[Co(Az)_4(NO_2)_2]Br\cdot 2H_2O\cdot LiBr$. *Inorg. Chem.* **1991**, *30* (19), 3750−3757.
(25) Atkinson, I. M.; Searle, G. H.; Keene, F. R. Conformational analyses of the isomers of the systems $[Co(men)n(en)3-n]^{3+}$ (men= N-methylethane-1, 2-diamine, en= ethane-1, 2-diamine; n= 1-3). *J. Chem. Soc., Dalton Trans.* **1991**, *1*, 45−51.
(26) Searle, G. H.; Keene, F. R. Cobalt (III) complexes with N-methylethane-1, 2-diamine (meen). Synthesis and characterization of the isomers of $[Co(meen)_3]^{3+}$,$[Co(meen)_2(en)]^{3+}$ and $[Co(meen)(en)_2]^{3+}$. *Inorg. Chim. Acta* **1989**, *155* (1), 125−138.
(27) Chia, Y.; Tay, M. An insight into fluorescent transition metal complexes. *Dalton Transactions* **2014**, *43* (35), 13159−13168.
(28) Lawaetz, A. J.; Stedmon, C. A. Fluorescence intensity calibration using the Raman scatter peak of water. *Appl. Spectrosc.* **2009**, *63* (8), 936−940.
(29) Dömötör, O.; Pelivan, K.; Borics, A.; Keppler, B. K.; Kowol, C. R.; Enyedy, É. A. Comparative studies on the human serum albumin binding of the clinically approved EGFR inhibitors gefitinib, erlotinib, afatinib, osimertinib and the investigational inhibitor KP2187. *J. Pharm. Biomed. Anal.* **2018**, *154*, 321−331.
(30) Graf, N.; Lippard, S. J. Redox activation of metal-based prodrugs as a strategy for drug delivery. *Adv. Drug Delivery Rev.* **2012**, *64* (11), 993−1004.
(31) Ware, D. C.; Palmer, H. R.; Pruijn, F. B.; Anderson, R. F.; Brothers, P. J.; Denny, W. A.; Wilson, W. R. Bis(dialkyl) dithiocarbamato cobalt (III) complexes of bidentate nitrogen mustards: synthesis, reduction chemistry and biological evaluation as hypoxia-selective cytotoxins. *Anticancer Drug Des.* **1998**, *13* (2), 81−103.
(32) Craig, P. R.; Brothers, P. J.; Clark, G. R.; Wilson, W. R.; Denny, W. A.; Ware, D. C. Anionic carbonato and oxalato cobalt (III) nitrogen mustard complexes. *Dalton Trans.* **2004**, *4*, 611−618.
(33) Failes, T. W.; Cullinane, C.; Diakos, C. I.; Yamamoto, N.; Lyons, J. G.; Hambley, T. W. Studies of a cobalt (III) complex of the MMP inhibitor marimastat: a potential hypoxia-activated prodrug. *Chem. - Eur. J.* **2007**, *13* (10), 2974−2982.
(34) Palmeira-Mello, M. V.; Caballero, A. B.; Ribeiro, J. M.; de Souza-Fagundes, E. M.; Gamez, P.; Lanznaster, M. Evaluation of cobalt (III) complexes as potential hypoxia-responsive carriers of esculetin. *J. Inorg. Biochem.* **2020**, *211*, 111211.
(35) Anderson, R.; Denny, W.; Ware, D.; Wilson, W. Pulse radiolysis studies on the hypoxia-selective toxicity of a colbalt-mustard complex. *Br. J. Cancer* **1996**, *27*, S48.
(36) Chang, J. Y.-C.; Lu, G.-L.; Stevenson, R. J.; Brothers, P. J.; Clark, G. R.; Botting, K. J.; Ferry, D. M.; Tercel, M.; Wilson, W. R.; Denny, W. A.; Ware, D. C. Cross-bridged cyclen or cyclam Co (III) complexes containing cytotoxic ligands as hypoxia-activated prodrugs. *Inorg. Chem.* **2013**, *52* (13), 7688−7698.
(37) SCQuery; The IUPAC Stability Constants Database (ver. 5.5). Academic Software, 1993−2005.
(38) Enyedy, É. A.; Mészáros, J. P.; Dömötör, O.; Hackl, C. M.; Roller, A.; Keppler, B. K.; Kandioller, W. Comparative solution equilibrium studies on pentamethylcyclopentadienyl rhodium complexes of 2, 2′-bipyridine and ethylenediamine and their interaction with human serum albumin. *J. Inorg. Biochem.* **2015**, *152*, 93−103.
(39) Griesser, R.; Sigel, H. Ternary complexes in solution. XI. Complex formation between the cobalt (II)-, nickel (II)-, copper (II)-, and zinc (II)-2, 2′-bipyridyl 1:1 complexes and ethylenediamine, glycinate, or pyrocatecholate. *Inorg. Chem.* **1971**, *10* (10), 2229−2232.
(40) Zékány, L.; Nagypál, I.; Leggett, D. *Computational methods for the determination of stability constants*; Plenum Press: New York, 1985.
(41) Schafer, F. Q.; Buettner, G. R. Redox environment of the cell as viewed through the redox state of the glutathione disulfide/glutathione couple. *Free Radical Biol. Med.* **2001**, *30* (11), 1191−1212.
(42) Fasman, G., Ed. *CRC Handbook of Biochemistry and Molecular Biology*; CRC Press: Cleveland, OH, 1976; p 122.
(43) Matsui, T.; Kitagawa, Y.; Okumura, M.; Shigeta, Y. Accurate standard hydrogen electrode potential and applications to the redox potentials of vitamin C and NAD/NADH. *J. Phys. Chem. A* **2015**, *119* (2), 369−376.
(44) Lovander, M. D.; Lyon, J. D.; Parr, D. L.; Wang, J.; Parke, B.; Leddy, J. Critical Review—Electrochemical Properties of 13 Vitamins: A Critical Review and Assessment. *J. Electrochem. Soc.* **2018**, *165* (2), G18−G49.
(45) Yu, Q.; Heikal, A. A. Two-photon autofluorescence dynamics imaging reveals sensitivity of intracellular NADH concentration and conformation to cell physiology at the single-cell level. *J. Photochem. Photobiol., B* **2009**, *95* (1), 46−57.
(46) Meister, A. Glutathione metabolism and its selective modification. *J. Biol. Chem.* **1988**, *263* (33), 17205−17208.
(47) Hunter, F. W.; Young, R. J.; Shalev, Z.; Vellanki, R. N.; Wang, J.; Gu, Y.; Joshi, N.; Sreebhavan, S.; Weinreb, I.; Goldstein, D. P.; et al. Identification of P450 oxidoreductase as a major determinant of

sensitivity to hypoxia-activated prodrugs. *Cancer Res.* **2015**, *75* (19), 4211−4223.
(48) Ahn, G.-O.; Botting, K. J.; Patterson, A. V.; Ware, D. C.; Tercel, M.; Wilson, W. R. Radiolytic and cellular reduction of a novel hypoxia-activated cobalt (III) prodrug of a chloromethylbenzindoline DNA minor groove alkylator. *Biochem. Pharmacol.* **2006**, *71* (12), 1683−1694.
(49) Dai, Z.-J.; Gao, J.; Ma, X.-B.; Yan, K.; Liu, X.-X.; Kang, H.-F.; Ji, Z.-Z.; Guan, H.-T.; Wang, X.-J. Up-regulation of hypoxia inducible factor-1α by cobalt chloride correlates with proliferation and apoptosis in PC-2 cells. *J. Exp. Clin. Cancer Res.* **2012**, *31* (1), 28.
(50) Stary, J.; Liljenzin, J. Critical evaluation of equilibrium constants involving acetylacetone and its metal chelates. *Pure Appl. Chem.* **1982**, *54* (12), 2557−2592.
(51) Enyedy, É. A.; Hollender, D.; Kiss, T. Lipophilicity of kinetically labile metal complexes through the example of antidiabetic Zn (II) and VO (IV) compounds. *J. Pharm. Biomed. Anal.* **2011**, *54* (5), 1073−1081.
(52) Irving, H.; Miles, M.; Pettit, L. A study of some problems in determining the stoicheiometric proton dissociation constants of complexes by potentiometric titrations using a glass electrode. *Anal. Chim. Acta* **1967**, *38*, 475−488.
(53) Gans, P; Sabatini, A; Vacca, A A. Vacca, Investigation of equilibria in solution. Determination of equilibrium constants with the HYPERQUAD suite of programs. *Talanta* **1996**, *43*, 1739−1753.
(54) Poljarevic, J. M.; Tamas Gal, G.; May, N. V.; Spengler, G.; Domotor, O.; Savic, A. R.; Grguric-Sipka, S.; Enyedy, E. A. Comparative solution equilibrium and structural studies of half-sandwich ruthenium-(II)(eta(6)-toluene) complexes of picolinate derivatives. *J. Inorg. Biochem.* **2018**, *181*, 74−85.

https://dx.doi.org/10.1021/acs.inorgchem.0c03083
Inorg. Chem. 2020, 59, 17794−17810

Supplementary material

Improving the stability of EGFR inhibitor cobalt(III) prodrugs

Marlene Mathuber[a], Hemma Schueffl[b], Orsolya Dömötör[c,d], Claudia Karnthaler[a], Éva A. Enyedy[c,d], Petra Heffeter[b,e], Bernhard K. Keppler[a,e] and Christian R. Kowol[a,e,*]

[a] Institute of Inorganic Chemistry, Faculty of Chemistry, University of Vienna, Waehringer Straße 42, 1090 Vienna, Austria

[b] Institute of Cancer Research and Comprehensive Cancer Center, Medical University of Vienna, Borschkegasse 8A, 1090 Vienna, Austria

[c] Department of Inorganic and Analytical Chemistry, University of Szeged, Dóm tér 7, H-6720 Szeged, Hungary

[d] MTA-SZTE Lendület Functional Metal Complexes Research Group, University of Szeged, Dóm tér 7, H-6720 Szeged, Hungary

[e] Research Cluster ''Translational Cancer Therapy Research'', University of Vienna and Medical University of Vienna, 1090 Vienna, Austria

* Corresponding author. E-mail address: christian.kowol@univie.ac.at

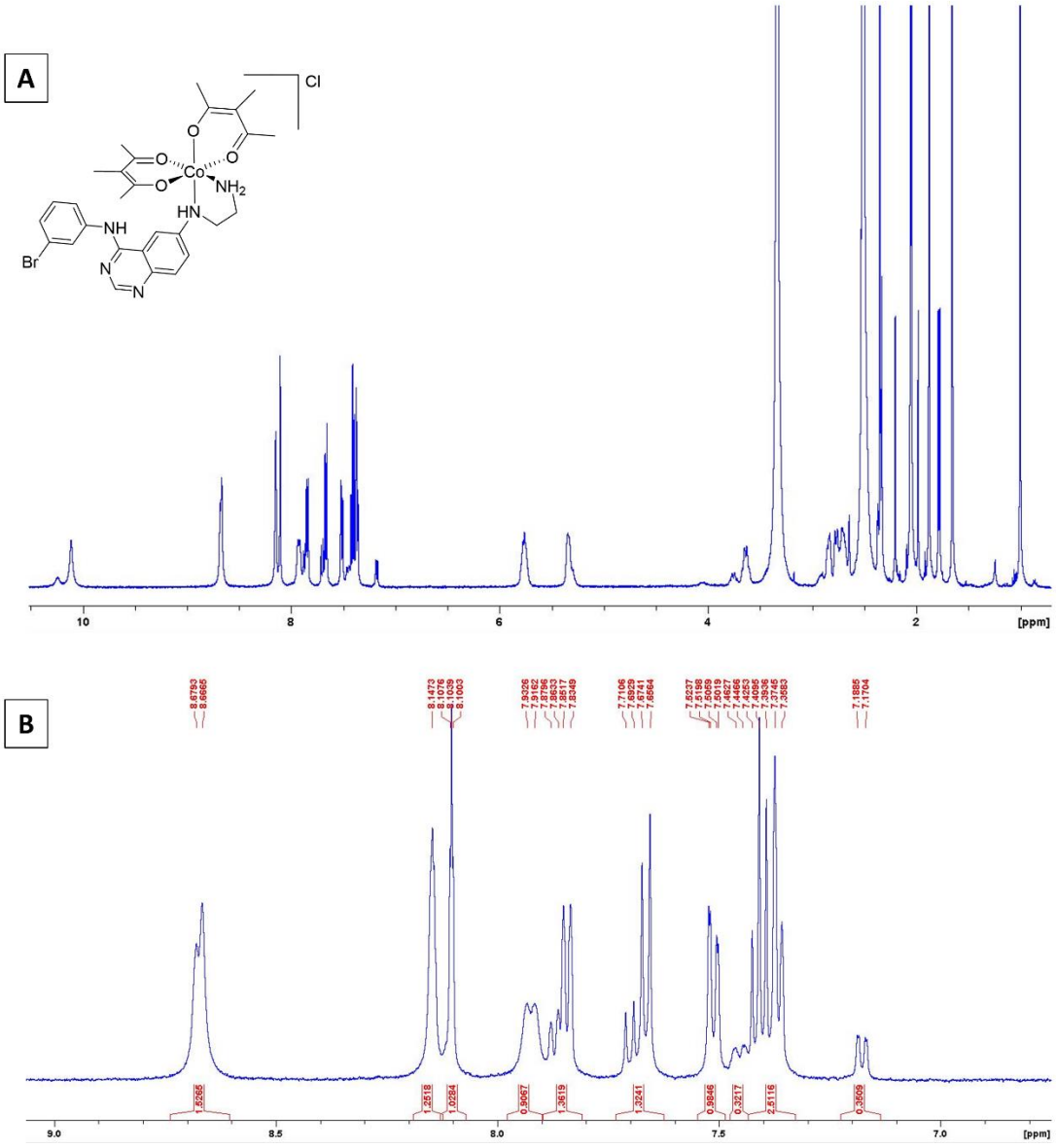

Figure S1: ^{1}H-NMR spectrum of **Co(Meacac)$_2$L$^+$,** showing the whole-range (A) and the aromatic area from ~7–9 ppm (B). Two stereoisomers can be observed.

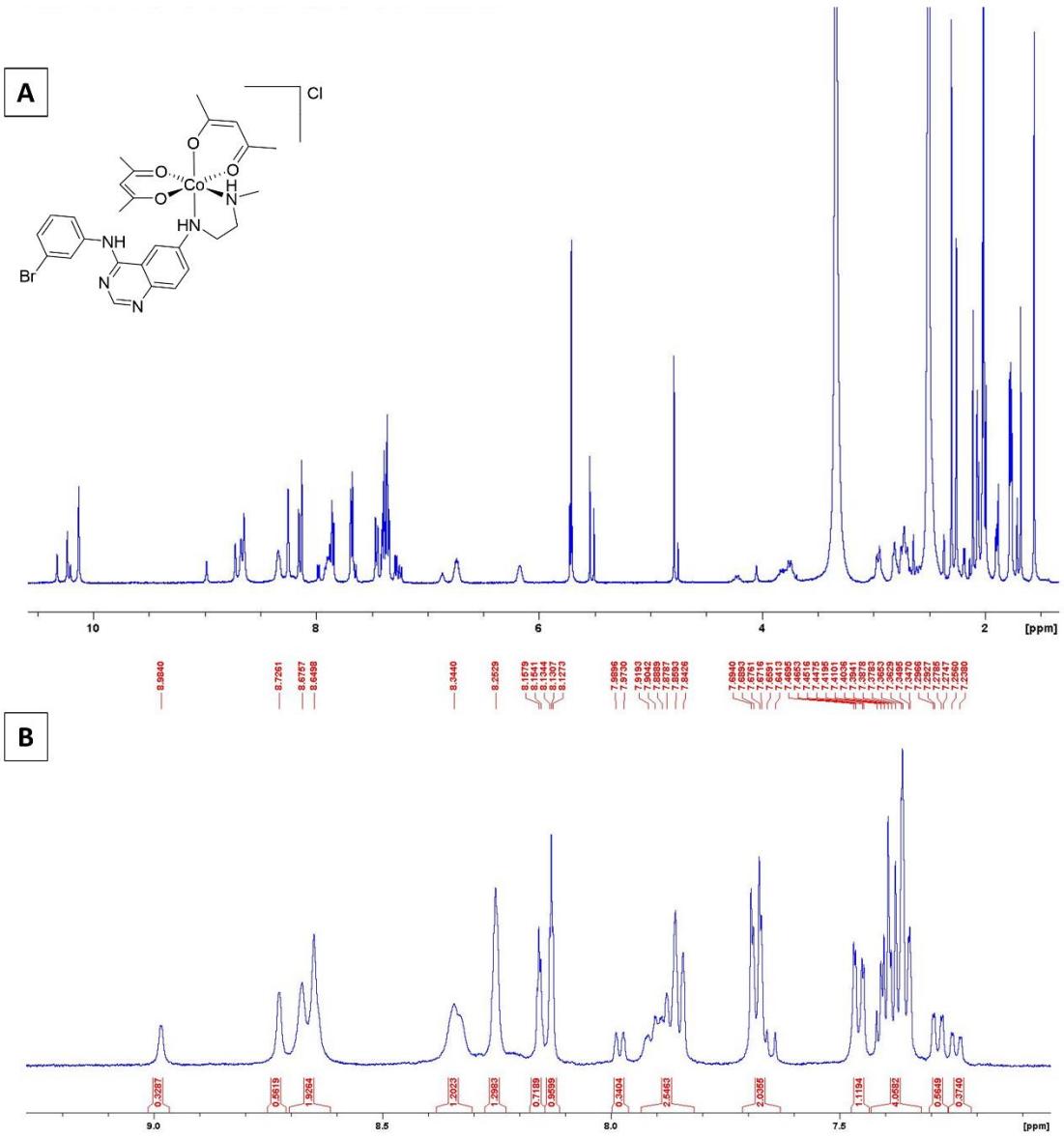

Figure S2: ^{1}H-NMR spectrum of **Co(acac)$_2$MeL$^+$,** showing the whole-range (A) and the aromatic area from ~7–9 ppm (B). Four stereoisomers can be observed.

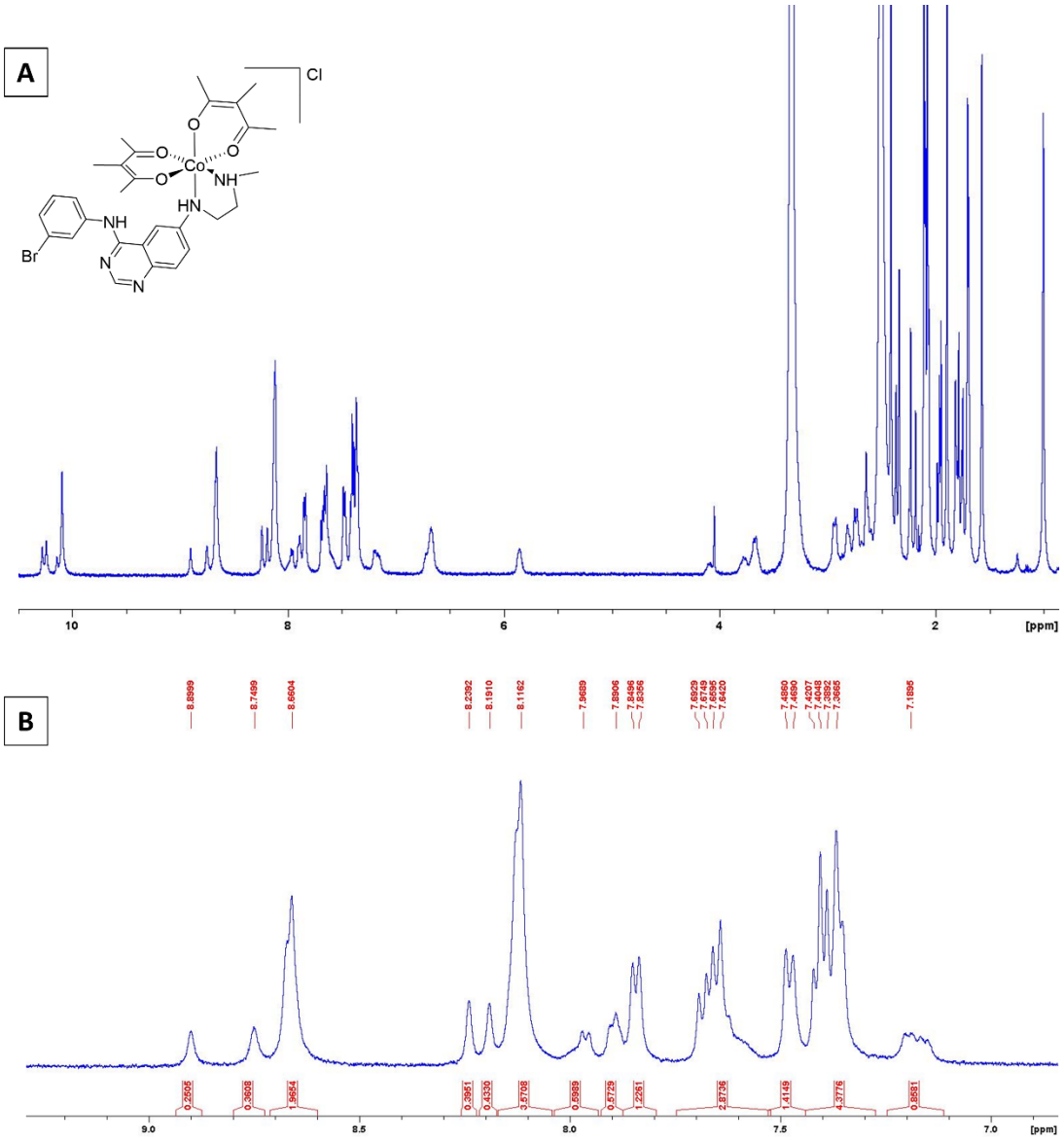

Figure S3: ^{1}H-NMR spectrum of **Co(Meacac)$_2$MeL$^+$,** showing the whole-range (A) and the aromatic area from ~7–9 ppm (B). Four stereoisomers can be observed.

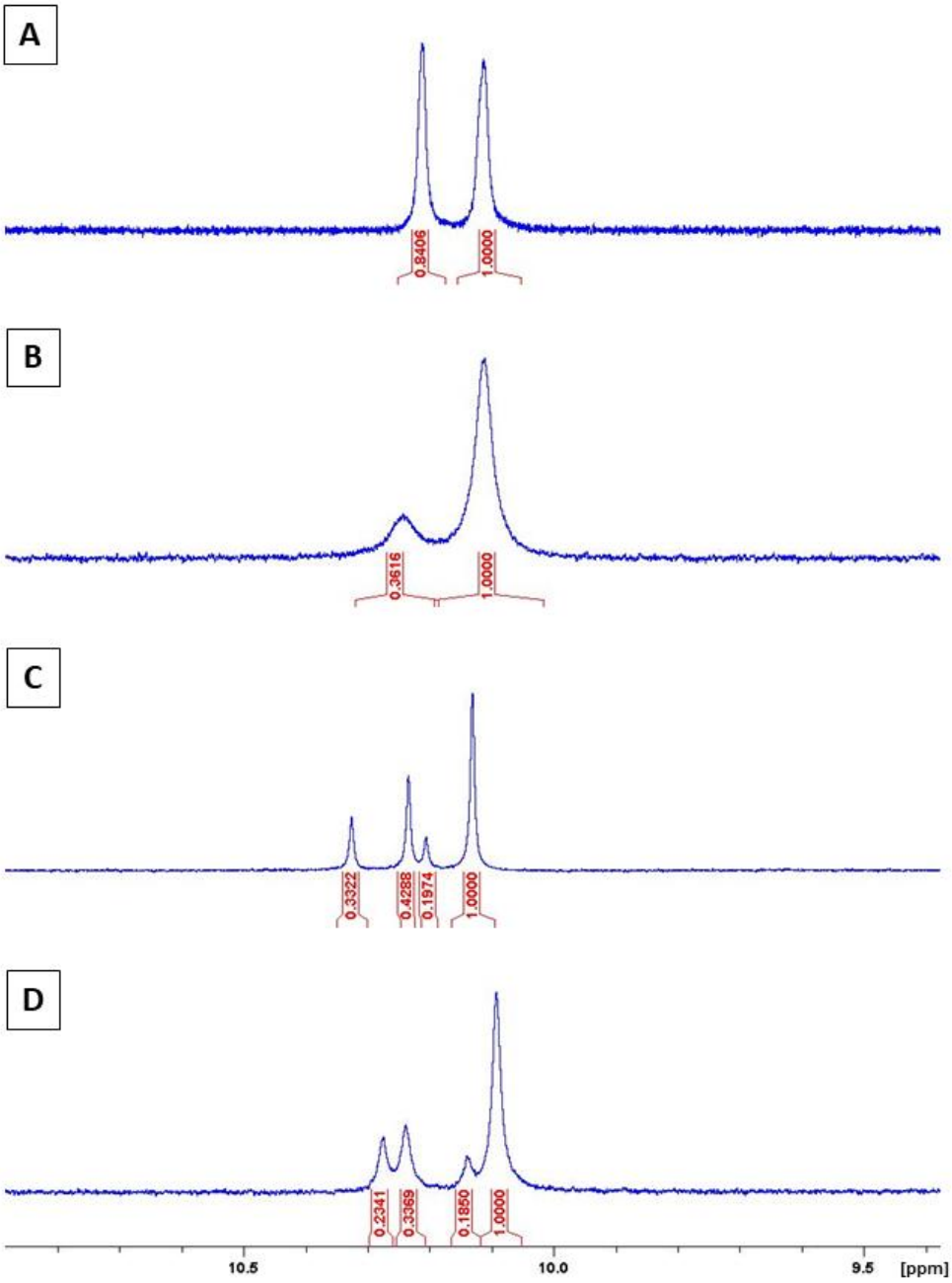

Figure S4: NH signals of the ^{1}H-NMR spectra of complexes **Co(acac)L^{+}** (A), **Co(Meacac)$_2$L^{+}** (B), **Co(acac)$_2$MeL^{+}** (C) and **Co(Meacac)$_2$MeL^{+}** (D). Depending on the number of stereogenic centres/isomers two or four separated singlets of the NH-group appear.

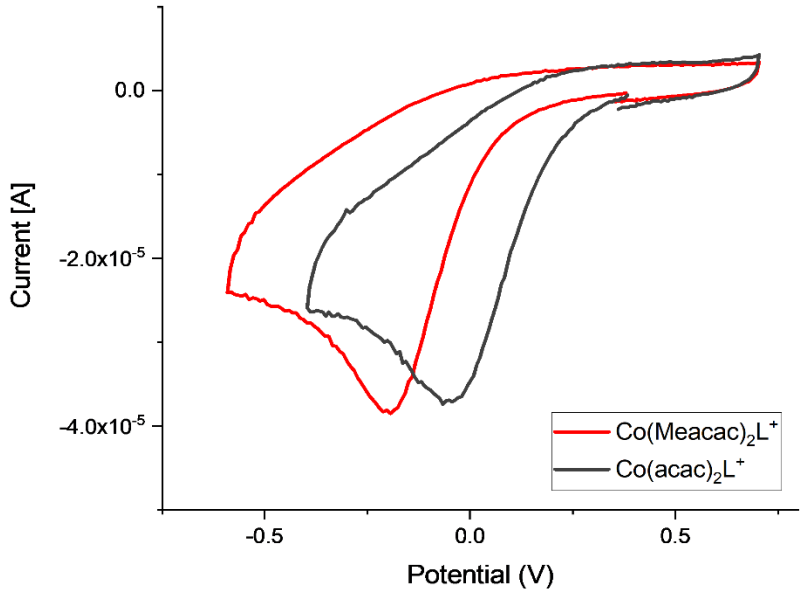

Figure S5: Cyclic voltammograms of **$Co(acac)_2L^+$** and **$Co(Meacac)_2L^+$** in 10 mM phosphate buffer pH = 7.40 [conc. complex = 1.5 mM; I = 0.10 M KCl; scan rate: 1000 mV/s, T = 25.0 °C]

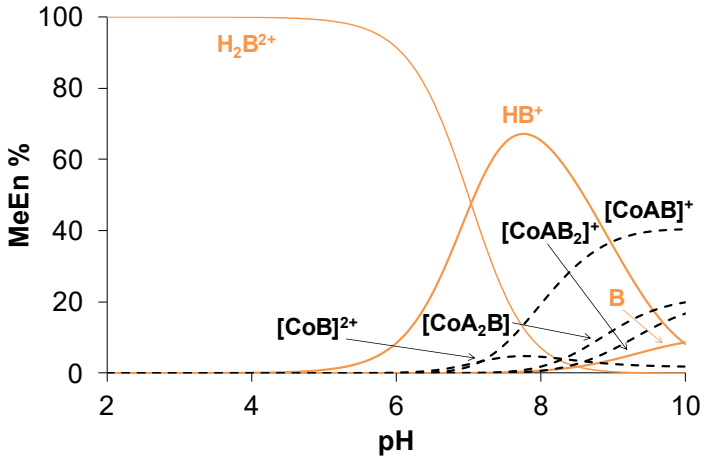

Figure S6: Concentration distribution diagram for cobalt(II)-acac-MeEn 1:2:1 system. A = acac; B = MeEn. [conc. cobalt(II) = 1 mM; I = 0.10 M (KCl); t = 25.0 °C]

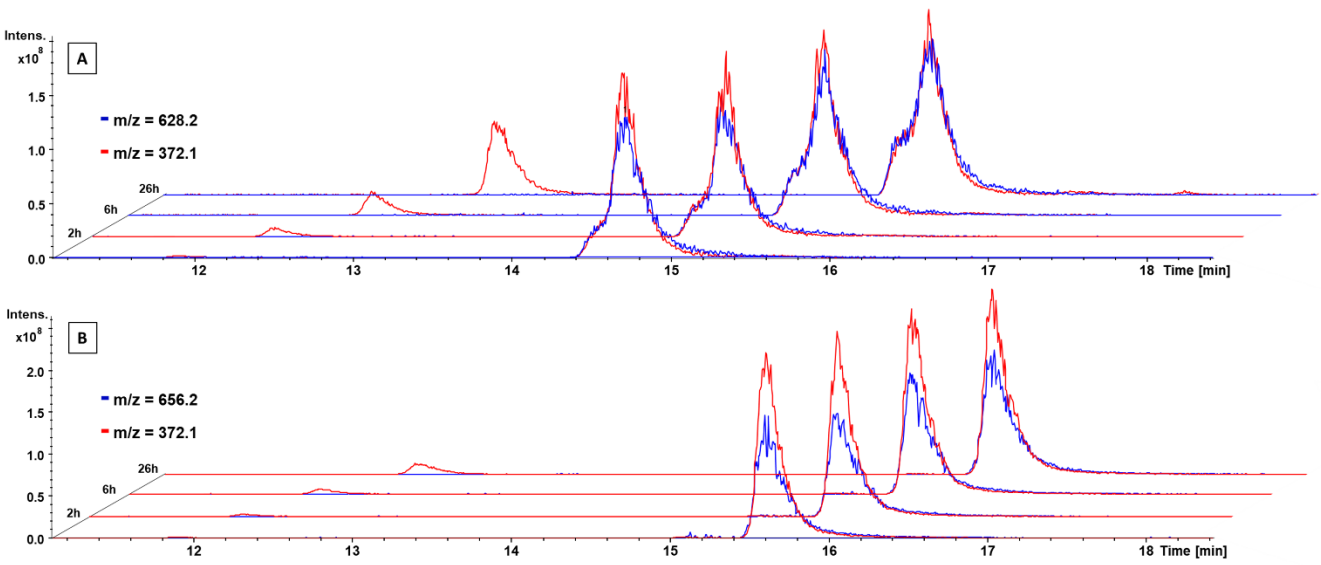

Figure S7: Time-dependent stability of **Co(acac)$_2$MeL$^+$** (A) **and Co(Meacac)$_2$MeL$^+$** (B) incubated in FCS at 37 °C (pH 7.4, 150 mM PB) monitored by HPLC–mass spectroscopy (depicted are the extracted ion mass chromatograms). Due to different ionisation properties the intensities of the free ligand (m/z 372.1) and the cobalt(III) complexes (m/z 628.2 or 656.2) cannot be directly compared.

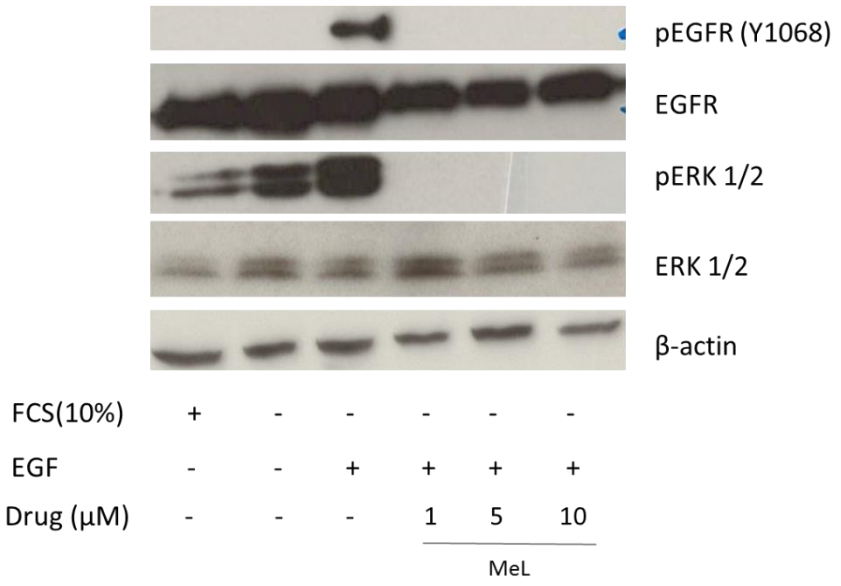

Figure S8: Impact of **MeL** on the EGFR signaling (pEGFR, pERK 1/2) under normoxic condition. A431 cells were grown in medium with or without FCS and treated with the indicated drug for 2 h. After EGFR stimulation with 50 ng/mL EGF for 10 min, cells were harvested, lysed and protein expression analyzed by Western blotting.

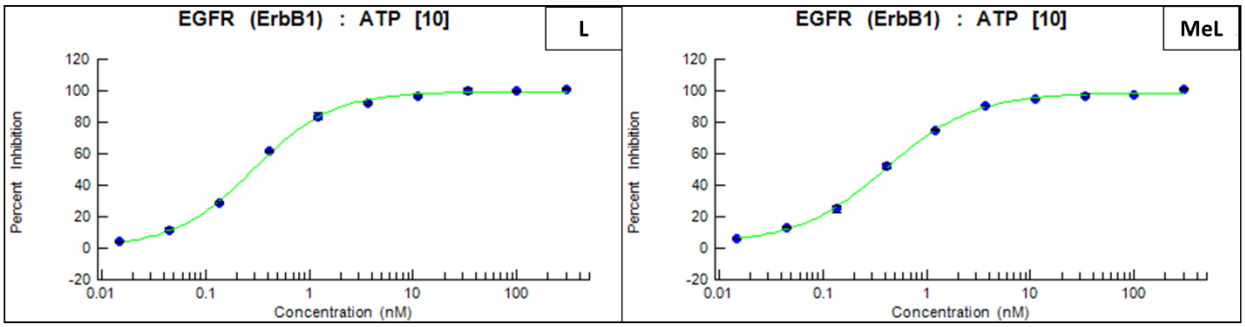

Figure S9: Data points of the cell-free EGFR kinase inhibition assay of the EGFR inhibitor ligands **L** and **MeL**.

7.2 Development of a cobalt(III)-based ponatinib prodrug system

Marlene Mathuber[a], Michael Gutmann[b], Mery La Franca[b,c], Petra Vician[b], Anna Laemmerer[b,d], Patrick Moser[b], Bernhard K. Keppler[a,d], Walter Berger[b,d]*and Christian R. Kowol[a,d]*

Inorganic Chemistry Frontiers, published on March 30th, 2021

[a] Institute of Inorganic Chemistry, Faculty of Chemistry, University of Vienna, Waehringer Straße 42, 1090 Vienna, Austria

[b] Institute of Cancer Research and Comprehensive Cancer Center, Medical University of Vienna, Borschkegasse 8A, 1090 Vienna, Austria

[c] Department of Biological, Chemical and Pharmaceutical Sciences and Technologies, University of Palermo, via Archirafi 32, 90123 Palermo, Italy

[d] Research Cluster ''Translational Cancer Therapy Research'', University of Vienna and Medical University of Vienna, 1090 Vienna, Austria

* Corresponding authors. E-mail address: christian.kowol@univie.ac.at; walter.berger@meduniwien.ac.at

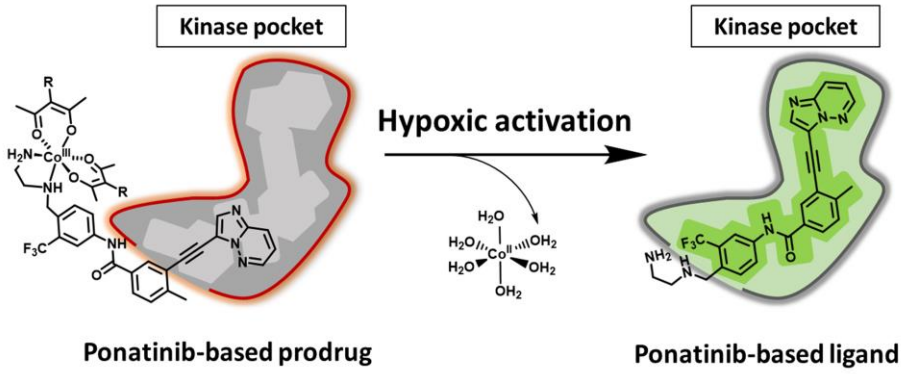

As the first author, I synthesized and characterized all compounds, determined their fluorescence properties, investigated their reduction potential, evaluated their stability under biological relevant conditions and wrote the majority of the manuscript.

INORGANIC CHEMISTRY
FRONTIERS

RESEARCH ARTICLE

View Article Online
View Journal | View Issue

Cite this: *Inorg. Chem. Front.*, 2021, **8**, 2468

Development of a cobalt(III)-based ponatinib prodrug system†

Marlene Mathuber,[a] Michael Gutmann,[b] Mery La Franca,[b,c] Petra Vician,[b] Anna Laemmerer,[b,d] Patrick Moser,[b] Bernhard K. Keppler,[a,d] Walter Berger *[b,d] and Christian R. Kowol *[a,d]

Receptor tyrosine kinase inhibitors have become a central part of modern targeted cancer therapy. However, their curative potential is distinctly limited by both rapid resistance development and severe adverse effects. Consequently, tumor-specific drug activation based on prodrug designs, exploiting tumor-specific properties such as hypoxic oxygen conditions, is a feasible strategy to widen the therapeutic window. After proof-of-principal molecular docking studies, we have synthesized two cobalt(III) complexes using a derivative of the clinically approved Abelson (ABL) kinase and fibroblast growth factor receptor (FGFR) inhibitor ponatinib. Acetylacetone (acac) or methylacetylacetone (Meacac) have been used as ancillary ligands to modulate the reduction potential. The ponatinib derivative, characterized by an ethylenediamine moiety instead of the piperazine ring, exhibited comparable cell-free target kinase inhibition potency. Hypoxia-dependent release of the ligand from the cobalt(III) complexes was proven by changed fluorescence properties, enhanced downstream signaling inhibition and increased *in vitro* anticancer activity in BCR-ABL- and FGFR-driven cancer models. Respective tumor-inhibiting *in vivo* effects in the BCR-ABL-driven K-562 leukemia model were restricted to the cobalt(III) complex with the higher reduction potential and confirmed in a FGFR-driven urothelial carcinoma xenograft model. Summarizing, we here present for the first time hypoxia-activatable prodrugs of the clinically approved tyrosine kinase inhibitor ponatinib and a correlation of the *in vivo* activity with their reduction potential.

Received 16th February 2021,
Accepted 17th March 2021

DOI: 10.1039/d1qi00211b

rsc.li/frontiers-inorganic

Introduction

Tyrosine kinases play an essential part in the signal transduction pathways of cells, by catalyzing the transfer of γ-phosphate groups of adenosine triphosphate (ATP).[1] Thus, they fulfil a crucial role in the control of *e.g.* cell growth, proliferation and differentiation. Dysregulations of these signaling processes have been linked to several diseases, including cancer initiation and progression.[2] The development of tyrosine kinase inhibitors (TKIs) is a promising targeted therapeutic approach and resulted in the approval of respective antibodies and small molecule inhibitors.[3,4] The latter competitively block the ATP-binding pockets in the active sites of tyrosine kinases.[3] One representative of this substance class is ponatinib, a multi-kinase inhibitor, which targets among others the Abelson kinase (ABL), fibroblast growth factor receptor (FGFR), and platelet-derived growth factor receptor (PDGFR) families.[5–7] Ponatinib is clinically approved as second line treatment for Philadelphia chromosome-positive chronic myeloid leukemia (Ph+ CML)/acute lymphoblastic leukemia (Ph+ ALL), especially in case of a BCR-ABLT315I mutation.[8–10] Its anti-tumorigenic potential is also evaluated in several other cancer types,[11] with the inhibition of FGFR being one major point of interest.[12,13] However, despite the specific targeting of oncogene-dependent cancer cells, adverse effects, caused by the lack of distinction between healthy and cancerous tissue, could be frequently noticed.[14] In a clinical phase III study severe arterial thrombotic events occured.[15,16] As a result, the maximum applicable dose of ponatinib for clinical routine was reduced and further safety measures were included.[15,17]

To optimize the therapeutic potential of ponatinib, a promising way could be the use of prodrug systems. In general, anticancer prodrugs consist of non-toxic, inactive compounds, which only release their active counterpart through specific activation in the tumor.[18] Cancerous tissue exhibits certain

[a]*Institute of Inorganic Chemistry, Faculty of Chemistry, University of Vienna, Waehringer Straße 42, 1090 Vienna, Austria*
[b]*Institute of Cancer Research and Comprehensive Cancer Center, Medical University of Vienna, Borschkegasse 8A, 1090 Vienna, Austria*
[c]*Department of Biological, Chemical and Pharmaceutical Sciences and Technologies, University of Palermo, via Archirafi 32, 90123 Palermo, Italy*
[d]*Research Cluster "Translational Cancer Therapy Research", University of Vienna and Medical University of Vienna, 1090 Vienna, Austria.*
E-mail: christian.kowol@univie.ac.at, walter.berger@meduniwien.ac.at
†Electronic supplementary information (ESI) available. See DOI: 10.1039/d1qi00211b

features, such as a hypoxic environment, which can be exploited for this kind of approach.[19,20] Hypoxia-activated prodrugs (HAPs) have been intensively explored over the past years for various substance classes with a focus on DNA alkylating agents.[21–23] Although some of these compounds (*e.g.* tirapazamine, evofosfamide, apaziquone) have entered advanced clinical studies, none of them received approval so far.[24,25] Surprisingly, until now this prodrug approach has been implemented only on a few TKI compounds,[26–28] with TH-4000 as one of the first examples.[29] Various chemical possibilities to exploit hypoxia are known with nitroimidazoles[27–29] and cobalt(III) metal complexes as important representatives.[26,30,31] The mechanism of the latter is based on distinct differences in ligand lability of the cobalt(III) (kinetically inert) and cobalt(II) (kinetically labile) oxidation state.[32,33] Due to its bulkiness, the intact cobalt(III) complex should not be able to bind to the ATP binding pocket of the respective kinase (Fig. 1). In healthy tissue (normoxic conditions) the complex is stable, thus the release of the bioactive ligand is prevented.[34]

In contrast, in the hypoxic environment of a tumor, the inactive prodrug will be irreversibly reduced. This results in the dissociation of the complex, with formation of $[Co(II)(H_2O)_6]^{2+}$ and release of the bioactive ligand with subsequent binding to the kinase pocket (Fig. 1).

In such a prodrug approach, a well-balanced equilibrium is important: on the one hand the cobalt(III) complex needs to have a high stability in healthy tissue, on the other hand the bioactive ligand should be efficiently released after reduction under hypoxic conditions. Seminal work of Ware *et al.* demonstrated that monodentate aziridine ligands could not sufficiently stabilized and therefore bidentate chelating ligands are preferred.[33]

In a previous study of our group, we established the concept of cobalt(III) prodrugs for EGFR-inhibitors, based on Erlotinib derivatives ($\mathbf{L_{EGFR}}$; Fig. 2).[26] We observed that, due to the direct connection of the ethylenediamine unit to the quinazoline ring system, the reduction potential of the respective cobalt(III) complex distinctly increased resulting in reduced stability in blood serum. In this study we focused on ponatinib, which is not only a highly active, clinically approved anticancer drug, but possesses also a $-CH_2$-spacer between the solubilizing piperazine moiety and the aromatic ring system ($\mathbf{L_{Pon}}$; Fig. 2). As ancillary ligands of the cobalt(III) complexes, acetylacetone (acac) or methylacetylaceton (Meacac) were used. The novel compounds were evaluated for their fluorescence properties, electrochemical potential, kinetic reduction behavior and serum stability. Additionally, their fluorescence properties and the biological activity were investigated under nor-

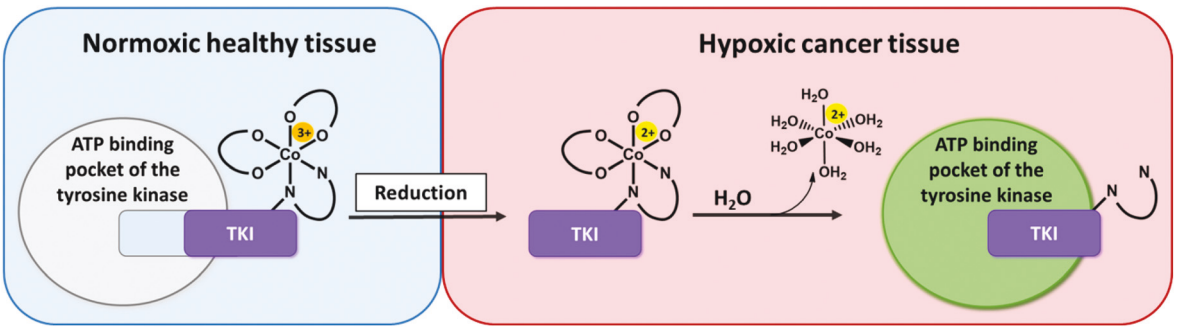

Fig. 1 Proposed mode of action of hypoxia-activated cobalt(III) prodrugs. **Normoxic, healthy tissue (left side):** The prodrug is inactive. Due to its bulkiness, the cobalt(III) complex does not fit into the ATP-binding pocket of the respective tyrosine kinase. **Hypoxic cancer tissue (right side):** The drug is active. In the hypoxic tissue of the tumor, the cobalt(III) complex is irreversibly reduced and the TKI ligand subsequently released able to inhibit the signaling processes of the target tyrosine kinases.

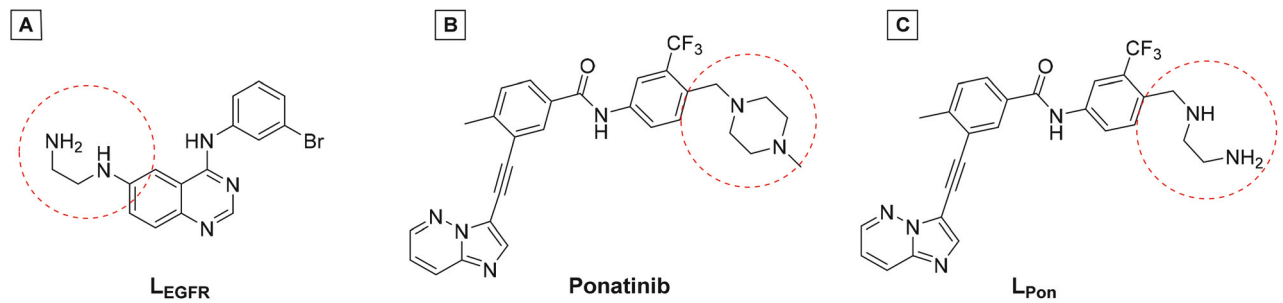

Fig. 2 (A) Chemical structure of the previously synthesized EGFR inhibitor ligand (L_{EGFR}) with a direct attachment of the ethylenediamine moiety to the aromatic ring system.[26] (B) The clinically approved ponatinib (Iclusig®). (C) Newly developed ponatinib derivative (L_{Pon}), where the metal-chelating ethylenediamine moiety is separated from the aromatic ring system.

moxic *vs.* hypoxic conditions in an FGFR- or ABL1-driven cancer cell background. Finally, the *in vivo* antitumor activity of the novel complexes was evaluated in the respective xenograft mouse models.

Results and discussion

Docking studies

To get a first indication if our proposed strategy is indeed promising, we performed docking studies of the novel ligand $\mathbf{L_{Pon}}$ and the two cobalt(III) complexes $\mathbf{Co(acac)_2L_{Pon}}$ and $\mathbf{Co(Meacac)_2L_{Pon}}$ (Scheme 1) compared to the approved parental compound ponatinib. In general, the anticancer effect of TKIs is based on their strong intermolecular, non-covalent interactions with target-specific residues mainly consisting of hydrogen bonds, van der Waals, and Coulomb interactions.[35] Consequently, molecular docking is a well-established tool in the field of TKI development.[36] As kinases, two of the main targets of ponatinib were chosen, namely FGFR1 (PDB ID: 4V04) and ABL1 (PDB ID: 4WA9). The results indicated that the replacement of the piperazine moiety of ponatinib by an ethylenediamine group ($\mathbf{L_{Pon}}$) did not change the binding mode in the pockets of FGFR1 (Fig. 3A and B) as well as ABL1 (Fig. 3C and D). In addition, the data of the complexes $\mathbf{Co(acac)_2L_{Pon}}$ and $\mathbf{Co(Meacac)_2L_{Pon}}$ convincingly showed that $\mathbf{L_{Pon}}$ attached to the cobalt(III) core is unable to interact with the active sites of FGFR1 and ABL1. The steric effects of the complexation prohibited all crucial interactions with FGFR1 and ABL1 (Fig. 3 and S1†). Summarizing, the molecular docking studies showed that $\mathbf{L_{Pon}}$ is comparable to ponatinib in its kinase binding ability and that the cobalt(III) complexes can be considered as promising prodrugs.

Synthesis and characterization

To obtain a suitable metal-binding moiety for the complexation with a cobalt precursor, the piperazine was exchanged with an ethylenediamine unit (Scheme 1). To this end, the aliphatic amino group of the commercially available 4-(aminomethyl)-3-(trifluoromethyl)aniline was protected using di-*tert*-butyl dicarbonate. For the subsequent coupling reaction between the free aromatic amino group and purchased 3-(2-{imidazo[1,2-*b*]pyridazin-3-yl}ethynyl)-4-methylbenzoic acid, the carboxylic acid was first converted into the corresponding acyl chloride using oxalylchloride $(COCl)_2$ in toluene.[37] Subsequently, the amino group was deprotected using HCl, followed by neutralization of the formed HCl salt. Reductive amination with *N*-boc-(metylamino)-acetaldehyde and sodium cyanoborhydride yielded in the introduction of the protected ethylenediamine moiety. Finally, a second deprotection step with trifluoroacetic acid (TFA) and purification by reversed-phase HPLC generated the ethylenediamine-bearing ponatinib derivative $\mathbf{L_{Pon}}$ as three-fold TFA salt.

For the synthesis of the cobalt complexes, acetylacetone (acac) or methylacetylacetone (Meacac) were used as ancillary ligands, since these ligands can also distinctly influence the reduction potential of the complex.[33,38] The cobalt(III) complexes were synthesized by reaction of $Na[Co(acac)_2(NO_2)_2]$ or $Na[Co(Meacac)_2(NO_2)_2]$ with $\mathbf{L_{Pon}}$ (after the *in situ* deprotonation of the ligand with NaOH) in methanol and the presence of activated charcoal following a slightly modified procedure

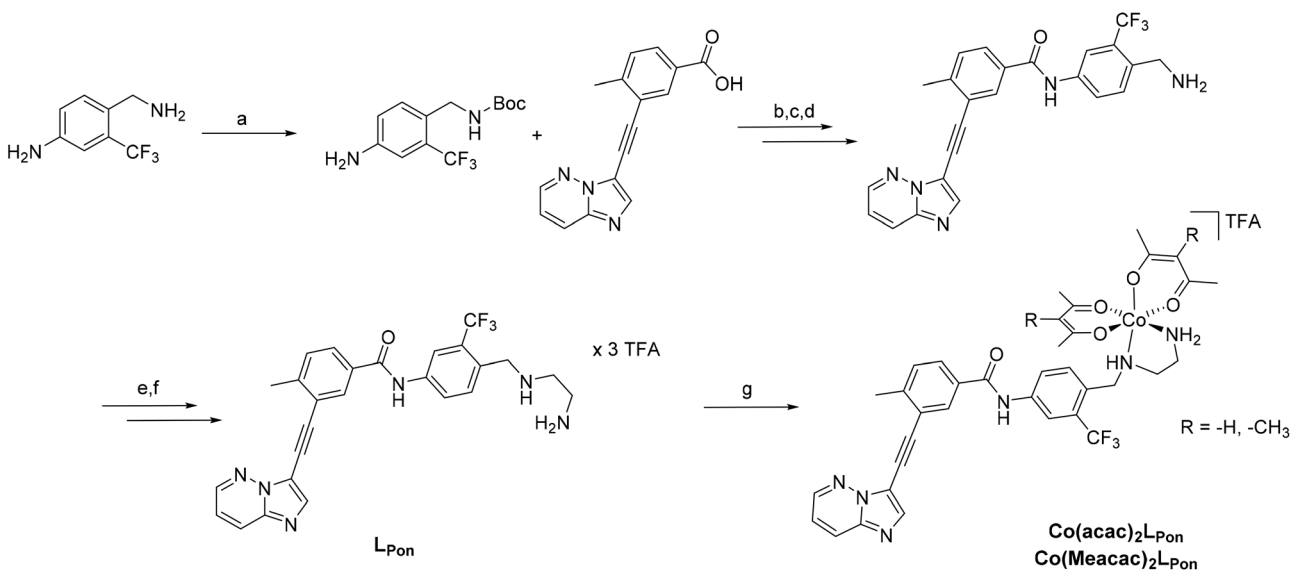

Scheme 1 Synthesis of L_{Pon} and its cobalt(III) complexes $\mathbf{Co(acac)_2L_{Pon}}$ and $\mathbf{Co(Meacac)_2L_{Pon}}$. Reagents and conditions: (a) Di-*tert*-butyl dicarbonat, THF, 81%; (b) $(COCl)_2$, abs. Toluol, NMM, DMAP, 68%; (c) 4 N HCl in dioxan/H_2O, 95%; (d) $NaHCO_3$ in EtOAc, 94%; (e) *N*-Boc-2-aminoacetaldehyde, sodium cyanoborhydride, abs. THF, molecular sieves (3–4 Å), 50%; (f) TFA in dichloromethane (ratio 1 : 1), 40%; (g) *in situ* deprotonation with NaOH, $Na[Co(acac)_2(NO_2)_2]$ or $Na[Co(Meacac)_2(NO_2)_2]$, activated charcoal in MeOH, 36% for $\mathbf{Co(acac)_2L_{Pon}}$ and 31% for $\mathbf{Co(Meacac)_2L_{Pon}}$.

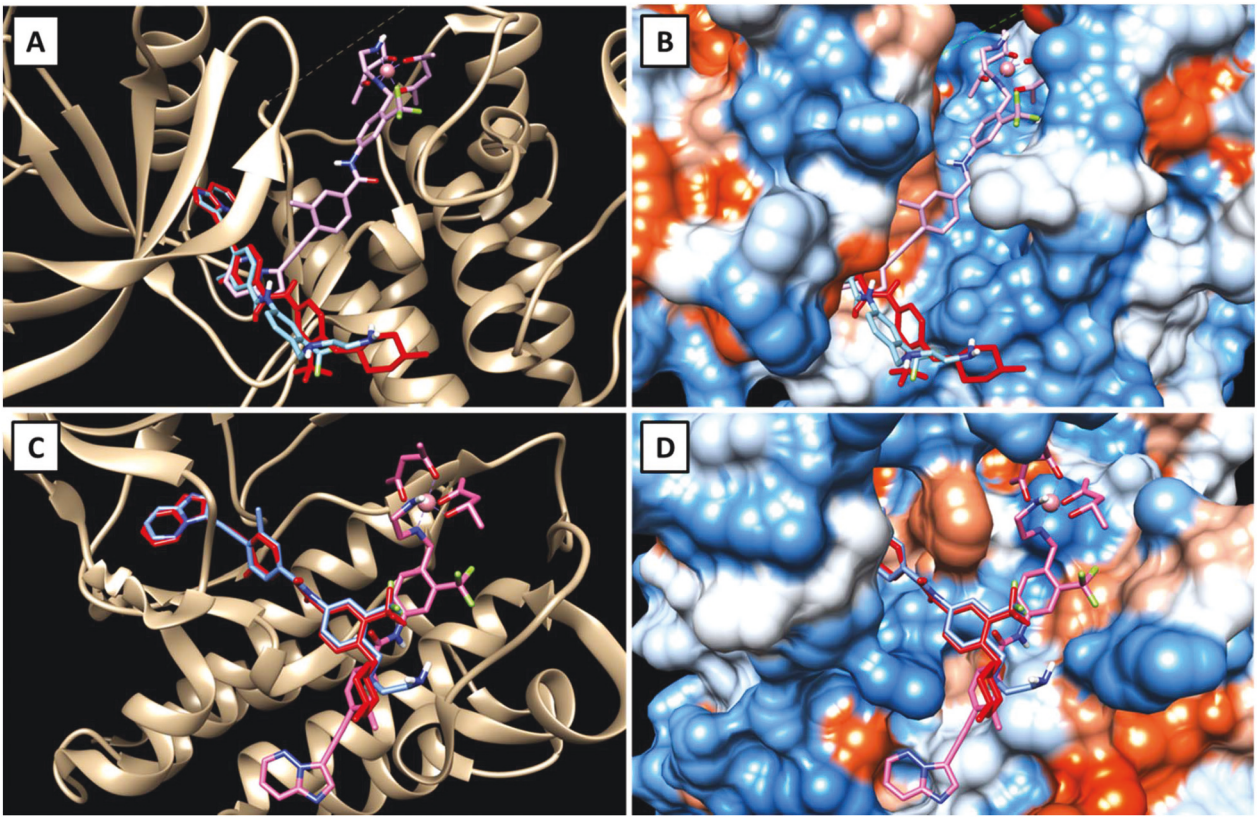

Fig. 3 Visualizations of the best docking poses of L_{Pon} and $Co(acac)_2L_{Pon}$ in comparison to ponatinib with FGFR1 (A and B) (PDB ID: 4V04) as well as ABL1 (C and D) (PDB ID: 4WA9). Ponatinib is shown in red, L_{Pon} in blue and $Co(acac)_2L_{Pon}$ in pink.

of Denny *et al.*[39] Afterwards, the crude products were directly purified by reversed-phase HPLC (with the addition of 0.1% TFA to the eluents) leading to the respective TFA salts of $\mathbf{Co(acac)_2L_{Pon}}$ and $\mathbf{Co(Meacac)_2L_{Pon}}$. Due to the two stereogenic centers (one from the propeller chirality of the complex itself and the other from the aliphatic NH-group of the ethylenediamine bridge), two isomers of the cobalt(III) complexes are present. For $\mathbf{Co(acac)_2L_{Pon}}$ we could separate the two isomers by adjusting the gradient of the preparative HPLC purification (Fig. S2†). All novel compounds were characterized by mass spectrometry as well as ^{1}H and ^{13}C one- and two-dimensional NMR spectroscopy and their purity was confirmed by elemental analysis. The amount of TFA was confirmed by ^{19}F-NMR measurements *via* the ratio of the fluorine signals between $\mathbf{L_{Pon}}$ and TFA.

The ^{1}H NMR spectra of the isomeric mixtures of the cobalt(III) complexes [~60% : 40% for $\mathbf{Co(acac)_2L_{Pon}}$ and ~70% : 30% for $\mathbf{Co(Meacac)_2L_{Pon}}$] show only one signal set in the aromatic area (with the exception of H23; see Experimental part), but two in the aliphatic area and of the –NH groups (Fig. S3 and S4†). This is in contrast to our previously synthesized cobalt(III) complex with $\mathbf{L_{EGFR}}$, where all signals could be observed twice.[26] An obvious explanation is that the conjugated system in the $\mathbf{L_{Pon}}$ ligand is much less extended compare to $\mathbf{L_{EGFR}}$ (Fig. 2). A clear indication, that we were indeed able to lower the impact of the ring system on the chelating ethylenediamine moiety and *vice versa*.

Following the successful isolation of the two isomers of $\mathbf{Co(acac)_2L_{Pon}}$, we studied their interconversion behavior in phosphate buffered saline (PBS) (pH 7.4, 10 mM) incubated at 37 °C. An interconversion is possible due to the chiral N of the ethylenediamine moiety, which can detach, invert and bind again, resulting in the other diastereomer. The results showed that the conversion from isomer 1 into isomer 2 proceeded with ~30% after 72 h (Fig. 4A). In contrast, the reverse reaction from pure isomer 2 into isomer 1 yielded in only ~20% conversion after 72 h (Fig. 4B). A higher kinetic stability of isomer 2 is also supported by data after 9 days, which reveal that initial pure isomer 1 is converted to a racemic mixture with isomer 2 (50%:50%). In case of pure isomer 2 still a ratio of ~60 : 40 is present after 9 days. At the same time, these experiments revealed that the complexes are highly stable in aqueous solution at pH 7.4 without any release of the ponatinib-like ligand. Because of the slow conversion rates the pure isomers of $\mathbf{Co(acac)_2L_{Pon}}$ were also biologically investigated (*vide infra*).

Fluorescence properties

We could recently show that ponatinib possesses distinct fluorescence properties with an emission maximum at 470 nm

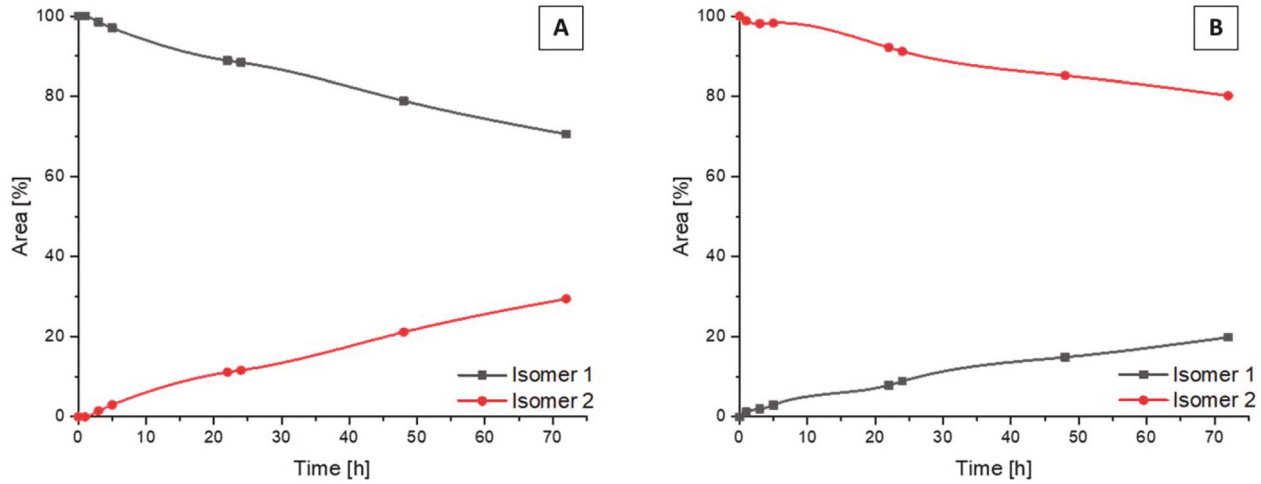

Fig. 4 Kinetic behavior of the isomers of **Co(acac)$_2$L$_{Pon}$** incubated in PBS at 37 °C (pH 7.4, 10 mM) and monitored by HPLC. Depicted is the conversion from pure isomer 1 (A) and pure isomer 2 (B) into the respective mixtures over a period of 72 h.

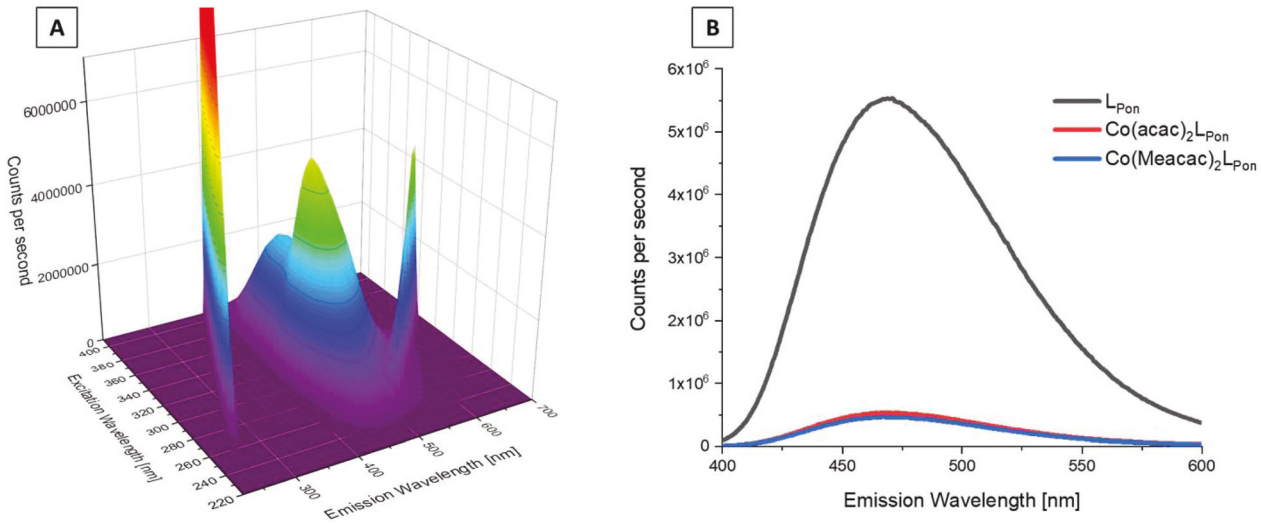

Fig. 5 Fluorescence properties of investigated ponatinib derivatives. (A) 3D full excitation–emission landscape of **L$_{Pon}$** (Rayleigh scattering of 1st and 2nd order appear as diagonal ridges). (B) Fluorescence emission spectra at λ_{ex} = 320 nm of **L$_{Pon}$**, **Co(acac)$_2$L$_{Pon}$**, and **Co(Meacac)$_2$L$_{Pon}$**. Measurements were performed in PBS at pH = 7.40 [conc. ligand/complex = 15 μM; T = 25.0 °C].

when irradiated at 320 nm (measured in PBS pH = 7.40, concentration = 15 μM).[40] Therefore, we also analyzed the fluorescence of the novel ligand **L$_{Pon}$** and its cobalt(III) complexes under the same conditions. The 3D spectrum of **L$_{Pon}$** showed a maximum and intensity similar to ponatinib (λ_{em} = 470 nm at λ_{ex} = 320 nm) (Fig. 5A). In contrast, for the cobalt(III) complexes a strongly quenched fluorescence in PBS was observed (Fig. 5B). This phenomenon can be explained by the metal center, which influences the conversion of singlet-excited states to triplet-excited states with extremely fast intersystem crossing rates (typical lifetimes are in the fs scale). Hence, ligand-based fluorescence is often difficult to observe in a metal coordinated form.[41] However, these distinct differences in the fluorescence properties between free ligand and cobalt(III) complex can be exploited for stability studies in cell culture (*vide infra*).

Cyclic voltammetry

Since the redox potential is a crucial characteristic for the activation of cobalt(III)-based prodrugs systems, we investigated the novel complexes by cyclic voltammetry in comparison to **Co(acac)$_2$L$_{EGFR}$**. Measurements were performed in dimethylformamide (DMF) (+0.2 M [n-Bu$_4$N][BF$_4$]) at a scan speed of 100 mV s^{-1}. The voltammograms revealed a single irreversible cathodic peak, which can be assigned to the reduction of

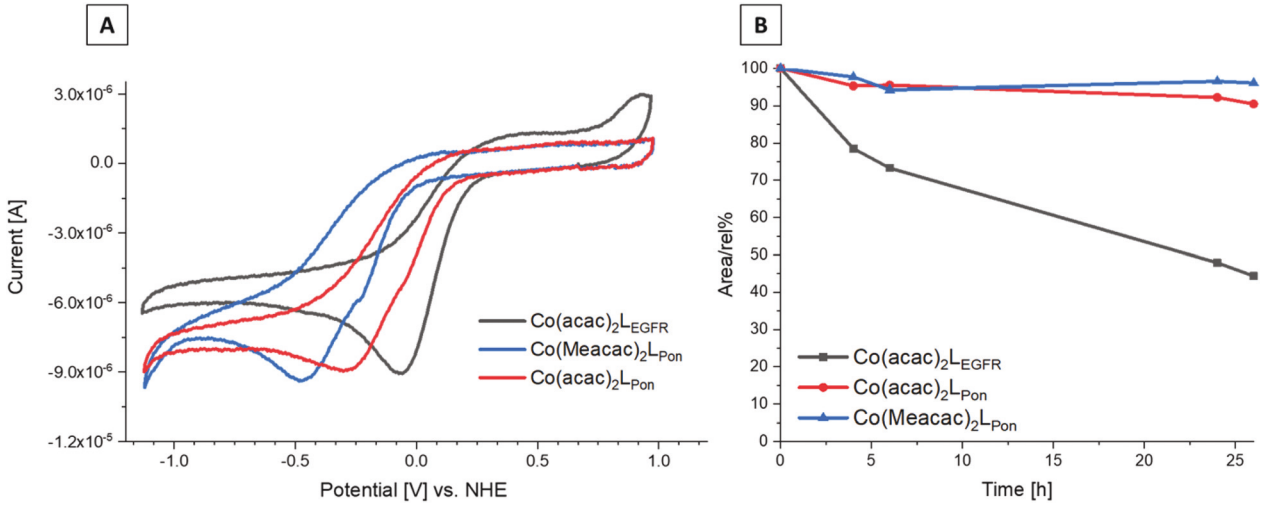

Fig. 6 (A) Cyclic voltammograms of **Co(acac)$_2$L$_{Pon}$**, **Co(Meacac)$_2$L$_{Pon}$** and **Co(acac)$_2$L$_{EGFR}$** in DMF (1.5 mM complex, I = 0.2 M [n-Bu_4N][BF_4], scan rate of 100 mV s^{-1}, 25.0 °C). (B) Stability measurements of **Co(acac)$_2$L$_{Pon}$**, **Co(Meacac)$_2$L$_{Pon}$** and **Co(acac)$_2$L$_{EGFR}$** incubated in pure FCS at 37 °C (pH 7.4, 150 mM phosphate buffer) analyzed by HPLC-MS over a time period of 26 h. The y-axis shows the relative ratio of the integrated peak areas of the intact complex over time (in percent) compared to the area at the starting point (0 h).

cobalt(III) to cobalt(II) (Fig. 6A). Even at a higher scan speed of 1000 mV s^{-1}, the redox processes were still completely irreversible for all complexes (Fig. S5†).

The data clearly showed that the "separation" of the chelating ethylenediamine moiety from the ring system in case of the ponatinib complex **Co(acac)$_2$L$_{Pon}$** resulted in the desired strongly decreased cathodic peak potential at −315 mV *vs.* NHE, compared to the directly attached EGFR-inhibitor reference **Co(acac)$_2$L$_{EGFR}$** at −57 mV *vs.* NHE. Methylation of the ancillary acetylacetone ligands in **Co(Meacac)$_2$L$_{Pon}$** further shifted the potential to −442 mV *vs.* NHE. This in line with literature data of other cobalt(III) prodrugs systems.[33,38] Investigation of the same complexes in a DMF/H_2O (7 : 3 v/v) mixture, resulted in similar shifts (Fig. S6†). In all measurements completely irreversible reduction processes were observed, regardless of the solvent or scan speed (100–1000 mV s^{-1}). This is of interest, since the proposed mechanism for cobalt(III) prodrugs is often associated with a reversible redox behaviour of these complexes. The frequently proposed model suggests that under normoxic conditions in healthy tissue the reduced cobalt(II) complex will immediately be re-oxidized by oxygen to the inert cobalt(III) complex and thus the release of the bioactive ligand is prevented.[34,42,43] Interestingly, for most cobalt(III) prodrugs reported in literature irreversible redox processes in aqueous solutions could be observed, which contradicts this hypothesis.[44–47]

Notably, pulse radiolysis studies of cobalt(III) nitrogen mustard complexes indeed suggested that the re-oxidation rate under normoxia is too slow and the cobalt(III) complexes rather compete with molecular oxygen for one-electron reductants.[48] Nevertheless, different cobalt(III) complexes with irreversible electrochemical behavior exhibited strong hypoxia-dependent activity against cancer cells *in vitro* and *in vivo*, proving the potential of such complexes.[26,45]

Serum stability measurements

Recently, we could show that even the EGFR-inhibitor cobalt(III) complex **Co(acac)$_2$L$_{EGFR}$** (with the highest redox potential) is completely stable in the presence of the natural low-molecular weight reducing agents ascorbic acid, glutathione or reduced nicotinamide adenine dinucleotide (NADH).[38] Therefore, we only investigated the stability of the novel complexes in fetal calf serum (FCS). As reference again **Co(acac)$_2$L$_{EGFR}$**[26] was included. The complexes were dissolved in 50 mM phosphate puffer and mixed 1 : 10 with fetal calf serum (FCS; buffered with 150 mM phosphate buffer to keep a stable pH of 7.4) to a final concentration of 50 μM. The samples were incubated at 37 °C and after 0, 2, 4, 6, 24 and 26 h extracted with acetonitrile and measured by HPLC-MS. Both ponatinib-derived complexes **Co(acac)$_2$L$_{Pon}$** and **Co(Meacac)$_2$L$_{Pon}$** were highly stable in FCS with ~90% intact complex after 26 h (Fig. 6B). In contrast, the reference **Co(acac)$_2$L$_{EGFR}$** showed less than 50% remaining complex after the same incubation time, in line with our previous results.[38] This indeed confirms, that by avoiding the direct attachment of the ethylenediamine moiety to an aromatic ring system, complexes with much higher stability can be generated. Since no distinct difference in stability between **Co(acac)$_2$L$_{Pon}$** and **Co(Meacac)$_2$L$_{Pon}$** within 26 h could be observed, measurements were repeated up to 72 h. Now the slightly increased stability of **Co(Meacac)$_2$L$_{Pon}$** at ~80% of intact compound compared to **Co(acac)$_2$L$_{Pon}$** at ~70% could be uncovered (Fig. S7†).

Biological investigations

Hypoxia-inducible intracellular ligand release

Prior to the evaluation of the anticancer activity of our novel derivatives in cell culture models, we examined the stability of

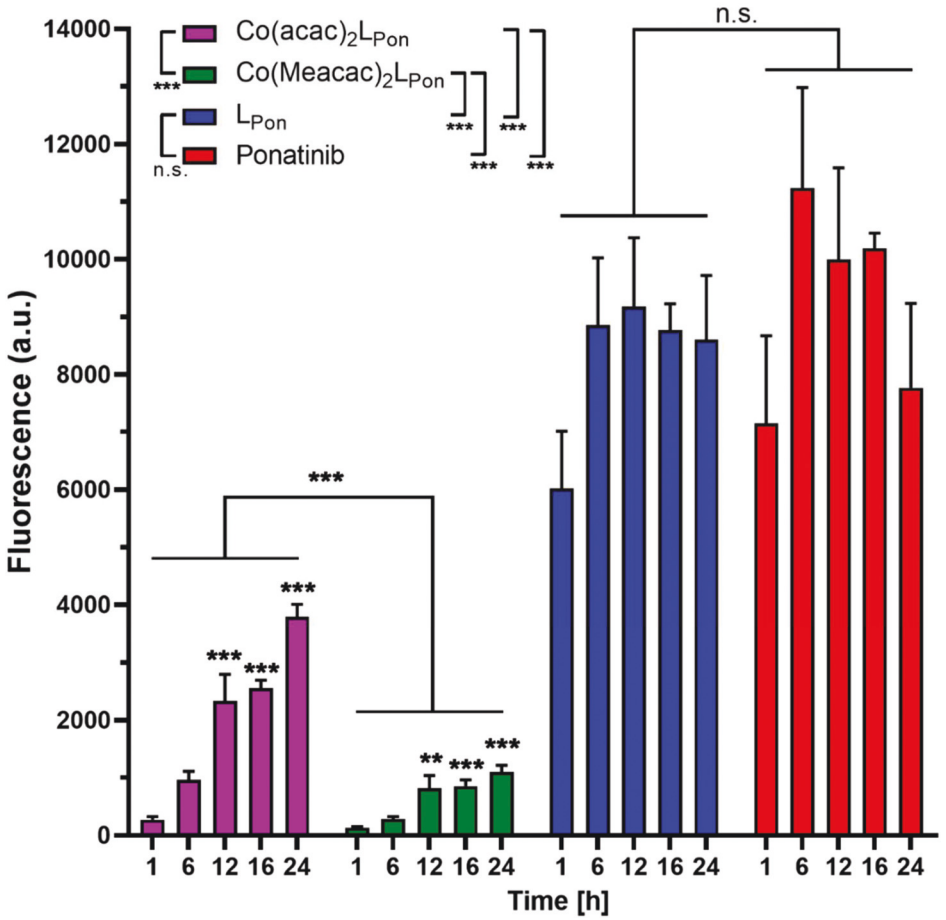

Fig. 7 Fluorescence-based evaluation of L_{Pon} release from **Co(acac)$_2$L$_{Pon}$** and **Co(Meacac)$_2$L$_{Pon}$** in K-562 cells under normoxic cell culture conditions by flow cytometry. Cells were incubated with 10 μM of the respective compounds for the indicated exposure times and mean fluorescence intensities were determined by flow cytometry (BD LSRFortessa X-20, pacific blue filter). Fluorescence intensities were normalized by subtracting the auto fluorescence of untreated cells. Data are given in arbitrary units (a.u.) as means ± SEM of five independent experiments. Statistical significance was calculated by two-way ANOVA with $p < 0.05$(*); <0.01 (**); <0.001 (***).

Co(acac)$_2$L$_{Pon}$ and **Co(Meacac)$_2$L$_{Pon}$** in the presence of cells under normoxic conditions. The stability was determined by the appearance of **L$_{Pon}$**-associated fluorescence (*vide supra*) in BCR-ABL-driven K-562 leukemia cells *via* flow cytometry. As shown in Fig. 7, both ponatinib and **L$_{Pon}$** were taken up rapidly and efficiently by K-562 cells with no significant increase in cell-associated fluorescence from 1 h exposure onwards. In contrast, exposure of K-562 cells to equimolar concentrations of both cobalt(III) complexes resulted in distinctly reduced cell-associated fluorescence levels, proving the pronounced stability of the complexes even in the presence of cells. Despite significant **L$_{Pon}$**-release from the two complexes over time (up to 24 h), in case of **Co(Meacac)$_2$L$_{Pon}$** cell-associated fluorescence remained more than 7.5-fold lower after 24 h as compared to the free ligand. Moreover, the fluorescence intensities of **Co(Meacac)$_2$L$_{Pon}$** were significantly reduced as compared to **Co(acac)$_2$L$_{Pon}$**, well in agreement with the higher reduction potential of the latter complex.

Next, the impact of hypoxia on the stability of our novel derivatives was evaluated by monitoring intracellular fluorescence intensities under normoxic (21% O_2) *vs.* hypoxic (0.1% O_2) conditions. In general, only in case of the cobalt(III) complexes, but not the free ligand **L$_{Pon}$** and ponatinib, a significant impact of oxygen conditions on cell-associated fluorescence was observed (Fig. 8). Hypoxic fluorescence activation in case of both cobalt(III) complexes was time-dependent, reaching significance after 6 h of compound incubation and resulting in 2- to 4-fold higher intensities. The activation ability tended to be higher in the more stable **Co(Meacac)$_2$L$_{Pon}$** complex, probably related to the lower spontaneous reduction under normoxic conditions (compare Fig. 7).

The enhanced stability of **Co(acac)$_2$L$_{Pon}$** under normoxia and its hypoxia-induced ligand release was subsequently confirmed by fluorescence microscopy. Fluorescence intensities indicated a ~2.8-fold decreased stability of the cobalt(III) complex under hypoxic *vs.* normoxic cell culture conditions. In case of the free ligand **L$_{Pon}$**, fluorescence intensities remained unaffected by different oxygen levels (Fig. S9†). These findings are well in agreement with the flow cytometric analysis of the intracellular ligand release, demonstrating reduced stability,

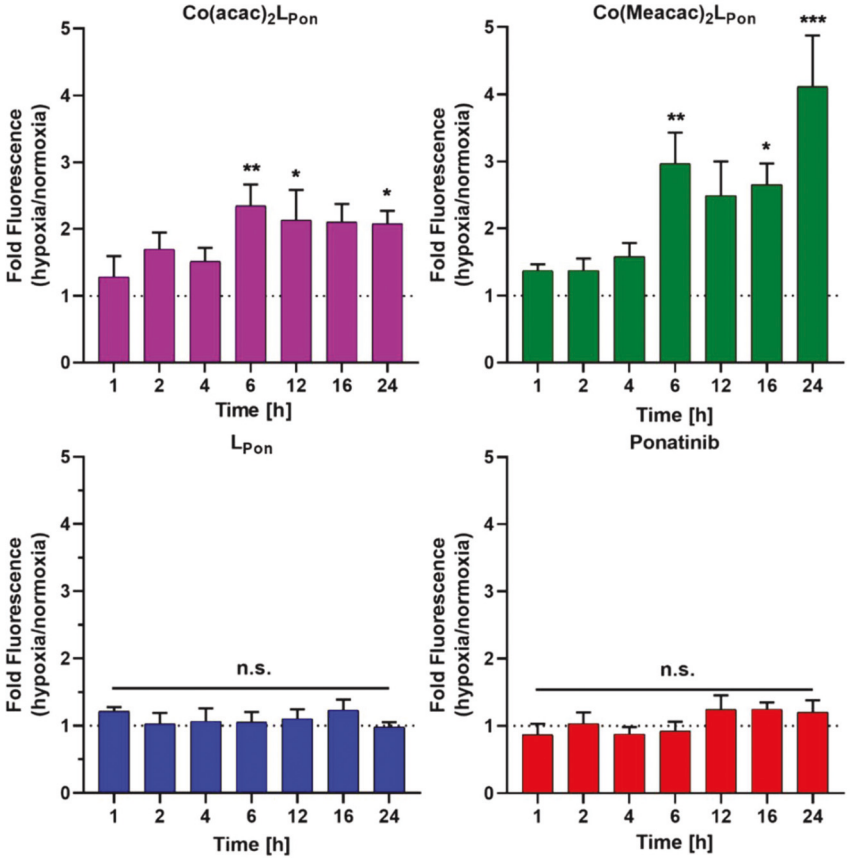

Fig. 8 Impact of hypoxia on cell-associated L_{Pon}-fluorescence from **Co(acac)$_2$L$_{Pon}$** and **Co(Meacac)$_2$L$_{Pon}$**. K-562 cells were incubated with 10 μM of compounds for the indicated time points under hypoxic and normoxic conditions and fluorescence intensities were determined by flow cytometry (BD LSRFortessa X-20, pacific blue filter). Fluorescence intensities were determined as described under Fig. 7 and mean fluorescence intensities under hypoxic cell culture conditions were normalized to the respective normoxic conditions. Data are given as means ± SEM of five independent experiments. Statistical significance was calculated by one-way ANOVA with Dunnett multiple comparison test with $p < 0.05$(*); <0.01 (**); <0.001 (***).

i.e. enhanced ligand release of the cobalt(III) complexes in hypoxic *vs.* normoxic environments.

Kinase screening

To investigate how the structural changes of the novel derivative affect its ABL1 and FGFR1 kinase-inhibitory potential in comparison to ponatinib, both substances were tested in cell-free kinase inhibition assays in the presence of a 10-fold excess of ATP (Fig. S8†). The IC_{50} values for ponatinib, which were 1.75 and 5.54 nM against ABL1 and FGFR1, are in the same range as reported in literature.[10]

In comparison, the IC_{50} values of **L_{Pon}** against ABL1 and FGFR1 was 1.93 and 25.9 nM, respectively. Consequently, the ABL1 inhibition potential of our new ligand is comparable to ponatinib, whereas the FGFR inhibition is distinctly weaker by a factor of ~5.

Anticancer activity against ABL1- and FGFR-driven cancer cell models

As a next step, the impacts of the novel derivatives on cell viability of the leukemia cancer cell line K-562 (BCR-ABL-dependent)[49] and the urothelial cancer cell line UM-UC-14 (FGFR3-dependent)[50] were evaluated under normoxic and hypoxic conditions. In general, a 72 h continuous cell exposure to all investigated compounds resulted in a dose-dependent reduction of cell vitality in the tested cell models under both oxygen conditions as determined by two independent methods, *i.e.* MTT assay (Fig. 9A) and ATP-based viability quantification (Fig. 9B).

Treatment of BCR-ABL-driven K-562 cells with ponatinib resulted in a pronounced reduction of cell vitality with IC_{50} in the nanomolar range. Notably, the anticancer activity of ponatinib was distinctly stronger as **L_{Pon}**. As in the above-mentioned cell-free kinase assay, IC_{50} values of both compounds against ABL1 were comparable (compare Fig. S8†), a reduced cellular uptake of **L_{Pon}** as compared to the more lipophilic ponatinib might be expected (calculated logP values[51]: ponatinib = 4.42; **L_{Pon}** = 3.39). Both cobalt(III) complexes were clearly less active as compared to the free ligand under normoxic conditions with **Co(Meacac)$_2$L$_{Pon}$** showing the highest IC_{50} value. Anticancer activities of ponatinib and **L_{Pon}** were only marginally altered under hypoxia, reaching significance only at a concentration of 0.5 nM ponatinib with both assays (Fig. 9A). In

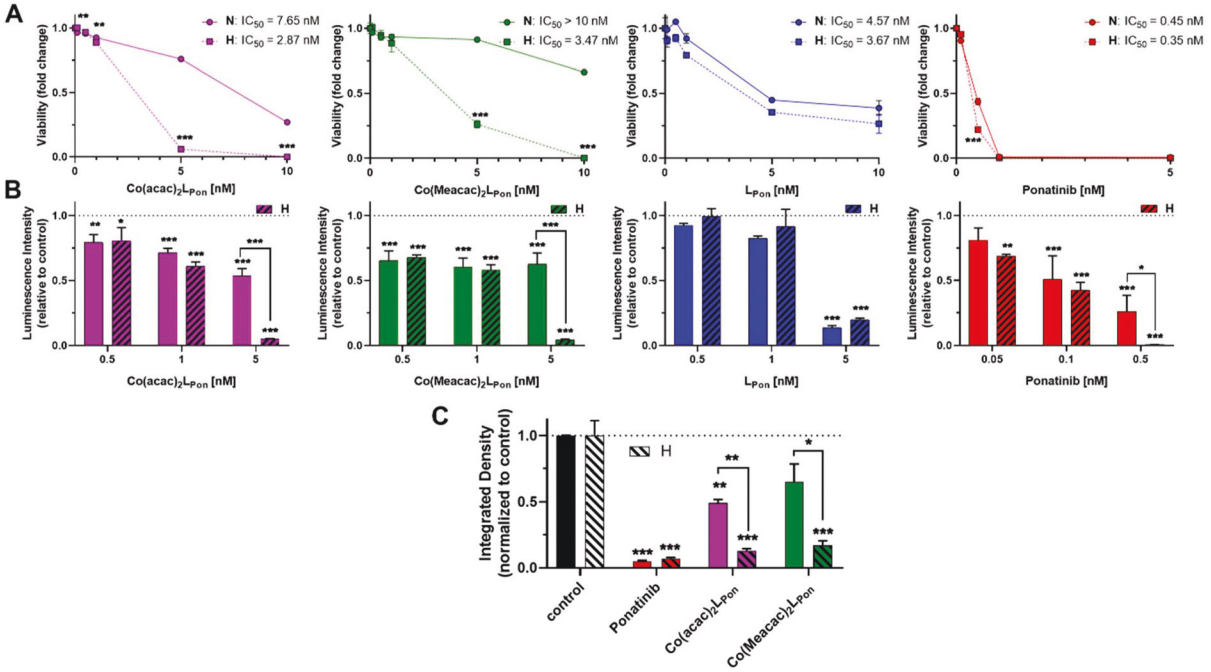

Fig. 9 Anticancer activity of **Co(acac)$_2$L$_{Pon}$**, **Co(Meacac)$_2$L$_{Pon}$**, **L$_{Pon}$** and ponatinib against human cancer cell models under normoxic (*N*) and hypoxic (*H*) conditions. (A) BCR-ABL-positive K-562 leukemic cell viability was measured by MTT vitality assay and (B) by luminescence assay based on ATP quantification (CellTiter-Glo) after 72 h. (C) Clonogenic cell growth of the FGFR3-driven UM-UC-14 urothelial cancer cell model determined by colony formation assay after 5 d of incubation. Data are given as means ± SD of one representative experiment performed in triplicates. Statistical significance was calculated by two-way ANOVA with Sidak multiple comparison test with $p < 0.05$(*); <0.01 (**); <0.001 (***).

contrast, reduction of oxygen to 0.1% massively increased the anticancer activity of **Co(acac)$_2$L$_{Pon}$** and **Co(Meacac)$_2$L$_{Pon}$** against K-562 cells at a concentration range between 5 and 10 nM.

In FGFR3-dependent UM-UC-14 cells a comparable activity pattern was observed but with IC_{50} values in the low micromolar range (Fig. S10†). Again, target cells could be strongly sensitized by oxygen reduction against both cobalt(III) complexes, but only marginally to ponatinib. The sensitizing effect in this cell model was more pronounced for **Co(acac)$_2$L$_{Pon}$** *vs.* **Co(Meacac)$_2$L$_{Pon}$** reflecting the differences in the reduction potentials. Purification of the novel compounds was performed in the presence of 0.1% TFA, leading to the respective TFA salts. MTT assays with TFA in UM-UC-14 cells elucidated, that TFA up to 25 μM had no impact on cell viability (Fig. S11†).

In order to investigate the impact of long-term oxygen restriction, clonogenic assays were performed in the FGFR3-dependent UM-UC-14 cell model (Fig. 9C). Under normoxic conditions both cobalt(III) complexes inhibited clonogenic cell growth by approximately 50% only, whereas ponatinib by 95%. In contrast, under hypoxic conditions all three compounds were comparably active with more than 80% inhibition of clone formation.

As mentioned above, two stereoisomers of **Co(acac)$_2$L$_{Pon}$** could be isolated. To clarify, whether there are differences in their anticancer activity, they were analyzed (in addition to the isomeric mixture) in UM-UC-14 cells by MTT assay. The impact on cell viability was moderately stronger for isomer 1 as compared to isomer 2 at normoxic conditions. Accordingly, values for the isomeric mixture positioned intermediate. As expected, both stereoisomers and the isomeric mixture were distinctly activated by hypoxic conditions. The moderately higher activity of isomer 1 remained also under hypoxic conditions (Fig. S12A†). Comparable effects were found in K-562 by luminescence assay-based ATP quantification (Fig. S12B†). Since no remarkable difference in anticancer activity could be observed for the pure isomers, the isomeric mixture was used for all other experiments.

It is known from literature that cobalt(II) ions (which are released after reduction of the cobalt(III) complexes) can cause cytotoxicity[52,53] and changes in the hypoxia inducible factor (HIF-1 alpha).[54] In our previous work we therefore investigated the effect of $CoCl_2$, and the two complexes [Co(II)(acac)$_2$en] and [Co(III)(acac)$_2$en]PF_6 ("en" = ethylenediamine) without an EGFR-targeting moiety on two cancer cell lines (A431 and H1975).[26] Notably, all compounds showed no significant cytotoxic activity under normoxic as well as hypoxic conditions. Consequently, a major contribution of cobalt(II) ions on the anticancer activity of our prodrugs can be widely excluded. Concerning upregulation of HIF-1 alpha signalling, it should be considered that our metal complexes are active in the nanomolar to the low micromolar range, while in most papers using $CoCl_2$ as hypoxia-mimicry, concentrations of 100 μM or even higher are used.[55]

Impact of hypoxia on downstream signalling inhibition

Next, the impact of both cobalt(III) complexes, $\mathbf{L_{Pon}}$ and ponatinib on the phosphorylation of the downstream targets ERK1/2 and S6 was evaluated under normoxic *vs.* hypoxic conditions by western blot analysis in BCR-ABL-driven K-562 cells (Fig. 10).

Generally, ERK1/2 phosphorylation, as readout of the MAPK pathway, tended to be enhanced under hypoxic conditions, while S6, as PI3K/AKT pathway indicator, tended to be reduced. Ponatinib and the free ligand $\mathbf{L_{Pon}}$ were equally active under the two oxygen conditions. However, comparable to the viability assays, the efficacy of $\mathbf{L_{Pon}}$ was lower as compared to ponatinib. The cobalt(III) complexes were distinctly more active

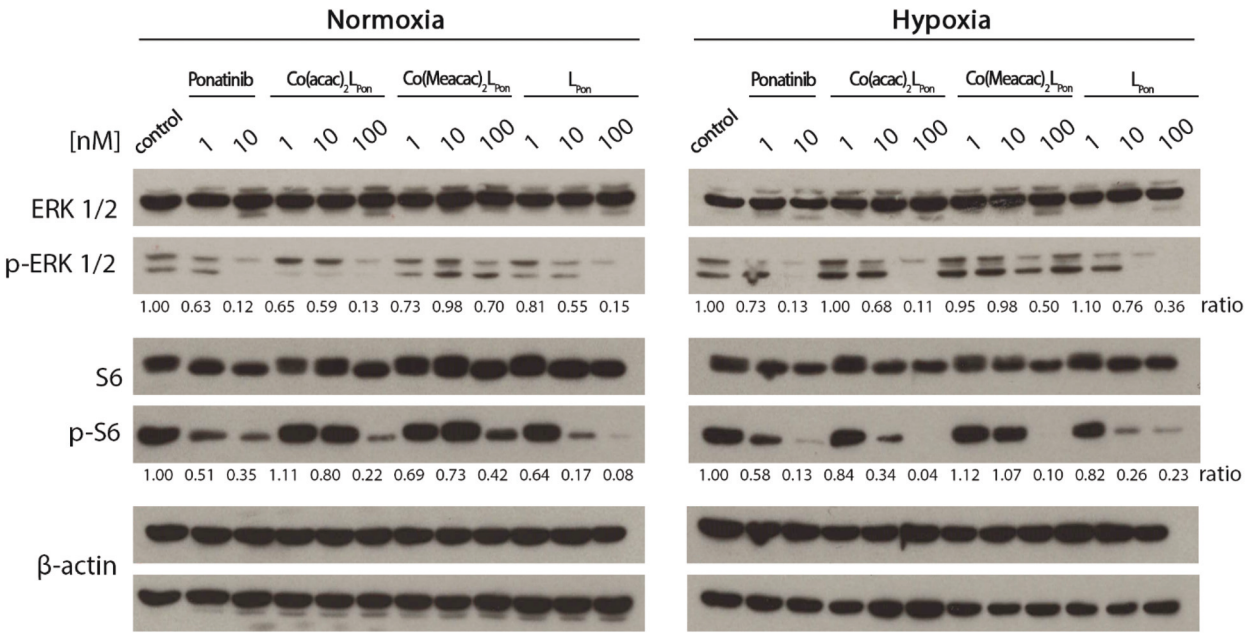

Fig. 10 Impact of the cobalt(III) complexes on the ERK1/2 and S6 under normoxic and hypoxic conditions. K-562 cells were treated with the compounds, after 12 h cell lysates were prepared and protein expression as well as phosphorylation levels of downstream pathways (p-ERK1/2 and p-S6) analyzed by western blotting. One representative experiment out of three is shown. The ratio of phosphorylated to total protein is given between the respective lanes.

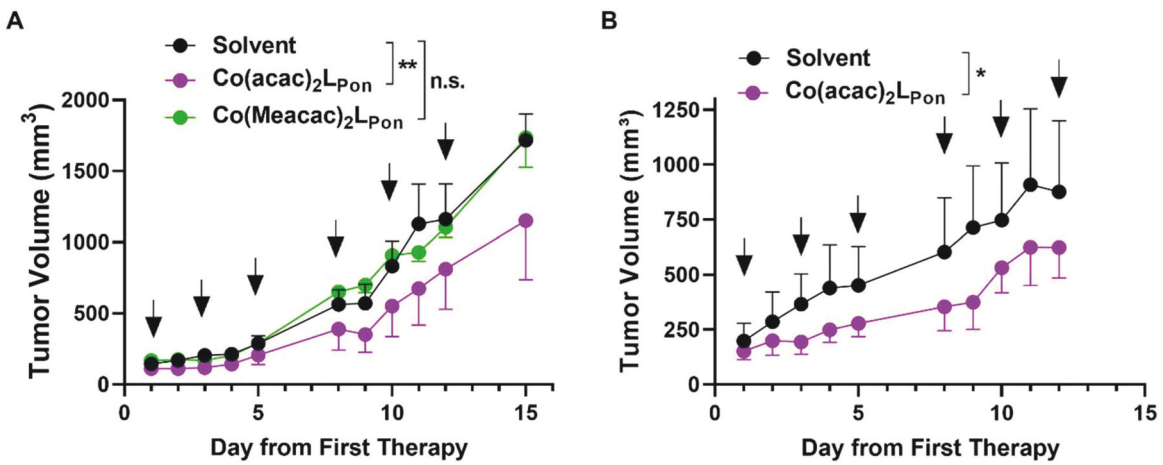

Fig. 11 *In vivo* anticancer activity of the investigated cobalt(III) complexes. (A) BCR-ABL-driven leukemic K-562 cells or (B) FGFR3-driven urothelial UM-UC-14 cells were injected s.c. into the right flank of male CB17/SCID mice (n = 4 animals per experimental group). When tumors were measurable (day 5 and day 7, respectively) compounds (10 mg kg^{-1} i.p.) were applied as indicated (black arrows). Tumor sizes were evaluated by caliper measurement. Data are given as means ± SEM. Statistical significance was calculated by two-way ANOVA with Sidak multiple comparison test with $p < 0.05$(*); <0.01 (**).

under hypoxic conditions, especially at the level of S6 phosphorylation. In this case, **Co(acac)$_2$L$_{Pon}$** turned out to be equally active as compared to ponatinib. The activity of **Co(Meacac)$_2$L$_{Pon}$** was generally weaker as compared to **Co(acac)$_2$L$_{Pon}$**.

In vivo anticancer activity

Based on this promising *in vitro* data, the antitumor activity of our novel cobalt(III) complexes **Co(acac)$_2$L$_{Pon}$** and **Co(Meacac)$_2$L$_{Pon}$** was evaluated in xenograft mouse models. As a first *in vivo* experiment, BCR-ABL-driven K-562 cells were injected subcutaneously (s.c.) and treated intraperitoneally (i.p.) with the test compounds at 10 mg kg^{-1} or the respective amount of solvent three times a week, for two weeks. Treatment with our novel derivatives was well tolerated and even after repeated i.p. applications no substantial body weight loss was observed (Fig. S13A†). Administration of **Co(acac)$_2$L$_{Pon}$** but not of the slower **L$_{Pon}$**-releasing **Co(Meacac)$_2$L$_{Pon}$** complex significantly reduced tumor growth of K-562 xenografts as compared to solvent controls (Fig. 11). Consequently, anticancer activity of **Co(acac)$_2$L$_{Pon}$** was also investigated against FGFR3-driven UM-UC-14 xenografts using the identical treatment regime. Again, administration of **Co(acac)$_2$L$_{Pon}$** displayed significant reduction of tumor volumes compared to control, without significant impact on body weight (Fig. 11, S13B†).

Conclusions

TKIs greatly improved cancer therapy since their first approval two decades ago. However, therapy resistance and severe side effects are limiting their clinical application. In this study, we developed the first ponatinib prodrugs with the aim to exploit the hypoxic environment present in the malignant tissue for cancer-specific drug activation. Molecular docking studies showed that both cobalt(III) prodrugs synthesized are unable to interact with the active sites of FGFR1 and ABL1 kinases and that the bioactive ligand **L$_{Pon}$** has comparable kinase inhibitory abilities as ponatinib. Cell-free kinase inhibition assays confirmed binding of the free ligand to the targeted kinases ABL1 and FGFR1, in the case of ABL1 with affinities comparable to ponatinib. Furthermore, investigation of the fluorescence properties demonstrated, that the intensities of **L$_{Pon}$** were comparable to ponatinib, whereas **Co(acac)$_2$L$_{Pon}$** and **Co(Meacac)$_2$L$_{Pon}$** exhibited a strongly quenched fluorescence. Both derivatives were highly stable in pure FCS with ~90% intact complex after 26 h. Nevertheless, according to cyclic voltammetry, **Co(Meacac)$_2$L$_{Pon}$** exhibited a clearly lower reduction potential as compared to **Co(acac)$_2$L$_{Pon}$**, suggesting higher stability and slower ligand release. This was confirmed, exploiting the distinct differences in the fluorescence properties between free ligand and cobalt(III) complexes. Flow cytometry confirmed significantly enhanced spontaneous release of the bioactive ligand from **Co(acac)$_2$L$_{Pon}$** as compared to **Co(Meacac)$_2$L$_{Pon}$** under normoxic conditions, but potent release of both compounds under hypoxia. Moreover, reduced oxygen levels significantly increased inhibition of FGFR3-downstream signaling and improved the anticancer activity of both cobalt(III) complexes against ABL- and FGFR-dependent human cancer cell models. Finally, **Co(acac)$_2$L$_{Pon}$**, but not **Co(Meacac)$_2$L$_{Pon}$** significantly reduced *in vivo* xenograft growth of the leukemic K-562 model. The *in vivo* activity of **Co(acac)$_2$L$_{Pon}$** was confirmed in an FGFR3 mutation-dependent urothelial carcinoma xenograft background. This suggests, that especially in the leukemic background hypoxic conditions might be too weak to activate **Co(Meacac)$_2$L$_{Pon}$** based on the lower reduction potential and, hence, higher stability. However, it needs to be considered that in the current study relatively small tumors were treated, due to a rapid tumor growth. Therefore, we currently aim to compare these drugs in slow growing cancer xenografts at later stages and to identify other solid tumor models, characterized by massive tumor hypoxia and driven by ponatinib targets. This will allow to further elucidate the interplay between cobalt(III)-based prodrug systems and its reduction kinetics, molecular targets and cancer hypoxia.

Experimental section

Docking studies

The 3D structures of the molecules (**L$_{Pon}$**, **Co(acac)$_2$L$_{Pon}$** and **Co(Meacac)$_2$L$_{Pon}$**) have been drawn and optimized with Avogadro version 1.2.0,[56] using Force Field GAFF (General AMBER Force Field).[57] The molecules obtained are those with minimum energy. The crystal structures of FGFR1 (PDB ID: 4V04) and ABL1 (PDB ID: 4WA9) have been obtained from the RCSB Protein Data Bank.[58] The *.pdb files from proteins were manipulated by elimination of adsorbed water and sulfur dioxide molecules, addition of missing hydrogen atoms, protonation of histidine residues, conversion of selenomethionines in methionines, addition and optimization of the side chain atoms. New *.pdb files were created of the proteins without the co-crystallized ligands and of the native ligands without the proteins using Chimera UCFS version 1.11.2.[59] The *.pdbqt files of drugs and proteins were generated using AutodockTools-1.5.7rc.[60] Ligand based molecular docking was performed with Autodock Vina 1.5 using ponatinib coordinates for FGFR1 and Axitinib for ABL1 to create the grid box.[61] The coordinates of the grid box are: FGFR1 (*x*-size: 30, *x*-center: 27.814, *y*-size: 46, *y*-center: 5.016, *z*-size: 54, *z*-center: 16.789); ABL1 (*x*-size: 48, *x*-center: 7.819, *y*-size: 46, *y*-center: 156.948, *z*-size: 46, *z*-center: 37.479). Docking studies were performed in triplicates and the calculated RMSD value was always less than 1.5 Å.[62]

Materials and methods

All solvents and reagents were obtained from commercial suppliers. They were, unless stated otherwise, used without further purification. Anhydrous MeOH and THF were bought

from Fisher Chemicals over molecular sieves. The cobalt(III) precursors $Na[Co(acac)_2(NO_2)_2]$ and $Na[Co(Meacac)_2(NO_2)_2]$ were obtained by following the protocol of Denny *et al.*[33] For all HPLC measurements Milli-Q water (18.2 MΩ cm, Merck Milli-Q Advantage, Darmstadt, Germany) was used. Preparative RP-HPLC was performed on an Agilent 1200 Series system controlled by Chemstation software. As stationary phase a XBridge BEH C18 OBD Prep Column (130 Å, 5 μm, 19 mm × 250 mm) from Waters Corp., Massachusetts, USA, was used. The general procedure included a flow rate of 17.06 mL min^{-1}, an injection volume of up to 10 mL and a column temperature of 25 °C. Milli-Q water and acetonitrile with addition of acids (0.1% TFA) were used as eluents unless stated otherwise. Elemental analyses were performed by the Microanalytical Laboratory of the University of Vienna on a PerkinElmer 2400 CHN Elemental Analyzer. The amount of TFA was also confirmed by ^{19}F NMR spectra. Electrospray ionization (ESI) mass spectra were recorded on a Bruker Amazon SL ion trap mass spectrometer in positive and/or negative mode by direct infusion.

High resolution mass spectra were measured on a Bruker maXis™ UHR ESI time of flight mass spectrometer. Expected and experimental isotope distributions were compared. ^1H and ^{13}C NMR, one- as well as two-dimensional, spectra were recorded in d_6-DMSO with a Bruker FT-NMR Avance III 500 MHz spectrometer at 500.10 (^1H) and 125.75 (^{13}C) MHz at 298 K. Chemical shifts (ppm) were referenced internal to the solvent residual peaks. For the description of the spin multiplicities the following abbreviations were used: s = singlet, d = doublet, t = triplet, q = quartet, m = multiplet.

Synthesis

***tert*-Butyl (4-amino-2-(trifluoromethyl)phenyl)carbamate.** 4-Amino-2-trifluoromethylbenzyl amine (2.03 g, 1.0 eq.) was dissolved in THF (20 mL) at room temperature and di-*tert*-butyl dicarbonate (2.58 g, 1.1 eq.) was added to the solution. After stirring overnight, the solvent was removed and a reddish, viscous oil was obtained. The crude product was purified *via* column chromatography (hexane : ethyl acetate 3 : 2), resulting in yellow crystals. Yield: 2.51 g (81%). ^1H NMR (500.1 MHz, DMSO-d_6): δ 7.24 (t, 1H), 7.11 (d, J = 8.4 Hz, 1H), 6.85 (d, J = 2.3 Hz, 1H), 6.75 (d, J = 8.3 Hz, 1H), 5.44 (s, 2H), 4.12 (d, J = 5.8 Hz, 2H), 1.39 (s, 9H) ppm. MS: calcd for $[C_{13}H_{17}F_3N_2O_2-H]^-$: 289.12, found: 288.97.

***tert*-Butyl (4-(3-(imidazo[1,2-*b*]pyridazin-3-ylethynyl)-4-methylbenzamido)-2-(trifluoromethyl)benzyl) carbamate.** 3-(2-{Imidazo[1,2-*b*]pyridazin-3-yl}ethynyl)-4-methylbenzoic acid (0.95 g, 1 eq.) was suspended in toluene (abs., 90 mL) under argon atmosphere. Then, *N*-methylmorpholine (1.12 mL, 3 eq.) and $(COCl)_2$ (1.79 mL, 1.1 eq., 2.0 M in dichloromethane) were added. The reaction was stirred at room temperature for 1.5 h, during which the solution become clear. The solvent was removed and the crude product was dried *in vacuo*, to remove any excess of $(COCl)_2$. The solid was again suspended in toluene (abs., 90 mL) under argon atmosphere. *N*-Methylmorpholine (0.56 mL, 1.5 eq.), *tert*-butyl (4-amino-2-(trifluoromethyl)phenyl)carbamate (990 mg, 1 eq.) and 4-dimethylaminopyridine (4-DMAP) as catalyst (33 mg, 5 mol%), were added. The reaction mixture turned into a bright yellow color and was stirred at room temperature for 1 h, then refluxed overnight. The solvent was removed and the crude product dried *in vacuo*. After purification *via* column chromatography (pure ethyl acetate), the product was obtained as bright yellow crystals. Yield: 1.27 g (68%). ^1H NMR (500.1 MHz, DMSO-d_6): δ 10.58 (s, 1H), 8.73 (dd, J = 4.4 Hz J = 1.5 Hz, 1H), 8.29–8.23 (m, 2H), 8.21 (dd, J = 8.6 Hz, J = 1.8 Hz, 2H), 8.07 (d, J = 8.4 Hz, 1H), 7.95 (dd, J = 8.0 Hz, J = 1.9 Hz, 1H),7.56 (d, J = 8.2 Hz, 1H), 7.49 (dd, J = 11.9 Hz, J = 7.2 Hz, 2H), 7.40 (dd, J = 9.2 Hz, J = 4.4 Hz, 1H), 4.29 (d, J = 5.7 Hz, 2H), 2.61 (s, 3H), 1.41 (s, 9H) ppm. MS: calcd for $[C_{29}H_{26}F_3N_5O_3+Na]^+$: 572.1880, found: 572.1878. Anal. calcd for $C_{29}H_{26}F_3N_5O_3$ (M_r = 549.55 g mol^{-1}): C, 63.38; H, 4.77; N, 12.74. Found: C, 63.06; H, 4.82; N, 12.47.

(4-(3-(Imidazo[1,2-*b*]pyridazin-3-ylethynyl)-4-methylbenzamido)-2-(trifluoromethyl)phenyl) methanaminium chloride. *tert*-Butyl (4-(3-(imidazo[1,2-*b*]pyridazin-3-ylethynyl)-4-methylbenzamido)-2-(trifluoromethyl)benzyl) carbamate (1.26 g, 1 eq.) was dissolved in 1,4-dioxane (16.6 mL,) and 4 N HCl in dioxane/water (2.86 mL, 5 eq.) was added. The reaction was stirred at room temperature for about 3 h. The resulting white precipitate was filtered off, washed with 1,4-dioxane and diethyl ether. Yield: 1.12 g (94%). ^1H NMR (500.1 MHz, DMSO-d_6): δ 10.76 (s, 1H), 8.76 (dd, J = 4.4 Hz, J = 1.3 Hz, 1H), 8.52 (s, 3H), 8.34–8.27 (m, 3H), 8.25 (d, J = 1.5 Hz, 1H), 8.21 (d, J = 8.4 Hz, 1H), 7.99 (dd, J = 8.1 Hz, J = 1.7 Hz, 1H), 7.77 (d, J = 8.5 Hz, 1H), 7.58 (d, J = 8.1 Hz, 1H), 7.44 (dd, J = 9.2 Hz, J = 4.4 Hz, 1H), 4.15 (d, J = 5.4 Hz, 2H), 2.62 (s, 3H) ppm. MS: calcd for $[C_{24}H_{18}F_3N_5O+H]^+$: 450.1536, found: 450.1533. Anal. calcd for $C_{24}H_{18}F_3N_5O{\cdot}HCl{\cdot}H_2O$ (M_r = 521.92 g mol^{-1}): C, 55.23; H, 4.44; N, 13.42. Found: C, 54.91; H, 4.19; N, 13.25.

***N*-(4-(Aminomethyl)-3-(trifluoromethyl)phenyl)-3-(imidazo[1,2-*b*]pyridazin-3-ylethynyl)-4-methylbenzamide.** (4-(3-(Imidazo[1,2-*b*]pyridazin-3-ylethynyl)-4-methylbenzamido)-2-(trifluoromethyl)phenyl) methanaminium chloride (240 mg, 1 eq.) was dissolved in deionized water and a saturated sodium bicarbonate solution was added until a slightly basic pH (7.5–8.0) was reached. The aqueous phase was extracted three times with ethyl acetate (3 × 50 mL). The organic layers were combined, dried over $MgSO_4$ and *in vacuo*, resulting in a bright yellow powder. Yield: 183 mg (89%). ^1H NMR (500.1 MHz, DMSO-d_6): δ 10.55 (s, 1H), 8.73 (dd, J = 4.4 Hz, J = 1.5 Hz, 1H), 8.27 (dd, J = 9.2 Hz, 1.6 Hz, 1H), 8.24 (s, 1H), 8.20 (dd, J = 21.5 Hz, 2.0 Hz, 2H), 8.07 (dd, J = 8.5 Hz, 1.9 Hz, 1H), 7.95 (dd, J = 8.0 Hz, 1.9 Hz, 1H), 7.77 (d, J = 8.5 Hz, 1H), 7.56 (d, J = 8.1 Hz, 1H), 7.40 (dd, J = 9.2 Hz, 4.4 Hz, 1H), 3.84 (s, 2H), 2.61 (s, 3H) ppm. MS: calcd for $[C_{24}H_{18}F_3N_5O+H]^+$: 450.15, found: 450.04.

***tert*-Butyl (2-((4-(3-(imidazo[1,2-*b*]pyridazin-3-ylethynyl)-4-methylbenzamido)-2-(trifluoromethyl) benzyl) amino) ethyl) carbamate.** *N*-(4-(Aminomethyl)-3-(trifluoromethyl)phenyl)-3-(imidazo[1,2-*b*]pyridazin-3-ylethynyl)-4-methylbenzamide (470 mg, 1 eq.) was dissolved in abs. MeOH (abs., 13.5 mL) under inert conditions, molecular sieves (3–4 Å) and *N*-boc-2-aminoacetaldehyde (200 mg, 1.2 eq.) were added to the solution. The reac-

tion was stirred at room temperature for 2 h. Subsequently, sodium cyanoborohydride (97 mg, 1.2 eq.) was added and the mixture was stirred overnight. The solvent was removed, the solid was dissolved in ethyl acetate (100 mL) and the molecular sieve was filtered off. The compound was extracted with saturated sodium bicarbonate solution (50 mL) and the organic phase was dried over $MgSO_4$ and *in vacuo*. Yield of the crude product (according to HPLC): 50%.

^{1}H NMR (500.1 MHz, DMSO-d_6): δ 10.58 (s, 1H), 8.74 (dd, J = 4.5 Hz, J = 1.5 Hz, 1H), 8.28 (dd, J = 9.2 Hz, 1.6 Hz, 1H), 8.25 (s, 1H), 8.23 (d, J = 2.0 Hz, 1H), 8.22 (d, J = 2.0 Hz, 1H), 8.08 (dd, J = 8.5 Hz, 1.9 Hz, 1H), 7.96 (dd, J = 8.0 Hz, 1.9 Hz, 1H), 7.75 (d, J = 8.5 Hz, 1H), 7.56 (d, J = 8.1 Hz, 1H), 7.40 (dd, J = 8.9 Hz, 4.4 Hz, 1H), 6.80 (s, 1H), 3.84 (s, 2H), 3.09–3.02 (m, 2H), 2.62 (s, 3H), 2.60–2.55 (m, 2H), 1.38 (s, 9H) ppm. MS: calcd for $[C_{31}H_{31}F_3N_6O_3+H]^+$: 593.2482, found: 593.2485.

N-(4-(((2-Aminoethyl)amino)methyl)-3-(trifluoromethyl)phenyl)-3-(imidazo[1,2-*b*]pyridazin-3 ylethynyl)-4-methylbenzamide·3TFA (L_{Pon}). *tert*-Butyl (2-((4-(3-(imidazo[1,2-*b*]pyridazin-3-ylethynyl)-4-methylbenzamido)-2-(trifluoromethyl) benzyl) amino) ethyl)carbamate (400.3 mg, 1 eq.) was dissolved in dichloromethane (9 mL), TFA (9 mL) was added and the reaction was stirred at room temperature for 1 h. By adding diethyl ether to the orange solution, the product was precipitated as white solid and filtered off. The crude product (280 mg) was purified by preparative RP-HPLC (Waters XBridge C18 column on an Agilent 1200 Series system; H_2O/ACN, both containing 0.1% TFA, 30.0–32.5% ACN gradient, 19 min per run) resulting in a beige, hygroscopic compound. Yield: 113 mg (40%). ^{1}H NMR (500.1 MHz, DMSO-d^6): δ 10.74 (s, 1H, H17), 9.62–9.09 (m, 2H, H26), 8.73 (s, 1H, H6), 8.32 (s, 1H, H19), 8.29–8.22 (m, 4H, H2, H4, H14, H24), 8.11–7.85 (m, 3H, H29), 7.96 (d, J = 8.0 Hz, 1H, H12), 7.78 (d, J = 8.5 Hz, 1H, H23), 7.58 (d, J = 7.6 Hz, H11), 7.40 (m, 1H, H5), 4.40–4.32 (m, 2H, H25), 3.34–3.28 (m, 2H, H27), 3.22–3.13 (m, 2H, H28), 2.62 (s, 3H, H15) ppm. ^{13}C NMR (125.75 MHz, DMSO-d_6): δ 164.8 (C16), 145.1 (C6), 143.8 (C10), 140.2 (C22), 139.7 (C3), 138.2 (C14), 132.1 (C23), 131.9 (C13), 130.2 (C24), 130.2 (C11), 128.5 (C12), 128.1 (C20), 126.2 (C4), 124.6 (C18), 123.6 (C2), 123.0 (C21), 121.8 (C9), 119.1(C5), 117.6 (C19), 111.6 (C1), 96.3 (C8), 81.2 (C7), 46.5 (C25), 44.3 (C27), 35.3 (C28), 20.4 (C15) ppm. MS: calcd for $[C_{26}H_{23}F_3N_6O+H]^+$: 493.1958, found: 493.1962. Anal. Calcd for $C_{26}H_{23}F_3N_6O$·3TFA (M_r = 834.57 g mol^{-1}): C, 46.05; H, 3.14; N, 10.07. Found: C, 46.28; H, 3.30; N, 9.89.

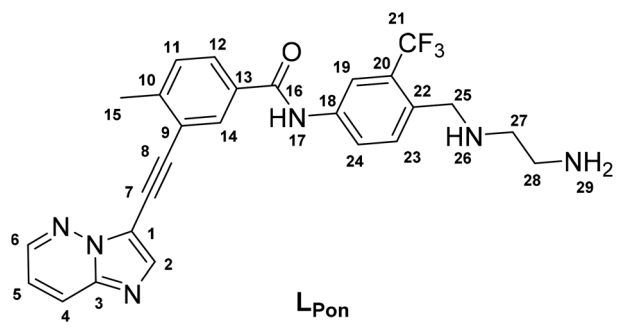

L_{Pon}

Bis(2,4-pentanedionato)N-(4-(((2-aminoethyl)amino)methyl)-3-(trifluoromethyl)phenyl)-3-(imidazo[1,2-*b*]pyridazin-3-ylethynyl)-4-methylbenzamide cobalt(III) 2,2,2-trifluoroacetate ($Co(acac)_2L_{Pon}$). $Na[Co(acac)_2(NO_2)_2]$ (39 mg, 1 eq.) was suspended in MeOH (3.66 mL). L_{Pon} (88 mg, 1 eq.) was dissolved in MeOH (4.12 mL) and neutralized by NaOH (14 mg, 3 eq.). To the resulting yellow solution a spatula tip activated charcoal was added. The reaction was stirred for 2 h at room temperature. Afterwards the solution was filtered through a syringe filter, which was washed with small amounts of MeOH. The solvent was evaporated and the violet, crude product was dried *in vacuo* (130 mg). Purification was performed by preparative RP-HPLC (Waters XBridge C18 column on an Agilent 1200 Series system; H_2O/ACN, both containing 0.1% TFA, isocratic gradient ACN 46%, 27 min per run) resulting in a violet, hygroscopic complex. Yield: 36 mg (36%). The ratio of the two isomers was 1 : 0.67.

Shifts of the main isomer; ^{1}H NMR (500.1 MHz, DMSO-d_6): δ 10.67 (s, 1H, H17), 8.73 (s, 1H, H6), 8.30–8.26 (m, 2H, H4, H19), 8.26–8.22 (m, 2H, H2, H14), 8.18–8.14 (m, 1H, H24), 7.97 (d, 1H, J = 9 Hz, H12), 7.78 (d, 1H, J = 8 Hz, H23), 7.58 (d, 1H, J = 9 Hz, H11), 7.43–7.39 (m, 1H, H5), 5.70 (s, 1H, CH, acac), 5.65 (s, 1H, CH, acac), 5.61 (s, 1H, H29), 5.26 (s, 1H, H26), 5.09 (s, 1H, H29), 3.89–3.79 (m, 2H, H25), 2.74–2.66 (m, 1H, H28), 2.63 (s, 3H, H15), 2.45–2.38 (m, 1H, H28), 2.55–2.45 (m, 1H, H27), 2.38–2.32 (m, 1H, H27), 2.15 (s, 3H, CH_3, acac), 2.13–2.10 (s, 6H, CH_3, acac), 2.06 (s, 3H, CH_3, acac) ppm. ^{13}C NMR (125.75 MHz, DMSO-d_6): δ 189.9 (C_Q, acac), 189.1 (C_Q, acac), 188.9 (C_Q, acac), 188.4 (C_Q, acac), 164.7 (C16), 145.1 (C6), 143.7 (C10), 139.7 (C3), 139.3 (C18), 138.3 (C14), 133.7 (C23), 132.0 (C13), 130.2 (C11 + C19), 128.5 (C12), 128.4 (C22), 126.9 (C20), 126.1 (C4), 124.8 (C21), 123.2 (C24), 121.8 (C9), 119.1 (C5), 117.5 (C2), 111.6 (C1), 98.1 (CH, acac), 97.9 (CH, acac), 96.4 (C8), 81.2 (C7), 52.2 (C27), 47.1 (C25), 42.5 (C28), 26.5 (CH_3, acac), 26.3 (CH_3, acac), 26.1 (CH_3, acac), 26.0 (CH_3, acac), 20.4 (C15) ppm.

Shifts of the minor isomer; ^{1}H NMR (500.1 MHz, DMSO-d_6): δ 10.67 (s, 1H, H17), 8.73 (s, 1H, H6), 8.30–8.26 (m, 2H, H4, H19), 8.26–8.22 (m, 2H, H2, H14), 8.18–8.14 (m, 1H, H24), 7.97 (d, 1H, J = 9 Hz, H12), 7.91 (d, 1H, J = 8 Hz, H23), 7.58 (d, 1H, J = 9 Hz, H11), 7.43–7.39 (m, 1H, H5), 5.74 (s, 1H, CH, acac), 5.65 (s, 1H, CH, acac), 5.61 (s, 1H, H26), 5.48 (s, 1H, H29), 5.39 (s, 1H, H29), 3.63–3.58 (m, 1H, H25), 3.11–3.04 (m, 1H, H25), 2.63 (s, 3H, H15), 2.55–2.45 (m, 2H, H28), 2.45–2.38 (m, 2H, H28), 2.19 (s, 3H, CH_3, acac), 2.13–2.10 (s, 6H, CH_3, acac), 2.05 (s, 3H, CH_3, acac) ppm. ^{13}C NMR (125.75 MHz, DMSO-d_6): δ 190.6 (C_Q, acac), 189.9 (C_Q, acac), 189.8 (C_Q, acac), 189.5 (C_Q, acac), 164.7 (C16), 145.1 (C6), 143.7 (C10), 139.7 (C3), 139.4 (C18), 138.3 (C14), 133.6 (C23), 132.0 (C13), 130.2 (C11 + C19), 128.5 (C12), 128.3 (C22), 126 126.6 (C20), 126.1 (C4), 124.8 (C21), 123.2 (C24), 121.8 (C9), 119.1 (C5), 117.5 (C2), 111.6 (C1), 98.1 (CH, acac), 98.0 (CH, acac), 96.4 (C8), 81.2 (C7), 50.9 (C27), 48.1 (C25), 42.3 (C28), 26.4 (CH_3, acac), 26.3 (CH_3, acac), 26.1 (CH_3, acac), 26.0 (CH_3, acac), 20.4 (C15) ppm.

MS: calcd For $[C_{36}H_{37}F_3N_6O_5Co]^+$: 749.2104, found: 749.2093. Anal. calcd for $C_{38}H_{37}F_6N_6O_7Co$·0.6TFA·1.5H_2O (M_r =

958.10 g mol^{-1}): C, 49.14; H, 4.27; N, 8.77. Found: C, 48.84; H, 3.96; N, 8.53.

Bis(3-methyl-2,4-pentanedionato) *N*-(4-(((2-aminoethyl)-amino)methyl)-3-(trifluoromethyl)phenyl)-3-(imidazo[1,2-*b*]-pyridazin-3-ylethynyl)-4-methylbenzamide cobalt(III) 2,2,2-trifluoroacetate ($Co(Meacac)_2L_{Pon}$). $Na[Co(Meacac)_2(NO_2)_2]$ (27.8 mg, 1 eq.) was suspended in MeOH (2.41 mL). L_{Pon} (88 mg, 1 eq.) was dissolved in MeOH (2.71 mL) and neutralized by NaOH (9.17 mg, 3 eq.). To the resulting yellow solution a spatula tip activated charcoal was added. The reaction was stirred for 2 h at room temperature. Afterwards the solution was filtered through a syringe filter, which was washed with small amounts of MeOH. The solvent was evaporated and the purple, crude product was dried *in vacuo* (85 mg). Purification was performed by preparative RP-HPLC (Waters XBridge C18 column on an Agilent 1200 Series system; H_2O/ACN, both containing 0.1% TFA, isocratic gradient ACN 50%, 27 min per run) resulting in a violet, hygroscopic lyophilisate. Yield: 22 mg (31%). The ratio of the two isomers was 1 : 0.43.

Shifts of the main isomer; ^{1}H NMR (500.1 MHz, DMSO-d_6): δ 10.66 (s, 1H, H17), 8.73 (s, 1H, H6), 8.30–8.21 (m, 4H, H2, H4, H14, H19), 8.17–8.13 (m, 1H, H24), 7.97 (d, 1H, J = 9 Hz, H12), 7.75 (d, 1H, J = 8 Hz, H23), 7.58 (d, 1H, J = 9 Hz, H11), 7.43–7.39 (m, 1H, H5), 5.52–5.42 (m, 1H, H29), 4.99 (s, 1H, H29), 4.81 (s, 1H, H26), 3.94–3.84 (m, 2H, H25), 2.72–2.65 (m, 1H, H28), 2.63 (s, 3H, H15), 2.47–2.42 (m, 1H, H27), 2.44–2.38 (m, 1H, H28), 2.38–2.33 (m, 1H, H27), 2.24 (s, 3H, CH_3, Meacac), 2.20 (s, 3H, CH_3, Meacac), 2.15 (s, 3H, CH_3, Meacac), 2.13 (s, 3H, CH_3, Meacac), 1.92 (s, 3H, CH_3, Meacac), 1.88 (s, 3H, CH_3, Meacac) ppm. ^{13}C NMR (125.75 MHz, DMSO-d_6): δ 188.1 ($2C_Q$, Meacac), 187.3 (C_Q, Meacac), 186.9 (C_Q, Meacac), 164.7 (C16), 145.1 (C6), 143.8 (C10), 139.7 (C3), 139.2 (C18), 138.3 (C14), 133.4 (C23), 132.0 (C13), 130.1 (C11 + C2), 128.5 (C12), 128.2 (C20), 127.3 (C22), 126.1 (C4), 124.8 (C21), 123.1 (C24), 121.9 (C9), 119.2 (C5), 117.5 (C19), 111.7 (C1), 100.8 (C_Q, Meacac), 100.7 (C_Q, Meacac), 96.4 (C8), 81.2 (C7), 52.1 (C27), 46.9 (C25), 42.4 (C28), 26.6 (CH_3, Meacac), 26.5 ($2CH_3$, Meacac), 26.2 (CH_3, Meacac), 20.4(C15), 14.9 (CH_3, Meacac), 14.8 (CH_3, Meacac) ppm.

Shifts of the minor isomer; ^{1}H NMR (500.1 MHz, DMSO-d_6): δ 10.66 (s, 1H, H17), 8.73 (s, 1H, H6), 8.30–8.21 (m, 4H, H2, H4, H14, H19), 8.17–8.13 (m, 1H, H24), 7.97 (d, 1H, J = 9 Hz, H12), 7.89 (d, 1H, J = 8 Hz, H23), 7.58 (d, 1H, J = 9 Hz, H11), 7.43–7.39 (m, 1H, H5), 5.52–5.42 (m, 1H, H29), 5.32 (s, 1H, H29), 5.12 (s, 1H, H26), 3.54–3.49 (m, 1H, H25), 2.99–2.93 (m, 1H, H25), 2.72–2.65 (m, 1H, H28), 2.63 (s, 3H, H15), 2.47–2.42 (m, 1H, H27), 2.44–2.38 (m, 1H, H28), 2.38–2.33 (m, 1H, H27) 2.28 (s, 3H, CH_3, Meacac), 2.23 (s, 3H, CH_3, Meacac), 2.18 (s, 3H, CH_3, Meacac), 2.11 (s, 3H, CH_3, Meacac), 1.92 (s, 3H, CH_3, Meacac), 1.87 (s, 3H, CH_3, Meacac) ppm. ^{13}C NMR (125.75 MHz, DMSO-d_6): δ 188.7 (C_Q, Meacac), 188.2 (C_Q, Meacac), 187.3 (C_Q, Meacac), 187.0 (C_Q, Meacac), 164.7 (C16), 145.1 (C6), 143.8 (C10), 139.7 (C3), 139.3 (C18), 138.3 (C14), 133.3 (C23), 132.0 (C13), 130.1 (C11 + C2), 128.5 (C12), 127.0 (C22), 126.1 (C4), 128.4 (C20), 123.1 (C24), 121.9 (C9), 119.2 (C5), 117.5 (C19), 111.7 (C1), 101.0 (C_Q, Meacac), 100.7 (C_Q, Meacac), 96.4 (C8), 81.2 (C7), 50.7 (C27), 48.0 (C25), 42.0 (C28), 26.4 (CH_3, Meacac), 26.3 (CH_3, Meacac), 26.2 ($2CH_3$, Meacac), 20.4 (C15), 14.9 (CH_3, Meacac), 14.8 (CH_3, Meacac) ppm.

MS: calcd for $[C_{38}H_{41}F_3N_6O_5Co]^+$: 777.2417, found: 777.2405. Anal. calcd for $C_{40}H_{41}F_6N_6O_7Co{\cdot}TFA{\cdot}H_2O$ (M_r = 1022.75 g mol^{-1}): C, 49.32; H, 4.34; N, 8.22. Found: C, 48.98; H, 4.19; N, 8.01.

Interconversion of the isomers

For the interconversion measurements, a stock solution of the two isomers of $Co(acac)_2L_{Pon}$ (5 mM in water) was prepared. The final concentration was reached by 1 : 100 dilution with PBS (pH 7.4, 10 mM). The samples were incubated at 37 °C. Measurements were performed on a Dionex UltiMate 3000 RS UPLC system with a Waters Acquity UPLC® BEH C18 column (3 × 50 mm, pore size 1.7 μm). Water and acetonitrile (both containing 0.1% TFA) were used as eluents, an isocratic gradient of 45% acetonitrile within 8 min was applied.

Fluorescence measurements

Fluorescence measurements were performed on a Horiba FluoroMax®-4 spectrofluorometer and the data was analyzed using the FluorEssence v3.5 software package. The tested solutions were dissolved immediately prior to analysis in PB (50 mM, pH 7.4) with a final concentration of 15 μM. Scans were run at room temperature with excitation and emission slit widths of 3 nm. Emission scans were run from 250–700 nm using an excitation wavelength of 320 nm. The 3D fluorescence spectra of L_{Pon} were determined at excitation wavelengths from 230–550 nm and emission was recorded within the range of 220–700 nm.

Cyclic voltammetry

The compounds were dissolved in DMF (+0.2 M [*n*-Bu_4N][BF_4]) to obtain a final concentration of 1.5 mM. Electrochemical experiments were conducted on an EG&G PARC 273A potentiostat/galvanostat with a scan rate of 100–1000 mV s^{-1} at room temperature. Argon was bubbled through the solution before every measurement to remove oxygen. A three-electrode configuration cell was used with a glassy carbon electrode as working electrode, which was polished before every measurement. The reference electrode was Ag/Ag^+/ACN (10 mM $AgNO_3$) and the auxiliary electrode was a platinum wire. The potentials were referenced to an internal standard redox couple of ferrocenium/ferrocene and calculated to the NHE ($E_{1/2}$ = +0.72 V *vs.* NHE).[63] For the cyclic voltammetry measurements in DMF/H_2O (7 : 3 v/v; aqueous phase was 10 mM phosphate buffer at pH 7.40 with 0.1 M KCl), a glassy carbon electrode as working electrode, a platinum auxiliary electrode, and an Ag/AgCl electrode containing 3.5 KCl were used. Redox potentials measured relative to the Ag/AgCl/KCl (3.5 M) reference electrode and converted to the NHE using +0.205 V. Measurements were at least repeated three times and the mean values were calculated.

Serum stability measurements

For serum stability measurements, 135 μL FCS, buffered with 150 mM phosphate (Na_2HPO_4/NaH_2PO_4) to maintain a pH

value of 7.4, were mixed with 15 μL of a 500 μM stock solution of the respective complex in 50 mM phosphate buffer to reach a final concentration of 50 μM. The samples were incubated at 37 °C. At different time points to 20 μL serum 40 μL of ACN were added. After vigorously shaking for 2 min the suspension was centrifuged at 6000 rpm for 10 min. The supernatant was taken with a syringe and directly measured *via* HPLC-MS. The samples were analyzed on an Agilent 1260 Infinity system using a Waters Atlantis T3 column (150 mm × 4.6 mm) coupled to a Bruker Amazon SL ESI-IT mass spectrometer. Water and acetonitrile (both containing 0.1% formic acid) were used as eluents with a gradient of 1–99% acetonitrile within 29 min.

Biological methods

Kinase screening

The ABL1 and FGFR1 kinase-inhibitory potentials of the novel derivative $\mathbf{L_{Pon}}$ in comparison to ponatinib were evaluated using the Select Screen® Biochemical Kinase Profiling Service at Life Technologies (ThermoFisher Scientific, Madison, USA). The test compounds were screened in a final concentration of 1% DMSO using the Z′-LYTE® Assay. Results are additionally depicted in Fig. S8.†

Cell lines, cell culture conditions and drug treatments

All reagents were purchased from Sigma-Aldrich (St Louis, USA) unless specified otherwise. The human leukemia cell line K-562 (chronic myeloid leukemia; BCR-ABL-positive) and human urothelial cancer cell line UM-UC-14 (FGFR3-dependent), obtained from the American Type Culture Collection (ATCC) (Rockville, MD, USA), were cultured in RPMI 1640 (K-562) or MEM (Minimum Essential Medium Eagle) (UM-UC-14) supplemented with 10% fetal calf serum (PAA, Linz, Austria) at 37 °C, 5% CO_2 in a humidified atmosphere. In case of hypoxic cell culture conditions, plated and treated cells were incubated at 37 °C, 5% CO_2 and 0.1% O_2 (ProOx Model C21 system, BioSpherix) in humidified incubators for the indicated time point before analysis. All investigated compounds were dissolved in dimethyl sulfoxide (DMSO) as 10 mM stock solutions and were stored at −20 °C. Dilutions in culture media supplemented with 10% fetal calf serum were made immediately before the experiments at the indicated concentrations. Corresponding dilutions of DMSO were used as untreated vehicle controls.

Cytotoxicity assay

Cells were seeded (3–7 × 10^4 cells per well) in 96-well plates and after 24 h recovery treated with increasing concentrations of compounds in triplicates. After 72 h drug exposure under normoxic or hypoxic cell culture conditions (0.1% O_2) (ProOx Model C21 system, BioSpherix), the proportion of viable cells was determined by 3-(4,5-dimethylthiazol-2-yl)-2,5-diphenyltetrazolium bromide (MTT)-vitality assay (EZ4U, Biomedica, Vienna, Austria) or by luminescence assay based on adenosine triphosphate quantification (CellTiter-Glo, Promega, Madison, Wisconsin) following the manufacturer's recommendations. Absorbance was measured at 450 nm (at 620 nm as reference) (MTT) and luminescence after 1000 ms (CellTiter-Glo) at the Tecan infinite 200Pro (Zurich, Switzerland). MTT-derived cytotoxicity was expressed as IC_{50} values calculated from full dose–response curves using GraphPad Prism software (La Jolla, CA).

Colony formation assay

UM-UC-14 cells were seeded at low densities of 3 × 10^3 cells per well in 24-well plates in 500 μL and after 24 h recovery treated with 100 μL of increasing concentrations of compounds in duplicates. Following drug exposure time of 5 days under normoxic or hypoxic (0.1% O_2) culture conditions, cells were washed with phosphate-buffered saline (PBS), fixed with ice-cold methanol for 30 min at 4 °C and stained with crystal violet. Digital photographs were taken using a Nikon D3200 camera and processed with ImageJ software. For quantification, crystal violet was eluted using 2% sodium dodecyl sulfate (SDS) and color absorbance was measured at 560 nm at the Tecan infinite 200Pro (Zurich, Switzerland). Values are given in arbitrary units (a.u.) as mean ± SD normalized to untreated control.

Flow cytometry

Cells were seeded (1 × 10^6 cells per well) in 96-well plates, dissolved compounds were added and cells were incubated under normoxic or hypoxic cell culture conditions. Samples were measured on a BD LSRFortessa X-20 cell analyzer high throughput sampler (HTS) (BD Biosciences, East Rutherford, NJ, USA). Compound fluorescence was detected using 405 nm excitation and pacific blue (450/50 nm) band pass emission filters. Data were analyzed using BD FACSDiva software and are given in arbitrary units (a.u.) as mean fluorescence intensities of cells normalized to the auto fluorescence of untreated control.

Fluorescence microscopy

UM-UC-14 cells were seeded (2.5 × 10^5 cells per well) in 12-well plates and after 24 h recovery treated with 10 μM of compounds. After 24 h incubation, the drug solutions were removed, cells were washed with PBS and microphotographs of the different treatments were taken using UV fluorescence microscopy (Nikon Eclipse Ti2 microscope with a DAPI filter and a high-pressure mercury lamp) and a 20× objective. The level of cellular fluorescence was determined from fluorescence microscopy images using ImageJ software.

Western blot analysis

K-562 cells were plated (5 × 10^5 cells per well) in 6-well plates and allowed to recover for 24 h. Subsequently, the cells were treated with the drugs in different concentrations. After 12 h cells were harvested, proteins were isolated, resolved by sodium dodecyl sulfate polyacrylamide gel electrophoresis (SDS/PAGE), and transferred onto a polyvinylidene difluoride membrane for western blotting. The following antibodies were

used: ERK1/2 (p44/42) rabbit monoclonal antibody (mAb) (137F5, #4695), phospho-ERK1/2 rabbit mAb (Thr202/Tyr204) (20G11, #4376), phospho-S6 rabbit pAb (Ser240/244, #2215) (Cell Signaling Technology, Beverly, MA, USA), S6 mouse mAb (C-8. #sc-74459) (Santa Cruz Biotechnology, TX, USA) and β-actin mouse mAb (#A5441, Sigma). All primary antibodies were used in 1 : 1000 dilutions (in Tris-buffered saline containing 0.1% Tween20 (TBST) + 3% bovine serum albumin (BSA)). Secondary goat anti-mouse-IgG (Fc specific)-peroxidase antibody (#A0168, Sigma) and horseradish peroxidase(HRP)-labeled mouse anti-rabbit IgG (#sc-2357, Santa Cruz Biotechnology) were used at working dilutions of 1 : 10 000 (in TBST + 1% BSA).

In vivo xenograft experiment

Eight-to nine-week-old male C.B.17/SCID mice were bread in-house (originally Harlan) and were kept in pathogen-free conditions and controlled environment with 12 h light–dark cycle. K-562 (5×10^6 in 100 μL serum-free RMPI medium, 20% Matrigel) or UM-UC-14 (1×10^6 in 100 μL serum-free RMPI medium) cells were injected into the right flank of male C.B.17/SCID mice. When all tumors were measurable (at day 5 and day 7, respectively), all animals were dosed i.p. with solutions (200 μL) containing $\mathbf{Co(acac)_2L_{Pon}}$ or $\mathbf{Co(Meacac)_2L_{Pon}}$ (10 mg kg^{-1}, 200 μL per 20 g, dissolved in 50 mM PBS, 2% DMSO). The control groups received solvent alone (200 μL, 50 mM PBS, 2% DMSO). Compounds were dissolved in the respective amount of DMSO and then added to PBS buffer for the desired end concentration allowing application of 200 μL per 20 g and dosing using 30 gauze needles. Tumor growth was evaluated by daily recording of tumor size by caliper measurement. Animals were sacrificed by cervical dislocation. All procedures were performed in a laminar flow hood. The animal experiments were performed according to the regulations of the Ethics Committee for the Care and Use of Laboratory Animals at the Medical University Vienna (proposal number BMBWF-V/3b 2020-0.380.502).

Statistical analysis

Data were analyzed using GraphPad Prism 8.0 software (GraphPad Software, Inc.) and are expressed as mean ± standard deviation (SD) of one independent experiment performed in triplicates, unless stated otherwise. One- or two-way analysis of variance (ANOVA) with multiple comparison test (Sidak, Bonferroni or Dunnett) was performed for statistical evaluation if not stated otherwise, p-values <0.05 were considered statistically significant [$p < 0.05$(*); <0.01 (**); <0.001 (***)].

Conflicts of interest

There are no conflicts to declare.

Acknowledgements

We gratefully acknowledge the Austrian Science Fund (FWF) for financial support. Grant P28853 to CK and grant FG3 to WB and CK.

References

1 M. A. Lemmon and J. Schlessinger, Cell signaling by receptor tyrosine kinases, *Cell*, 2010, **141**, 1117–1134.
2 Z. Du and C. M. Lovly, Mechanisms of receptor tyrosine kinase activation in cancer, *Mol. Cancer*, 2018, **17**, 58.
3 P. Wu, T. E. Nielsen and M. H. Clausen, FDA-approved small-molecule kinase inhibitors, *Trends Pharmacol. Sci.*, 2015, **36**, 422–439.
4 S. M. Chiavenna, J. P. Jaworski and A. Vendrell, State of the art in anti-cancer mAbs, *J. Biomed. Sci.*, 2017, **24**, 1–12.
5 W.-S. Huang, C. A. Metcalf, R. Sundaramoorthi, Y. Wang, D. Zou, R. M. Thomas, X. Zhu, L. Cai, D. Wen and S. Liu, Discovery of 3-[2-(imidazo [1, 2-b] pyridazin-3-yl) ethynyl]-4-methyl-N-{4-[(4-methylpiperazin-1-yl) methyl]-3-(trifluoromethyl) phenyl} benzamide (AP24534), a potent, orally active pan-inhibitor of breakpoint cluster region-abelson (BCR-ABL) kinase including the T315I gatekeeper mutant, *J. Med. Chem.*, 2010, **53**, 4701–4719.
6 S. M. Hoy, Ponatinib: a review of its use in adults with chronic myeloid leukaemia or Philadelphia chromosome-positive acute lymphoblastic leukaemia, *Drugs*, 2014, **74**, 793–806.
7 F. H. Tan, T. L. Putoczki, S. S. Stylli and R. B. Luwor, Ponatinib: a novel multi-tyrosine kinase inhibitor against human malignancies, *OncoTargets Ther.*, 2019, **12**, 635–645.
8 J. E. Cortes, D.-W. Kim, J. l. Pinilla-Ibarz, P. Le Coutre, R. Paquette, C. Chuah, F. Nicolini, J. Apperley, H. Khoury and M. Talpaz, A phase 2 trial of ponatinib in Philadelphia chromosome–positive leukemias, *New Eng. J. Med.*, 2013, **369**, 1783–1796.
9 M. C. Mueller, F. Cervantes, H. Hjorth-Hansen, J. J. Janssen, D. Milojkovic, D. Rea and G. Rosti, Ponatinib in chronic myeloid leukemia (CML): Consensus on patient treatment and management from a European expert panel, *Crit. Rev. Oncol. Hematol.*, 2017, **120**, 52–59.
10 T. O'Hare, W. C. Shakespeare, X. Zhu, C. A. Eide, V. M. Rivera, F. Wang, L. T. Adrian, T. Zhou, W.-S. Huang and Q. Xu, AP24534, a pan-BCR-ABL inhibitor for chronic myeloid leukemia, potently inhibits the T315I mutant and overcomes mutation-based resistance, *Cancer Cells*, 2009, **16**, 401–412.
11 F. Musumeci, C. Greco, G. Grossi, A. Molinari and S. Schenone, Recent studies on ponatinib in cancers other than chronic myeloid leukemia, *Cancers*, 2018, **10**, 430.
12 R. Roskoski Jr., The role of fibroblast growth factor receptor (FGFR) protein-tyrosine kinase inhibitors in the treatment of cancers including those of the urinary bladder, *Pharmacol. Res.*, 2020, **151**, 104567.
13 J. M. Gozgit, M. J. Wong, L. Moran, S. Wardwell, Q. K. Mohemmad, N. I. Narasimhan, W. C. Shakespeare, F. Wang, T. Clackson and V. M. Rivera, Ponatinib (AP24534), a multitargeted pan-FGFR inhibitor with activity in multiple FGFR-amplified or mutated cancer models, *Mol. Cancer Ther.*, 2012, **11**, 690–699.

14 O. Chan, C. Talati, L. Isenalumhe, S. Shams, L. Nodzon, M. Fradley, K. Sweet and J. Pinilla-Ibarz, Side-effects profile and outcomes of ponatinib in the treatment of chronic myeloid leukemia, *Blood Adv.*, 2020, **4**, 530–538.
15 J. F. Gainor and B. A. Chabner, Ponatinib: accelerated disapproval, *Oncologist*, 2015, **20**, 847.
16 J. H. Lipton, C. Chuah, A. Guerci-Bresler, G. Rosti, D. Simpson, S. Assouline, G. Etienne, F. E. Nicolini, P. le Coutre and R. E. Clark, Ponatinib versus imatinib for newly diagnosed chronic myeloid leukaemia: an international, randomised, open-label, phase 3 trial, *Lancet Oncol.*, 2016, **17**, 612–621.
17 D. J. Dorer, R. K. Knickerbocker, M. Baccarani, J. E. Cortes, A. Hochhaus, M. Talpaz and F. G. Haluska, Impact of dose intensity of ponatinib on selected adverse events: multivariate analyses from a pooled population of clinical trial patients, *Leuk. Res.*, 2016, **48**, 84–91.
18 F. Kratz, I. A. Müller, C. Ryppa and A. Warnecke, Prodrug strategies in anticancer chemotherapy, *ChemMedChem*, 2008, **3**, 20–53.
19 Y. A. Fouad and C. Aanei, Revisiting the hallmarks of cancer, *Am. J. Cancer Res.*, 2017, **7**, 1016.
20 R. M. Phillips, Targeting the hypoxic fraction of tumours using hypoxia-activated prodrugs, *Cancer Chemother. Pharmacol.*, 2016, **77**, 441–457.
21 K. M. Johnson, Z. D. Parsons, C. L. Barnes and K. S. Gates, Toward hypoxia-selective DNA-alkylating agents built by grafting nitrogen mustards onto the bioreductively activated, hypoxia-selective DNA-oxidizing agent 3-amino-1, 2, 4-benzotriazine 1, 4-dioxide (tirapazamine), *J. Org. Chem.*, 2014, **79**, 7520–7531.
22 V. Liapis, I. Zinonos, A. Labrinidis, S. Hay, V. Ponomarev, V. Panagopoulos, A. Zysk, M. DeNichilo, W. Ingman and G. J. Atkins, Anticancer efficacy of the hypoxia–activated prodrug evofosfamide (TH–302) in osteolytic breast cancer murine models, *Cancer Med.*, 2016, **5**, 534–545.
23 R. M. Phillips, H. R. Hendriks, J. B. Sweeney, G. Reddy and G. J. Peters, Efficacy, pharmacokinetic and pharmacodynamic evaluation of apaziquone in the treatment of non-muscle invasive bladder cancer, *Expert Opin. Drug Metab. Toxicol.*, 2017, **13**, 783–791.
24 A. Sharma, J. F. Arambula, S. Koo, R. Kumar, H. Singh, J. L. Sessler and J. S. Kim, Hypoxia-targeted drug delivery, *Chem. Soc. Rev.*, 2019, **48**, 771–813.
25 L. Spiegelberg, R. Houben, R. Niemans, D. de Ruysscher, A. Yaromina, J. Theys, C. P. Guise, J. B. Smaill, A. V. Patterson and P. Lambin, Hypoxia-activated prodrugs and (lack of) clinical progress: The need for hypoxia-based biomarker patient selection in phase III clinical trials, *Clin. Transl. Radiat. Oncol.*, 2019, **15**, 62–69.
26 C. Karnthaler-Benbakka, D. Groza, K. Kryeziu, V. Pichler, A. Roller, W. Berger, P. Heffeter and C. R. Kowol, Tumor–Targeting of EGFR Inhibitors by Hypoxia–Mediated Activation, *Angew. Chem., Int. Ed.*, 2014, **53**, 12930–12935.
27 C. Karnthaler-Benbakka, D. Groza, B. Koblmüller, A. Terenzi, K. Holste, M. Haider, D. Baier, W. Berger, P. Heffeter and C. R. Kowol, Targeting a targeted drug: an approach toward hypoxia-activatable tyrosine kinase inhibitor prodrugs, *ChemMedChem*, 2016, **11**, 2410–2421.
28 B. Bielec, H. Schueffl, A. Terenzi, W. Berger, P. Heffeter, B. K. Keppler and C. R. Kowol, Development and biological investigations of hypoxia-sensitive prodrugs of the tyrosine kinase inhibitor crizotinib, *Bioorg. Chem.*, 2020, 103778.
29 A. V. Patterson, S. Silva, C. Guise, M. Bull, M. Abbattista, A. Hsu, J. D. Sun, C. P. Hart, T. E. Pearce and J. B. Smaill, TH-4000, a hypoxia-activated EGFR/Her2 inhibitor to treat EGFR-TKI resistant T790M-negative NSCLC, *J. Clin. Oncol.*, 2015, **33**(15 suppl).
30 C. R. Munteanu and K. Suntharalingam, Advances in cobalt complexes as anticancer agents, *Dalton Trans.*, 2015, **44**, 13796–13808.
31 N. Yamamoto, A. K. Renfrew, B. J. Kim, N. S. Bryce and T. W. Hambley, Dual targeting of hypoxic and acidic tumor environments with a cobalt(III) chaperone complex, *J. Med. Chem.*, 2012, **55**, 11013–11021.
32 U. Jungwirth, C. R. Kowol, B. K. Keppler, C. G. Hartinger, W. Berger and P. Heffeter, Anticancer activity of metal complexes: involvement of redox processes, *Antioxid. Redox Signal.*, 2011, **15**, 1085–1127.
33 D. C. Ware, B. D. Palmer, W. R. Wilson and W. A. Denny, Hypoxia-selective antitumor agents. 7. Metal complexes of aliphatic mustards as a new class of hypoxia-selective cytotoxins. Synthesis and evaluation of cobalt(III) complexes of bidentate mustards, *J. Med. Chem.*, 1993, **36**, 1839–1846.
34 M. C. Heffern, N. Yamamoto, R. J. Holbrook, A. L. Eckermann and T. J. Meade, Cobalt derivatives as promising therapeutic agents, *Curr. Opin. Chem. Biol.*, 2013, **17**, 189–196.
35 X.-Y. Meng, H.-X. Zhang, M. Mezei and M. Cui, Molecular docking: a powerful approach for structure-based drug discovery, *Curr. Comput.-Aided Drug Des.*, 2011, **7**, 146–157.
36 Z. Gagic, D. Ruzic, N. Djokovic, T. Djikic and K. Nikolic, In silico methods for design of kinase inhibitors as anticancer drugs, *Front. Chem.*, 2020, **7**, 873.
37 D. H. Zou, W.-S. Thomas, R. M. Romero, J. A. C. Qi, J. Wang, Y. Zhu, X. Shakespeare, W. C. Sundaramoorthi, R. Metcalf, C. A. Dalgarno III and D. C. Sawyer, T. K., Bicyclic heteroaryl compounds, *W.O. Patent* 2007/075869A2, 2007.
38 M. Mathuber, H. Schueffl, O. Dömötör, C. Karnthaler, E. v. A. Enyedy, P. Heffeter, B. K. Keppler and C. R. Kowol, Improving the Stability of EGFR Inhibitor Cobalt(III) Prodrugs, *Inorg. Chem.*, 2020, **59**, 17794–17810.
39 D. C. Ware, H. R. Palmer, P. J. Brothers, C. E. Rickard, W. R. Wilson and W. A. Denny, Bis-tropolonato derivatives of cobalt(III) complexes of bidentate aliphatic nitrogen mustards as potential hypoxia-selective cytotoxins, *J. Inorg. Biochem.*, 1997, **68**, 215–224.
40 B. Englinger, A. Laemmerer, P. Moser, S. Kallus, C. Röhrl, C. Pirker, D. Baier, T. Mohr, L. Niederstaetter, S. M. Meier-Menches, C. Gerner, L. Gabler, J. Gojo, G. Timelthaler, J. Senkiv, W. Jäger, C. R. Kowol, P. Heffeter and W. Berger,

Lipid droplet–mediated scavenging as novel intrinsic and adaptive resistance factor against the multikinase inhibitor ponatinib, *Int. J. Cancer*, 2020, 1680–1693.
41 Y. Chia and M. Tay, An insight into fluorescent transition metal complexes, *Dalton Trans.*, 2014, **43**, 13159–13168.
42 N. Graf and S. J. Lippard, Redox activation of metal-based prodrugs as a strategy for drug delivery, *Adv. Drug Delivery Rev.*, 2012, **64**, 993–1004.
43 A. K. Renfrew, E. S. O'Neill, T. W. Hambley and E. J. New, Harnessing the properties of cobalt coordination complexes for biological application, *Coord. Chem. Rev.*, 2018, **375**, 221–233.
44 D. C. Ware, H. R. Palmer, F. B. Pruijn, R. F. Anderson, P. J. Brothers, W. A. Denny and W. R. Wilson, Bis (dialkyl) dithiocarbamato cobalt(III) complexes of bidentate nitrogen mustards: synthesis, reduction chemistry and biological evaluation as hypoxia-selective cytotoxins, *Anticancer Drug Des.*, 1998, **13**, 81–103.
45 P. R. Craig, P. J. Brothers, G. R. Clark, W. R. Wilson, W. A. Denny and D. C. Ware, Anionic carbonato and oxalato cobalt(III) nitrogen mustard complexes, *Dalton Trans.*, 2004, 611–618.
46 T. W. Failes, C. Cullinane, C. I. Diakos, N. Yamamoto, J. G. Lyons and T. W. Hambley, Studies of a cobalt(III) complex of the MMP inhibitor marimastat: a potential hypoxia–activated prodrug, *Chem. – Eur. J.*, 2007, **13**, 2974–2982.
47 I. C. A. de Souza, S. de Souza Santana, J. G. Gómez, G. P. Guedes, J. Madureira, S. M. de Ornelas Quintal and M. Lanznaster, Investigation of cobalt(III)–phenylalanine complexes for hypoxia-activated drug delivery, *Dalton Trans.*, 2020, 16425–16439.
48 R. Anderson, W. Denny, D. Ware and W. Wilson, Pulse radiolysis studies on the hypoxia-selective toxicity of a colbalt-mustard complex, *Br. J. Cancer*, 1996, **27**, S48.
49 B. B. Lozzio and C. B. Lozzio, Properties and usefulness of the original K-562 human myelogenous leukemia cell line, *Leuk. Res.*, 1979, **3**, 363–370.
50 M. Miyake, M. Ishii, N. Koyama, K. Kawashima, T. Kodama, S. Anai, K. Fujimoto, Y. Hirao and K. Sugano, 1-tert-butyl-3-[6-(3, 5-dimethoxy-phenyl)-2-(4-diethylamino-butylamino)-pyrido [2, 3-d] pyrimidin-7-yl]-urea (PD173074), a selective tyrosine kinase inhibitor of fibroblast growth factor receptor-3 (FGFR3), inhibits cell proliferation of bladder cancer carrying the FGFR3 gene mutation along with up-regulation of p27/Kip1 and G1/G0 arrest, *J. Pharmacol. Exp. Ther.*, 2010, **332**, 795–802.
51 PerkinElmer, *ChemBioDraw Ultra 13.0*.
52 C. Bresson, C. Darolles, A. Carmona, C. Gautier, N. Sage, S. Roudeau, R. Ortega, E. Ansoborlo and V. Malard, Cobalt chloride speciation, mechanisms of cytotoxicity on human pulmonary cells, and synergistic toxicity with zinc, *Metallomics*, 2013, **5**, 133–143.
53 J. N. Lee, J. Park, S.-G. Kim, M. S. Kim, J.-Y. Lim and S.-K. Choe, 3-Aminotriazole protects against cobalt(II) chloride-induced cytotoxicity by inhibiting reactive oxygen species formation and preventing mitochondrial damage in HepG2 cells, *Mol. Cell. Toxicol.*, 2017, **13**, 125–132.
54 Z.-J. Dai, J. Gao, X.-B. Ma, K. Yan, X.-X. Liu, H.-F. Kang, Z.-Z. Ji, H.-T. Guan and X.-J. Wang, Up-regulation of hypoxia inducible factor-1α by cobalt chloride correlates with proliferation and apoptosis in PC-2 cells, *J. Exp. Clin. Cancer Res.*, 2012, **31**, 28.
55 Y. Yuan, G. Hilliard, T. Ferguson and D. E. Millhorn, Cobalt inhibits the interaction between hypoxia-inducible factor-α and von Hippel-Lindau protein by direct binding to hypoxia-inducible factor-α, *J. Biol. Chem.*, 2003, **278**, 15911–15916.
56 M. D. Hanwell, D. E. Curtis, D. C. Lonie, T. Vandermeersch, E. Zurek and G. R. Hutchison, Avogadro: an advanced semantic chemical editor, visualization, and analysis platform, *J. Cheminf.*, 2012, **4**, 17.
57 J. Wang, R. M. Wolf, J. W. Caldwell, P. A. Kollman and D. A. Case, Erratum: Development and testing of a general amber force field (Journal of Computational Chemistry (2004) 25 (1157)), *J. Comput. Chem.*, 2005, **26**, 1157–1174.
58 H. M. Berman, J. Westbrook, Z. Feng, G. Gilliland, T. N. Bhat, H. Weissig, I. N. Shindyalov and P. E. Bourne, The protein data bank, *Nucleic Acids Res.*, 2000, **28**, 235–242.
59 E. F. Pettersen, T. D. Goddard, C. C. Huang, G. S. Couch, D. M. Greenblatt, E. C. Meng and T. E. Ferrin, UCSF Chimera—a visualization system for exploratory research and analysis, *J. Comput. Chem.*, 2004, **25**, 1605–1612.
60 R. Harris, A. J. Olson and D. S. Goodsell, Automated prediction of ligand–binding sites in proteins, *Proteins*, 2008, **70**, 1506–1517.
61 O. Trott and A. J. Olson, AutoDock Vina: improving the speed and accuracy of docking with a new scoring function, efficient optimization, and multithreading, *J. Comput. Chem.*, 2010, **31**, 455–461.
62 I. Kufareva and R. Abagyan, in *Homology Modeling*, Springer, 2011, pp. 231–257.
63 W. C. Barrette, H. Johnson and D. T. Sawyer, Voltammetric evaluation of the effective acidities (pKa') for Broensted acids in aprotic solvents, *Anal. Chem.*, 1984, **56**, 1890–1898.

Supplementary material

Development of a ponatinib-based cobalt(III) prodrug system

Marlene Mathuber[a], Michael Gutmann[b], Mery La Franca[b,c], Petra Vician[b], Anna Laemmerer[b,d], Patrick Moser[b], Bernhard K. Keppler[a,d], Walter Berger[b,d]*and Christian R. Kowol[a,d]*

[a] Institute of Inorganic Chemistry, Faculty of Chemistry, University of Vienna, Waehringer Straße 42, 1090 Vienna, Austria

[b] Institute of Cancer Research and Comprehensive Cancer Center, Medical University of Vienna, Borschkegasse 8A, 1090 Vienna, Austria

[c] Department of Biological, Chemical and Pharmaceutical Sciences and Technologies, University of Palermo, via Archirafi 32, 90123 Palermo, Italy

[d] Research Cluster ‘‘Translational Cancer Therapy Research’’, University of Vienna and Medical University of Vienna, 1090 Vienna, Austria

* Corresponding authors. E-mail address: christian.kowol@univie.ac.at; walter.berger@meduniwien.ac.at

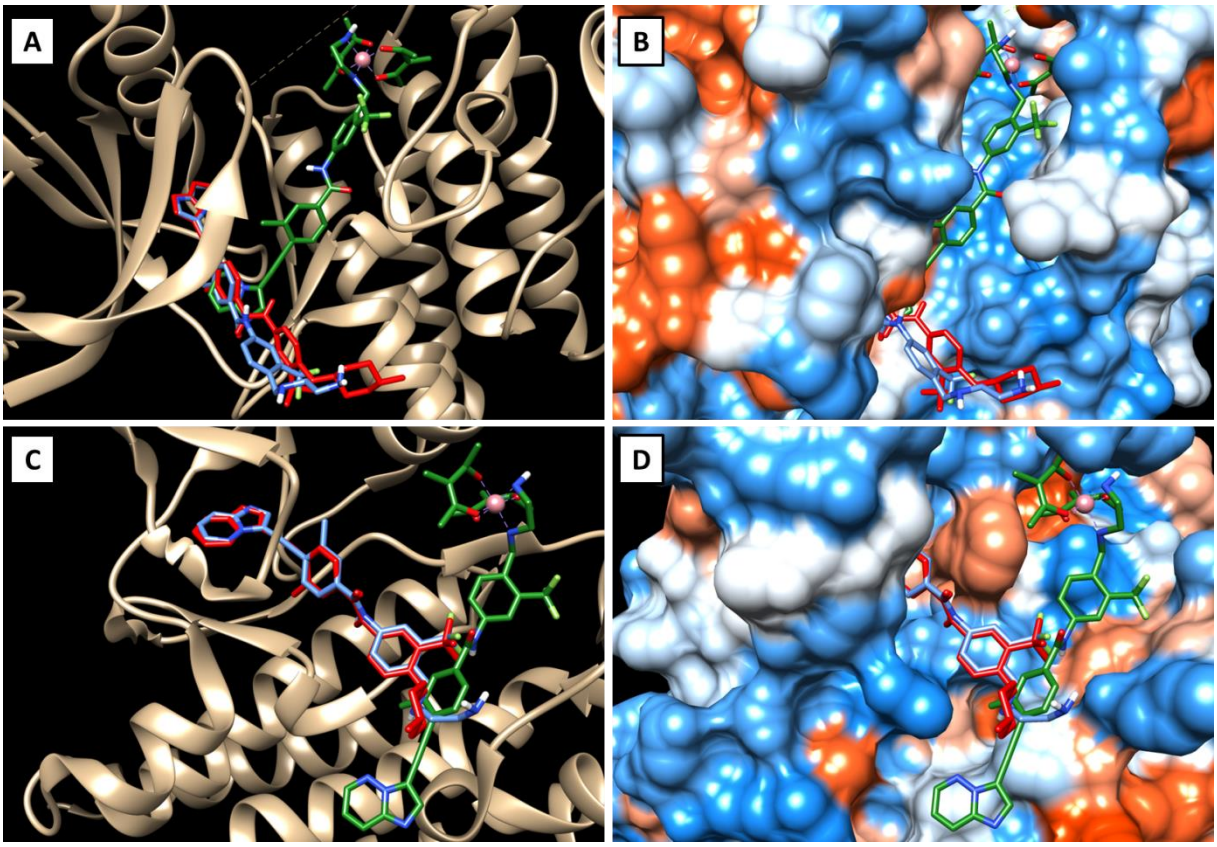

Figure S1: Visualizations of the best docking poses of $\mathbf{L_{Pon}}$ and $\mathbf{Co(Meacac)_2L_{Pon}}$ in comparison to ponatinib with FGFR1 (A and B) (PDB ID: 4V04) as well as ABL1 (C and D) (PDB ID: 4WA9). Ponatinib is shown in red, $\mathbf{L_{Pon}}$ in blue and $\mathbf{Co(Meacac)_2L_{Pon}}$ in green.

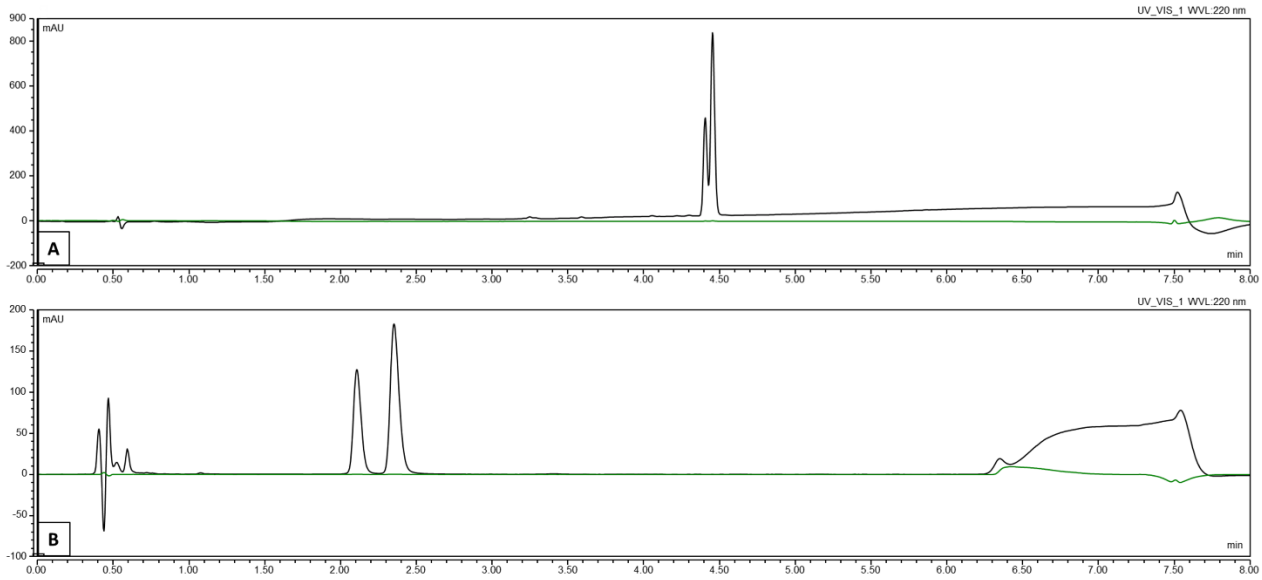

Figure S2: HPLC measurements of $\mathbf{Co(acac)_2L_{Pon}}$: A) Gradient from 5-95 % ACN (+0.1 % TFA), both isomers are visible, but strongly overlapping. B) Adjusted gradient 45 % ACN (+0.1 % TFA) isocratic, essential for separation via preparative HPLC.

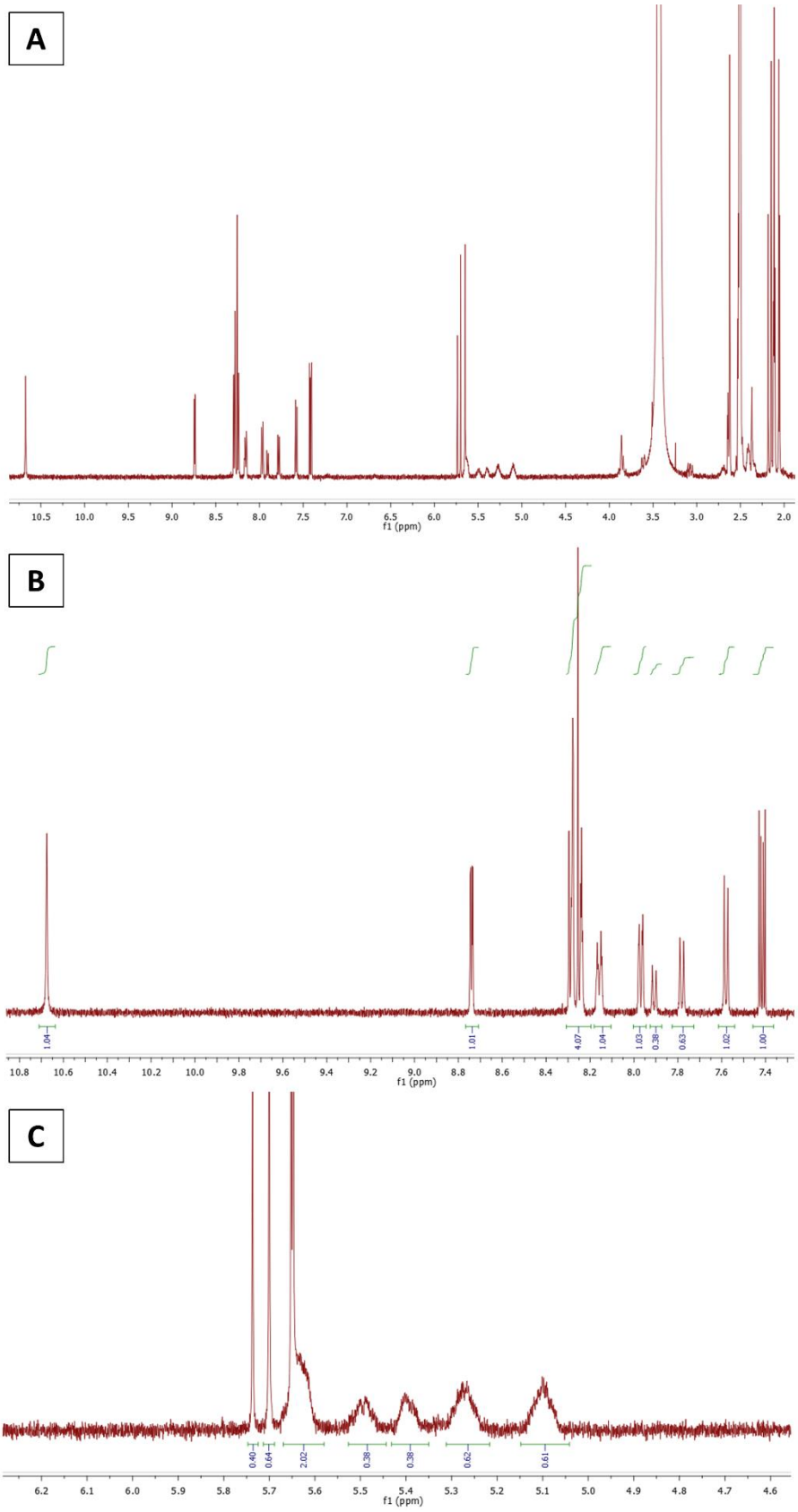

Figure S3: ^{1}H-NMR spectrum of **$Co(acac)_2L_{Pon}$,** showing (A) the whole-range, (B) the aromatic area from ~7–11 ppm and (C) the aliphatic area from ~4–6 ppm . Two sets of signals can be observed, but only in the aliphatic region and for the proton at 7.78/7.91 ppm.

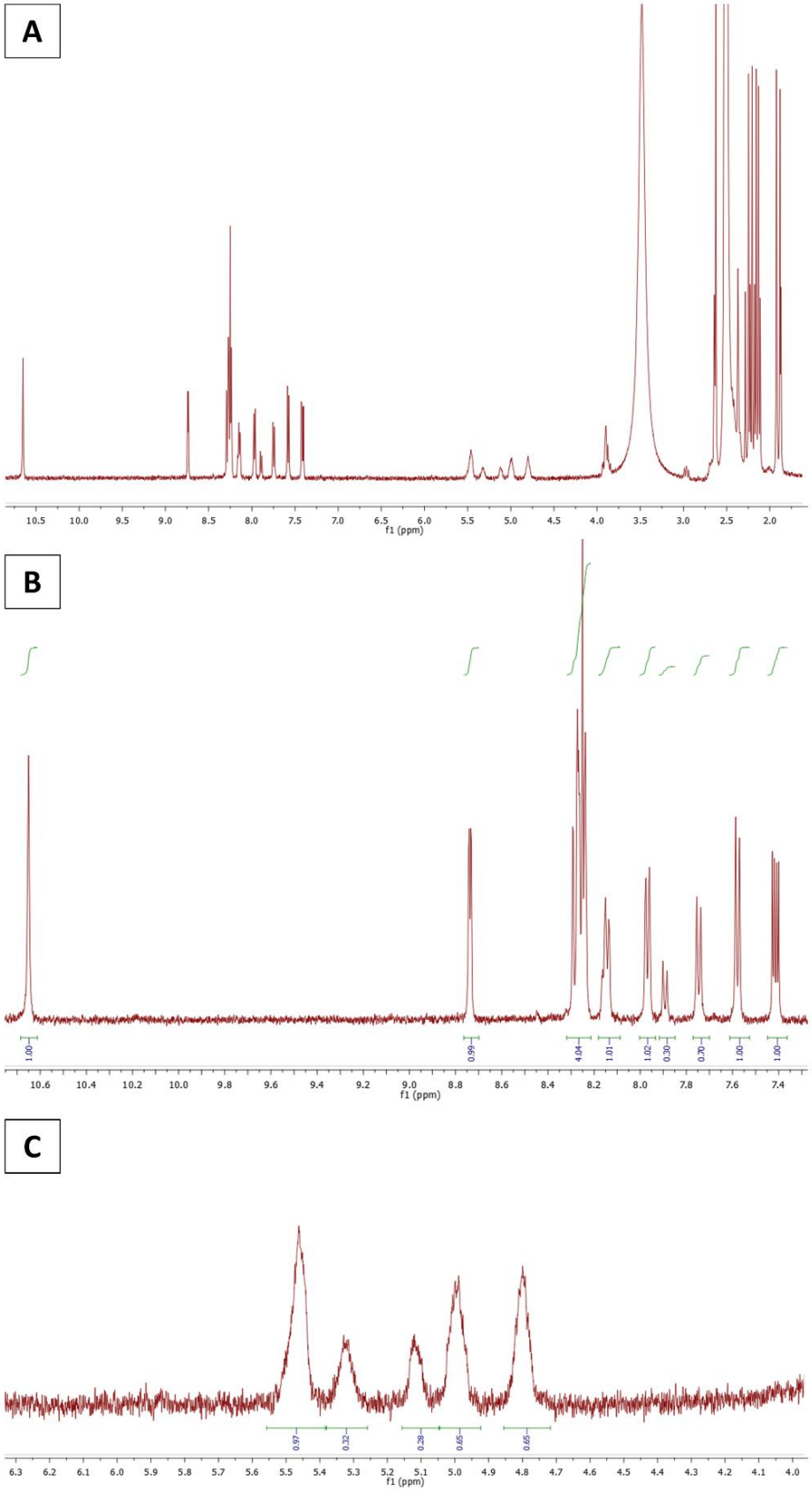

Figure S4: ^{1}H-NMR spectrum of **Co(Meacac)$_2$L$_{Pon}$,** showing (A) the whole-range, (B) the aromatic area from ~7–11 ppm and (C) the aliphatic area from ~4–6 ppm . Two sets of signals can be observed, but only in the aliphatic region and for the proton at 7.75/7.89 ppm.

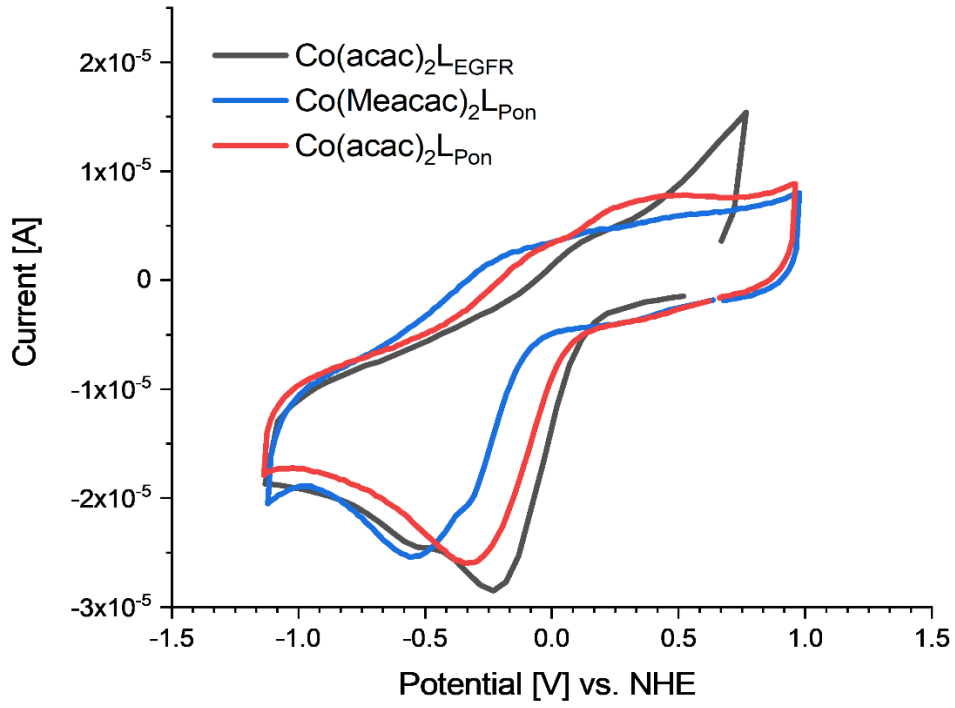

Figure S5: Cyclic voltammograms of **$Co(acac)_2L_{Pon}$**, **$Co(Meacac)_2L_{Pon}$** and **$Co(acac)_2L_{EGFR}$** in DMF (1.5 mM complex, I = 0.2 M [n-Bu_4N][BF_4], scan rate of 1000 mV/s, 25.0 °C).

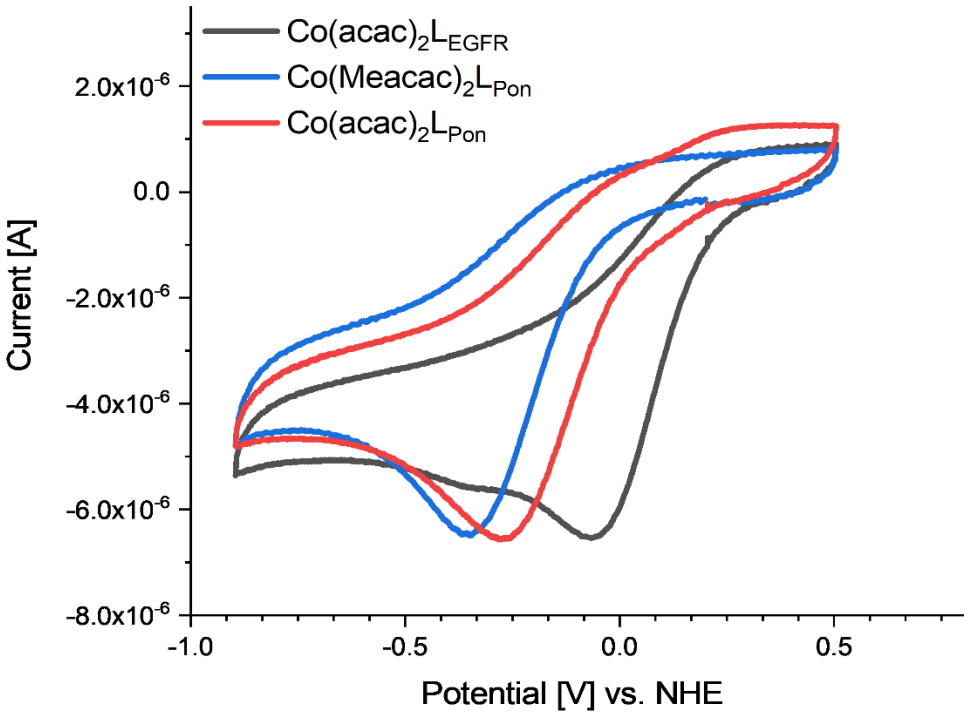

Figure S6: Cyclic voltammograms **$Co(acac)_2L_{Pon}$**, **$Co(Meacac)_2L_{Pon}$** and **$Co(acac)_2L_{EGFR}$** in 7:3 DMF/H_2O (1.5 mM complex, I = 0.2 M [n-Bu_4N][BF_4] for DMF, aqueous phase = 10 mM phosphate buffer at pH 7.40 with I = 0.1 M KCl, scan rate of 100 mV/s, 25.0 °C).

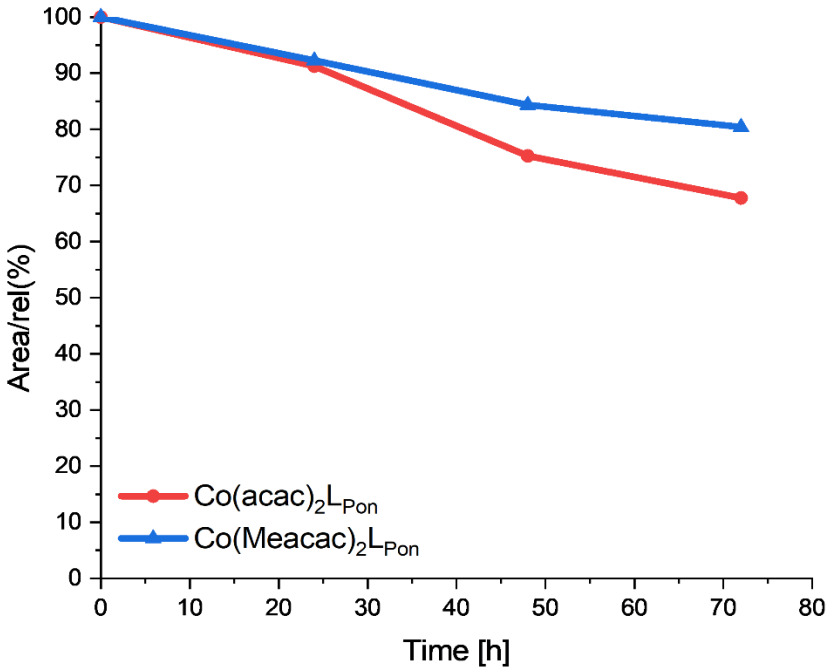

Figure S7: Stability measurements of **$Co(acac)_2L_{Pon}$** and **$Co(Meacac)_2L_{Pon}$** incubated in FCS at 37°C (pH 7.4, 150 mM phosphate buffer) analyzed by HPLC-MS over a time period of 72 h. The y-axis shows the relative ratio of the integrated peak areas of the intact complex over time (in percent) compared to the area at the starting point (0 h).

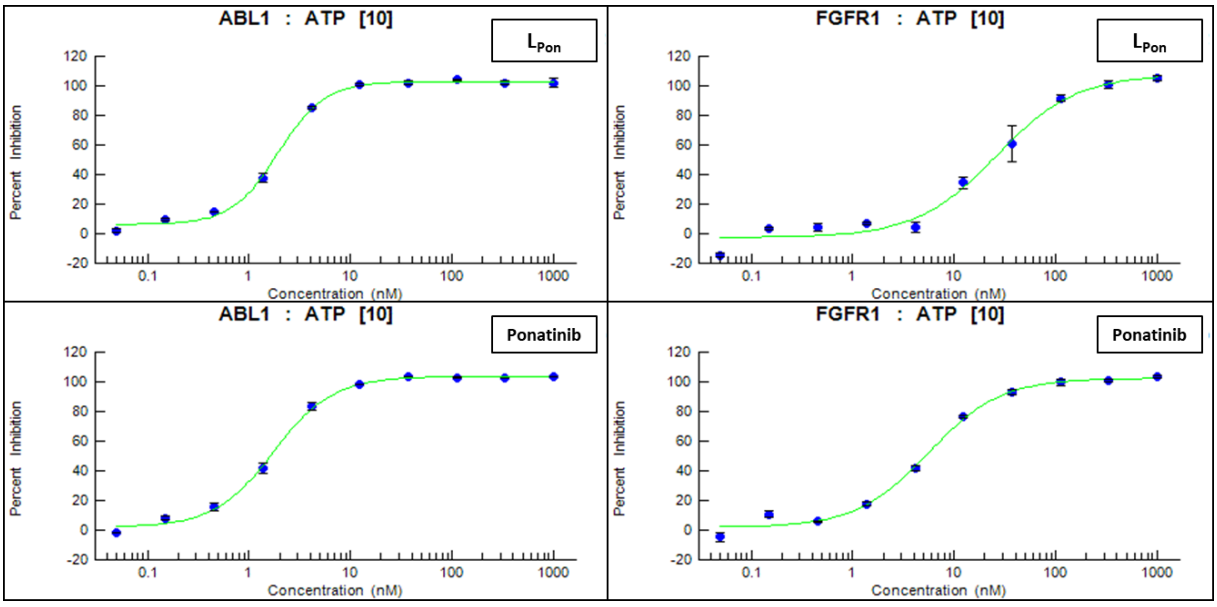

Figure S8: Data points of the cell-free ABL1 (left) and FGFR1 (right) kinase inhibition assay of **L_{Pon}** and ponatinib.

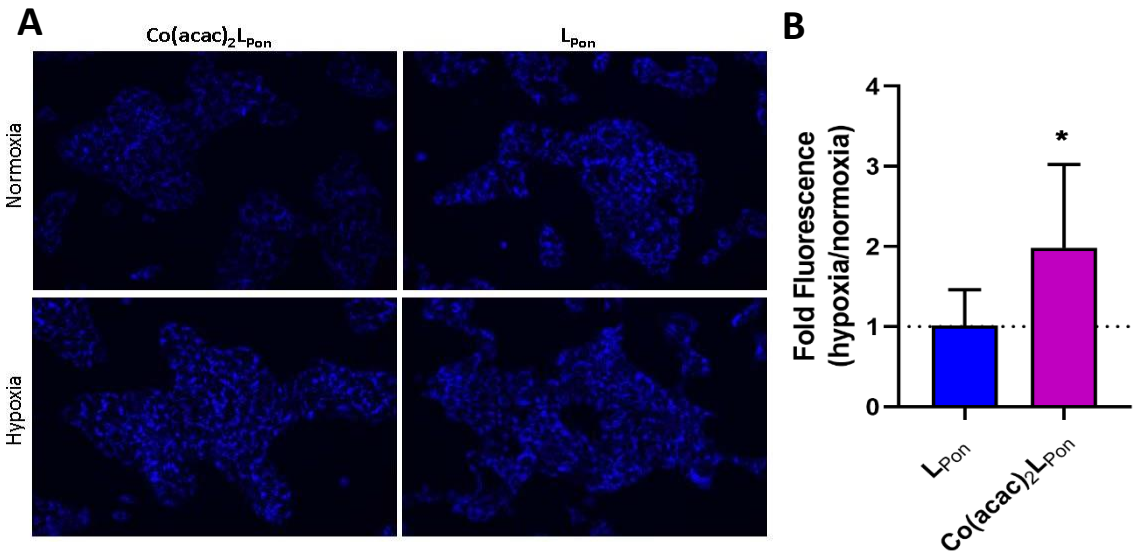

Figure S9: Ligand release of **$Co(acac)_2L_{Pon}$** under normoxic and hypoxic cell culture conditions in comparison to **L_{Pon}** using UV fluorescence microscopy. UM-UC-14 cells were incubated with 10 µM of compounds for 24 h. Images of the different treatments were taken by UV fluorescence microcopy (20X objective) and the corrected total cell fluorescence was evaluated using ImageJ software. Data in Figure S9B are given as means ± SD of ten analyzed microphotographs per compound. Statistical significance was calculated by unpaired t test with $p < .05$(*).

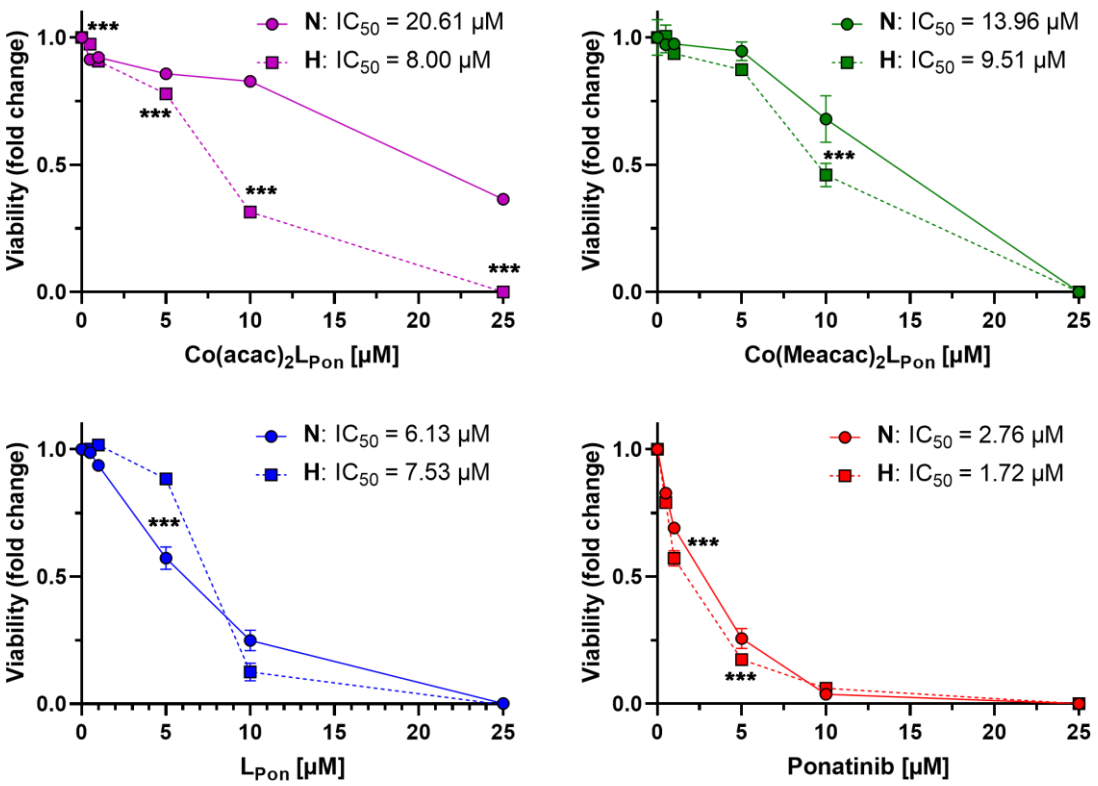

Figure S10: Cytotoxic activity of **$Co(acac)_2L_{Pon}$**, **$Co(Meacac)_2L_{Pon}$**, **L_{Pon}** and **ponatinib** against the UM-UC-14 cell line. Cells were incubated with the compounds under normoxic (21% O_2) or hypoxic conditions (0.1% O_2). ***N*** = normoxia; ***H*** = hypoxia. Cell viability was measured by MTT vitality assay after 72 h. Values are given as means ± SD of one representative experiment, performed in triplicates. Statistical significance was calculated by two-way ANOVA with Sidak multiple comparison test with $p < .05$(*); < .01 (**); < .001 (***).

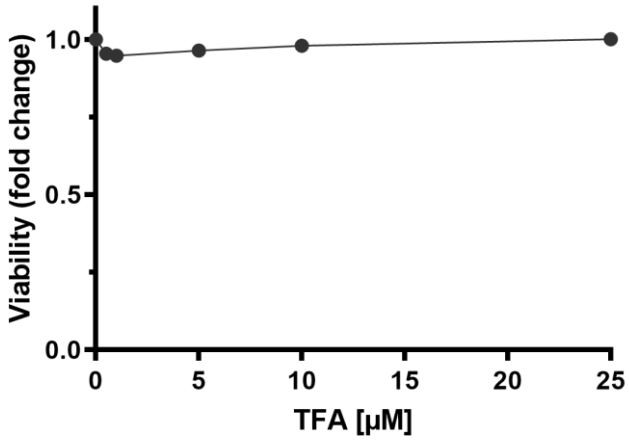

Figure S11: Cytotoxic activity of TFA against the UM-UC-14 cell line. Cells were incubated with TFA and cell viability was measured by MTT vitality assay after 72 h. Values are given as means ± SD of one representative experiment.

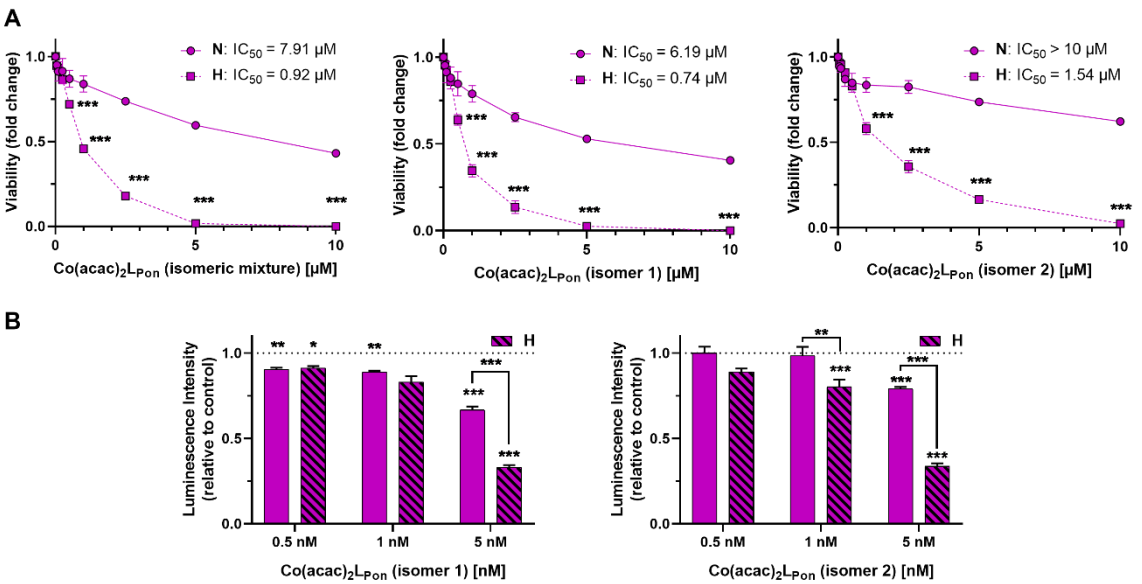

Figure S12: Cytotoxic activity of both pure isomers of **$Co(acac)_2L_{Pon}$** against human cancer cell models under normoxic (*N*) and hypoxic (*H*) conditions. A) FGFR3-driven UM-UC-14 urothelial cell viability was measured by MTT vitality assay and (B) cell viability of BCR-ABL-positive K-562 by luminescence assay based on ATP quantification (CellTiter-Glo) after 72 h. Data are given as means ± SD of one representative experiment performed in triplicates. Statistical significance was calculated by two-way ANOVA with Sidak multiple comparison test with $p < .05$(*); $< .01$ (**); $< .001$ (***).

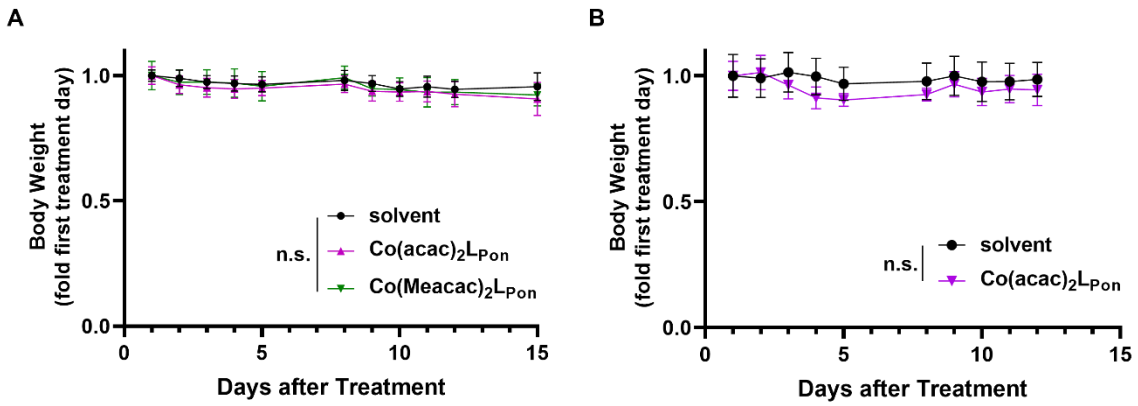

Figure S13: Animal weights of xenograft experiments. (A) BCR-ABL-driven leukemic K-562 cells or (B) FGFR3-driven urothelial UM-UC-14 cells were injected s.c. into the right flank of male CB17/SCID mice (n=4 animals per experimental group). When tumors were measurable (day 5 and day 7, respectively) compounds (10 mg kg^{-1} i.p.) were applied and animal weights were determined. Data are given as means ± SEM. Statistical significance was calculated by two-way ANOVA with Sidak multiple comparison test.

7.3 Liposomal formulations of anticancer copper(II) thiosemicarbazone complexes

Marlene Mathuber[a], Sonja Hager[b,c], Bernhard K. Keppler[a,c], Petra Heffeter[b,c] and Christian R. Kowol[a,c,*]

Dalton Transactions, in submission

[a] Institute of Inorganic Chemistry, Faculty of Chemistry, University of Vienna, Waehringer Straße 42, 1090 Vienna, Austria

[b] Institute of Cancer Research and Comprehensive Cancer Center, Medical University of Vienna, Borschkegasse 8A, 1090 Vienna, Austria

[c] Research Cluster ''Translational Cancer Therapy Research'', University of Vienna and Medical University of Vienna, 1090 Vienna, Austria

* Corresponding author. E-mail address: christian.kowol@univie.ac.at

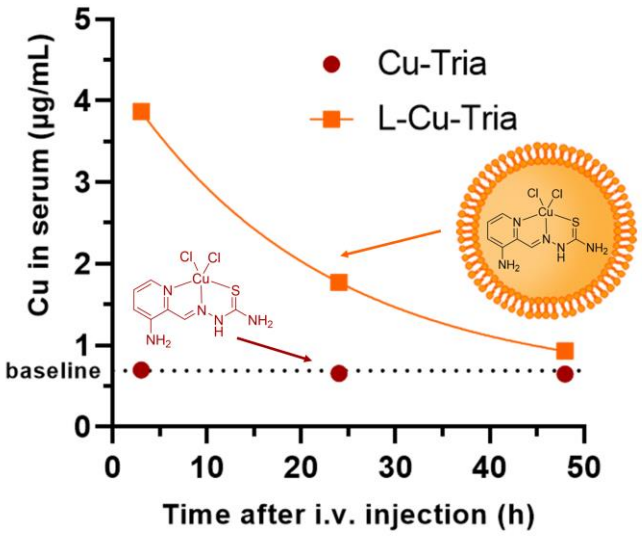

As the first author, I synthesized and characterized the liposomal formulations, evaluated their stability as well as release kinetics and wrote the majority of the manuscript.

Liposomal formulations of anticancer copper(II) thiosemicarbazone complexes

Marlene Mathuber[a], Sonja Hager[b,c], Bernhard K. Keppler[a,c], Petra Heffeter[b,c] and Christian R. Kowol[a,c,*]

[a] Institute of Inorganic Chemistry, Faculty of Chemistry, University of Vienna, Waehringer Straße 42, 1090 Vienna, Austria

[b] Institute of Cancer Research and Comprehensive Cancer Center, Medical University of Vienna, Borschkegasse 8A, 1090 Vienna, Austria

[c] Research Cluster ''Translational Cancer Therapy Research'', University of Vienna and Medical University of Vienna, 1090 Vienna, Austria

E-mail address: christian.kowol@univie.ac.at

Abstract

The a-*N*-heterocyclic thiosemicarbazones Triapine and COTI-2 are currently investigated as anticancer therapeutics in clinical trials. However, especially against solid tumor types, Triapine was widely inactive so far. A likely explanation is the short half-life plasma time and fast metabolism. One promising approach to overcome such drawbacks is the encapsulation of the drug into nanoparticles (passive drug-targeting). In a previous work we showed that it was not possible to stably encapsulate free Triapine into liposomes. Hence, in this manuscript we present the successfully preparation of liposomal formulations of the copper(II) complexes of Triapine and COTI-2. To this end, various drug-loading strategies were examined and the resulting liposomes were characterized regarding their physico-chemical characteristics. Especially for liposomal Cu-Triapine, a decent encapsulation efficacy and a slow drug release behavior could be observed. Subsequent *in vitro* studies in different cell lines showed the expected strongly reduced cytotoxicity and DNA damage induction due to stably encapsulated Cu-Triapine. Also *in vivo* distinctly higher copper plasma levels and a continuous release could be observed for the liposomal formulation compared to free Cu-Triapine. Taken together, the here presented nanoformulation of Cu-Triapine is an important step further to increase the plasma-half-life time and tumor targeting properties of anticancer thiosemicarbazones.

Introduction

α-*N*-Heterocyclic thiosemicarbazones possess a distinctive N,N,S-donor ligand set, which characterizes them as strong metal chelators.[1] Both, the free ligands as well as their metal complexes (e.g. with Cu, Fe, Ru, Ga, etc.) exhibit extraordinary antibacterial, antiviral and antitumor activity.[2] Regarding their mode of action as anticancer drugs, recent studies proposed that thiosemicarbazones can impact on several iron-dependent biological pathways by chelation of both iron(II) and iron(III) ions. Thus, they are generally considered as "iron-interacting" drugs.[3-4] Moreover, another important mechanism (for at least a part) of this compound class is their interaction with cellular copper ions.[5-7] 3-Aminopyridine-2-carboxaldehyde thiosemicarbazone (Triapine; Figure 1) is the most prominent and well-studied representative, with its main target being the iron-dependent enzyme ribonucleotide reductase (RR).[3-4] Triapine has been already evaluated in more than 30 clinical phase I/II trials against different cancer types.[8] Noteworthy, recently Triapine entered a clinical phase III study in combination with cisplatin and radiation therapy against cervical or vaginal cancer patients (study number NCT02466971, clinicaltrials.gov).[9] Although Triapine showed especially promising results against hematological cancers (e.g. advanced leukemia)[10] hardly any activity was found against solid cancers (e.g. renal cell carcinoma

or non-small-cell lung cancer).[11-12] The inefficacy of Triapine most likely results from rapid metabolism/excretion[13] and/or insufficient tumor accumulation.[14-15] More recently also new thiosemicarbazones have been clinically investigated namely di-2-pyridylketone 4-cyclohexyl-4-methyl-3-thiosemicarbazone (DpC) and 4-(pyridine-2-yl)-N-([(8E)-5,6,7,8-tetrahydroquinolin-8-ylidene] amino)piperazine-1-carbothio-amide (COTI-2; Figure 1). DpC entered a phase I clinical trial for patients with advanced solid tumors in 2016 (study number NCT02688101, clinicaltrials.gov).[16] COTI-2 is currently studied in a phase Ib/IIa clinical trial for the treatment of gynecologic malignancies (study number NCT02433626, clinicaltrials.gov).[17] COTI-2 showed nanomolar cytotoxicity against various cancer cells *in vitro* and promising activity *in vivo*.[18] Biological investigations revealed that COTI-2 could restore the tumor suppressor functionality of mutated p53.[19-20]

A general approach to distinctly prolong the plasma half-life time and simultaneously increase the tumor-specificity/accumulation (also resulting in reduced adverse effects), is the encapsulation of therapeutics into nanoparticulate drug formulations such as liposomes.[21] Via the enhanced permeability and retention (EPR) effect nanoformulations can accumulate in tumor tissue (by passive targeting) due to the combination of leaky blood vessels together with a defective lymphatic drainage system.[22-23] Several liposomal formulations of anticancer drugs are already approved, such as Doxil© (liposomal doxorubicin), Depocyt© (liposomal cytarabine) and Marqibo© (liposomal vincristine).[24] Previously, we already synthesized the first liposomal nanoformulations of Triapine. However, a burst release of the drug occurred and no stable encapsulation could be achieved.[21] In this work, we investigated, if the copper(II) complex of Triapine (Cu-Tria; Figure 1) is a suitable derivative for encapsulation into liposomes. The underlying idea is that it is already known that the copper complex of Triapine (Cu-Tria) can act as a "prodrug" with release of the Triapine ligand after reduction.[5, 25] Furthermore, we investigated the encapsulation potential of COTI-2 and its copper(II) complex (Cu-COTI; Figure 1). Drug loading was performed either by the remote loading approach (also used for preparation of e.g. the clinically approved Doxil©[26]) or by adding the drugs directly to the lipid mixture.[27] The obtained liposomal formulations were physico-chemically characterized and subsequently tested for their anticancer activity on different cancer cell lines in comparison to the free ligands. In addition, the impact on methemoglobin formation (a common side effect of Triapine in clinical trials) was examined.[28] Finally, the plasma levels *in vivo* have been compared to prove an enhanced retention time of the liposomal drugs compared to the free ligands.

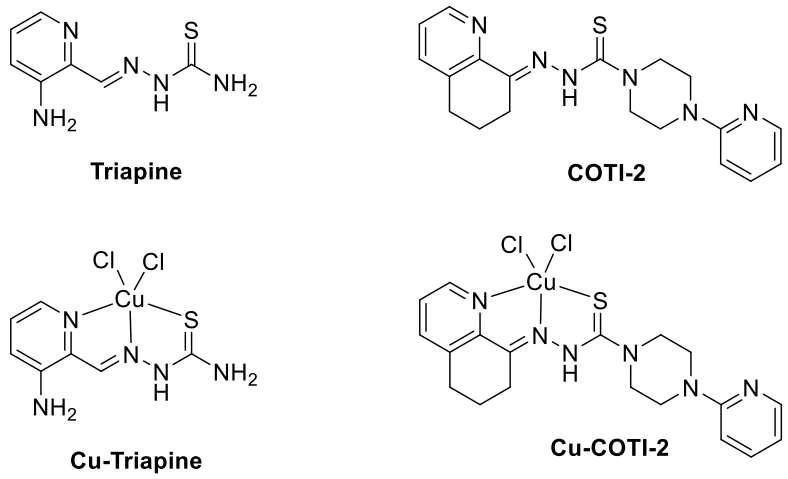

Figure 1: Chemical structures of the clinically investigated thiosemicarbazones Triapine and COTI-2 as well as their copper(II) complexes.

Results and Discussion

Liposome preparation

The liposomal preparation method is crucial for the final properties of the nanoparticles such as particle size and encapsulation efficacy (EE). In this work, two methods were applied: 1) where the respective drug is added to the lipid mixture at the beginning of the preparation (Scheme 1) commonly applied for highly lipophilic (and water-insoluble) compounds.[27] 2) the remote-loading approach which is preferably used for (fairly) water-soluble compounds (Scheme 2).[29] For both methods the liposomal building blocks DSPC/CHOL/DSPE-mPEG (2000) 55:40:5 mol/mol (DSPC = 1,2-distearoyl-sn-glycero-3-phosphocholine; CHOL = cholesterol; DSPE-mPEG 2000 = 1,2-distearoyl-sn-glycero-3-phosphoethanolamine-N-[methoxy(polyethylene glycol)-2000)] were used, a formulation, which is well established in literature.[21, 26, 30]

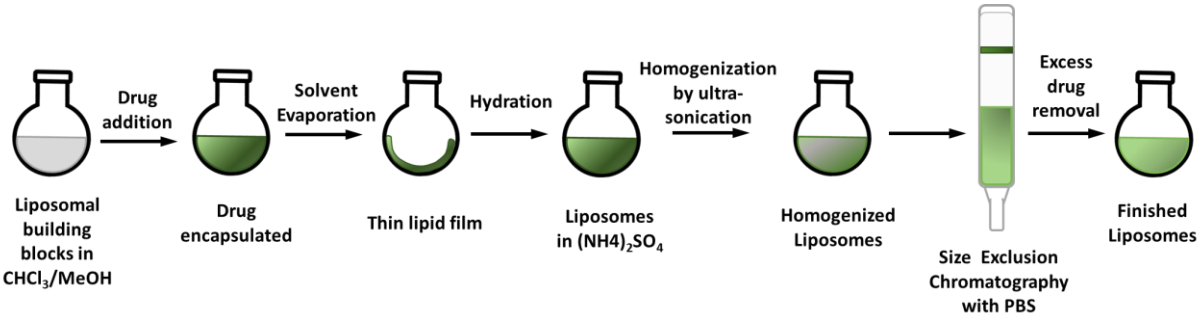

Scheme 1: Preparation of the liposomal formulations by addition of the drug at the beginning of the synthetic procedure.

COTI-2 is highly lipophilic (logP of +2.89)[31] and is therefore suitable for the approach depicted in Scheme 1. Briefly, the building blocks and the drug were dissolved together in a mixture of chloroform and methanol. After refluxing at 65 °C for 1.5 h, the solvents were removed and the thin film of lipid left dried *in vacuo*. This film was then rehydrated in an aqueous solution of choice (e.g. 0.3 M $(NH_4)_2SO_4$) to form the liposomes (so called thin lipid hydration method).[32] To achieve the required size reduction and homogenization, subsequently ultra-sonication with a micro-tip was performed. Non-encapsulated drug was removed by size exclusion chromatography (Sephadex G50) with phosphate-buffered saline (PBS) at pH 7.4. Hardly any free COTI-2 could be observed on the column correlating with a high encapsulation efficacy. However, overnight (despite storage at 4 °C) large amounts of precipitate formed, indicating a burst release of COTI-2. A switch in the rehydrating solvent from $(NH_4)_2SO_4$ to KCl (0.15 M) did not change the encapsulation stability. Therefore, we next tried to encapsulate its copper(II) complex, which was synthesized from a 1:1 mixture of COTI-2 and $CuCl_2$ in methanol[31] bearing a neutral thiosemicarbazone and two chlorido ligands (Figure 1). However, similar results to the free COTI-2 were obtained, a high EE followed by rapid precipitation, which could not even be prevented by storage at –20 °C. Therefore, we decided to change the metal salt by *in situ* complexation of COTI-2 with either $Cu(NO_3)_2$ or $CuSO_4$. Subsequently, the liposomal building blocks were added to the respective reaction solution and synthesis continued as described above. By complexation with $Cu(NO_3)_2$, no stable encapsulation could be obtained either. However, applying the same approach to the complex synthesized with $CuSO_4$, we succeeded in a stable liposomal formulation (named L-Cu-COTI; figure S1), which was further characterized and biologically tested (see below). Unfortunately, only a low EE of 21 ± 3 % (n = 5) was achieved for L-Cu-COTI. No precipitations could be observed up to two weeks when stored at 4°C.

After successfully encapsulation of Cu-COTI, we tried the same approach also for the synthesis of liposomal formulations of Cu-Tria (as mentioned before, it was not possible to stably encapsulate free Triapine into liposomes[21]). To this end, we used the preformed Cu(Triapine)Cl_2 complex as well as the *in situ* complexation of Triapine with $CuSO_4$. Nonetheless, no sufficient encapsulation of the complexes could be observed, probably due to a distinctly higher hydrophilicity compared to Cu-COTI. We also experimented with complexation directly in the liposomes by adding Triapine to a liposomal formulation with an intra-liposomal copper solution. However, this resulted in complex formation mainly outside the liposomal particles. Therefore, we changed the general method to the remote-loading approach (Scheme 2).[29]

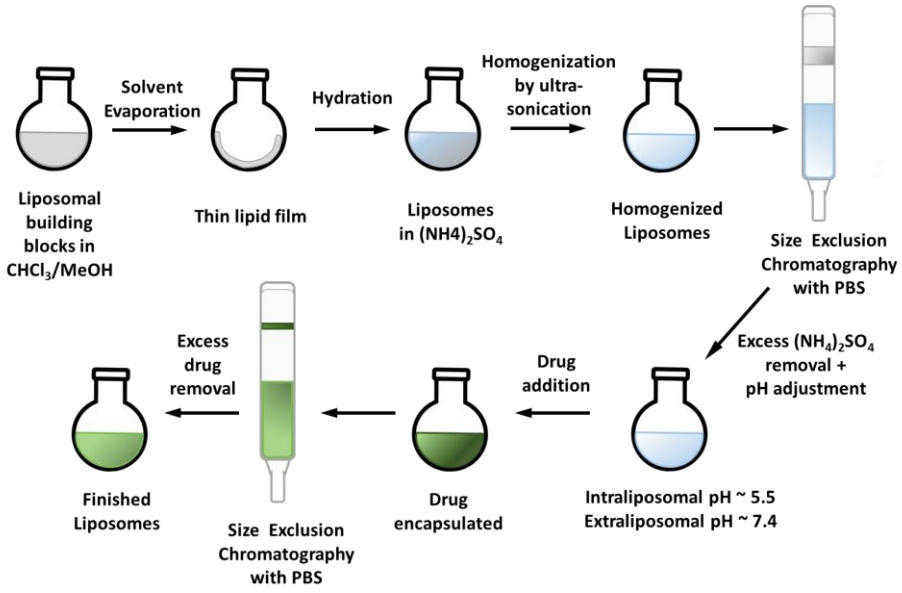

Scheme 2: Preparation of the liposomal formulations by the remote-loading approach.

Via an ammonium sulfate gradient (lower intra-liposomal pH compared to the pH of the extra-liposomal solution) the drug can be "absorbed" into the liposomes.[33] The drugs should have a $logD_{7.0}$ in the range of −2.5 to 2 and a pKa ≤ 11, to be suitable for this technique.[29] For the remote-loading approach, the thin lipid film was prepared as described before,[27] however, without addition of the drug. Rehydration was again performed with a 0.3 M $(NH_4)_2SO_4$ solution and size reduction by ultra-sonication. Afterwards, size exclusion chromatography (Sephadex G50) with phosphate-buffered saline (PBS) at pH 7.4 to remove any access of $(NH_4)_2SO_4$ and create the required pH gradient. Cu-Tria (synthesized from a 1:1 mixture of Triapine and $CuCl_2$[34]) was encapsulated by addition to the freshly prepared liposomes and the resulting solution was stirred for 1 h at 65°C. A second size exclusion column (same conditions as before) removed unloaded drug and generated the liposomal formulation L-Cu-Tria (Figure S1). Indeed, hardly any free drug retained on the column and the formed liposomes were stable. Despite the successful encapsulation, the EE varied over a series of experiments. Since the performance of the remote-loading approach strongly depends on the right pH gradient, we analyzed the pH value after addition of Cu-Tria to the liposomal solution and a pH drop from 7.2 to ~6.9 could be observed. This could be circumvented by using higher volumes of the liposomal solution (3.5 mL), maintaining the essential intra-liposomal (~pH 5.3) versus extra-liposomal (~pH 7.2) pH difference. Additional modifications such as increasing the buffer strength or re-buffering the liposomal solution after addition Cu-Tria did not result in higher EE, even when increasing the amount of drug. Consequently, to reach a higher drug loading, the volume of the solution was reduced to ~1/2 on a rotary evaporator. Afterwards, another size exclusion column was carried out to ensure that Cu-Tria was still completely

encapsulated. With this modification in the protocol, an EE of 64 ± 5 % (n = 15) with high reproducibility and high stability (no precipitate formed after >70 days at 4°C) could be obtained.

Liposome characterization

One of the most important characteristics of liposome is their size and size distribution, which can be examined by dynamic light scattering (DLS). Measurements were performed in PBS (pH 7.4) at room temperature and the average size as well as polydispersity index (PDI) were highly reproducible (in general, a PDI below 0.15 indicates a narrow size distribution).

The L-Cu-COTI-loaded liposomes showed a size of 99 ± 1 nm and a PDI 0.09 ± 0.01 (Figure S2). For the liposomes with encapsulated L-Cu-Tria, a size of 90 ± 2 nm and a PDI of 0.12 ± 0.02 were obtained (Figure 2A). After reduction of the volume, we again checked the size and size distribution of L-Cu-Tria by DLS to confirm that there was no degradation or agglomeration of the liposomes (Figure S3). The average size and PDI of L-Cu-Tria was well reproducible with a size of 93 ±5 nm and a PDI of 0.13 ± 0.02 over the synthesis of 14 batches.

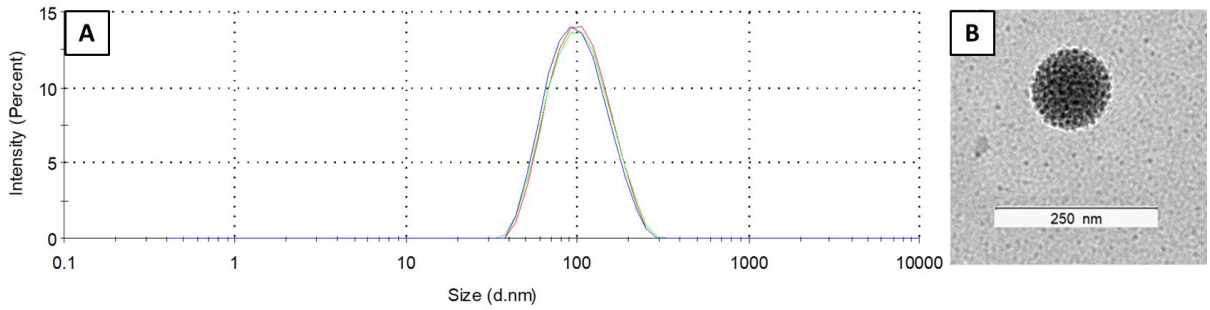

Figure 2: A) Size distribution of L-Cu-Tria (by intensity) measured by DLS (each line represents measurements in triplicate). B) Transmission electron microscopy (TEM) image of L-Cu-Tria; samples were prepared by negative staining with Uranyless.

In addition, the zeta potential (= the electrostatic repulsion of the particle surface) was examined in PBS (pH 7.4), resulting in slightly negative values for L-Cu-Tria at −1.3 ± 0.6 mV and for L-Cu-COTI at −1.5 ± 0.8 mV, which can be expected for PEGylated liposomes.[35-36]

Furthermore, we examined the morphology of L-Cu-Tria by negative stain transmission electron microscopy (TEM) measurements. A representative picture can be seen in Figure 2B (the whole image can be found in Figure S4), which nicely depicts the spherical shape of the liposomes and confirms the size of ~ 100 nm measured by DLS.

Drug release from liposomes

To investigate the drug release of the liposomal formulation L-Cu-Tria, the dialysis diffusion technique was applied. To this end, the liposomal formulations were transferred into a dialysis bag

(molecular weight cut-off 14 kDa), which were then immersed into a PBS solution (pH 7.4) at 37 °C. Over a period of 48 h, samples were removed from this solution and the released drug amount was measured by UV-Vis spectroscopy. In addition, reference measurements with Cu-Tria only were performed under the same conditions. In these experiments a low release of 9 % after 48 h was observed, which indicates stable drug encapsulation and a controlled release behavior over time. In contrast, free Cu-Tria showed the expected fast release out of the dialysis bag of nearly 100 % already after 1 h. This method could not be applied for the evaluation of the liposomal formulation of L-Cu-COTI, since the free Cu-COTI complex possesses hardly any aqueous solubility and immediately precipitates after release. Therefore, the stability of the L-Cu-COTI encapsulation was indirectly evaluated via their biological activity on different cancer cell lines.

Biological investigations

Anticancer activity and uptake of L-Cu-Tria in human cancer cells

It is well known from the literature,[37-39] that a PEGylated surface reduces the attachment of liposomes to the plasma membrane and, consequently, hampers endocytic cellular uptake, e.g., via macrophages. Thus, such nanocarriers are frequently referred to as “stealth liposomes”. Noteworthy, this type of liposomes is also characterized by a distinctly reduced uptake into cancer cells. In fact, their *in vivo* mode of action seems to be based mainly on enhanced accumulation in the malignant tissue by the EPR effect followed by continuous drug release over a longer time.[37, 39] To evaluate whether our thiosemicarbazone nanoformulations act as “stealth liposomes”, ICP-MS measurements of intracellular copper levels of cancer cells treated for 3 h with either the free copper complex or the liposomal formulation were performed. Indeed, at 50 µM significantly lower copper level were detected in L-Cu-Tria-treated cells compared to Cu-Tria (Figure 3), confirming the “stealth nature” of the nanocarriers.

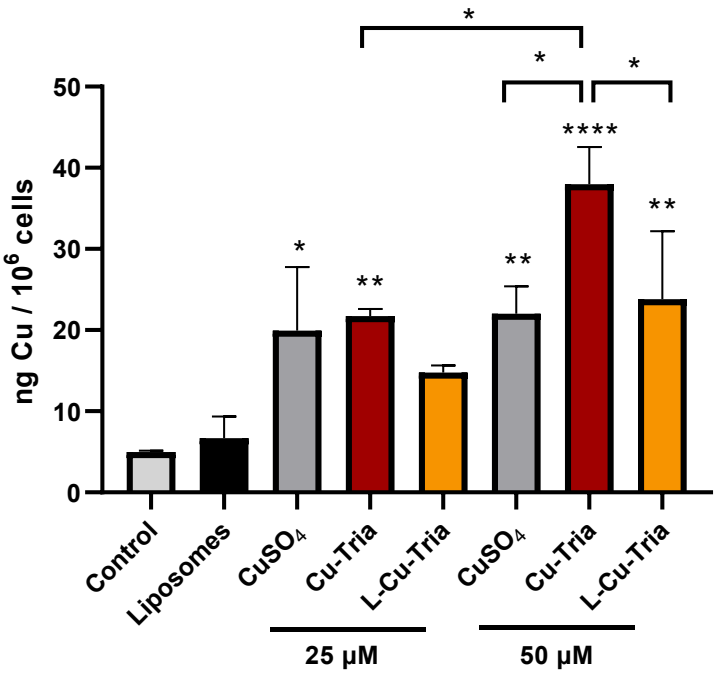

Figure 3: Cellular copper levels of SW480 cells measured by ICP-MS after treatment with empty liposomes, $CuSO_4$, Triapine, Cu-Tria or L-Cu-Tria at the indicated concentrations for 3 h. Values given are the mean ± standard deviation (SD) of triplicates. Significance to control (stars above bars) and to other treatments (stars above brackets between bars) was calculated by one-way ANOVA and Tukey's multiple comparison test (* $p < 0.05$; ** $P < 0.01$; **** $p < 0.0001$).

The biological activity of the liposomal formulations compared to the free complexes was studied by MTT viability assays in SW480 and HCT-116 cells after 48 and 72 h drug treatment (Table 1 and Figure 4A). In comparison, also the activity of the metal-free ligands (Triapine and COTI-2) as well as the unloaded liposomes were analyzed (Table 1 and Figure 4A). In general, unloaded liposomes had no observable effects on cell viability. While for Triapine complexation with copper decreased its anticancer activity in both cell models and time points, for COTI-2, the copper complex displayed similar or even increased activity (Table 1), which is in line with previous publications.[5, 31] L-Cu-Tria displayed an over 7- and 14-fold lower anticancer activity (in HCT-116 and SW480 cells, respectively) compared to free Cu-Tria after 48 h of treatment. This is in agreement with the lower drug uptake (Figure 3), but additionally reveals that the complexes are stably encapsulated into the liposomes, preventing the cells from the cytotoxic activity. After 72 h, the difference decreased especially in SW480 cells to an 8-fold lower anticancer activity, indicating drug release from the liposomes over several days. Further prolongation of the exposure time to 10 days additionally enhanced the activity of L-Cu-Tria (Figure 4B and 4C).

With regards to the liposomal COTI formulation, L-Cu-COTI, cell viability was similar when compared to the treatment with free Cu-COTI (Table 2). This indicates a fast release of the drug from the liposomes and, consequently, a rather low loading stability. Consequently, L-Cu-COTI has not the appropriate drug release profile that allows a stable transport of the intact liposomes into the malignant tissue, where it is released in a tumor-specific manner. Based on these results, no further *in vitro* or *in vivo* experiments were performed with this drug panel.

Table 1: IC_{50} values (mean ± SD) after 48 and 72 h of the metal-free ligands, the free complexes and their liposomal formulations in SW480 and HCT-116 cells.

	SW480 IC_{50} (µM)		**HCT-116 IC_{50} (µM)**	
	48h	**72h**	**48h**	**72h**
Liposomes	> 50	> 50	> 50	> 50
Triapine	0.91 ± 0.08	0.62 ± 0.12	1.40 ± 0.69	0.81 ± 0.07
Cu-Tria	2.99 ± 1.66	0.90 ± 0.14	5.53 ± 0.57	3.38 ± 0.45
L-Cu-Tria	>44	7.29 ± 1.93	>42	26.77 ± 8.10
Ratio L-Cu-Tria/Cu-Tria	>14.7	8.0 ± 1.2**	>7.6	7.9 ± 1.9*
COTI-2	n.d.	0.25 ± 0.09	n.d.	0.06 ± 0.02
Cu-COTI	0.44 ± 0.06	0.16 ± 0.12	0.13 ± 0.05	0.07 ± 0.01
L-Cu-COTI	0.43 ± 0.06	0.12 ± 0.06	0.09 ± 0.03	0.06 ± 0.02
Ratio L-Cu-COTI/Cu-COTI	$0.9 \pm 0.2^{n.s}$	$0.8 \pm 0.2^{n.s}$	$0.7 \pm 0.2^{n.s}$	$0.8 \pm 0.2^{n.s}$

* $p < 0.05$; ** $p < 0.01$; n.s. not significant, calculated by one sample t test against 1.

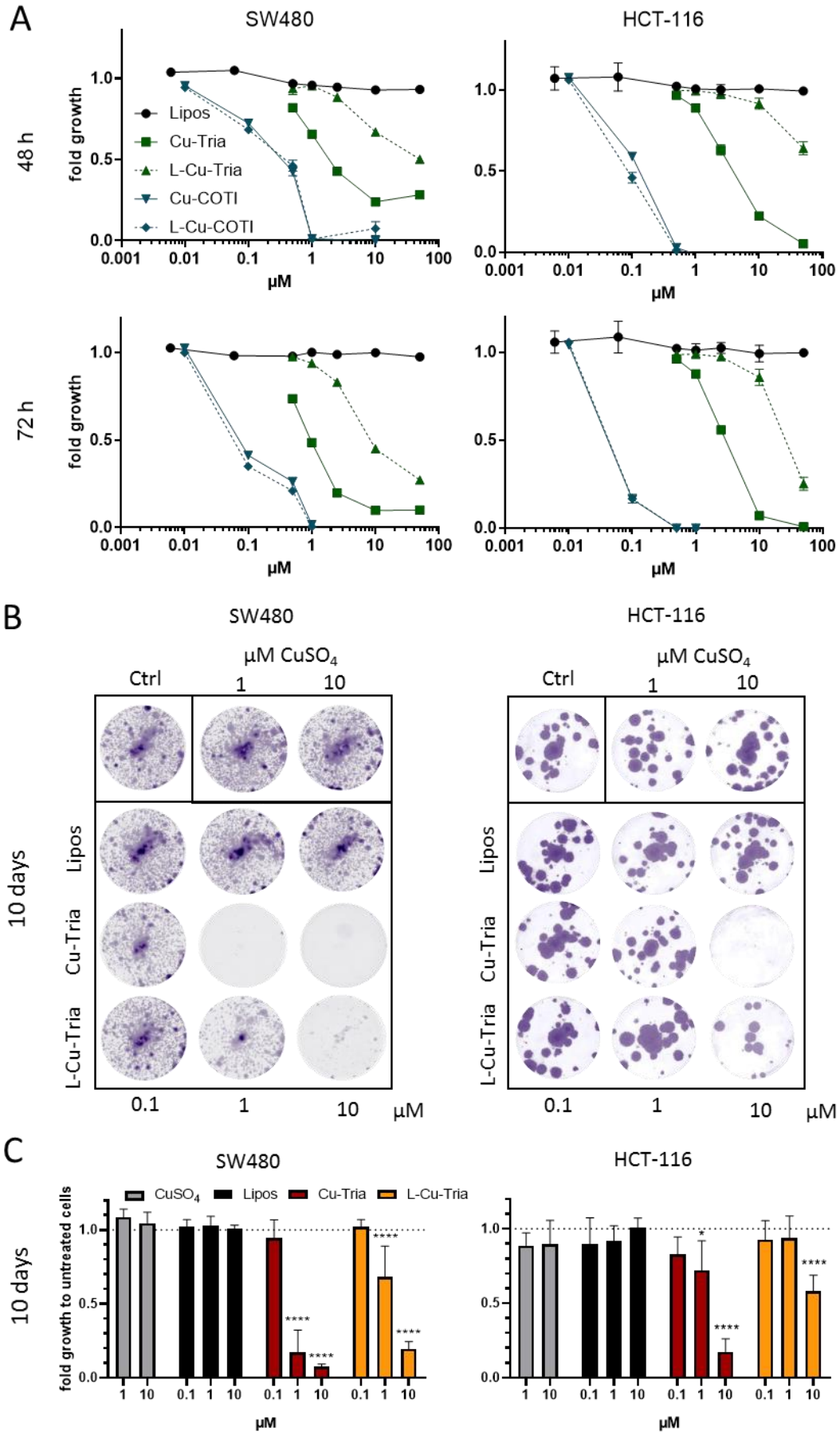
A
SW480
HCT-116
48 h
72 h
fold growth
Lipos
Cu-Tria
L-Cu-Tria
Cu-COTI
L-Cu-COTI
μM
B
SW480
HCT-116
μM CuSO4
Ctrl
1
10
10 days
Lipos
Cu-Tria
L-Cu-Tria
0.1
1
10
μM
C
SW480
HCT-116
10 days
CuSO4
Lipos
Cu-Tria
L-Cu-Tria
fold growth to untreated cells
μM

Figure 4: **A**: Cell viability of SW480 and HCT-116 cells treated with free complexes, drug-free or -loaded liposomes measured by MTT assay after 48 and 72h. Values given in the graph are the mean ± SD of triplicates from one representative experiment out of three. **B:** Cell viability after long-term treatment of SW480 and HCT-116 cells with $CuSO_4$, free complexes, drug-free or -loaded liposomes. After 10 days, cells were fixed, stained with crystal violet. Representative images of stained cells (violet) are shown. Fold growth to untreated cells was calculated from integrated density analyzed with Image J and shown in **C**. Values given are the mean ± SD of duplicates from three experiment. Significance to control was calculated in with two-way ANOVA and Dunnett's multiple comparison test (**** $p < 0.0001$, * $p \leq 0.05$).

The prolonged replication stress induced by the RR inhibition of Triapine was previously reported to result in DNA double-strand breaks, assumingly due to the collapse of DNA replication forks.[40] Accordingly, also when looking at pH2AX (by immunofluorescence staining and Western blot analysis) as a marker for DNA damage and Triapine activity, encapsulation into liposomes prevented DNA damage generated by Triapine-induced RR inhibition in 24 h experiments (Figure 5). $CuSO_4$ and the empty liposomes had either no or only minor effects in these experiments (Figure 5C and Figure S5). However, upon prolonged incubation (7 days), the pH2AX levels became similar (HCT-116 cells) or even higher (SW480 cells) in the L-Cu-Tria samples compared to the free copper complex (Figure 5C). This indicates a slow but continuous release of Cu-Tria from the liposomes.

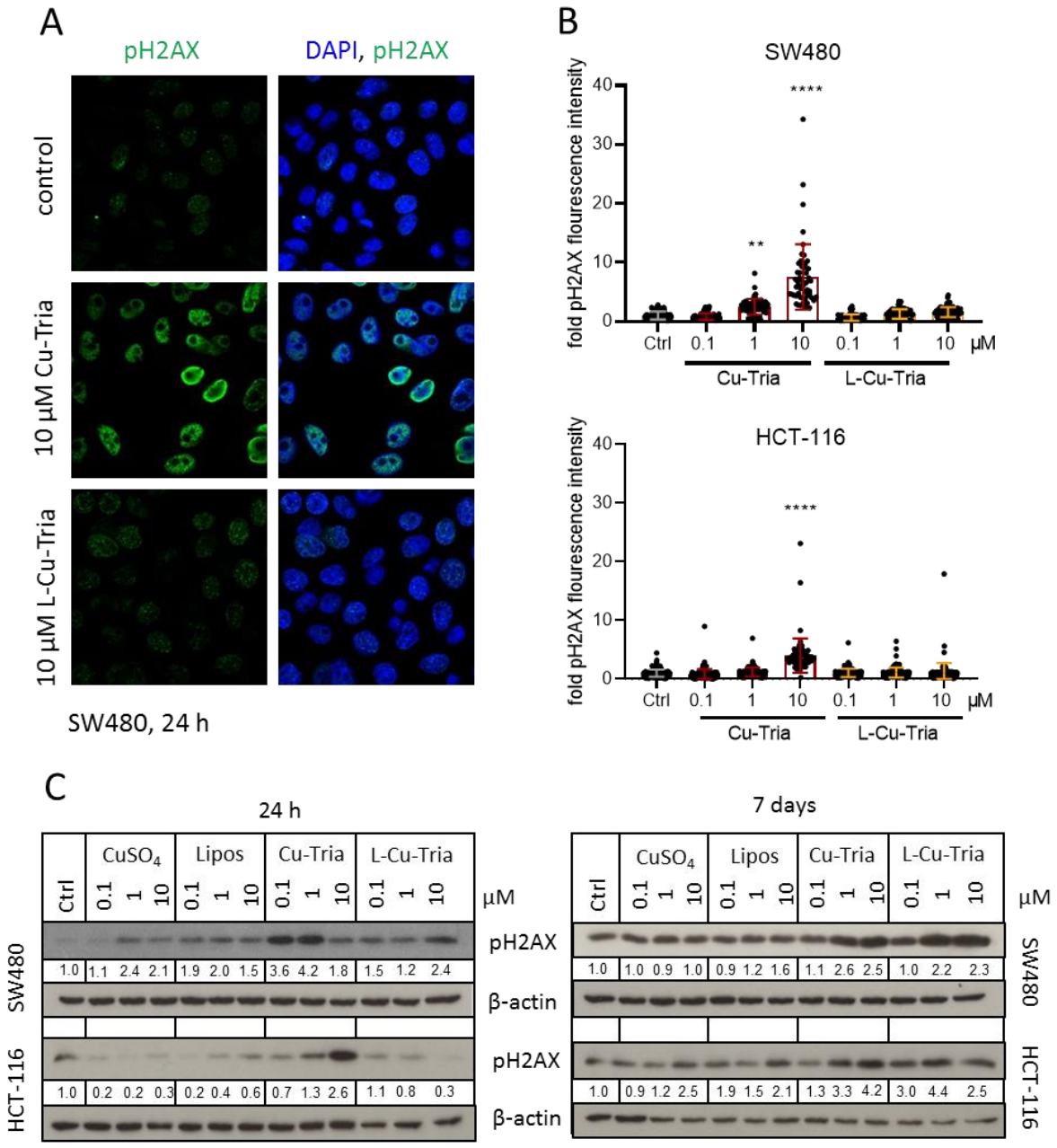

Figure 5: **A**: Representative images of pH2AX immunofluorescence staining (green) in nuclei (DAPI, blue) of SW480 cells treated as indicated **B**: Quantification of immunofluorescence intensities in the nucleus of the DNA damage marker pH2AX in SW480 and HCT-116 cells treated with the indicated drugs and concentrations for 24 h. Values given are the mean fold intensities ± SD per nucleus. Significance to control was calculated in with two-way ANOVA and Dunnett's multiple comparison test (**** $p < 0.0001$, ** $p \leq 0.01$). **C**: Western blot analysis of pH2AX expressed by SW480 and HCT-116 cells treated with indicated drugs and concentrations 24 h and 7 days. β-actin was used as a loading control. Normalized pH2AX values to β-actin and compared to control are given below the bands.

Impact of the liposomal formulation on the serum half-life time *in vivo*

To get first indications on the pharmacokinetics of L-Cu-Tria in comparison to Cu-Tria, copper levels in serum of mice treated with equimolar drug concentrations were determined via ICP-MS. As a first step, the basal serum levels of animals (0.7 µg Cu/mL serum) were assessed 7 days before treatment. Then the mice were treated intravenously (i.v.) with 1.75 mg/kg Cu-Tria either as a free complex or in form of the liposomal formulation and blood was collected by the facial vein after 3, 24 and 48 h (Figure 6). Treatment with Cu-Tria did not result in measurable changes of the serum copper levels at the investigated time points. In contrast, injection of the liposomal Cu-Tria increased serum copper levels significantly. Thus, after 3 h serum copper concentration of around 4 µg/mL were detected, which decreased to 1.7 µg/mL after 24 h and returned to baseline copper levels after 48 h (1 µg/mL). In general, the undetectable copper levels upon treatment with the free complex were not unexpected, as we (and others) previously reported that the serum half-life time of metal-free Triapine is below 1 h in mice based on the relatively fast excretion/metabolism of the drug.[13-14] In addition, there is already a rather high copper content in the serum (due to copper-containing enzymes such ceruloplasmin and albumin),[41-42] which decreases the sensitivity of the measurements. However, considering that the theoretical elevation of copper blood levels by the drugs at time of injection would be ~5 µg/mL, our preliminary data indicate that L-Cu-Tria is characterized by a distinctly prolonged serum half-life (> 10 h). This would be in good agreement with other liposomal drugs such as DOXIL®, which had a reported serum half-life of 13 h in female C57BL/6 mice.[43]

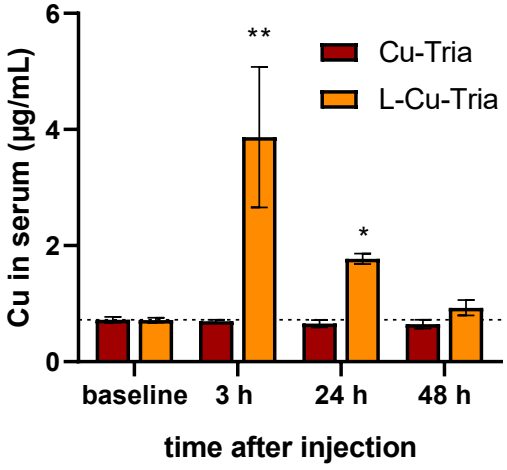

Figure 6: Serum copper levels of female Balb/c mice treated i.v either with 1.75 mg/kg Cu-Tria or L-Cu-Tria and blood drawn via the facial vein at the indicated time points. Samples for baseline were collected from the same mice 7 days prior drug treatment. Values given are mean ± standard error of the mean (SEM) and significance was calculated by Kruskal-Wallis test against the baseline with false discovery rate by Benjamini and Hochberg (* $p < 0.05$; ** $p < 0.01$).

Investigation of methemoglobin formation

The occurrence of methemoglobinemia, where oxyhemoglobin (HbO_2) is oxidized to methemoglobin (metHb), is a side effect frequently observed in clinical trials of Triapine.[44] It is caused by iron(III) Triapine complexes, which are formed in the bloodstream and, subsequently, can oxidize hemoglobin.[45] We investigated, therefore, whether L-Cu-Tria in the presence of iron(III) leads to the formation of metHb. To this end, L-Cu-Tria and Triapine, which was included as positive control, were incubated with $Fe(NO_3)_3$ in a 2:1 ration for 10 min at r.t. The subsequent reaction with HbO_2 was monitored by UV-Vis spectroscopy[46-47]. For Triapine the typical decrease in the absorption of the HbO_2 bands (at 539 and 577 nm) and the hypsochromic shift could be observed (Figure 7A), which indicates the formation of metHb and is comparable with the results of our previous work.[21] For L-Cu-Tria no changes in the UV-Vis spectra were measured over time, suggesting that no redox-active iron(III) complex was formed, in agreement with the high stability constant of Cu-Tria[48] (also in case of Cu-Tria alone no redox reaction occurred, data not shown). Therefore, these data demonstrates the stable complexation of Triapine in form of Cu-Tria preventing the generation of methemoglobinemia.

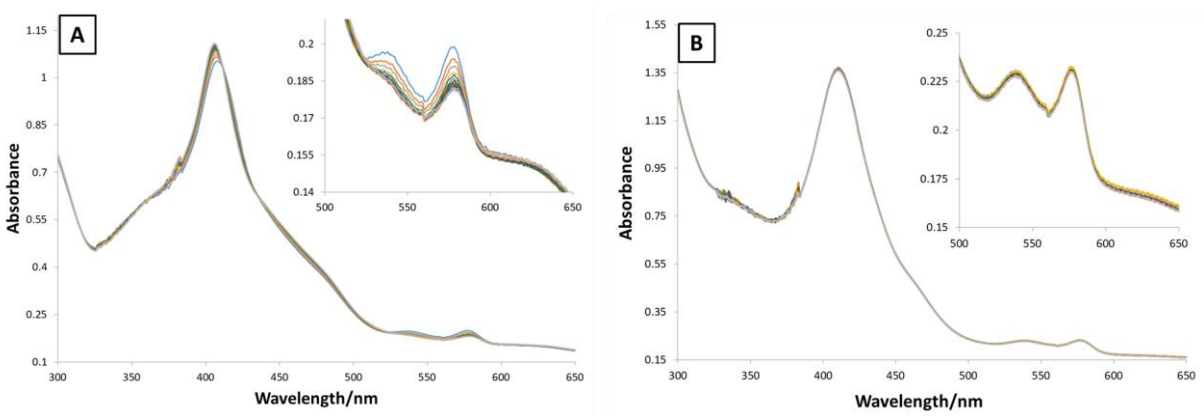

Figure 7: Time resolved UV-Vis spectroscopy of the reaction between human HbO_2 and A) Triapine and B) L-Cu-Tria in the presence of iron(III) during 21 min (inset zoom of the range 500–650 nm).

Conclusions

α-*N*-Heterocyclic thiosemicarbazones are promising anticancer drugs and various compounds have already be studied in clinical trials. Nevertheless, the most prominent representative Triapine did not exhibit distinct antitumor activity against most solid tumor types. The underlying reasons are most probably rapid metabolization and a short plasma half-life time. To increase the retention of a drug in the body and simultaneously enhance its concentration at the tumor site, the passive drug targeting approach represents a promising and frequently used strategy. The drug is encapsulated

into nanoparticles, which then accumulate in the tumor tissue utilizing the EPR effect. This concept is already successfully applied in the clinics e.g., for doxorubicin, daunorubicin, vincristine and irinotecan.[24] For the development of nanocarriers, several parameters such as size, zeta potential, EE and reproducibility have to be considered.[49] Most importantly, the drug release profile, which is crucial for the therapeutic effectiveness, has to be balanced: On the one hand, the drug is inactivated by encapsulation into the nanoformulation, on the other hand, a too rapid release leads to loss of selectivity. We demonstrated in a previous study that free Triapine is not suitable for this method, as only a fast drug release from the nanoformulations could be observed.[21] Therefore, in this work we chose the copper(II) complex (Cu-Tria) as derivative for encapsulation, since it can be considered as prodrug, releasing Triapine after reduction to copper(I).[5, 25] Additionally, the clinically studied third-generation thiosemicarbazone COTI-2 and its copper(II) complex (Cu-COTI) were investigated. Owing to the lipophilic nature of COTI-2, the most suitable technique for encapsulation was the addition to the thin lipid film at the beginning of the synthesis. As for the more water-soluble Cu-Tria, the remote-loading approach (used for the preparation of Doxil©) was applied. *In vitro* tests confirmed the stable encapsulation and slow drug release behavior of L-Cu-Tria, in line with DNA damage experiments and drug release studies. However, for the liposomal formulations of COTI-2 as well as of Cu-COTI, only a fast burst release could be observed. This clearly shows that the exact chemical structure strongly impacts on the ability to generate stable liposomal formulations, when comparing Cu-Triapine vs. Cu-COTI but also Cu-Triapine vs. Triapine. Consequently, *in vivo* test were only performed with L-Cu-Tria and indeed a distinctly prolonged half-life time compared to Cu-Tria was achieved. Furthermore, the formation of methemoglobin, which is a side effect from Triapine, could be completely prevented in the presence of L-Cu-Tria. Taken together, we could show that liposomal formulations are a promising method to increase the plasma half-life time of Cu-Triapine, which is an important step further to generate successful thiosemicarbazone nanopreparations.

Materials and methods

Chemicals

All solvents and reagents were purchased from commercial suppliers. They were, unless stated otherwise, of analytical grade and used without further purification. 1,2-Distearoyl-sn-glycero-3-phosphocholine (DSPC), 1,2-distearoyl-sn-glycero-3-phosphoethanolamine-N-[methoxy(polyethylene glycol)-2000] (ammonium salt) (DSPE-mPEG(2000)) and cholesterol were obtained from Avanti Polar Lipids Inc. (Alabaster, AL). Human hemoglobin was acquired from Sigma Aldrich. Milli-Q water was obtained from a Millipore Advantage A10 185 UV Ultrapure Water

System (18.2 MΩ; Molsheim, France). Cu-Tria was synthesized according Kowol *et al*,[34] COTI-2 and Cu-COTI following procedures from Bormio Nunes *et al*.[31]

Preparation of drug-loaded liposomes

Liposomal formulation of Cu-COTI (L-Cu-COTI)

The liposomes of Cu-COTI were prepared by *in situ* complexation of COTI-2 (2 mg) with $CuSO_4 \cdot 5\,H_2O$ (1.36 mg) in 1 mL of $CHCl_3$/MeOH (4:1, v/v). Afterwards, 20 mg DSPC, 6.5 mg DSPE-mPEG(2000), 7.2 mg cholesterol were dissolved in 4 mL of a mixture of $CHCl_3$/MeOH (4:1, v/v), transferred to the complex solution and stirred for 1.5 h at 65 °C. The solvent was then carefully removed under reduced pressure to form a thin, yellowish film, which was dried *in vacuo* overnight. Afterwards, the film was rehydrated with 2 mL of a 0.3 M $(NH_4)_2SO_4$ solution and 15 glass beads were added. The mixture was rotated on a rotary evaporator for 1.5 h at 65 °C. Subsequently, the suspension was decanted and refilled to 2 mL with 0.3 M $(NH_4)_2SO_4$ solution. To homogenize the suspension by ultra-sonication, the Bandelin ultrasonic homogenizer HD 3100 with a maximum amplitude of 20% for 3 min, 5 min, 7 min, 5 min and 12 min (each with few seconds break) was used. Non-encapsulated drug was removed by size exclusion chromatography (Sephadex G50) using PBS (0.01 M, pH 7.4) as eluent, resulting in L-Cu-COTI. The liposomes were stored at 4 °C until further usage.

Liposomal formulation of Cu-Tria (L-Cu-Tria)

Liposomal formulations of Cu-Tria were prepared using the remote-loading approach.[29] 20 mg DSPC, 6.5 mg DSPE-mPEG(2000) and 7.2 mg cholesterol were dissolved in 5 mL $CHCl_3$/MeOH (4:1, v/v) and the resulting solution was stirred for 1.5 h at 65 °C. The solvent was carefully removed under reduced pressure to form a thin, opaque film, which was dried *in vacuo* overnight. Afterwards, the film was rehydrated with 2 mL of a 0.3 M $(NH_4)_2SO_4$ solution and 15 glass beads were added. The mixture was rotated on a rotary evaporator for 1.5 h at 65 °C. Subsequently, the suspension was decanted and refilled to 2 mL with 0.3 M $(NH_4)_2SO_4$ solution. To homogenize the suspension by ultra-sonication, the Bandelin ultrasonic homogenizer HD 3100 with a maximum amplitude of 20% for 3 min, 5 min, 7 min, 5 min and 12 min (each with few seconds break) was used. Excess ammonium sulfate was removed by size exclusion chromatography (Sephadex G50) using PBS (0.01 M, pH 7.4) as eluent. Cu-Tria (1.2 mg) was doused with the purified liposomes (around 3.5 mL) and stirred for further 1.5 h at 65 °C. To remove non-encapsulated drug, another size exclusion column was performed (same conditions as before). About half of the aqueous solution was evaporated at 40 °C on a rotary evaporator to increase the concentration. The liposomes were stored at 4 °C until further usage.

Particles size and surface charge (zeta potential)

The PDI and particle sizes were determined by DLS with a Malvern ZetaSizer Nano ZS (Malvern Instruments Ltd., Malvern, UK) equipped with a 4 mW He-Ne, 632.8 nm laser beam at 25 °C and at a scattering angle of 173°. Prior to the particle size measurement, the liposomes and nanoparticles were diluted (1 : 9 v/v) with PBS and measured in disposable cuvettes (UV-cuvette micro, Brand GmbH + Co KG, Germany). The zeta-potential was determined in disposable folded capillary cells using the same instrument.

TEM measurements

The liposomes were analyzed by negative stain electron microscopy using a Carl Zeiss Libra 120 electron microscope. The liposomal formulation was diluted (1:10 v/v, with Millipore water), 10 µL of the resulting solution were pipetted on a carbon-coated G240-mesh Nylon grid (Agar Scientific) and the grid was allowed to dry overnight. At the next day, the grid was placed on a drop of Uranyless (seated on a piece of parafilm tape) for 1 min. Excess solvent was removed with a filter paper and the grid was dried for 10 min. The grid was then again placed on a fresh drop of Uranyless and after 1 min the excess was drawn off with a filter paper. After drying for 3 h, the grid was analyzed with the electron microscope.

Determination of encapsulated drug amount

Aliquots of 50 µL of the liposome probes were dried under reduced pressure by rotary evaporation and then *in vacuo* for 10 min. The resulting film was dissolved in methanol and sonicated in an ultrasonic bath for 2 min. The amount of encapsulated drug was determined by UV-Vis spectroscopy on an Agilent 8453 UV-Vis spectrophotometer (Agilent Technologies, Germany) using 10 mm path length quartz cuvettes. To examine the concentration of the samples a calibration curve of the drug was measured.

Drug release studies

For examination of the drug release, the dialysis bag diffusion technique was used. Freshly prepared L-Cu-Tria was filled into a dialysis membrane (average flat width of 10 mm and molecular weight cut off of 14 kDa; Sigma Aldrich, Austria). The membrane was sealed and immersed into 25 mL PBS (pH = 7.4) at 37 ± 1 °C with continuous stirring at 200 rpm. To examine the amount of drug that diffused through the dialysis membrane, 1 mL-samples were withdrawn from the solution at fixed time intervals (0 min, 1 h, 3 h, 6 h, 24 h and 48 h) and replaced by 1 mL of fresh PBS. The drug concentration was measured by UV-Vis spectroscopy on an Agilent 8453 UV-Vis spectrophotometer (Agilent Technologies, Germany). As a positive control, a stock solution of the free drug Cu-Tria in water was diluted with PBS to the concentration of the drug in the liposomes. This solution was

also placed into the dialysis bag and the drug content in the outer compartment was determined as described above. All experiments were performed in duplicates.

Biological investigations

Cell culture

The following human cell lines were used: the colon carcinoma cell lines SW480 and HCT-116 (both obtained from American Type Culture Collection, Manassas, VA). SW480 cells were cultured in minimal essential medium and HCT-116 cell lines in McCoy's 5a medium supplemented with 2 mM glutamine (from Sigma-Aldrich, MO, US) containing 10% fetal bovine serum and kept at 37°C and 5 % CO_2.

Cellular copper levels

Cells were seeded ($3x10^5$/well) in 1 mL in 6-well plates and left to recover for 24 h at 37 °C and 5 % CO_2. The liposome-free compounds were dissolved in PBS (1 mM) and then further diluted in growth medium. Drug dilutions were added in 1 mL/well for 3 h in triplicates. Then, cells were washed twice with PBS, left to dry overnight and lysed with 500 µl/well HNO_3. After one-hour incubation, 400 µl of each well were removed and diluted with 7.6 mL H_2O for copper measurement with ICP-MS (see below).

Viability assay

Cells were seeded ($2x10^4$ cells/well) in 100 µl/well in 96-well plates and allowed to attach for 24 h at 37 °C and 5 % CO_2. The liposome-free compounds were diluted in PBS (1 mM) and then further diluted in growth medium. Drug dilutions were added in 100 µl/well, with the final concentrations depending on the compound and the cell line. After drug treatment, cells were incubated for 48 h or 72 h at 37°C and 5 % CO_2. The proportion of viable cells was determined by 3-(4,5-dimethylthiazole-2-yl)-2,5-diphenyltetrazolium assay (MTT) following the manufacturer's recommendations (EZ4U, Biomedica, Vienna, Austria). Anticancer activity was expressed as IC_{50} values (drug concentrations inducing 50% reduction of cell survival in comparison to the control) calculated from full dose-response curves using GraphPad Prism software.

Clonogenic assay

For long-term drug exposure, 200 cells/well were seeded in 24-well plates and allowed to recover for 24 h. Then, the cells were exposed to the compounds for 10 days. The cells were fixed with methanol (–20°C, 20 min) and after washing with PBS stained with crystal violet (1 h, 100µg/ml, Sigma-Aldrich, Austria). The washed and dried plates were then measured for fluorescence (with

633 nm excitation and 610/30 nm BP emission filter) with the imager Typhoon Trio (GE Healthcare Life Sciences). The sum of fluorescence intensities per well (integrated density) was measured with ImageJ and, after background subtraction, normalized to untreated cells.

Immunofluorescence

Cells ($8x10^4$/mL) were seeded in 50 µL on 10-well PTFE printed spot slides (Science Services, Austria). After 24 h recovery, cells were treated with indicated drug concentrations and fixed with 4% paraformaldehyde for 10 min at room temperature and (after washing with PBS) blocked and permeabilized with a solution containing 5% bovine serum albumin (BSA), 0.3% Triton-X-100 in PBS for 1 h. The primary antibody pH2A.X (#2577, Cell Signaling Technology, Austria) was added 1:200 in a solution contacting 1% BSA and 0.3% Triton-X-100 in PBS overnight at 4°C. After washing with PBS, the cells were incubated with anti-rabbit secondary antibody conjugated to AlexaFluor488 (#A-11008, Thermo Fisher, 1:500 in 1% BSA and 0.3% Triton-X-100 in PBS) for 1 h. The cells were again washed and counterstained with 4',6-diamidine-2'-phenylindole dihydrochloride (DAPI; 1 µg/mL) in PBS for 10 min. The dyes were removed, and the cells mounted in Vectashield mounting medium (Vector Laboratories, CA, USA) with a coverslip. Images were taken with a Zeiss LSM 700 Olympus (Carl Zeiss AG, Oberkochen, Germany) confocal microscope and pH2A.X fluorescence intensities per nucleus were measured using ImageJ.

Protein isolation and Western blot

Cells were seeded $2x10^5$/well or $2x10^4$/well in 6-well plates. After 24 h recovery, cells were treated for 24 h or 7 days, respectively, with the indicated concentrations of the compounds. Cells were scratched into the medium and after washing with PBS, lysed in lysis buffer (50 mM Tris, 300 mM NaCl, 0.5% Triton-X-100) containing a phosphorylation inhibitor cocktail (Complete and Phospho-Stop, Roche, Austria) for 45 min on ice. After 5 min ultrasound bath, lysates were centrifuged for 15 min at 14 000 rpm at 4°C. Protein concentration of supernatant was quantified using Micro BCA Protein Assay (Pierce, Thermo Fisher, Austria). 15 µg of proteins were separated by SDS-PAGE (10 % gels), and transferred onto a polyvinylidene difluoride membrane for Western blotting as described previously.[50] The following primary antibodies were used: anti-pH2AX monoclonal rabbit (Cell Signaling, #2577) and anti-β-actin monoclonal mouse (Sigma Aldrich, #A5441). Secondary, horseradish peroxidase-labeled antibodies were anti-rabbit monoclonal mouse (sc-2357, Santa Cruz Biotechnology, Austria) and anti-mouse polyclonal goat (Merck, #A0168) were used in working dilutions of 1:10 000.

Animals

Eight-to twelve-week-old BALB/c mice were purchased from Janvier (France). The animals were kept in a pathogen-free environment and every procedure was done in a laminar airflow cabinet. Experiments were done according to the regulations of the Ethics Committee for the Care and Use of Laboratory Animals at the Medical University Vienna (proposal number BMWF-66.009/0157-V/3b/2019), the U.S. Public Health Service Policy on Human Care and Use of Laboratory Animals as well as the United Kingdom Coordinating Committee on Cancer Prevention Research's Guidelines for the Welfare of Animals in Experimental Neoplasia. To ensure animal welfare throughout the experiment, the body weight of the mice was assessed once a day. At weight loss exceeding 10 % (in less than two days), animals were sacrificed by cervical dislocation.

Pharmacokinetic experiments

In order to reduce the number of used animals (following the "3R" guidelines), rotation design was used for this experiments. In more detail, as a first step, blood was sampled from six untreated female BALB/c mice via the facial vein. Seven days later, the animals received their first i.v. treatment (three animals per group) with either 1.75 mg/kg Cu-Tria (in 5 % glucose in physiological saline) or L-Cu-Tria (in PBS, 100 µl/ 20 g mouse). In each treatment group, blood was again drawn via facial vein after 3, 24 or 48 h from one mouse per group. After a wash-out/recovery period of seven days, the process was repeated different collection time points for each mouse. This was then performed a third time. Thus, of each mouse 3, 24 and 48 h time point was collected in total. After blood coagulation, serum was separated from the blood pellet by two centrifugation steps (3 000 g, 10 min) and stored at –20°C for ICP-MS analysis.

ICP-MS measurements

The copper levels in cell lysates and serum were determined by ICP-MS. The cell lysates were prepared as described above (see Materials and Methods: Cellular copper levels). Preparation of the serum samples was performed via digestion, parameters are stated below (Table2):

Table 2: Experimental parameters of sample preparation for the ICP-MS measurements

Sample Preparation	
Type	Open vessel graphite digestion
Solution	2 mL HNO_3 (20%) + 0.1 mL H_2O_2 (30%)
Vial material	PFA
Vial size	25 mL
Weighing	approx. 10–30 mg

For measurements the ICP-MS Agilent 7800® (Agilent Technologies, Tokyo, Japan) was equipped with an Agilent SPS 4 autosampler (Agilent Technologies, Tokyo, Japan) and a MicroMist nebulizer at a sample uptake rate of approx. 0.2 mL/min. The Agilent MassHunter® software package (Workstation Software, version C.01.04, Build 544.17, Patch 3, 2018) was used for data processing. The experimental parameters for ICP-MS are summarized in the Table 3 below. The instrument was tuned on a daily basis to achieve maximum sensitivity. The instrumental LOQ (LOQ = blank average + 10*stdev) was calculated by measuring a clean blank 5 times. All Cu-values were blank corrected.

Table 3: Experimental parameters of the ICP-MS measurements

	ICP-MS Agilent 7800
RF power [W]	1550
Cone material	Nickel
Carrier gas [L/min]	1.07
Plasma gas [L/min]	15
Monitored isotopes	^{115}In, ^{63}Cu, ^{65}Cu
Mode	no gas, O_2
Integration time [s]	0.1
Number of replicates	10
Number of sweeps	100

Investigation of methemoglobin formation

Fresh solutions of HbO_2 were prepared by dissolving human hemoglobin (20 mg) in 1 mL of PBS and reducing the metalloprotein by incubation with an excess of sodium dithionite (~4 mg) for 1.5 h at room temperature. Afterwards, the resulting solution was purified by gel filtration (Sephadex G-25 and PBS as eluent). The final concentration of HbO_2 was determined by UV-Vis spectroscopy from the extinction coefficient of the protein at 542 nm.[47] Stock solutions of Cu-Tria (5 mM) and $Fe(NO_3)_3$ (50 mM) were prepared in MeOH. L-Cu-Tria and Cu-Tria were then incubated with $Fe(NO_3)_3$ in a 2 : 1 molar ratio for 10 min at room temperature and diluted with PBS. For the kinetic studies, the incubated solutions (final concentration of compounds: 50 µM) and HbO_2 (final concentration: 5 µM total heme) in PBS were measured over a period of 22 min using a Perkin Elmer UV-Vis spectrometer Lambda 35 over 15 cycles (300–650 nm; scan-speed 480 nm/min). As negative control, all compounds were additionally measured without prior incubation with $Fe(NO_3)_3$ (final concentration of compounds: 50 µM and HbO_2: 5 µM total heme) and no changes in the UV-Vis spectra could be observed (data not shown). For quantification the concentrations of HbO_2 and metHb were determined at 577 nm and 630 nm after subtraction of the controls (HbO_2 or the compound alone at 630 nm) from the extinction coefficient.[47]

Acknowledgements

We are thankful to Sophie Neumayer, Tatjana Schafarik and Martin Schaier for ICP-MS measurements. We also thank Mag. Gerhard Zeitler for devoted animal care. Dr. Norbert Cyran of the "Core Facility of Cell Imaging and Ultrastructure Research" of the University of Vienna for introduction and help regarding the TEM measurements. Sonja Hager is a recipient of a DOC fellowship of the Austrian Academy of Sciences. We gratefully acknowledge the Austrian Science Fund (FWF) grant P31923 (to CK) for financial support.

References

1. Lobana, T. S.; Sharma, R.; Bawa, G.; Khanna, S., Bonding and structure trends of thiosemicarbazone derivatives of metals—an overview. *Coordination Chemistry Reviews* **2009,** *253* (7-8), 977-1055.
2. Beraldo, H.; Gambino, D., The wide pharmacological versatility of semicarbazones, thiosemicarba-zones and their metal complexes. *Mini reviews in medicinal chemistry* **2004,** *4* (1), 31.
3. Yu, Y.; Kalinowski, D. S.; Kovacevic, Z.; Siafakas, A. R.; Jansson, P. J.; Stefani, C.; Lovejoy, D. B.; Sharpe, P. C.; Bernhardt, P. V.; Richardson, D. R., Thiosemicarbazones from the old to new: iron chelators that are more than just ribonucleotide reductase inhibitors. *Journal of medicinal chemistry* **2009,** *52* (17), 5271-5294.
4. Heffeter, P.; Pape, V. F.; Enyedy, É. A.; Keppler, B. K.; Szakacs, G.; Kowol, C. R., Anticancer thiosemicarbazones: chemical properties, interaction with iron metabolism, and resistance development. *Antioxidants & redox signaling* **2019,** *30* (8), 1062-1082.
5. Hager, S.; Pape, V. F.; Pósa, V.; Montsch, B.; Uhlik, L.; Szakács, G.; Tóth, S.; Jabronka, N.; Keppler, B. K.; Kowol, C. R., High copper complex stability and slow reduction kinetics as key parameters for improved activity, paraptosis induction and impact on drug-resistant cells of anticancer thiosemicarbazones. *Antioxidants and Redox Signaling* **2020,** (ja).
6. Santini, C.; Pellei, M.; Gandin, V.; Porchia, M.; Tisato, F.; Marzano, C., Advances in copper complexes as anticancer agents. *Chemical reviews* **2014,** *114* (1), 815-862.
7. Lovejoy, D. B.; Jansson, P. J.; Brunk, U. T.; Wong, J.; Ponka, P.; Richardson, D. R., Antitumor activity of metal-chelating compound Dp44mT is mediated by formation of a redox-active copper complex that accumulates in lysosomes. *Cancer research* **2011,** *71* (17), 5871-5880.
8. Miah, A.; Harrington, K.; Nutting, C., Triapine in clinical practice. *The European Journal of Clinical & Medical Oncology* **2010,** *2* (1), 1.
9. Kunos, C. A.; Ivy, S. P., Triapine radiochemotherapy in advanced stage cervical cancer. *Frontiers in oncology* **2018,** *8*, 149.
10. Karp, J. E.; Giles, F. J.; Gojo, I.; Morris, L.; Greer, J.; Johnson, B.; Thein, M.; Sznol, M.; Low, J., A Phase I study of the novel ribonucleotide reductase inhibitor 3-aminopyridine-2-carboxaldehyde thiosemicarbazone (3-AP, Triapine®) in combination with the nucleoside analog fludarabine for patients with refractory acute leukemias and aggressive myeloproliferative disorders. *Leukemia research* **2008,** *32* (1), 71-77.
11. Ma, B.; Goh, B. C.; Tan, E. H.; Lam, K. C.; Soo, R.; Leong, S. S.; Wang, L. Z.; Mo, F.; Chan, A. T.; Zee, B., A multicenter phase II trial of 3-aminopyridine-2-carboxaldehyde thiosemicarbazone (3-AP, Triapine®) and gemcitabine in advanced non-small-cell lung cancer with pharmacokinetic evaluation using peripheral blood mononuclear cells. *Investigational new drugs* **2008,** *26* (2), 169-173.
12. Knox, J. J.; Hotte, S. J.; Kollmannsberger, C.; Winquist, E.; Fisher, B.; Eisenhauer, E. A., Phase II study of Triapine® in patients with metastatic renal cell carcinoma: a trial of the National

Cancer Institute of Canada Clinical Trials Group (NCIC IND. 161). *Investigational new drugs* **2007,** *25* (5), 471-477.
13. Pelivan, K.; Frensemeier, L.; Karst, U.; Koellensperger, G.; Bielec, B.; Hager, S.; Heffeter, P.; Keppler, B. K.; Kowol, C. R., Understanding the metabolism of the anticancer drug triapine: electrochemical oxidation, microsomal incubation and in vivo analysis using LC-HRMS. *Analyst* **2017,** *142* (17), 3165-3176.
14. Pelivan, K.; Miklos, W.; van Schoonhoven, S.; Koellensperger, G.; Gille, L.; Berger, W.; Heffeter, P.; Kowol, C. R.; Keppler, B. K., Differences in protein binding and excretion of Triapine and its Fe (III) complex. *Journal of inorganic biochemistry* **2016,** *160*, 61-69.
15. Feun, L.; Modiano, M.; Lee, K.; Mao, J.; Marini, A.; Savaraj, N.; Plezia, P.; Almassian, B.; Colacino, E.; Fischer, J., Phase I and pharmacokinetic study of 3-aminopyridine-2-carboxaldehyde thiosemicarbazone (3-AP) using a single intravenous dose schedule. *Cancer chemotherapy and pharmacology* **2002,** *50* (3), 223-229.
16. Guo, Z.-L.; Richardson, D. R.; Kalinowski, D. S.; Kovacevic, Z.; Tan-Un, K. C.; Chan, G. C.-F., The novel thiosemicarbazone, di-2-pyridylketone 4-cyclohexyl-4-methyl-3-thiosemicarbazone (DpC), inhibits neuroblastoma growth in vitro and in vivo via multiple mechanisms. *Journal of hematology & oncology* **2016,** *9* (1), 1-16.
17. Salim, K. Y.; Maleki Vareki, S.; Danter, W. R.; Koropatnick, J., COTI-2, a new anticancer drug currently under clinical investigation, targets mutant p53 and negatively modulates the PI3K/AKT/mTOR pathway. *European Journal of Cancer* **2016,** *69*, S19.
18. Salim, K. Y.; Vareki, S. M.; Danter, W. R.; Koropatnick, J., Abstract A25: COTI-2, a novel small molecule that is effective against multiple human cancer cell lines in vitro and in vivo. AACR: 2017.
19. Lindemann, A.; Patel, A. A.; Tang, L.; Liu, Z.; Wang, L.; Silver, N. L.; Tanaka, N.; Rao, X.; Takahashi, H.; Maduka, N. K.; Zhao, M.; Chen, T.-C.; Liu, W.; Gao, M.; Wang, J.; Frank, S. J.; Hittelman, W. N.; Mills, G. B.; Myers, J. N.; Osman, A. A., COTI-2, a novel thiosemicarbazone derivative, exhibits antitumor activity in HNSCC through p53-dependent and -independent mechanisms. *Clinical Cancer Research* **2019,** *25*, 5650-5662.
20. Salim, K. Y.; Maleki Vareki, S.; Danter, W. R.; Koropatnick, J., COTI-2, a novel small molecule that is active against multiple human cancer cell lines in vitro and in vivo. *Oncotarget* **2016,** *7*, 41363-41379.
21. Fischer, B.; Kryeziu, K.; Kallus, S.; Heffeter, P.; Berger, W.; Kowol, C. R.; Keppler, B. K., Nanoformulations of anticancer thiosemicarbazones to reduce methemoglobin formation and improve anticancer activity. *RSC advances* **2016,** *6* (61), 55848-55859.
22. Portney, N. G.; Ozkan, M., Nano-oncology: drug delivery, imaging, and sensing. *Analytical and bioanalytical chemistry* **2006,** *384* (3), 620-630.
23. Maeda, H.; Nakamura, H.; Fang, J., The EPR effect for macromolecular drug delivery to solid tumors: Improvement of tumor uptake, lowering of systemic toxicity, and distinct tumor imaging in vivo. *Advanced drug delivery reviews* **2013,** *65* (1), 71-79.
24. Bulbake, U.; Doppalapudi, S.; Kommineni, N.; Khan, W., Liposomal formulations in clinical use: an updated review. *Pharmaceutics* **2017,** *9* (2), 12.
25. Popović-Bijelić, A.; Kowol, C. R.; Lind, M. E.; Luo, J.; Himo, F.; Enyedy, É. A.; Arion, V. B.; Gräslund, A., Ribonucleotide reductase inhibition by metal complexes of Triapine (3-aminopyridine-2-carboxaldehyde thiosemicarbazone): a combined experimental and theoretical study. *Journal of inorganic biochemistry* **2011,** *105* (11), 1422-1431.
26. Barenholz, Y. C., Doxil®—the first FDA-approved nano-drug: lessons learned. *Journal of controlled release* **2012,** *160* (2), 117-134.
27. Sharma, A.; Sharma, U. S., Liposomes in drug delivery: progress and limitations. *International journal of pharmaceutics* **1997,** *154* (2), 123-140.
28. Kunos, C. A.; Radivoyevitch, T.; Ingalls, S. T.; Hoppel, C. L., Management of 3-aminopyridine-2-carboxaldehyde thiosemicarbazone-induced methemoglobinemia. *Future Oncology* **2012,** *8* (2), 145-150.

29. Zucker, D.; Marcus, D.; Barenholz, Y.; Goldblum, A., Liposome drugs' loading efficiency: a working model based on loading conditions and drug's physicochemical properties. *Journal of controlled release* **2009,** *139* (1), 73-80.
30. Kallus, S.; Englinger, B.; Senkiv, J.; Laemmerer, A.; Heffeter, P.; Berger, W.; Kowol, C. R.; Keppler, B. K., Nanoformulations of anticancer fgfr inhibitors with improved therapeutic index. *Nanomedicine: Nanotechnology, Biology and Medicine* **2018,** *14* (8), 2632-2643.
31. Bormio Nunes, J. H.; Hager, S.; Mathuber, M.; Pósa, V.; Roller, A.; Enyedy, E. v. A.; Stefanelli, A.; Berger, W.; Keppler, B. K.; Heffeter, P., Cancer Cell Resistance Against the Clinically Investigated Thiosemicarbazone COTI-2 Is Based on Formation of Intracellular Copper Complex Glutathione Adducts and ABCC1-Mediated Efflux. *Journal of medicinal chemistry* **2020**.
32. Bangham, A.; De Gier, J.; Greville, G., Osmotic properties and water permeability of phospholipid liquid crystals. *Chemistry and physics of lipids* **1967,** *1* (3), 225-246.
33. Barenholz, Y., Liposome application: problems and prospects. *Current opinion in colloid & interface science* **2001,** *6* (1), 66-77.
34. Kowol, C. R.; Heffeter, P.; Miklos, W.; Gille, L.; Trondl, R.; Cappellacci, L.; Berger, W.; Keppler, B. K., Mechanisms underlying reductant-induced reactive oxygen species formation by anticancer copper (II) compounds. *JBIC Journal of Biological Inorganic Chemistry* **2012,** *17* (3), 409-423.
35. Nakamura, K.; Yamashita, K.; Itoh, Y.; Yoshino, K.; Nozawa, S.; Kasukawa, H., Comparative studies of polyethylene glycol-modified liposomes prepared using different PEG-modification methods. *Biochimica et Biophysica Acta (BBA)-Biomembranes* **2012,** *1818* (11), 2801-2807.
36. Garbuzenko, O.; Zalipsky, S.; Qazen, M.; Barenholz, Y., Electrostatics of PEGylated micelles and liposomes containing charged and neutral lipopolymers. *Langmuir* **2005,** *21* (6), 2560-2568.
37. Nag, O. K.; Awasthi, V., Surface engineering of liposomes for stealth behavior. *Pharmaceutics* **2013,** *5* (4), 542-569.
38. Hioki, A.; Wakasugi, A.; Kawano, K.; Hattori, Y.; Maitani, Y., Development of an in vitro drug release assay of PEGylated liposome using bovine serum albumin and high temperature. *Biological and Pharmaceutical Bulletin* **2010,** *33* (9), 1466-1470.
39. Immordino, M. L.; Dosio, F.; Cattel, L., Stealth liposomes: review of the basic science, rationale, and clinical applications, existing and potential. *International journal of nanomedicine* **2006,** *1* (3), 297.
40. Ishiguro, K.; Lin, Z. P.; Penketh, P. G.; Shyam, K.; Zhu, R.; Baumann, R. P.; Zhu, Y.-L.; Sartorelli, A. C.; Rutherford, T. J.; Ratner, E. S., Distinct mechanisms of cell-kill by triapine and its terminally dimethylated derivative Dp44mT due to a loss or gain of activity of their copper (II) complexes. *Biochemical pharmacology* **2014,** *91* (3), 312-322.
41. Kirsipuu, T.; Zadorožnaja, A.; Smirnova, J.; Friedemann, M.; Plitz, T.; Tõugu, V.; Palumaa, P., Copper (II)-binding equilibria in human blood. *Scientific reports* **2020,** *10* (1), 1-11.
42. Raju, K. S.; Alessandri, G.; Ziche, M.; Gullino, P. M., Ceruloplasmin, copper ions, and angiogenesis. *Journal of the National Cancer Institute* **1982,** *69* (5), 1183-1188.
43. Han, H. D.; Lee, A.; Song, C. K.; Hwang, T.; Seong, H.; Lee, C. O.; Shin, B. C., In vivo distribution and antitumor activity of heparin-stabilized doxorubicin-loaded liposomes. *International journal of pharmaceutics* **2006,** *313* (1-2), 181-188.
44. Quach, P.; Gutierrez, E.; Basha, M. T.; Kalinowski, D. S.; Sharpe, P. C.; Lovejoy, D. B.; Bernhardt, P. V.; Jansson, P. J.; Richardson, D. R., Methemoglobin formation by triapine, di-2-pyridylketone-4, 4-dimethyl-3-thiosemicarbazone (Dp44mT), and other anticancer thiosemicarbazones: identification of novel thiosemicarbazones and therapeutics that prevent this effect. *Molecular pharmacology* **2012,** *82* (1), 105-114.
45. Basha, M. T.; Bordini, J.; Richardson, D. R.; Martinez, M.; Bernhardt, P. V., Kinetico-mechanistic studies on methemoglobin generation by biologically active thiosemicarbazone iron (III) complexes. *Journal of inorganic biochemistry* **2016,** *162*, 326-333.
46. Basha, M. T.; Rodríguez, C.; Richardson, D. R.; Martínez, M.; Bernhardt, P. V., Kinetic studies on the oxidation of oxyhemoglobin by biologically active iron thiosemicarbazone

complexes: relevance to iron-chelator-induced methemoglobinemia. *JBIC Journal of Biological Inorganic Chemistry* **2014,** *19* (3), 349-357.
47. Zijlstra, W. G.; Buursma, A.; Meeuwsen-van der Roest, W. P., Absorption spectra of human fetal and adult oxyhemoglobin, de-oxyhemoglobin, carboxyhemoglobin, and methemoglobin. *Clinical Chemistry* **1991,** *37* (9), 1633-1638.
48. Enyedy, É. A.; Nagy, N. V.; Zsigó, É.; Kowol, C. R.; Arion, V. B.; Keppler, B. K.; Kiss, T., Comparative Solution Equilibrium Study of the Interactions of Copper (II), Iron (II) and Zinc (II) with Triapine (3-Aminopyridine-2-carbaldehyde Thiosemicarbazone) and Related Ligands. *European Journal of Inorganic Chemistry* **2010,** *2010* (11), 1717-1728.
49. Kratz, F.; Senter, P.; Steinhagen, H., *Drug delivery in oncology: from basic research to cancer therapy*. John Wiley & Sons: 2013.
50. Towbin, H.; Staehelin, T.; Gordon, J., Electrophoretic transfer of proteins from polyacrylamide gels to nitrocellulose sheets: procedure and some applications. *Proceedings of the national academy of sciences* **1979,** *76* (9), 4350-4354.

Supporting Information

Liposomal formulations of anticancer copper(II) thiosemicarbazone complexes

Marlene Mathuber[a], Sonja Hager[b,c], Bernhard K. Keppler[a,c], Petra Heffeter[b,c] and Christian R. Kowol[a,c,*]

[a] Institute of Inorganic Chemistry, Faculty of Chemistry, University of Vienna, Waehringer Straße 42, 1090 Vienna, Austria

[b] Institute of Cancer Research and Comprehensive Cancer Center, Medical University of Vienna, Borschkegasse 8A, 1090 Vienna, Austria

[c] Research Cluster ''Translational Cancer Therapy Research'', University of Vienna and Medical University of Vienna, 1090 Vienna, Austria

E-mail address: christian.kowol@univie.ac.at

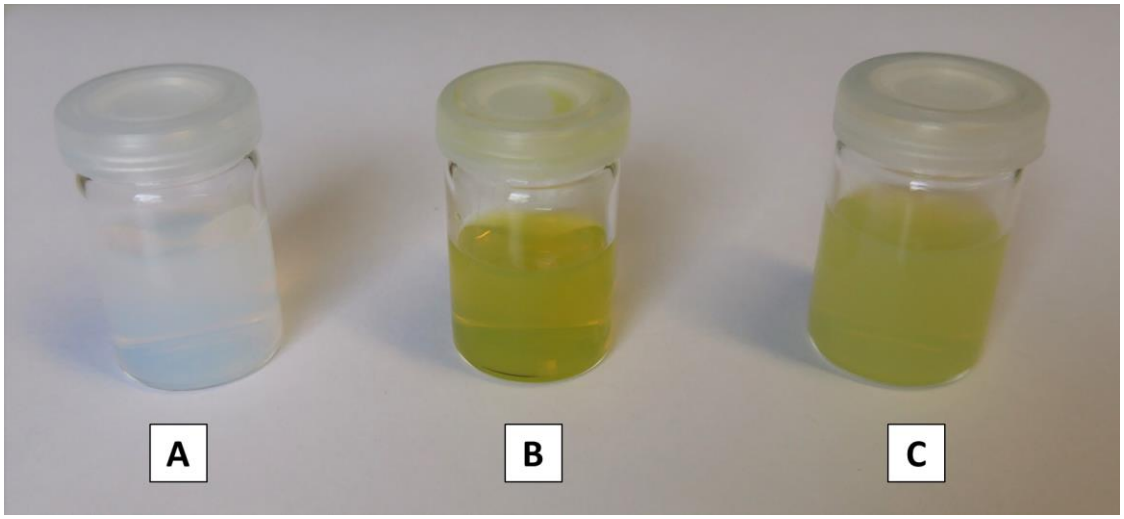

Figure S1: Pictures of (A) unloaded liposomes, (B) **L-Cu-Tria** and (C) **L-Cu-COTI**.

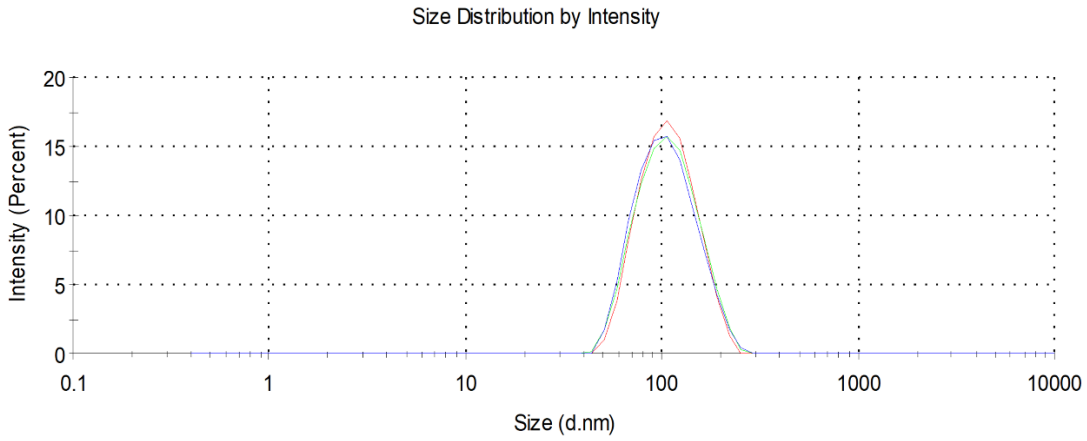

Figure S2: Size distribution of **L-Cu-COTI** (by intensity) measured by dynamic light scattering (each line represent measurements in triplicate).

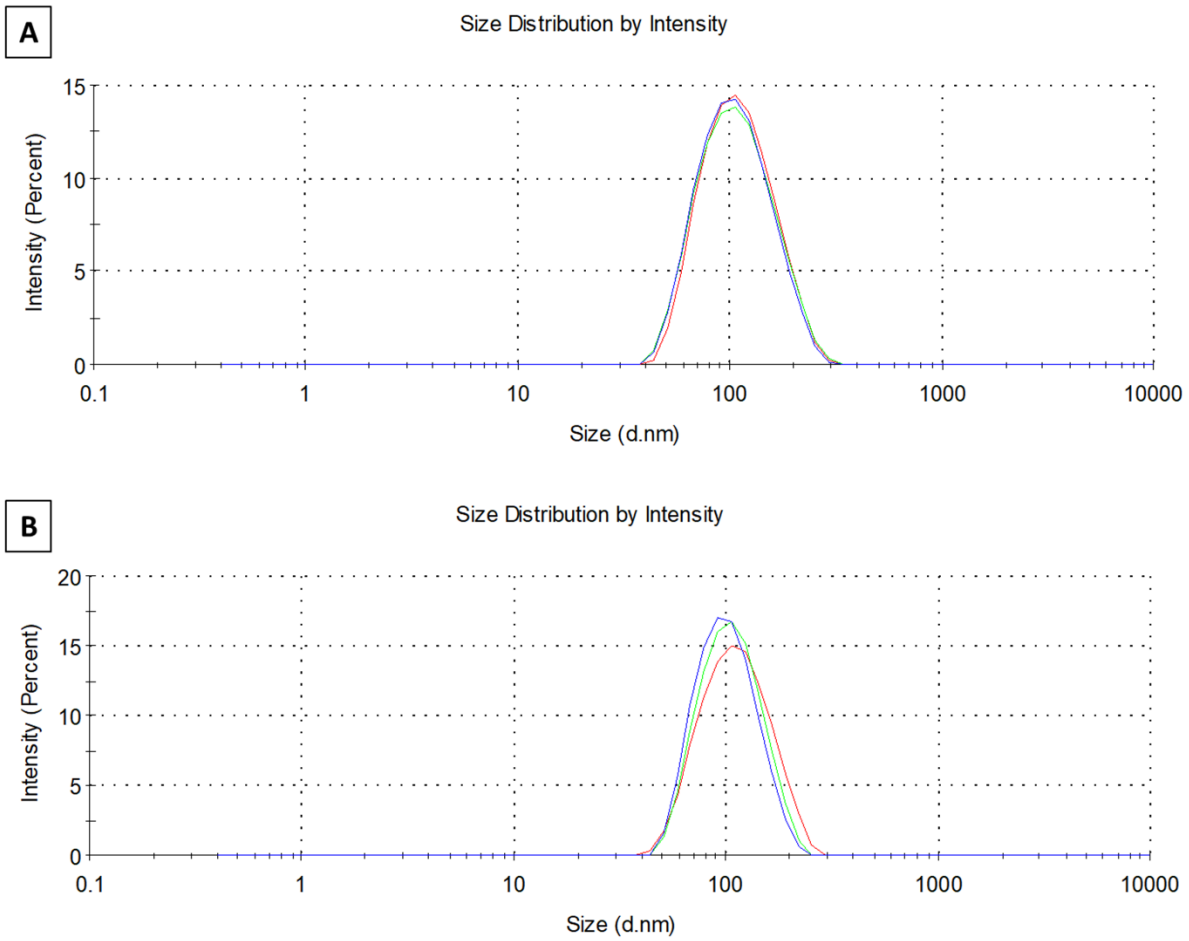

Figure S3: Size distribution of **L-Cu-Tria** (by intensity) measured by dynamic light scattering (each line represent measurements in triplicate). A) Directly after the second size exclusion chromatography B) after reducing the solution by approximately half of its volume.

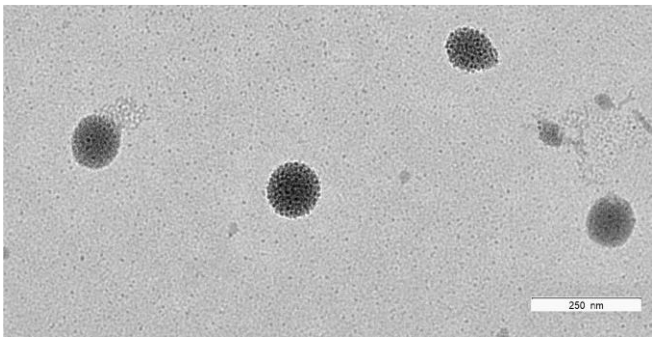

Figure S4: Transmission electron microscopy image of **L-Cu-Tria**; samples were prepared by negative staining with Uranyless.

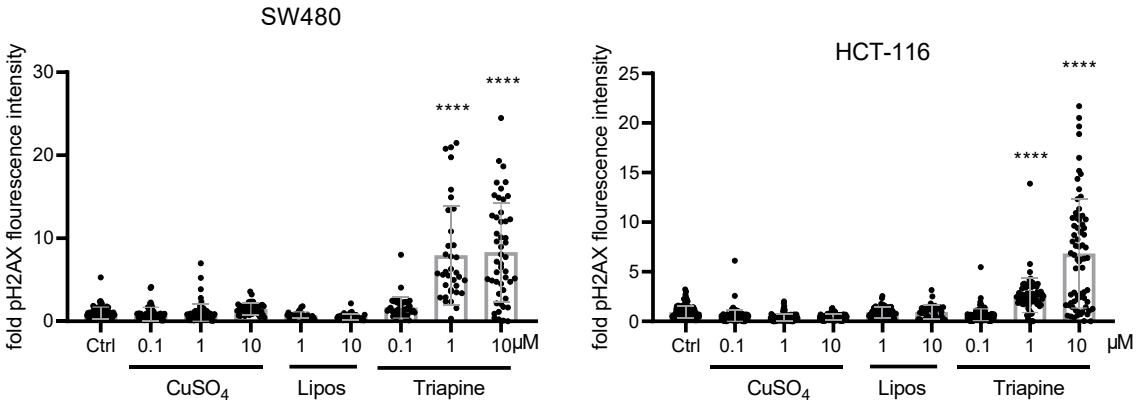

Figure S5: Quantification of immunofluorescence intensities in the nucleus of the DNA damage marker pH2AX in SW480 and HCT-116 cells treated with indicated concentrations of $CuSO_4$, empty liposomes (equivalent concentration to loaded liposomes) or Triapine for 24 h. Values given are the mean fold intensities ± SD per nucleus. Significance to control was calculated by two-way ANOVA and Dunnett's multiple comparison test (**** $p < 0.0001$).

8 CONCLUSION

Cancer is still one of the leading causes of death worldwide, in spite of all scientific development and various available therapy options. The greatest restriction of anticancer therapeutics are treatment-induced adverse effects, which are caused by a lack of tumor specificity and frequently lead to dose-reductions or therapy discontinuation. In addition, the occurrence of resistances, sometimes only after a short period of time, represents another major issue. Thus, the aim of this thesis was to develop prodrug and passive drug targeting systems for two different compound classes of anticancer drugs in order to overcome their respective drawbacks.

The first part of this thesis focused on small molecule TKIs, a subclass of targeted therapeutics, which dramatically improved cancer treatment over the last two decades. However, despite their oncogenic targets, in the clinics TKIs suffer from severe side effects and rapidly arising resistances. One promising strategy to address these issues is the administration of TKIs in form of prodrugs, which are specifically activated at the target site. In this thesis cobalt(III) complexes were used a hypoxia-activatable prodrug systems. Previously we developed for the first time a cobalt(III) prodrug with a small molecule TKI (EGFR inhibitor) as ligand. Despite encouraging *in vitro* and first *in vivo* experiments, the lead compound (Co-EGFR) was not as stable as expected in blood plasma. Consequently, the aim of the first project was to increase the stability of the original complex by reducing its redox potential. To this end, methyl groups as electron donators were inserted at different positions (ligand and/or ancillary moiety). Cyclic voltammetry studies showed that by using methyl acetylacetone (Meacac) instead of acetylacetone (acac) as auxiliary groups the reduction potential could be successfully lowered. In contrast, the methylation of the ligand did not result in the expected effect. Notably, the fluorescence property of the coordinated ligands is almost completely quenched, which is useful for the distinction between free ligand and complex. Thus, a strong correlation between the decreased reduction potential and increased stability could be confirmed by physico-chemical and biological fluorescence measurements. *In vitro* tests revealed that the most stable complexes could be still activated under hypoxic conditions. Nevertheless, their IC_{50} values did not reach those of the free ligands, suggesting a slow activation. For the second project another strategy was applied to increase the stability of TKI-bearing cobalt(III) prodrugs. We assumed that the high reduction potential of the previously synthesized complex Co-EGFR was caused by the direct bonding of the metal-chelating moiety to the aromatic ring system. Therefore, ponatinib, a clinically approved mulitkinase inhibitor, was chosen as ligand motif as its molecular structure 1) allows the introduction of the necessary ethylenediamine group (instead of the original piperazine moiety) and more importantly 2) has a $–CH_2$ spacer unit between the aromatic ring system and piperazine moiety. This spacer unit was assumed to

weaken the electron withdrawing effect of the aromatic rings. Molecular docking studies revealed a similar binding mode of ponatinib and the novel ligand as well as the prodrug potential of the cobalt(III) complexes (again with acac or Meacac as ancillary ligands). Cyclic voltammetry measurements showed that the $–CH_2$ group indeed fulfilled its purpose as distinctly reduced reduction potentials were achieved compared to Co-EGFR. Cell tests confirmed the higher stability and activation by hypoxia for the novel cobalt(III) complexes. Notably, *in vivo* experiments revealed that the complex with the lowest reduction potential (Meacac ligands) was less effective than the analogue with acac as auxiliary ligands.

In summary, in both subprojects the reduction potential of the respective complexes could be successfully lowered, while maintaining their hypoxia activatable properties in a biological environment. However, the *in vitro* as well as *in vivo* results indicate that the complexes with the lowest reduction potential became too stable to be completely activated (at least under the applied conditions). Consequently, future research should focus on finding the right balance of adequate stability and activity (e.g. by synthesizing and investigating a larger panel of different complexes) as they are the crucial factors for this kind of approach. Additionally, all compounds showed an irreversible redox behavior, which is not in line the suggested mode of action for organic hypoxia-activated prodrug systems (immediate re-oxidization of the prodrug by molecular oxygen after the one-electron reduction step). Therefore, of great interest is the elucidation of the exact activation mechanism for hypoxia-activatable cobalt(III) prodrugs.

The second part of this thesis addressed the compound class of TSCs. While Triapine, one of their leading representatives, achieved encouraging outcomes in several clinical trials against hematological cancers, hardly any efficacy against solid tumors could be observed. This very likely results from a fast metabolization and short retention time of Triapine in the body. To distinctly improve the anticancer potential of TSCs, the plasma half-life needs to be significantly extended and the tumor specificity enhanced. A promising strategy to meet these requirements is the passive drug targeting approach. With this concept, the respective compound is encapsulated into nanoparticles, which then accumulate at the target site *via* the enhanced permeability and retention (EPR) effect. Additionally, an improved solubility (especially useful for highly lipophilic compounds) can be achieved. Notably, this method is already an approved cancer therapy in the form of e.g. liposomal doxorubicin (Doxil®) or vincristine (Marqibo®). However, in a previous work we revealed that this strategy could not be applied to Triapine as no stable encapsulation into nanoformulations could be obtained. Thus, within the third project of this thesis, liposomal formulations of copper(II) Triapine (Cu-Tria) were prepared as this complex behaves like a prodrug, releasing Triapine after being reduced. Furthermore, we included a clinically investigated

third-generation TSC, namely COTI-2, as well as its copper(II) complex into our studies. Depending on the chemical nature of the respective drug, different encapsulation techniques were used. A strongly decreased cytotoxicity and DNA damaging for liposomal Cu-Tria compared to the free Cu-Tria was observed *in vitro*, indicating a stable encapsulation. In addition, a slow continuous release of Cu-Triapine could be confirmed, an essential feature for the therapeutic effectiveness of nanoformulations. Unfortunately, neither COTI-2 nor its copper(II) complex could be stably encapsulated. Consequently, only liposomal Cu-Tria was investigated *in vivo*, where a slow and constant release could be confirmed by monitoring the copper levels in plasma *via* ICP-MS. Additionally, methemoglobinemia, a frequently noticed adverse event of Triapine during clinical studies, was completely prevented by the liposomal formulation. Therefore, the encapsulation into nanoparticles is a promising strategy to enhance the plasma half-life time of Cu-Tria and presents an encouraging basis for further research. Subsequent animal tests will reveal the anticancer potential of liposomal Cu-Tria compared to the free drug. The obtained results of Cu-Tria compared to Cu-COTI impressively show how crucial the exact chemical structure is for this approach. Quite small differences can dramatically influence the encapsulation efficacy and the release kinetics. Furthermore, it is worth mentioning that an encapsulation limit has been reached for the micromolar active Cu-Tria. Thus, future studies should focus on TSCs, which are active within the nanomolar range. Achieving then loading concentrations comparable to Cu-Tria should ultimately lead to a higher anticancer activity.

Taken together, in this thesis prodrug as well as passive targeting strategies have been applied to two different classes of antineoplastic agents (namely TKIs and TSCs) with the aim to improve their therapeutic index. Each approach could be successfully correlated with biologically experiments and showed potential for future investigations. Concluding, the outcome of this work will hopefully help to increase the tolerability and scope of the studied anticancer drugs.

Ich habe mich bemüht sämtliche Inhaber der Bildrechte ausfindig zu machen und ihre Zustimmung zur Verwendung der Bilder in dieser Arbeit eingeholt. Sollte dennoch eine Urheberrechtsverletzung bekannt werden, ersuche ich um umgehende Meldung bei mir.

Marlene Mathuber, 12.08.2021